

Final Report on NASA Contract

NAS9-5911

The Apollo Lunar Surface Experiment Package

Suprathermal Ion Detector Experiment

Department of Space Physics and Astronomy

Rice University

Houston, Texas 77001

July, 1975.

## TABLE OF CONTENTS

	Page
Introduction	1
The Lunar Ionosphere	3
The Electric Potential of the Lunar Surface	5
The Lunar Nightside	6
Bow Shock Protons	7
Magnetosheath	8
Magnetotail	9
Solar Wind--Neutral Gas Cloud Interactions	10
Rocket Exhaust Products	10
Synoptic and Secular Studies and Transient Events	11
Penetrating Solar Particles	12
Future Research	13
Summary	15
References	16
Bibliography	17
Appendices	
1. Data Users Handbook	
2. One-Year Report	
3. Full copies of Papers cited in the text.	

## Introduction

The Suprathermal Ion Detector Experiment (SIDE) was deployed on the Apollo 12, 14 and 15 missions. Table 1 gives the deployment locations and dates.

Table 1

	<u>Longitude</u>	<u>Latitude</u>	<u>M. D. Y.</u>
Apollo 12	23.4°W	3.2°S	11 19 69
Apollo 14	17.4°W	3.6°S	2 5 71
Apollo 15	3.6°E	26.1°N	7 31 71

At the time of preparation of this report the Apollo 12 and 15 SIDEs are returning useful data although the Apollo 12 SIDE mass analyzer is noisy and the absolute intensity calibration of the total ion detector is no longer trustworthy. The Apollo 14 SIDE returned useful data until mid-December of 1974, when it failed to operate after having drawn excessive current.

In all some 13 years, 9 months of cumulative data have been received from the three instruments. The raw data is stored on several thousand reels of magnetic tape. The majority of this data has been converted to a scientifically useful format and deposited in the National Space Science Data Center at Greenbelt, Maryland. This data is in a usefully condensed format and occupies approximately 74 reels of magnetic tape. A copy of the Experiment Users

Guide that accompanies that data is attached to this report (Appendix 1) and serves as a convenient description of the instrument and the data format. A copy of the One-Year report on the SIDE contract is also attached, as Appendix 2.

The principal scientific objectives of the Suprathermal Ion Detector Experiment were to explore the lunar ionic environment and to measure the electric potential of the lunar surface. The experiment was highly successful in that both of these objectives were accomplished. Furthermore, an additional objective, the investigation of the magnetospheric tail at lunar distances, was also successful and a new region of magnetospheric plasma was discovered above and below the plasma sheet; the lobe plasma.

A measure of the success of the experiment can be seen in the length of the attached Bibliography of papers and theses pertaining to the SIDE data. Approximately 200 pages of published material have appeared in books or scientific journals, and over 45 papers have been presented in scientific meetings. In addition ~~same~~ 1200 pages of M. S. and Ph.D. thesis material has been written resulting in 9 M. S. degrees and 3 Ph.D. degrees. Two more Ph.D. degrees based on SIDE data are expected in November 1975.

A glance at the attached bibliography also shows the wide range of subjects explored by the SIDE data. We now provide a brief current summary of the principal results from some of these subject areas.



### The Lunar Ionosphere

Because the lunar ionosphere is promptly accelerated by the solar wind electric field the majority of SIDE data on the ionosphere comes from the terminator regions. Here the orientation between the electric field and the detector look axes is such that the ions can be accelerated into the SIDE field of view. The observed fluxes of ions in the mass range about 20 AMU/q (probably neon) are highly variable, depending on solar wind magnetic field conditions and local time. Typical values for the stronger events are approximately  $10^5$  ions  $\text{cm}^{-2} \text{sec}^{-1}$  in the energy range 10-3500 eV. Assuming accepted values for the U.V. and charge exchange ionization rates leads to neon neutral number densities of  $5 \times 10^4$  to  $10^5$  atoms/cm. Although we have seen events in which ions in the mass 40 AMU/q range were represented these events are not as clean and we are not able to quote fluxes and number densities for Argon ions and atoms.

A particularly interesting feature of the terminator ion data is the ion energy spectrum itself. This spectrum has proven to be quite tractable and illuminating. Several examples are given in the attached paper "The Lunar Terminator Ionosphere", by Benson et al., 1975 (Appendix 3-1). The differential energy spectrum is exponential above the main peak owing to the exponential nature of the lunar atmosphere and the homogeneous solar wind electric field.

The e-folding energy gives the product of the neutral gas scale height and the solar wind electric field strength. Since the scale height is determined independently this provides direct measure of the solar wind electric field. The peak energy is a rough measure of the lunar surface electric potential which is found to be negative near the terminator. The shape of the dip in the spectrum below the peak energy indicates the rate at which the lunar surface electric field falls off with height. Fits to an exponential function indicate an e-folding height of several kilometers, a much larger distance than the free streaming solar wind Debye length of several meters. These spectra provide a great deal of information on the electric field environment of the moon as well as the ion environment.

When the solar wind electric field is not oriented such as to accelerate ions into the SIDE at the terminator, ion fluxes are sometimes still observed. These fluxes are due to atmospheric ions accelerated toward the lunar surface by the lunar surface electric field alone. The differential energy spectrum of these ions (see figure 4 of "The lunar Terminator Ionosphere", Benson et al., 1975, Appendix 3-1) is very narrow and in fact rarely seen in more than one SIDE energy channel. Because the spectrum is so narrow it is not mathematically tractable except to calculate that the peak energy is a direct measure of the local electric potential of the the lunar surface, usually between - 10 and - 100

volts in the terminator region.

The SIDEs also detect the lunar ionosphere on the dayside of the moon. In this case the accelerating electric field is provided by the SIDE itself. A stepped voltage supply provides a potential difference between the ground plane grid and the ion entrance aperture. When the aperture is negative relative to the lunar surface ions can be accelerated into the detectors. This mode of operation is used to determine the dayside lunar surface potential due to photo electrons, (see "The Electric Potential of the Lunar Surface", Fenner et al., 1973, Appendix 3-2). It also provides a measure of the ion number density at the surface. This number is found to lie between 1 and 7 ions/cm in the solar wind or magnetosheath plasma. As expected this ion number density does not exceed that of the solar wind.

#### The Electric Potential of the Lunar Surface

As indicated above, the surface potential in sunlight is determined by the energy spectrum of ions accelerated by the ground plane stepper supply. Since this electric field extends about 1 Debye length or less from the SIDE it provides a measure of the lunar potential relative only to the immediate surrounding plasma i.e., the surface potential due chiefly to the photoelectrons. This potential is found to be about +10 volts from solar zenith angles of 0 to about 45°. Beyond 45° the potential falls rapidly to values as

low as - 100 volts near the terminator. The lunar surface potential is not symmetric with regard to positive and negative zenith angles. At about  $+50^\circ$  the potential rises abruptly to about +18 volts. No equivalent peak is seen at negative angles. As shown by the CPLEE data (Burke et al., 1975) the potential of the lunar surface on the dayside relative to the solar wind may be considerably higher in regions where there exists a substantial surface magnetic field. Further details of the surface potential can be found in "Lunar Electric field, Surface Potential and Associated Plasma Sheath Effects", Freeman and Ibrahim, 1975, Appendix 3-3.

#### The Lunar Nightside

Ions in the energy range 250 eV to 1500 eV are seen on the nightside of the moon. These ions may be seen throughout almost the entire lunar night but activity increases in the period 1 to 6 days prior to local sunrise and has a strong peak 2 to 3 days before sunrise as seen with the Apollo 14 and 15 SIDEs. The Apollo 12 SIDE shows an equivalent activity following sunset.

The ion energies are generally less than solar wind energies. The spectra vary from mono-energetic at 250 eV to 500 eV to broad. There is an indication that the peak energy changes with lunar local time reaching a maximum of 750 eV 3 to 4 days before sunrise.

The ion fluxes are of the order of  $10^6$  ions/cm<sup>2</sup>-sec-ster. They occur in bursts usually less than 1 hour in duration. They show no  $K_p$  dependence.

These ions are not understood. Their energy suggests that they are of solar wind origin. They are of too high energy to be detected by the SIDE mass analyzer. Possible explanations include:

1. Atmospheric ions accelerated by the solar wind into circumlunar trajectories.
2. Solar wind protons escaping from a lunar limbshock as recompression shock.
3. The positive ion sheath of the lunar nightside negative surface potential.

For further details see "An Observation of Lunar Night-time Ions", by Henry Emil Schneider, 1975, (Appendix 3-4).

#### Bow Shock Protons

Protons and other solar wind ions accelerated in the earth's bow shock can escape upstream along magnetic field lines. The SIDEs established that these ions can travel at least as far as the lunar orbit. At the moon these ions have energies ranging from 250 eV to beyond the upper limit of the SIDE at 3500 eV. Integral fluxes of the order of  $10^5$  ions/cm<sup>2</sup> sec -ster are typical. Their arrival at the moon is correlated with the interplanetary magnetic field direction. Further details can be found in "Bow Shock

Protons in the Lunar Environment", by Benson et al., 1975, Appendix 3-5 and the related thesis by Benson.

### Magnetosheath

The moon offers a good platform from which to study the distant magnetotail and magnetosheath. Using SIDE energy spectra the plasma parameters bulk velocity, temperature, number density, pressure, and energy density ratio were computed for 10 lunations throughout the magnetosheath. These parameters generally follow the predictions of laminar flow. The presence of non-thermal particles concentrating in a high energy tail of the energy spectrum is observed to increase near the bow shock in the dusk magnetosheath.

An unexpected result is an asymmetry in the correlation between this high energy tail and  $K_p$ . The dusk magnetosheath shows a good correlation but the dawn magnetosheath shows no such correlation. This result is believed to be related to the presence of oblique shocks at the dawn magnetosheath. Further information can be found in "Dawn-Dusk Magnetosheath Plasma Asymmetries at 60 RE", by M. A. Fenner and J. W. Freeman 1975, (Appendix 3-6), and the related thesis by Fenner.

### Magnetotail

Perhaps the most important and least expected result from the SIDE data is the discovery of a new plasma regime in the high latitude lobes of the geomagnetic tail. Principally because of the SIDE's high sensitivity to low energy ions it detects what we refer to as the "lobe plasma".

The lobe plasma consists of protons of energy 50 to 250 eV streaming along the geomagnetic tail field lines away from the earth. Integral fluxes range from  $10^5$  to  $10^8$  ions/cm<sup>2</sup> sec ster, temperatures  $4 \times 10^4$  to  $5 \times 10^5$ °K and number densities 0.1 to 5/cm<sup>3</sup>. See "A New Plasma Regime in the Distant Geomagnetic Tail", Hardy et al., 1975, (Appendix 3-7) and the related thesis by Hardy.

This plasma is found to be sometimes but not always contiguous with the plasma sheet. It is believed to convect toward the plasma sheet from the polar magnetopause and to form the source region for the plasma sheet. Its frequency of occurrence in certain areas of the tail appears correlated with the east-west component of the interplanetary magnetic field, thus providing convincing evidence for the highly controversial magnetic merging on the dayside magnetopause.

Detailed investigations of the plasma sheet using the SIDE data are only now getting underway. One feature of interest is the appearance of multiple bulk flow velocities. Also the correlation of plasma sheet flow with substorm activity remains a promising subject to be investigated.

### Solar Wind-Neutral Gas Cloud Interactions

An important aspect of cosmic physics is the interaction between neutral and ionized gas streams. An opportunity to investigate such an interaction accrued following the impact of the Apollo 13 S-IVB stage rocket 140 km west of the Apollo 12 ALSEP site. Both the SIDE and the Solar Wind Spectrometer observed a large flux of positive ions (maximum flux  $\sim 3 \times 10^8$  ions/cm<sup>2</sup> sec ster). Two separate streams of ions were seen: a horizontal flux that appeared to be deflected solar wind ions and a smaller vertical flux of predominantly heavy ions ( $> 10$  AMU/q) which probably consisted of material vaporized from the S-IVB stage. The important result is that hot electrons (50eV) were created and were an important ionization mechanism in the impact-produced neutral gas cloud. Thus strong ionization and acceleration were seen under near collisionless conditions. For further information refer to "The Interaction Between an Impact - Produced Neutral Gas Cloud and the Solar wind at the Lunar Surface", by Lindeman et al., 1974 (Appendix 3-8).

### Rocket Exhaust Products

Along with ions from the ambient atmosphere the SIDEs detect ions arising from exhaust gases from the Apollo missions. The Apollo 12 SIDE data was studied briefly with the object of determining the dissipation rates of these



gases. Two mass analyzer spectra were examined: one 14 hours after the Apollo 12 landing; the other 2 months later. Both spectra showed good agreement with the predicted mass spectra for exhaust gases. When fitted to an exponential decay curve an e-folding time of approximately 30 days was obtained for the majority of the gases ("Suprathermal Ions Near the Moon", Freeman et al., 1972, Appendix 3-9). This study has not been completed. The lifetimes of individual gases have not been examined in detail nor have the data from the Apollo 14 and 15 SIDEs been carefully examined with a study of exhaust gases as the principal object.

#### Synoptic and Secular Studies and Transient Events

Due to the sporadic nature of the lunar ionosphere measurements it has been difficult to make secular and synoptic measurements. It has been observed, however, that ion densities computed from data taken about 6 months after the deployment of the Apollo 15 instrument are about a factor of 10 higher than those computed from data taken 2 years after deployment. The numbers quoted earlier in this report are from the later data. These agree with the neutral number densities for neon found by the Lunar Atmospheric Composition Experiment on Apollo 17 [Hoffman et al., 1973].

A possible explanation for this apparent change is calibration drifts in the instruments. Several independent tests of the long term calibration integrity are under way

but have not been completed. An alternative explanation is that the early data are in some way still affected by contaminants from the landing or a locally enhanced neon flux due to the heating of the lunar surface by the rocket plume. A final possibility is that there has occurred a natural secular variation in the atmospheric neon concentration. We will withhold judgement on this until all possibilities have been thoroughly investigated.

In 1973 we reported a 14-hour period during which water vapor ions dominated the ion mass per unit charge spectrum at the Apollo 14 site ("Observations of Water Vapor ions at The Lunar Surface", Freeman et al., 1973, Appendix 3-10). By examining all possible sources of contamination and extra-lunar sources, we concluded that the ions were probably of lunar origin. Since this time no additional water vapor events have been found. Consequently it appears unlikely that the water vapor came from a lunar source, although the details of the ion production are still unclear. Aside from this enigmatic event no evidence exists in the SIDE data for transient events.

#### Penetrating Solar Particles

The SIDE was designed to measure 10-3500 eV ions which enter the detector aperture. However, particles of sufficiently high energy can penetrate the instrument from any direction and be detected. Such was the case during the

intense solar flare activity of early August, 1972. High energy solar protons produced by the flares constituted an isotropic flux by the time they reached the vicinity of Earth, and were recorded by the SIDEs although the instruments were on the night side of the moon. The penetrating particles produced a high counting rate in all channels of all three SIDEs, and the event was observed for several days. A most unusual feature of the event was a sudden sharply increased flux which lasted for about two hours and ended as suddenly as it began. This so-called "square wave" was discussed in "The Solar Cosmic Ray Square-Wave of August, 1972" by Medrano et al., 1975 (Appendix 3-11), as well as in earlier conference reports and collected papers on the topic, and in the Ph.D. thesis of Medrano. Other instruments on several other spacecraft have also reported such observations and multi-spacecraft intercomparisons may shed more light on the nature of the disturbance which produced this event.

#### Future Research

The success of the SIDE experiments is characterized by the variety of phenomena the data provide information about. This wide range of phenomena has made it difficult to find time to examine all the phenomena in great depth. A great deal of data analysis remains to be done. The in depth study so far has been limited to the lunar ionosphere. The

lunar surface electric potential, the night side ions, the magnetotail, and the bow shock data have been skimmed for the gross features, but a number of specific features need investigating further. A partial list of these is as follows:

1. Investigation of the asymmetry in the lunar surface potential to determine its cause.
2. Correlation between SIDE and CPLEE lunar surface potential data in the magnetotail.
3. Correlation of the night side energetic ion fluxes with the interplanetary magnetic field to determine the origin of these fluxes.
4. Correlation between the lobe plasma and magnetospheric substorm data from ground and satellites.
5. Determination of plasma sheet parameters and their correlation with other magnetospheric data.
6. Statistical studies on the location of the magnetopause and bow shock front.
7. High resolution studies of the plasma parameters at the magnetopause and bow shock front.
8. Studies of the decay rates of the individual rocket exhaust product gases.
9. Investigation of the interaction between a rocket exhaust neutral gas cloud and the magnetosheath plasma.

10. Investigation of the cause of a background enhancement near the terminator possibly due to dust movement above the lunar surface.
11. Investigation of long-term variations in the intensities of several phenomena observed. Preliminary work indicates definite variations due to seasonal and longer-term periodicities in the lunar orbit and directions with respect to the sun. When these effects can be recognized and removed, the magnitude of secular variations, if any, can be investigated.

#### Summary

The ALSEP/SIDE has been a very fruitful investigation with the data rich in information about a variety of different areas. It has been a multidisciplinary experiment. A great deal of analysis remains to be done, particularly in the areas pertaining to the magnetosphere.

## REFERENCES

- Burke, W. J., P. H. Reiff, and D. L. Reasoner, "The Effect of Local Magnetic Fields on the Lunar Photo-Electron Layer While the Moon is in the Plasma Sheet." Proc. Sixth Lunar Sci. Conf., Geochim. et Cosmochim. Acta, Suppl. 6, 3, Pergamon Press, 1975.
- Hoffman, J. H., R. R. Hodges, Jr., F. S. Johnson, and D. E. Evans, "Lunar Atmospheric Composition Results from Apollo 17." Proc. Fourth Lunar Sci. Conf., Geochim. et Cosmochim. Acta, Suppl. 4, 3, pp. 2865-2875, Pergamon Press, 1973.

ADDENDUM to Page 17

- 2.a "Lunar Atmosphere as a Source of Lunar Surface Elements," R. H. Manka and F. C. Michel, Proc. Second Lunar Sci. Conf., Geochim. et Cosmochim. Acta, Supp. 2, 2, pp. 1717-1728, 1971.

Bibliography of ALSEP/SIDE Research

Papers Published

1. "Suprathermal Ion Detector Experiment", J. W. Freeman, Jr., H. Balsiger, and H. K. Hills, Apollo 12 Preliminary Science Report, NASA SP-235, pp. 83-92, 1970.
2. "Some Results from the Apollo 12 Suprathermal Ion Detector", J. W. Freeman, Jr., H. K. Hills, and M. A. Fenner, Proc. Second Lunar Sci. Conf., Geochim. et Cosmochim. Acta, Supp. 2, 3, pp. 2093-2102, 1971.
3. "Suprathermal Ion Detector Experiment (Lunar Ionosphere Detector)", H. K. Hills and J. W. Freeman, Jr., Apollo 14 Preliminary Science Report, NASA SP-272, pp. 175-183, 1971.
4. "Plasma Sheet Ions at Lunar Distance Preceding Substorm Onset", H. B. Garrett, T. W. Hill, and M. A. Fenner, Planet. Space Sci., 19, pp. 1413-1416, 1971.
5. "Suprathermal Ion Detector Experiment", H. K. Hills, J. C. Meister, R. R. Vondrak, and J. W. Freeman, Jr., Apollo 15 Preliminary Science Report, NASA SP-289, 1972.
6. "Water Vapor: Whence Comest Thou?", J. W. Freeman, Jr., H. K. Hills, and R. R. Vondrak, Proc. Third Lunar Sci. Conf., Geochim. et Cosmochim. Acta, Suppl. 3, 3, pp. 2217-2230, 1972.
7. "Energetic Ion Bursts on the Night Side of the Moon", J. W. Freeman, Jr., J. Geophys. Res., 77, pp. 239-243, 1972.



ADDENDUM to Page 18

- 15.a. "Plasma and Potential at the Lunar Surface", R. H. Manka, Photon and Particle Interactions with Surfaces in Space, pp. 429-442, D. Reidel, Pub., Dordrecht, Holland, 1973.

8. "Suprathermal Ions Near the Moon", J. W. Freeman, Jr., M. A. Fenner, H. K. Hills, R. A. Lindeman, R. Medrano and J. Meister, *Icarus*, 16, pp. 328-338, 1972.
9. "Observations of Water Vapor Ions at the Lunar Surface", J. W. Freeman, Jr., H. K. Hills, R. A. Lindeman, and R. R. Vondrak, *The Moon*, 8, pp. 115-128, 1973.
10. "Electric Potential of the Moon in the Solar Wind", J. W. Freeman, Jr., M. A. Fenner, and H. K. Hills, *J. Geophys. Res.*, 78, pp. 4560-4567, 1973.
11. "Suprathermal Ion Detector Results from Apollo Space Missions", J. W. Freeman, Jr., *Space Research XIII*, pp. 821-830, Akademie-Verlag, Berlin, Pub., 1973.
12. "The Electric Potential of the Lunar Surface", M. A. Fenner, J. W. Freeman, Jr., and H. K. Hills, *Proc. Fourth Lunar Sci. Conf., Geochim. et Cosmochim. Acta*, Supp. 4, 3, pp. 2877-2887, 1973.
13. "Ions from the Lunar Atmosphere", R. Lindeman, J. W. Freeman, Jr., and R. R. Vondrak, *Proc. Fourth Lunar Sci. Conf., Geochim. et Cosmochim. Acta*, Supp. 4, 3, pp. 2888-2896, 1973.
14. "Lunar Ion Energy Spectra and Surface Potential", R. H. Manka and F. C. Michel, *Proc. Fourth Lunar Sci. Conf., Geochim. et Cosmochim. Acta*, Supp. 4, 3, pp. 2897-2908, 1973.
15. "Lunar Ion Flux and Energy", R. H. Manka and F. C. Michel, *Photon and Particle Interactions with Surfaces in Space*, pp. 429-442, D. Reidel, Pub., Dordrecht-Holland, 1973.

16. "The Electric Potential of the Moon <sup>in the Solar Wind</sup>", J. W. Freeman, Jr., M. A. Fenner and H. K. Hills, Photons and Particle Interactions with Surfaces in Space, pp. 363-368, D. Reidel, Pub., Dordrecht-Holland, 1973.
17. "Penetrating Solar Flare Particle and Solar Wind Observations in the Lunar Night, August, 1972", R. A. Medrano, J. W. Freeman, Jr., H. K. Hills, and R. R. Vondrak, Collected Data Reports on August, 1972, Solar-Terrestrial Events, H. E. Coffey, Editor, pp. 361-370, Report UAG-28, Part II, World Data Center A for Solar-Terrestrial Physics, Boulder, Colorado, 1973.
18. "The Interaction Between an Impact-Produced Neutral Gas Cloud and the Solar Wind at the Lunar Surface", R. A. Lindeman, R. R. Vondrak, J. W. Freeman, and C. W. Snyder, J. Geophys. Res., 79, pp. 2287-2296, 1974.
19. "Measurements of Lunar Atmosphere Loss Rate", R. R. Vondrak, J. W. Freeman, and R. A. Lindeman, Proc. Fifth Lunar Sci. Conf., Geochim. et Cosmochim. Acta, Supp. 5, 3, pp. 2945-2954, 1974.
20. "Creation of an Artificial Lunar Atmosphere", R. R. Vondrak, Nature, 248, pp. 657-659, 1974.
21. "The Solar Cosmic Ray Square-Wave of August, 1972", R. A. Medrano, C. J. Bland, J. W. Freeman, H. K. Hills, and R. R. Vondrak, J. Geophys. Res., 80, pp. 1735-1743, 1975.
22. "A New Plasma Regime in the Distant Geomagnetic Tail", D. A. Hardy, H. K. Hills, and J. W. Freeman, Geophys. Res. Let., 2, pp. 169-172, 1975.

23. "The Lunar Terminator Ionosphere", J. Benson, J. W. Freeman, and H. K. Hills, Proc. Sixth Lunar Sci. Conf., Geochim. et Cosmochim. Acta, Supp. 6, 3, 1975.
24. "Dawn-Dusk Magnetosheath Plasma Asymmetries at 60  $R_E$ ", M. A. Fenner and J. W. Freeman, J. Geophys. Res., 1975.
25. "Lunar Electric Fields, Surface Potential and Associated Plasma Sheaths", J. W. Freeman and M. Ibrahim, The Moon, 2, pp. 368-379, 1975.
26. "Energetic Lunar Nighttime Ion Events", H. E. Schneider and J. W. Freeman, The Moon, 2, pp. 297-303, 1975.
27. "Bow Shock Protons in the Lunar Environment", J. Benson, J. W. Freeman, H. K. Hills, and R. R. Vondrak, The Moon, 2, pp. 290-296, 1975.

Theses (Rice University)

1. "A Suprathermal Ion Accelerator", David Thad Young, M.S., 1967 (127 pages)
2. "Design and Calibration of the Suprathermal Ion Detector Experiment (SIDE)", Robert L. Shane, M.S., 1969 (72 pages).
3. "Solar Plasma Disturbance Observed by a Suprathermal Ion Detector on the Moon", René A. Medrano-Balboa, M. S., 1971 (84 pages).
4. "Recurring Ion Events at the Lunar Surface", Robert A. Lindeman, M. S., 1971 (68 pages).
5. "Magnetosheath Plasma at 60  $R_E$ ", Martha Ann Fenner, M.S., 1971 (88 pages).
6. "Lunar Atmosphere and Ionosphere", Robert Hall Manka, Ph.D., 1972 (141 pages).
7. "Unusual Solar Wind and Solar Proton Events Observed on the Lunar Surface", René A. Medrano-Balboa, Ph.D., 1973 (153 pages).
8. "Observation of Ions from the Lunar Atmosphere", Robert A. Lindeman, Ph.D., 1973 (115 pages).
9. "Observations of Magnetosheath Plasma at the Lunar Orbit", Martha A. Fenner, Ph.D., 1974 (70 pages).
10. "Observation of Low Energy Protons in the Geomagnetic Tail at Lunar Distances, David A. Hardy, M.S., 1974 (47 pages).
11. "Observations of Bow Shock Protons at the Lunar Orbit", John L. Benson, M.S., 1974 (174 pages).
12. "An Observation of Lunar Nighttime Ions", Henry Emil Schneider, M.S., 1975 (39 pages).

13. "The Electric Potential of the Lunar Surface", Mohamed Esam Ibrahim, M.S., 1975 (41 pages).

Papers Presented at Scientific Meetings

1. Preliminary Results from the Apollo 12 ALSEP Lunar Ionosphere Detector: I General Results, J. W. Freeman, H. Balsiger, and H. K. Hills, 51st Annual A.G.U. Meeting, Washington, D. C., April, 1970.
2. Preliminary Results from the Apollo 12 ALSEP Lunar Ionosphere Detector: II The Ion Mass Spectrometer, H. Balsiger, J. W. Freeman, and H. K. Hills, *ibid.*
3. Energetic Protons Observed at the Lunar Surface on the Night Side of the Moon, H. K. Hills, J. W. Freeman, and H. Balsiger, *ibid.*
4. Positive Ions at the Apollo 12 ALSEP site resulting from the Apollo 13 S-IV B lunar impact, J. W. Freeman and H. K. Hills, Fall annual A.G.U. Meeting, San Francisco, 1970.
5. Results from the Apollo 12 Suprathermal Ion Detector, 1971 Lunar Science Conference, Houston, January, 1971.
6. Magnetosheath Plasma Observations at the Moon's Surface, M. A. Fenner, H. K. Hills, R. A. Medrano, J. W. Freeman, and R. A. Lindeman, 52nd Annual A.G.U. Meeting, Washington, D. C., April, 1971.
7. Ion Bursts at the Lunar Distance in the Tail Preceding Substorm Onset, H. B. Garrett, T. W. Hill, and M. A. Fenner, *ibid.*
8. Recurring Ions Clouds at the Lunar Surface, R. A. Lindeman, J. W. Freeman, and H. K. Hills, *ibid.*

9. An Interplanetary Disturbance as Seem from the Lunar Surface, René A. Medrano, J. W. Freeman, and M. A. Fenner, *ibid.*
10. Suprathermal Ions Near the Moon, J. W. Freeman, Jr., M. A. Fenner, H. K. Hills, R. Lindeman, R. Medrano, and J. Meister, 15th I.U.G.G. General Assembly, Moscow, U.S.S.R., August, 1971.
11. Impact-generated ions observed simultaneously at widely separated sites on the lunar surface, J. C. Meister and H. K. Hills, Fall annual A.G.U. Meeting, San Francisco, 1971.
12. Observed effect of an expanding gas cloud on magnetosheath ions at the lunar surface, R. R. Vondrak, H. K. Hills, and J. A. Meister, *ibid.*
13. Evidence for Acceleration of Lunar Ions, R. H. Manka, F. C. Michel, J. W. Freeman, P. Dyal, C. W. Parkin, D. S. Colburn, and C. P. Sonett, 3rd Lunar Science Conference, Houston, January, 1972.
14. Gases on and in the Moon, H. K. Hills, American Chemical Society, Boston, April, 1972.
15. Suprathermal Ion Detector Results from Apollo Mission, J. W. Freeman, 15th Plenary Meeting, COSPAR, Madrid, Spain, May, 1972.
16. Observations of Lunar Module Exhaust Gases at the Lunar Surface, H. K. Hills, R. R. Vondrak, and J. W. Freeman, 53rd annual A.G.U. Meeting, Washington, D.C., April, 1972.



17. Energy Spectrum of Lunar Ions, R. H. Manka, F. C. Michel, J. W. Freeman, and H. K. Hills, *ibid.*
18. Magnetosheath Structure Observed by 3 ALSEP/SIDE Plasma Detectors, M. A. Fenner, J. W. Freeman, H. K. Hills, and R. Lindeman, *ibid.*
19. Fine Structure of a Solar Flare Associated Shock Wave, R. A. Medrano, J. W. Freeman, and R. R. Vondrak, *ibid.*
20. Suprathermal Ion Detector Results from Apollo Missions, H. K. Hills and J. W. Freeman, Jr., IAP Technical Session, 24th International Geological Congress, Montreal, August, 1972.
21. Penetrating Particles on the Night Side of the Moon Associated with the August, 1972, Solar Flares, R. A. Medrano, J. W. Freeman, and H. K. Hills, Fall annual A.G.U. Meeting, San Francisco, 1972.
22. Observations of an Anomalous Neutral Gas--Solar Wind Interaction at the Lunar Surface, R. A. Lindeman, R. R. Vondrak, and J. W. Freeman, *ibid.*
23. The Electric Potential of the Moon in the Solar Wind, J. W. Freeman, M. A. Fenner, and H. K. Hills, *ibid.*
24. Ions from the Lunar Ionosphere, R. A. Lindeman, J. W. Freeman, and R. R. Vondrak, Fourth Lunar Science Conference, Houston, March, 1973.
25. Acceleration of Lunar Exospheric Ions, J. W. Freeman, M. A. Fenner, H. K. Hills, R. A. Lindeman, and R. R. Vondrak, 54th Annual A.G.U. Meeting, Washington, D. C., April, 1973.

26. Electric Fields near the Moon, J. W. Freeman, 2nd General Scientific Assembly, IAGA, Kyoto, Japan, September, 1973.
27. The Solar Energetic Particle Square Wave During the August, 1972, Solar Storm, R. A. Medrano, C. J. Bland, and J. W. Freeman, *ibid.*
28. Loss of Gases from the Lunar Ionosphere, R. R. Vondrak, R. A. Lindeman, and J. W. Freeman, Fall annual A.G.U. Meeting, San Francisco, 1973.
29. Measurements of Lunar Atmospheric Loss Rate, R. R. Vondrak, J. W. Freeman, and R. A. Lindeman, 5th Lunar Science Conference, Houston, March, 1974.
30. Electric Field Acceleration of Lunar Exospheric Ions, J. W. Freeman and R. R. Vondrak, 55th Annual A.G.U. Meeting, Washington, D.C., April, 1974.
31. Observation of Bow Shock Protons at the Lunar Orbit, J. L. Benson, H. K. Hills, J. W. Freeman, and R. R. Vondrak, *ibid.*
32. Low Energy Protons in the Geomagnetic Tail, D. A. Hardy, H. K. Hills, and J. W. Freeman, *ibid.*
33. Dawn-Dusk Magnetosheath Plasma Asymmetries at  $60 R_E$ , M. A. Fenner and J. W. Freeman, *ibid.*
34. Energetic Lunar Nighttime Ion Events, H. E. Schneider and J. W. Freeman, Conference on Interactions of the Interplanetary Plasma with the Ancient and Modern Moon, Lake Geneva, October, 1974.

35. Bow Shock Protons in the Lunar Environment, J. Benson,  
H. K. Hills, J. W. Freeman, and R. R. Vondrak, *ibid.*
36. First Observation of Low Energy Protons in the Geomagnetic  
Tail at Lunar Distance, D. A. Hardy and J. W. Freeman,  
*ibid.*
37. Electric Fields, The Lunar Electric Potential and Plasma  
Sheath Effects, J. W. Freeman and M. Ibrahim, *ibid.*
38. The Lunar Ionosphere, R. R. Vondrak and J. W. Freeman, *ibid.*
39. Lunar Electric Models and Applications to Planets, R. H.  
Manka, *ibid.*
40. Low Energy Plasma in the Geomagnetic Tail at Lunar Distance:  
I General Features, D. A. Hardy, H. K. Hills, and  
J. W. Freeman, Fall Annual A.G.U. Meeting, San Fran-  
cisco, December, 1974.
41. Low Energy Plasma in the Geomagnetic Tail at Lunar Dis-  
tance: II Joint Observations, P. R. Moore, D. A.  
Hardy, and W. J. Burke, *ibid.*
42. The Lunar Surface Potential and Plasma Sheath Effects,  
J. W. Freeman, H. K. Hills, and M. Ibrahim, *ibid.*
43. Low Energy Mass Spectra of the Lunar Ionosphere, J. Benson  
and J. W. Freeman, *ibid.*
44. The Lunar Ionosphere, J. Benson, J. W. Freeman, H. K. Hills,  
M. Ibrahim, and H. Schneider, 6th Lunar Science Con-  
ference, Houston, March, 1975.
45. Low Energy Plasma in the Tail Lobes, D. A. Hardy, J. W.  
Freeman, and H. K. Hills, Conference on Quantitative  
Magnetospheric Models, LaJolla, California, May, 1975.

46. Lunar Ion Energy Spectra Produced by Interplanetary Electric Field Acceleration, J. Benson, J. W. Freeman, Spring Annual A.G.U. Meeting, Washington, D.C., June, 1975.
47. Plasma Sheet Protons at Lunar Distance, H. K. Hills and D. A. Hardy, *ibid.*
48. Detailed Analysis of Low Energy Plasma in the Geomagnetic Tail at Lunar Distance, D. A. Hardy, H. K. Hills, and J. W. Freeman, *ibid.*
49. Low Energy Proton Regime in the Geomagnetic Tail at Lunar Distance, H. K. Hills, D. A. Hardy, and J. W. Freeman, Tenth ESLAB Symposium (IMS), Vienna, Austria, June, 1975.



## 9. SUPRATHERMAL ION DETECTOR EXPERIMENT

The suprathermal ion detector experiment (SIDE) was designed to achieve the following objectives: (1) provide information on the energy and mass spectra of the positive ions close to the lunar surface (the lunar exosphere), (2) measure the flux and energy spectra of positive ions in the magnetotail and magnetosheath during the periods when the Moon passes through the magnetic tail of the Earth, (3) provide data on the plasma interaction between the solar wind and the Moon, and (4) determine a preliminary value for the electric potential of the lunar surface.

### DESCRIPTION

Three SIDE instruments were deployed (at the Apollo 12, 14, and 15 sites). The SIDE consists of two positive-ion detectors, the mass analyzer (MA) and the total ion detector (TID). Both use curved plate analyzers for energy per unit charge discrimination. The MA also uses a Wien velocity filter (crossed electric and magnetic fields), because knowledge of the energy per unit charge and the velocity is sufficient to allow determination of the mass per unit charge. The MA measures a 20-channel mass spectrum at each of six energy levels: 48.6, 16.2, 5.4, 1.8, 0.6, and 0.2 eV. The mass ranges covered are approximately 10 to 1000 atomic mass units per charge (amu/Q) for the Apollo 12 unit, 6 to 750 amu/Q for Apollo 14, and 1 to 90 amu/Q for Apollo 15. While each mass spectrum is being observed by the MA, the TID measures a 20-channel differential energy spectrum (including all masses) from 3500 eV/Q down to 10 eV/Q. Each 20-channel spectrum is obtained in 24 sec.

Each detector has a field of view that is roughly a square solid angle,  $6^\circ$  on a side. Numerous commands are possible, some of which allow certain measurements to be omitted to devote more time to other measurements. To establish electrical reference to the lunar surface, a wire screen (the lunar-surface ground plane in figure 9-1) is deployed on the surface beneath the SIDE. This screen is connected to the SIDE ground through a power supply that can cycle through 24 steps from -27.6 to +27.6 V. The effects of stepping this voltage through its cycle can be used in certain circumstances to determine the lunar-surface potential. A schematic diagram of the SIDE instrument is

shown in figure 9-1, a cutaway view of the SIDE in figure 9-2, and the SIDE as deployed at the Apollo 12 and 14 sites in figure 9-3.

The look direction of each instrument was angled  $15^\circ$  east (Apollo 14 and 15) or west (Apollo 12) from the local meridian plane. The Apollo 15 instrument (at latitude  $26^\circ$  N) was deployed tilted  $26^\circ$  from vertical toward the south, so that the sensor look directions of all three instruments included the ecliptic plane (fig. 9-4).

#### OPERATIONAL HISTORY

This section summarizes the time periods when the instruments were in full operation and returning science data. Periods when only housekeeping data were returned are not included. The design goal was full operation continuously after an initial period to allow for outgassing during the lunar daytime. Summaries of SIDE operation for Apollo 12, 14, and 15 are as follows.

##### Apollo 12 SIDE

<u>Period</u>	<u>Description</u>
November 19 and 20, 1969	Deployment and operation during mission activities.
December 1969 to January 1970	Operation during lunar night (and a short time before and after).
February 1970 to August 1972	Operation during lunar night, plus cyclic operation for approximately 10 days centered on local noon. Cyclic operation involves 2 hr on and 10 hr, or more, off. More coverage was obtained during continuous real-time support of Apollo lunar surface experiments package (ALSEP) missions (i.e., the first 45 days of the mission).

September 1972 to August 1973

Operation as for preceding period but with intermittent loss of data during lunar night (for periods of minutes to periods of many days) during the months of September, November, and December 1972, and during January, June, and August 1973.

Apollo 14 SIDE

<u>Period</u>	<u>Description</u>
February 5 to 7, 1971	Deployment and operation during mission activities.
February 1971 to July 1971	Operation during the night and part of the day but off for approximately 8 days centered on noon.
August 1971 to October 1971	Operation as for preceding period, plus short cycles of operation periodically for approximately 8 days near noon.
November 1971 to March 1973	Continuous operation.
April 1973 to August 1973	Operation during the night from approximately 1 day before sunset until sunrise.

Apollo 15 SIDE

<u>Period</u>	<u>Description</u>
July 31, 1971 to August 3, 1973	Deployment and operation during mission activities.
August 1971 to September 1971	Operation except during approximately 10 days centered on local noon.



October 1971 to November 1971

Operation as for preceding period, plus short intervals of operation intermittently for approximately 4 to 7 days near noon.

December 1971 to April 1972

Operation except during 3 to 5 days centered on local noon.

May 1972 to August 1973

Continuous operation.

#### DATA SETS AND AVAILABILITY THROUGH NSSDC

The following list gives the SIDE data sets, their form, and their availability through the National Space Science Data Center (NSSDC).

<u>Data_set</u>	<u>Form</u>	<u>Availability</u>
1. Machine plots (MA and TID on same plot) of counting rates as a function of frame number	16-mm micro-film	Data for times after about August 1972 are (or soon will be) available at NSSDC. Data for times from about June 1971 to August 1972 will be available at NSSDC after production of copies.
2. Listings of counting rates as a function of frame number, with limited amount of house-keeping data	16-mm micro-film	Same as preceding set.
3. Machine plots (three-dimensional) of TID average energy spectra as a function of time	76 by 91 cm (30 by 36 in.) paper	All data will eventually be available at NSSDC.

- |    |  |  |  |
|----|--|--|--|
| 4. | Machine plots<br>(three-dimensional)<br>of MA average<br>mass spectra<br>as a function<br>of time  | 76 by 91 cm<br>(30 by 36 in.)<br>paper | Same as preceding<br>set.  |
| 5. | TID spectra as a<br>function of<br>time  | Digital, on<br>magnetic tape           | Same as preceding<br>set.  |
| 6. | MA spectra as a<br>function of<br>time   | Digital, on<br>magnetic tape           | Same as preceding<br>set.  |
| 7. | Engineering<br>parameters  | Digital, on<br>magnetic tape           | Data for times<br>after about June<br>1971 will be<br>available at<br>NSSDC. |
| 8. | TID and MA data,<br>including every-<br>thing telem-<br>etered from<br>SIDE, plus eval-<br>uations of data<br>quality and in-<br>strument mode<br>of operation.<br>Called "NPAK"<br>by Rice Uni-<br>versity. | Digital, on<br>magnetic tape           | Data available only<br>at Rice University.                                   |

#### DESCRIPTION OF NSSDC DATA TAPES

Data tapes are standard 731.5-m (2400 ft), 1.27-cm (0.5 in.), 7-track IBM-compatible tapes, recorded at 800 bpi with odd parity. Words are 24-bit binary integers with negative numbers represented as 2's complement; with 28 such words per logical record (for both MA and TID). Physical records are fixed-length, blocked, with 100 logical records per physical record, and with no record-length description or control words. There is only one file per reel, *containing 1850 physical records.*

~~Each tape is labeled with the name of the data set and the date of recording. A standard tapemark is written after the last record. The last reel of a calendar year's data is the one that will have less than a full reel and the only one that will~~

have less than 100 logical records in its last physical record. The TID and MA data are written on separate tapes but have almost identical formats; the first word in the logical record allows them to be distinguished from each other. The 28 words in a logical record contain time, 20 channels (mass for MA, energy for TID) of accumulated counts, and housekeeping parameters (including energy for the MA data). Where reliable data are not available, the value -1 is inserted.

#### SUMMARY OF PRINCIPAL RESULTS

1. Lunar ions accelerated by the solar-wind-induced field ( $E = -\vec{V} \times \vec{B}$ ) were observed (where  $\vec{E}$  is the electric field and  $-\vec{V} \times \vec{B}$  is the negative cross product of velocity and magnetic field).

2. During lunar night, 1 to 3 keV protons (considered to be protons from the bow shock of the Earth) were observed.

3. Ion mass spectra due to the LM exhaust gas were observed, and the intensity decay rate was determined.

4. Multisite observation was made of the energetic ion characteristics in the Earth magnetosheath and at its boundaries, and correlation with geomagnetic activity was made.

5. The effects of the lunar module (LM) ascent engine exhaust on magnetosheath ion fluxes were observed.

6. Multisite observations of apparent motions of ion "clouds" related to lunar impact events and observations of mass spectra during the events were made.

7. Ion fluxes were monitored during local solar eclipses; no changes were observed.

8. Energetic ions were observed during lunar night when the site was shielded from the solar-wind direction.

9. Observation of ion events near terminators suggests a turbulent region of solar-wind plasma interaction with the solid Moon.

10. Positive ion fluxes were monitored while in the geomagnetic tail and correlated with geomagnetic storm activity.

11. Mass spectra of ions were observed from the ambient atmosphere, including a single observation of water vapor ions, possibly of natural origin.

12. The electric potential of the lunar surface was determined (a) in the magnetosheath or solar wind and (b) near the terminators.

13. Solar wind was observed during interplanetary storms.

14. Penetrating ions from solar flares were observed.

# BIBLIOGRAPHY

Fenner, M. A.: Magnetosheath Plasma at 60 R<sub>E</sub>. M. S. Thesis, Rice Univ., 1971.

Fenner, M. A.; Freeman, J. W., Jr.; and Hills, H. K.: The Electric Potential of the Lunar Surface. Proceedings of the Fourth Lunar Science Conference, vol. 3, Pergamon Press (New York), 1973, pp. 2877-2889.

Freeman, J. W., Jr.: Energetic Ion Bursts on the Night Side of the Moon. J. Geophys. Res., vol. 77, no. 1, Jan. 1, 1972, pp. 239-243.

Freeman, J. W., Jr.: Suprathermal Ion Detector Results from Apollo Missions. Space Res. <sup>XIII</sup> ~~XIV~~, Proceedings of the 16th Plenary Meeting of CCSPAR (Committee on Space Research), *Madrid* May 23 to June 5, 1973. *1972*

Freeman, J. W., Jr.; Balsiger, H.; and Hills, H. K.: Suprathermal Ion Detector Experiment (Lunar Ionosphere Detector). Sec. 6 of Apollo 12 Preliminary Science Report, NASA SP-235, 1970.

Freeman, J. W., Jr.; Fenner, M. A.; and Hills, H. K.: The Electric Potential of the Moon in the Solar Wind. J. Geophys. Res., vol. 78, no. 22, Aug. 1, 1973, pp. 4560-4567. *Madison*

Freeman, J. W., Jr.; Fenner, M. A.; Hills, H. K.; Lindeman, R. A.; *et al.*: Suprathermal Ions Near the Moon. Icarus, vol. 16, no. 2, April 1972, pp. 328-338.

Freeman, J. W., Jr.; Hills, H. K.; and Fenner, M. A.: Some Results from the Apollo 12 Suprathermal Ion Detector. Proceedings of the Second Lunar Science Conference, vol. 3. A. A. Levinson, ed., MIT Press (Cambridge, Mass.), 1971, pp. 2093-2102.

Freeman, J. W., Jr.; Hills, H. K.; Lindeman, R. A.; and Vondrak, R. R.: Observations of Water Vapor Ions at the Lunar Surface. The Moon, vol. 8, nos. 1/2, 1973, pp. 115-128.

Freeman, J. W., Jr.; Hills, H. K.; and Vondrak, R. R.: Water Vapor, Whence Comest Thou? Proceedings of the Third Lunar Science Conference, vol. 3, David R. Criswell, ed., MIT Press (Cambridge, Mass.), 1972, pp. 2217-2230.

- Garrett, H. B.; Hill, T. W.; and Fenner, M. A.: Plasma-Sheet Ions at Lunar Distance Preceding Substorm Onset. Planet. Space Sci., vol. 19, 1971, pp. 1413-1418.
- Hills, H. K.; and Freeman, J. W., Jr.: Suprathermal Ion Detector Experiment (Lunar Ionosphere Detector). Sec. 8 of Apollo 14 Preliminary Science Report, NASA SP-272, 1971.
- Hills, H. Kent; Meister, Jurg C.; Vondrak, Richard R.; and Freeman, John W., Jr.: Suprathermal Ion Detector Experiment (Lunar Ionosphere Detector). Sec. 12 of Apollo 15 Preliminary Science Report, NASA SP-289, 1972.
- Lindeman, R. A.: Observations of Ions from the Lunar Atmosphere. Ph. D. Dissertation, Rice Univ., 1973. X
- Lindeman, Robert A.: Recurring Ion Clouds at the Lunar Surface. M. S. Thesis, Rice Univ., 1971.
- Lindeman, R.; Freeman, J. W., Jr.; and Vondrak, R. R.: Ions from the Lunar Atmosphere. Proceedings of the Fourth Lunar Science Conference, vol. 3, Pergamon Press (New York), 1973, pp. 2889-2896. X
- Manka, Robert Hall: Lunar Atmosphere and Ionosphere. Ph. D. Dissertation, Rice Univ., 1972.
- Manka, R. H.; and Michel, F. C.: Lunar Atmosphere as a Source of Ar-40 and Other Lunar Surface Elements. Science, vol. 169, no. 3942, July 17, 1970, pp. 278-280. X
- Manka, R. H.; and Michel, F. C.: Lunar Ion Energy Spectra and Surface Potential. Proceedings of the Fourth Lunar Science Conference, vol. 3, Pergamon Press (New York), 1973, pp. 2897-2908.
- Paris Colman, Sweet*  
Manka, R. H.; Michel, F. C.; Freeman, J. W., Jr.; Dyal, P.; et al.: Evidence for Acceleration of Lunar Ions. Lunar Science-III (Rev. abs. of the Third Lunar Science Conference (Houston, Tex.), Jan. 10-13), pp. 504-506.
- Medrano, Rene A.; Freeman, John W., Jr.; Hills, H. Kent; Vondrak, Richard R.: Penetrating Solar Flare Particle and Solar Wind Observations in the Lunar Night, August 1972. Collected Data Reports on August 1972 Solar-Terrestrial Events, Rept. UAG-28, pt. II, H. E. Coffey, ed., World Data Center A for Solar-Terrestrial Physics, Boulder, Colo., 1973.
- Medrano-Balboa, R. A.: Unusual Solar Wind and Solar Proton Events Observed on the Lunar Surface. Ph. D. Dissertation, Rice Univ., 1973.

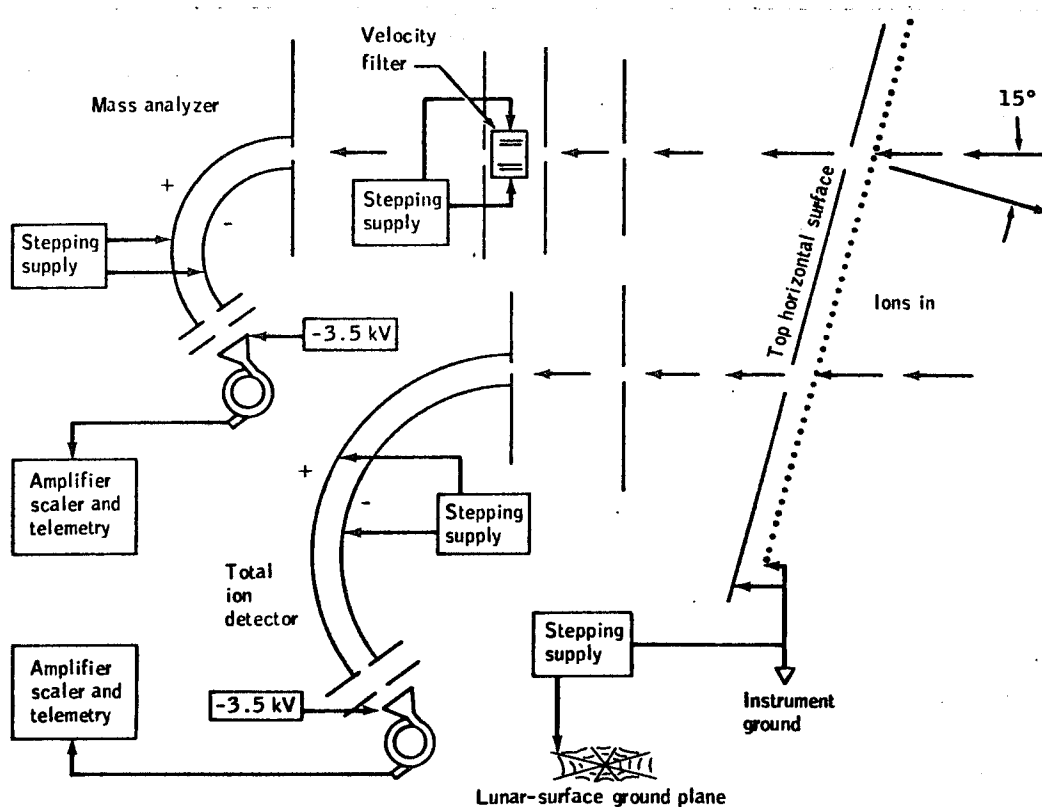


Figure 9-1.- Schematic diagram of SIDE.

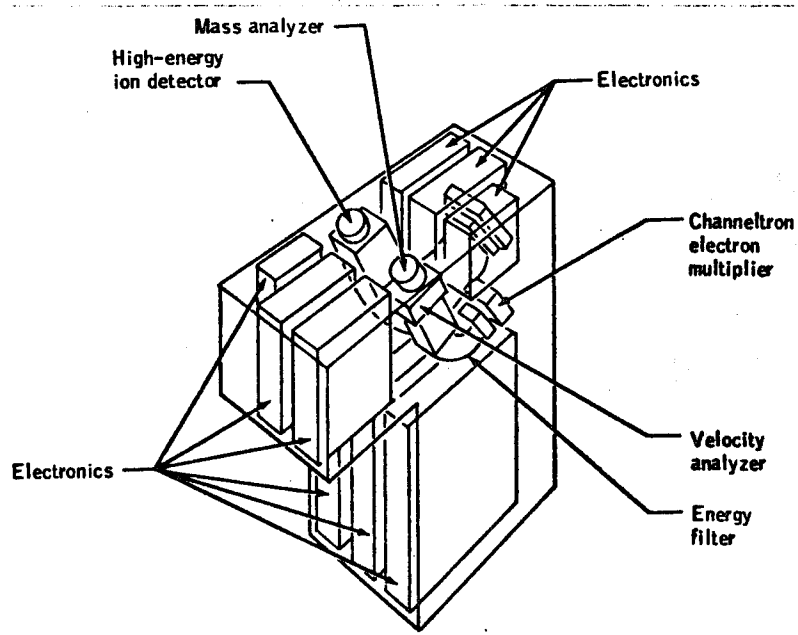


Figure 9-2.- Cutaway view of SIDE.

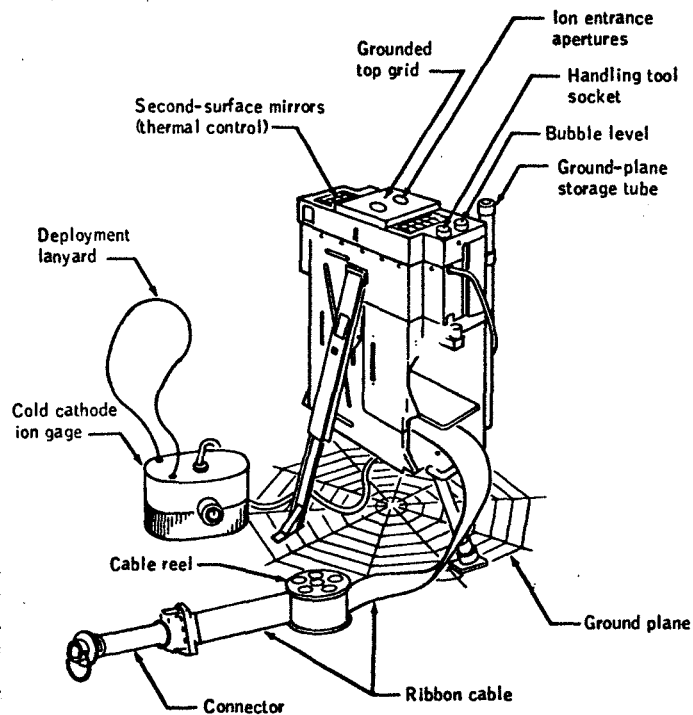


Figure 9-3.- The SIDE configuration as deployed at the Apollo 12 and 14 sites.

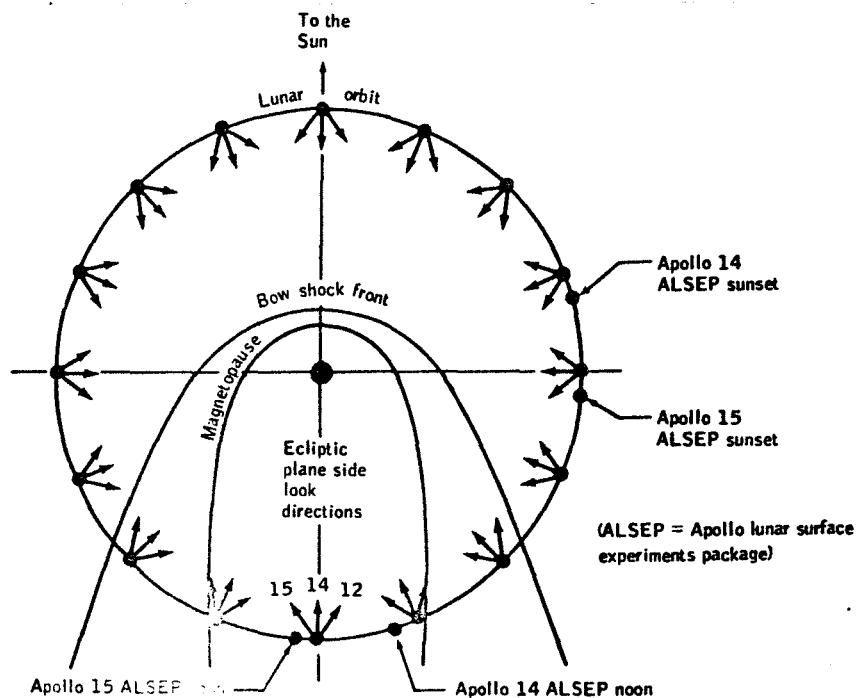


Figure 9-4.- Sensor look directions of SIDE instruments deployed at the Apollo 12, 14, and 15 sites.





Apollo XII  
Suprathermal Ion Detector Experiment

One Year Report  
October, 1970

Prepared by Rice University under NASA Contract NAS9-5911



## SUPRATHERMAL ION DETECTOR EXPERIMENT

(Lunar Ionosphere Detector)

This report reviews the lunar surface operation of the Suprathermal Ion Detector Experiment (SIDE) and gives the status of the experiment as of September 1, 1970, including observations of scientific and engineering interest which have been made since the 45-day preliminary report (reference 1). The SIDE is designed to achieve the following experimental objectives:

- (1) Provide information on the energy and mass spectra of positive ions close to the lunar surface, whether these ions are of natural origin such as the moon or the solar wind, or are due to the Apollo vehicle and life-support systems.
- (2) Measure the flux and energy spectrum of positive ions in the Earth's magnetotail and magnetosheath during those periods when the moon passes through the magnetic tail of the Earth.
- (3) Provide data on the interaction between the solar wind plasma and the Moon.
- (4) Determine a preliminary value for the electric potential of the lunar surface.

The SIDE consists of two positive ion detectors, called the total ion detector and the mass analyzer. The total ion detector registers ions in twenty energy ranges from 10eV through 3500eV, and the mass analyzer covers the mass-per-unit-charge range 10 through 1000amu/q (this mass range varies from unit to unit) with 20 channels at each of 6 energy

levels from 0.2 to 48.6 eV. The sensor fields of view are roughly square solid angles  $6^\circ$  on a side, and include the ecliptic plane. The look axes are canted  $15^\circ$  from the local vertical and to the west, with the look directions at various points along the lunar orbit as shown in Figure 1. The sensitivities of the total ion detector and of the mass analyzer are approximately  $5 \times 10^{17}$  and  $10^{17}$  counts/sec/amp of entering positive ion flux, respectively. The entrance aperture areas are approximately  $24\text{mm}^2$  and  $16\text{mm}^2$ , respectively. A more detailed description of the instrument is given in the preliminary report (reference 1).

#### Performance

The performance of the SIDE continues to be excellent. All temperatures and voltages have been nominal and no new anomalies in operation have appeared since the preliminary report. The calibration signal for the total ion detector has been intermittent for a short time on several occasions. This is used as a diagnostic check on the digital logic and is not essential as long as the digital logic functions properly.

The detector high voltage ( $-3.5$  kV) power supply had to be commanded off for a period of about 11 days centered on lunar noon during the first three lunar cycles after deployment. This was done because of the spontaneous execution of mode change commands by the SIDE when its temperature exceeded some threshold value. Since these spurious commands were assumed to be caused by high voltage corona or arcing in the SIDE, probably due to outgassing as the temperatures increased, the high voltage was commanded

off after such a mode change in order to prevent further arcing and possible damage to components. The threshold temperature above which spontaneous mode changes occurred increased significantly (from  $36^{\circ}$  to  $51^{\circ}\text{C}$ ) on the 2nd lunar day, apparently as outgassing proceeded. However, improvement has been slow since then and the current critical temperature range is about  $50\text{--}55^{\circ}\text{C}$ . An operational method has been devised to circumvent this problem, and has resulted in acquisition of very interesting data in the earth's tail and magnetosheath regions. When the SIDE temperature reaches  $50\text{--}55^{\circ}\text{C}$ , or after a spontaneous mode change occurs, the instrument power is cycled off and on, which produces a temperature history such as that shown in Figure 2, keeping the package below about  $55^{\circ}\text{C}$  and hence obtaining data without undue risk of high voltage arcing damage to components. In the lunar afternoon the instrument is turned on and left on until it is necessary to cycle it off and on again in the next lunar day. The duty cycle can be increased above what is shown in Figure 2, but a high duty factor has been utilized only in periods of highly interesting data. The remainder of the time the normal 2hr/day real-time support periods have been utilized to obtain data for monitoring purposes.

The thermal design of SIDE kept the internal temperatures within the desired nominal operating range of  $-20^{\circ}\text{C}$  to  $+80^{\circ}\text{C}$ . The peak operating temperatures reached  $79^{\circ}\text{C}$  during each of the three lunar days when the power was left on continuously. During the night-time the internal temperatures are maintained at constant values ( $-9^{\circ}\text{C}$  to  $+22^{\circ}\text{C}$ , depending on proximity to the heaters) by means

of 4 watts of heater power dissipation in addition to the 6 watts dissipated in the electronics. A study of the temperature vs sun-angle data from deployment until the present shows that there has been no degradation of the thermal control during this time (about 9 months).

The Cold Cathode Gauge Experiment (CCGE) electronics are carried in the SIDE package, and the CCGE high voltage (4.5 kv) power supply failed at about 14 hours after deployment. Extensive testing and failure analysis of similar units subsequently indicated that a transistor in this power supply was susceptible to failure in this application due to transient noise. A different transistor, better suited for this application, has been installed in the Apollo XIV and XV flight units to improve the reliability of the instrument. Additional care has also been taken to minimize the likelihood of high voltage corona within the instrument.

### General Results

#### Low-Energy Events

As reported in references 1 and 2, several low-energy (10 to 250 eV) events were detected by the total ion detector shortly after initial turn-on of the SIDE. These ions appeared as intermittent clouds, several of which were accompanied at the outset by higher energy ions (500 to 750 eV). One arrival of such a cloud was coincident with a magnetometer variation that indicated the passage of a current sheet nearby. At the same time these low-energy events were seen by the total ion detector, the mass analyzer detected ions in the 48.6 eV range, with the peak of the mass spectrum in the mass-per-unit-charge range of

18 to 50 amu/q. It should be noted that the light gases H, H<sub>2</sub>, and He cannot be detected by the Apollo XII mass analyzer; they can be detected only by the total ion detector.

Other low-energy ion events have often been seen by the total ion detector only. Since the sensitivity of the mass analyzer is lower than that of the total ion detector, this could be because there were few of the heavier ions present, but it could also be because of the small fraction of the time that the energy channel of the mass analyzer coincides with a similar energy channel of the total ion detector. A study is currently in progress to investigate possible long-term low-level mass spectra in the mass analyzer data. Sometimes the ions in these low-energy events have rather broad spectra covering two or three energy channels, although frequently the spectrum is quite monoenergetic, with all energies falling within a single energy channel.

The frequent appearance of these suprathermal ions suggests the operation of a general acceleration mechanism. One interesting possibility to speculate on is the  $\vec{E} \times \vec{B}$  drift acceleration by the solar wind. This mechanism has been proposed as the source of large quantities of Ar<sup>40</sup> found in the lunar surface samples (reference 3). We may therefore have direct evidence for such a process.

#### Higher Energy Phenomena

Reference 1 also reported the detection of high energy (1 to 3 keV) ions sporadically in the portion of the lunar orbit near, and up to 4 days after, sunset at the ALSEP



site. In the earlier part of this time period there are lower energy ions, also. These ions have been tentatively identified as protons escaping from the Earth's bow shock front and moving generally along the interplanetary magnetic field lines at the "garden hose" angle. Such observations have been reported at the much closer Earth orbit of the Vela satellites (reference 4).

Low-energy protons escaping from the bow shock cannot drift upstream as close to the interplanetary field direction as higher energy protons can. Thus there should be a change to a more energetic spectrum at later times, as is observed. However, the actual energies and directions of such escaped protons are expected to be modified in an unknown manner by magnetic and electric fields in the vicinity of the moon, of both local and long-range scale. Note that the ALSEP magnetometer measures a steady 36 $\gamma$  magnetic field which is probably of local origin (reference 5).

Ions of solar wind energy observed several days before local sunrise, as if due to a deflection of the solar wind, were previously reported (reference 1). These have been observed each lunar cycle. Intermittent day-time events are also seen each cycle.

#### Earth's Wake in the Solar Wind

Beginning in February, 1970, observations were made during many short segments of time throughout the region of the Earth's magnetospheric tail and the magnetosheath region between the bow shock front and the tail. Very intense ion fluxes are observed in the magnetosheath as

the moon leaves the magnetospheric tail, while only very low and sporadic ion fluxes are seen in the magnetosheath where the moon enters the tail. The detector is looking roughly "upstream" parallel to the bow shock front in the former case, whereas in the latter the detector looks almost perpendicular to the shock front. In both cases when the moon is outside the shock front the detector look direction is such that the solar wind in interplanetary space is undetectable. The intense fluxes of ions are observed behind the bow shock, so they do not constitute the undisturbed solar wind, but rather the solar wind after passing through the bow shock. There is also an indication that effects of the solar wind interaction with the moon are being observed as well. A preliminary description of this data has been presented in reference 6. A general factor of the magnetosheath data is the observation of three characteristic types of spectra, which appear at different times. Typical spectra of each of these types are exhibited in figure 3, each panel of which displays total ion detector counts per frame for three scans through the energy spectrum. The intensity and constancy of the fluxes, and the presence of higher energy ions, as listed in the figure, are used to characterize the different types of spectra shown. As a simplified description, the type I spectra are typically observed near the magnetopause, shortly after entering the magnetosheath. The more intense type II spectra appear later, and type III spectra are typically observed near the bow shock, as the moon is leaving the magnetosheath.

The magnetosheath is a very complex region, and it is expected that further SIDE data from this region will yield extremely useful information on the interaction and acceleration mechanisms operating there, both in magnetically disturbed times and in relatively quiet times.

#### Impact Events

The impacts of the Apollo XII lunar module (LM) ascent stage and of the Apollo XIII S-IVB rocket, which were crashed into the lunar surface as known sources of seismic signals, both created ion clouds which were detected by the SIDE for periods of a few minutes. The ions observed from the LM impact had energies of about 250 eV to 500 eV, mainly, which is far above the range detectable by the mass analyzer. However, the ions from the S-IVB impact had energies of about 50 to 70 eV, and consequently were visible to the mass analyzer. At least 10% and perhaps most of these ions had masses between 10 and 80 amu/q. We have learned that an impact such as that of the S-IVB produces a gas cloud of sufficient density to deflect the solar wind in the vicinity of the impact and accelerate the gas cloud ions to suprathermal energies. Figure 4 shows the time history of the maximum intensity per channel from the spectra recorded at S-IVB impact. The energy corresponding to each channel is noted. The decrease and later increase in energy of the most abundant ions is of particular interest. A more detailed discussion of the complex effects on the ions of the cloud and of the solar wind is in preparation (references 7 and 8).

There have been several large natural impact events detected by the Apollo XII Passive Seismic Experiment (G. Lathan, private communication, 1970), and there remains the possibility that a large enough natural impact may occur close enough to produce a detectable flux of ions at the ALSEP site. In the first several months of operation there have been no clear ion events of this type.

### Eclipses

Partial lunar eclipses have occurred twice (February 21 and August 16, 1970) since the deployment of ALSEP, and both constituted partial solar eclipses as seen from the ALSEP site. The February eclipse was very slight at ALSEP and produced no effects discernible in the SIDE ion flux data. There was a cooling effect on the instrument package, as expected, with the temperature sensor in the CCGE package (in contact with the lunar surface) indicating a temperature drop from 364°K down to 294°K. Very interesting activity in the form of highly variable ion fluxes was observed in the SIDE data during the August eclipse. However, this may have been due to a time coincident intense solar flare event which resulted in a large magnetic storm at Earth. Data from additional magnetic storms and eclipses will be necessary to resolve this ambiguity.

In view of the large and rapid temperature decrease observed during an eclipse, a total eclipse is more interesting than a partial one for observations of possible gas liberation. Thus the total lunar eclipse of February 10, 1971 will be of special interest. It should be noted that Apollo XIV is scheduled for launch January 31, 1971,

and that the Apollo XII SIDE is still operating properly so there is a chance that both the Apollo XII and the Apollo XIV SIDE instruments will be able to observe this total eclipse. There is also a second total lunar eclipse in 1971 on August 6.

#### Present and Future Data Analysis Activities

The following list represents the distribution of effort of various project scientific personnel and their present areas of concentration:

1. Dr. J. W. Freeman is analyzing the Apollo XIII S-IVB impact event. This analysis is nearly complete and a paper is in preparation that will be presented at the December (1970) Western National Meeting of the American Geophysical Union. A paper on this subject will be submitted jointly with Drs. Conway Snyder and H. Kent Hills (for publication) (reference 7).
2. Dr. Kent Hills is interested in the night side high-energy phenomena. A paper on this subject was presented by him at the April (1970) National Meeting of the American Geophysical Union (reference 9). A paper for publication will be in preparation shortly.
3. Dr. Jürg Meister is investigating possible SIDE data correlations with optical lunar transient events reported by the LION network. Dr. Meister is an ESRO/NASA International Post-Doctoral Fellow who only recently arrived at Rice to work with the SIDE group.
4. Miss Martha Fenner (a Rice Space Science graduate student) has been pursuing the data from the outbound magnetosheath passes. She presented a paper on the SIDE data from this region at the April (1970) National Meeting of the American Geophysical Union (reference 6).

5. Mr. Robert Lindeman (a Rice Space Science graduate student) is preparing a computer program to analyze low-level night side events by computing long-term averages.
6. Mr. René Medrano (a Rice Space Science graduate student) is performing a power spectrum analysis to determine the origin of the mass analyzer counting rates seen during the lunar day.
7. Mr. Tom Rich (a Rice undergraduate) is performing a hand analysis of pre-dawn solar wind energy ion-cloud events to determine their distribution along the lunar orbit.

The following list represents a partial enumeration of areas awaiting detailed investigations:

1. The ground plane voltage influence on SIDE counting rates. (This will provide information on the lunar surface electric field.)
2. Long-term averages of the mass analyzer fluxes during the lunar day.
3. Quiet-time and seasonal plasma fluxes in the magnetotail.
4. Analysis of lunar eclipse data.
5. Investigation of the variation in the fluxes seen during large geomagnetic storms.
6. More complete examination of the concept of a general acceleration mechanism for thermal ions in the lunar ionosphere (reference 8).
7. Correlation of SIDE data with PSE data (detected natural impact events) and with LSM data.

It should be noted that most of these specific areas of research will be greatly aided by data from the SIDE's on additional ALSEP missions. This is true because of

the different locations and SIDE detector look directions planned for future ALSEP's, hopefully with time concurrent data.

### Conclusion

A brief summary of the salient features of this report follows.

- (1) The SIDE continues to operate normally, with no indication of degradation of performance or of thermal control capabilities.
- (2) Mass spectra of 50 eV ions were obtained soon after deployment. These show concentrations of ions in the 18 to 50 amu/q mass-per-charge range.
- (3) Clouds of 10 to 250 eV ions have been detected, as well as other events, which suggests the operation of a general acceleration mechanism.
- (4) Solar wind energy ions are observed several days before local sunrise.
- (5) Ions of 250 to 3000 eV presumed to be protons which escaped from the bow shock, are observed in the time period between sunset and midnight.
- (6) Data on the complex features of the interaction of the solar wind with the earth's magnetic field and with the moon are being accumulated.
- (7) The Apollo XIII S-IVB impact resulted in a cloud of 50 to 70 eV ions being detected at the SIDE, with a large number of ions of mass about 10 to 80 amu/q. No mass data is available from the Apollo XII LM impact, which resulted in ions of 250 to 500 eV at the SIDE.

(8) Two partial lunar eclipses have been monitored, but no ion events have been clearly attributed to an eclipse. High fluxes during the second eclipse may be associated with a large solar flare rather than with the eclipse.



## References

1. Freeman, J.W., Jr., H. Balsiger, and H.K. Hills:  
Suprathermal Ion Detector Experiment. Sec.6  
of Apollo XII Preliminary Science Report,  
NASA SP-235 (1970).
2. Balsiger, H., J.W. Freeman, Jr., and H.K. Hills:  
Preliminary Results from Apollo XII ALSEP  
Lunar Ionosphere Detector: I. General Results.  
Transactions, Amer. Geophys. Union, 51, 7,  
p.589 (1970) (Revised abstract).
3. Heymann, D., A. Yaniv, J.A.S. Adams, and G.E. Fryer:  
Inert Gases in Lunar Samples. Science 167,  
pp.555-558 (1970).
4. Asbridge, J.R., S.J. Bame, and I.B. Strong: Outward  
Flow of Protons from the Earth's Bow Shock.  
J. Geophys. Res., 73, pp.5777-5782 (1968).
5. Dyal, P., C.W. Parkin, and C.P. Sonett: Apollo  
XII Magnetometer: Measurement of a Steady  
Magnetic Field on the Surface of the Moon.  
Science, 169, pp.762-764 (1970).
6. Freeman, J.W., Jr., M.A. Fenner, H.K. Hills, and  
H. Balsiger: Preliminary Results from Apollo  
XII ALSEP Lunar Ionosphere Detector: II.  
Detection of Ions of Solar Wind Energies.  
Transactions, Amer. Geophys. Union, 51, 7,  
p.590 (1970) (Revised abstract).
7. Freeman, J.W., Jr. and H.K. Hills: Positive Ions  
Resulting from the Apollo XIII S-IVB Lunar  
Impact. In preparation.
8. Balsiger, H., J.W. Freeman, Jr., and H.K. Hills:  
Acceleration of Thermal Ions at the Lunar  
Surface: Apollo XII Observations. Rice  
University Report, June, 1970.

9. Hills, H.K., J.W. Freeman, Jr., and H. Balsiger:  
Energetic Protons Observed at the Lunar  
Surface on the Night Side of the Moon.  
Transactions, Amer. Geophys. Union, 51, 4,  
p.407 (1970) (Abstract).

Figure Captions

- Figure 1. The look directions of the SIDE at various points along the lunar orbit. The Earth is not drawn to scale.
- Figure 2. Temperature history during the cyclic operation of the SIDE. The dashed curve was taken from earlier times when the power was left on, and only the internal high voltage supplies were turned off.
- Figure 3. Three typical spectra observed in the magnetosheath region with the total ion detector. Each frame is 1.2 seconds long, and the counts are accumulated in that time interval. Each panel shows three scans of the spectrum, starting with the 3500 eV channel, then repeating. Some characteristics of each type of spectra are tabulated below the spectra.
- Figure 4. Maximum counts per channel of the total ion detector during the S-IVB impact event. Each bar represents the maximum count in a 20-frame spectrum scan, and is labeled with its appropriate energy. Note that the spectrum peak was at 50 and 70 eV initially, and shifted down to 10 eV, then increased to several hundred eV.

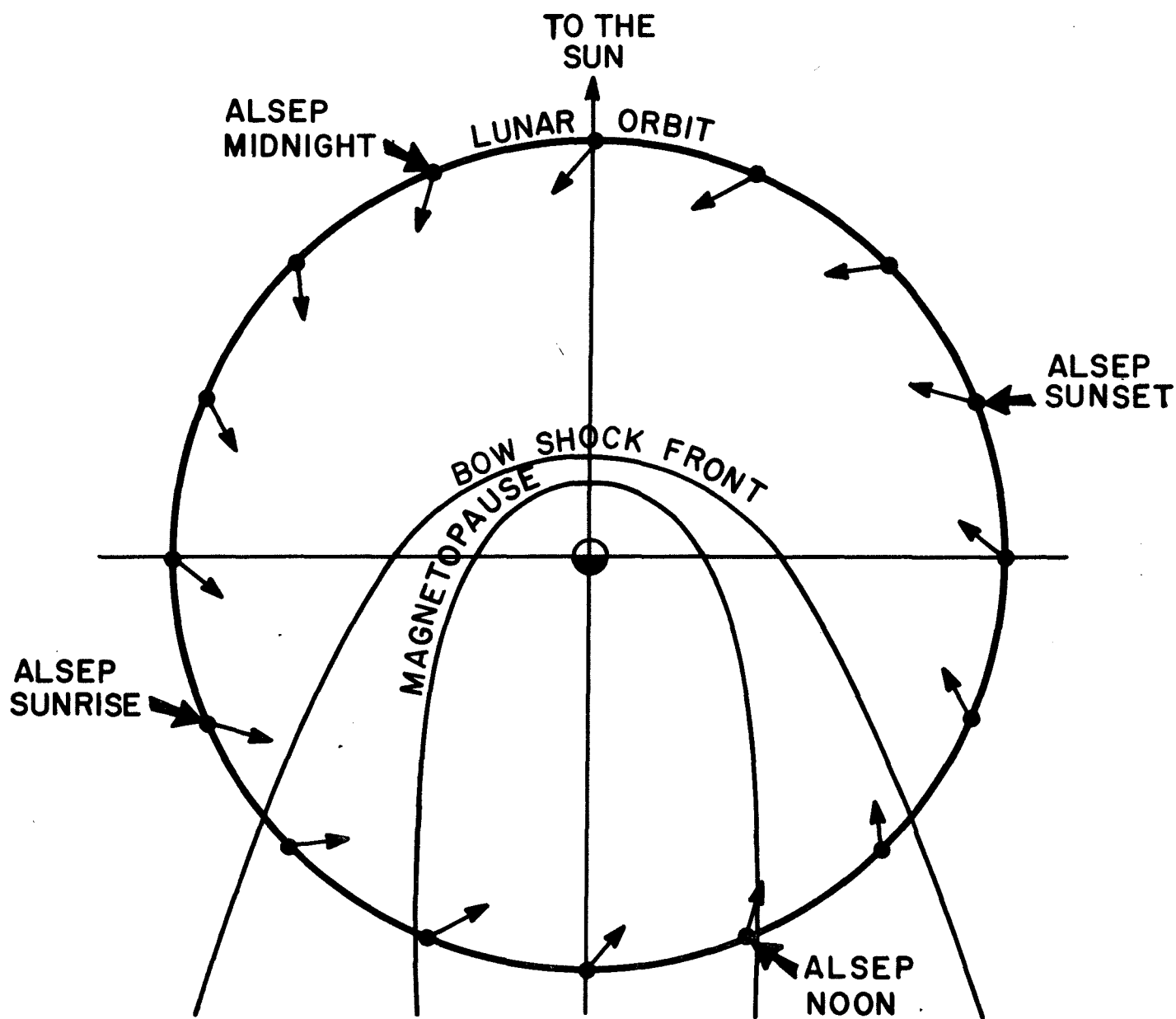


FIGURE 1

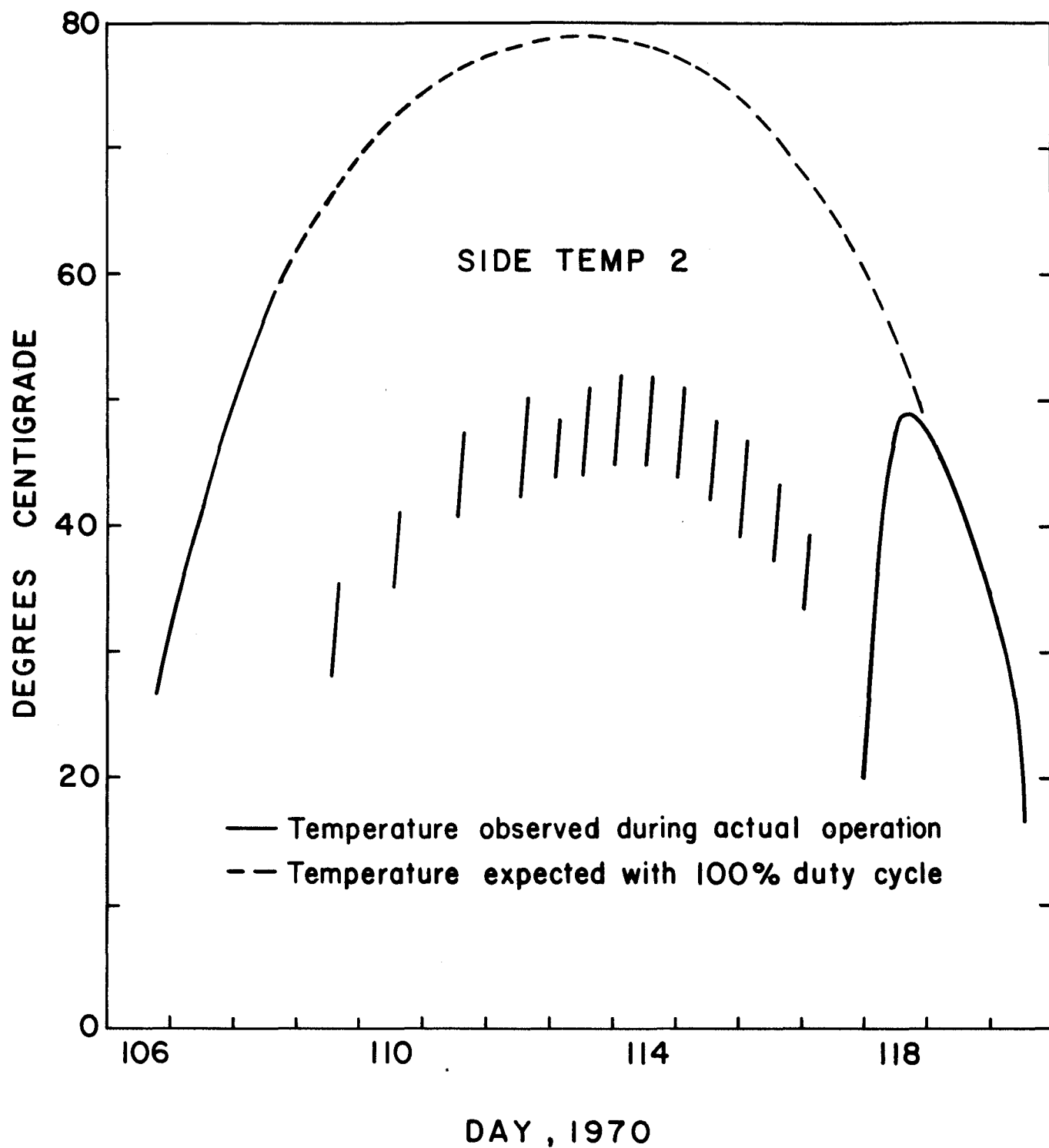


FIGURE 2

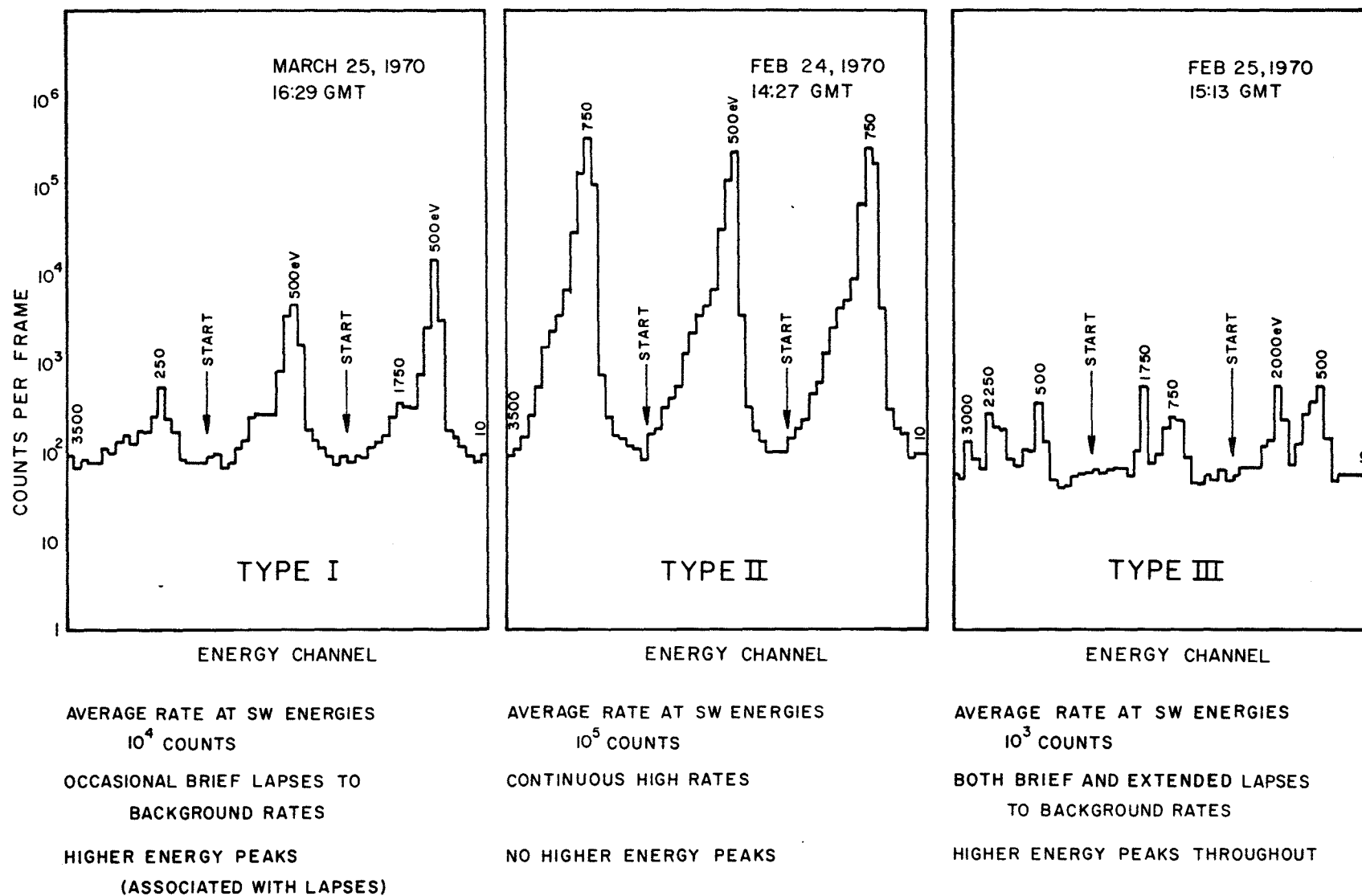
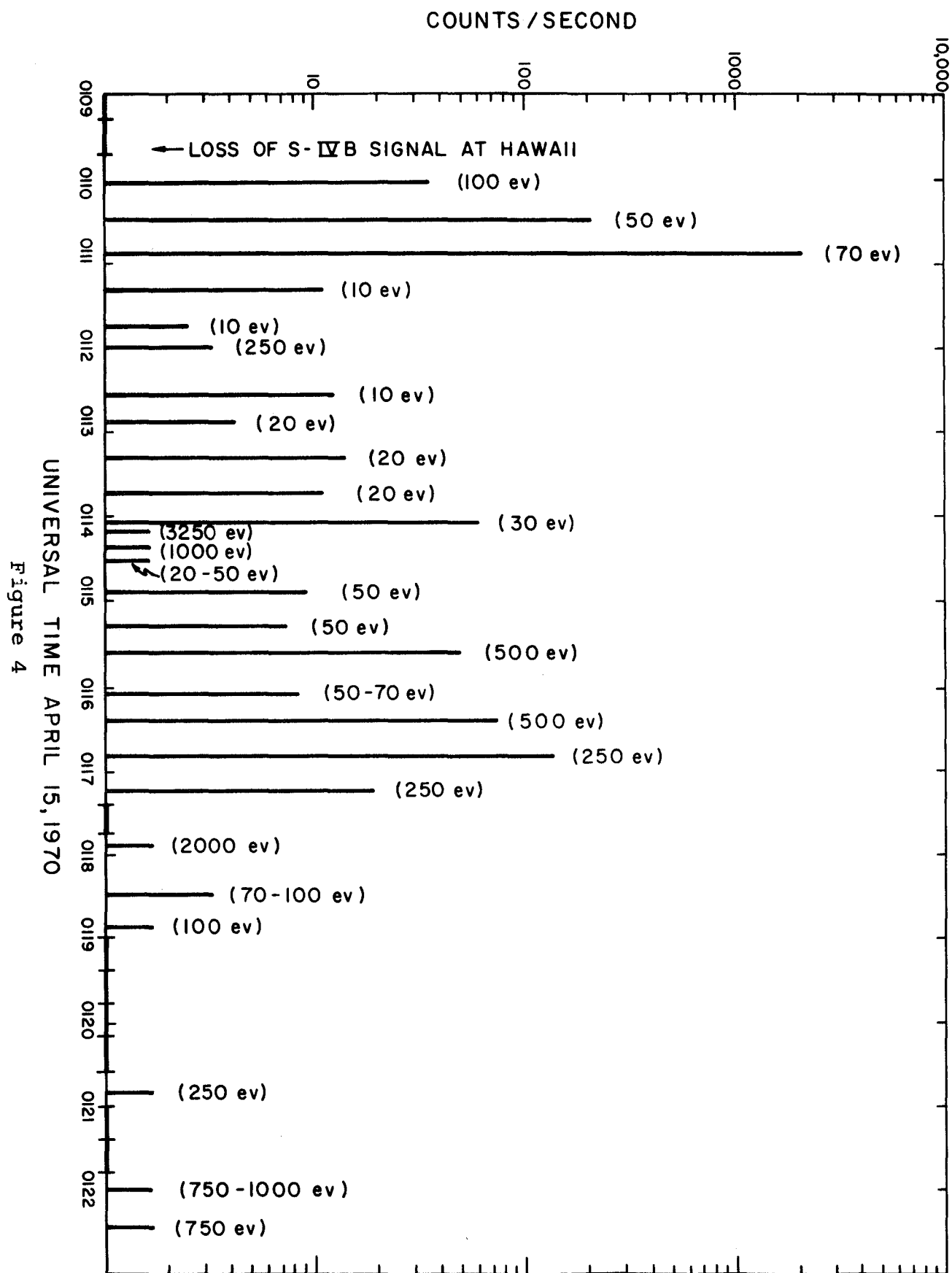


FIGURE 3







The Lunar Terminator Ionosphere\*

by

J. Benson, J. W. Freeman, and H. K. Hills

Department of Space Physics and Astronomy

Rice University  
Houston, Texas 77001  
U.S.A.

\*Based on a paper presented at the 6th Lunar Science Conference,  
Houston, Texas, March, 1975.

*Proc. Sixth Lunar Sci. Conf., Geochimica et Cosmochimica  
Acta, Suppl. 6, 3, 1975.*

### ABSTRACT

The extended ionosphere is seen by the Suprathermal Ion Detector Experiments (SIDE) near the terminator. An analysis of the energy and mass spectra of these ions accelerated by the interplanetary electric field indicates the following: (1) the principal ion species are in the mass per unit charge ranges consistent with neon and argon; (20-28 amu/q and 40-44 amu/q; (2) the lunar atmosphere in these mass ranges is distributed exponentially; (3) the terminator region surface number density for  $^{20}\text{Ne}$  is of the order of  $10^5 \text{ cm}^{-3}$ ; (4) the terminator region lunar surface potential is negative from about 10 to 100 volts; and (5) this potential has a screening length of the order of a kilometer.

## INTRODUCTION

The interplanetary electric field,  $\vec{E}_i$ , continuously accelerates ions generated in the lunar atmosphere by photoionization and by charge transfer with the solar wind. These ions are detectable by the Supra-thermal Ion Detector Experiments (SIDEs) near the lunar terminators. Manka and Michel [1973] and Vondrak et al. [1974] have discussed the energy spectra of these ions. In this paper we present a new method of analysis of these spectra which includes a model of the electric field due to the lunar surface potential. This model and its application to recent SIDE data result in a new determination of the surface number density of neon near the terminator and an estimate of the magnitude of the surface potential and its screening length.

### Theory

The interplanetary electric field is given by

$$\vec{E}_i = -\vec{V}_{sw} \times \vec{B}_i ,$$

$\vec{V}_{sw}$  is the solar wind velocity and  $\vec{B}_i$  the interplanetary magnetic field strength.  $\vec{E}_i$  can be assumed to be homogeneous over the lunar atmospheric scale height,

$$h = \frac{kT}{mg}$$

## INTRODUCTION

The interplanetary electric field,  $\vec{E}_i$ , continuously accelerates ions generated in the lunar atmosphere by photoionization and by charge transfer with the solar wind. These ions are detectable by the Supra-thermal Ion Detector Experiments (SIDEs) near the lunar terminators. Manka and Michel [1973] and Vondrak et al. [1974] have discussed the energy spectra of these ions. In this paper we present a new method of analysis of these spectra which includes a model of the electric field due to the lunar surface potential. This model and its application to recent SIDE data result in a new determination of the surface number density of neon near the terminator and an estimate of the magnitude of the surface potential and its screening length.

### Theory

The interplanetary electric field is given by

$$\vec{E}_i = -\vec{V}_{sw} \times \vec{B}_i ,$$

$\vec{V}_{sw}$  is the solar wind velocity and  $\vec{B}_i$  the interplanetary magnetic field strength.  $\vec{E}_i$  can be assumed to be homogeneous over the lunar atmospheric scale height,

$$h = \frac{kT}{mg}$$

and zero-energy intercept

$$I = \ln \left( \frac{n_0 p}{q E_i} \right) \quad (5)$$

If the value of  $E_i$  is known, eq. 4 gives the scale height; and if the ionization rate  $p$  is also known, eq. 5 gives the surface number density of the neutrals  $n_0$ . Alternatively, if  $h$  is known,  $E_i$  can be calculated from eq. 4.

Now consider the effect of a second electric field resulting from the negative lunar surface potential at the terminator [Lindeman, 1973a] and [Lindeman et al., 1973b]. As seen by a detector at the lunar surface the positive atmospheric ions will have their energies shifted upward by an amount  $q\phi_0$ . Equations (1) becomes

$$\epsilon(z) = qE_i z + q\phi_0 \quad (6)$$

where  $\phi_0$  is the magnitude of the negative lunar surface potential. This equation is correct only for ions created well above the screening length of the lunar surface electric field. Its effect is to shift the linear semi-log energy spectrum line toward higher energies. To correct for this, when evaluating the zero-energy intercept, equation (5), we must shift the energy axis by an amount  $q\phi_0$ . The  $pn_0$  product can then be determined from eq. 5. However eq. 5 is not strictly valid at  $\epsilon = q\phi_0$  so that  $pn_0$  determined from this eq. is an estimate.

We can improve the analysis of the spectrum by modeling the height distribution of the lunar surface electric field and if a successful fit

to the data is obtained the parameters of the fitting function are determined directly.

We model the surface field by assuming an exponential height distribution of the form

$$\phi(z) = \phi_0 \exp[-z/\lambda] \quad (7)$$

where  $\lambda$  is the screening length. The ion energy at the surface will be given by

$$\epsilon(z) = q(E_i z + \phi_0 (1 - \exp(-z/\lambda))) \quad (8)$$

and the differential flux by

$$\frac{dJ}{d\epsilon}(z) = \frac{n_0 p \exp(-z/h)}{q[E_i + \frac{\phi_0}{\lambda} \exp(-z/\lambda)]} \quad (9)$$

In this case the flux as a function of energy  $\epsilon$  can be obtained by plotting eq. 9 vs. eq. 8.

For  $z \gg \lambda$  eqs. 8 and 9 reduce to

$$\epsilon(z) \approx qE_i z + q\phi_0 \quad (10)$$

in agreement with eq. (6) and

$$\frac{dJ}{d\epsilon} \approx \left( \frac{n_0 p}{qE_i} \right) e^{-z/h} \quad (11)$$

Solving (10) for  $z$  and using this in (11) gives,

$$\left(\frac{dJ}{d\epsilon}\right)_{z \gg \lambda} \approx \left(\frac{n_o p}{qE_i}\right) e^{-\frac{\epsilon - q\phi_o}{qE_i h}} \quad (12)$$

or

$$\ln \left(\frac{dJ}{d\epsilon}\right)_{z \gg \lambda} \approx \ln\left(\frac{n_o p}{qE_i}\right) - \frac{1}{qE_i h} (\epsilon - q\phi_o) \quad (13)$$

It is clear from eq. 13 that eq. 4 is still valid for the slope. Hence  $E_i$  can still be estimated from the slope if  $h$  is known. When eq. 13 is evaluated at  $\epsilon = q\phi_o$ , the intercept is given by eq. 5 in agreement with the ideas discussed above.

The method of analysis of the data in the next section was to estimate the parameters of the fitting function (equations 8 and 9) from the data using eqs. 4 and 5. The final value of the parameters  $pn_o$ ,  $E_i$ ,  $\phi_o$  and  $\lambda$  were determined from the fit.

### Observations

Figure 1 shows a  $\vec{V}_{sw} \times \vec{B}_i$  event observed by the Apollo 15 SIDE in 1974. The portion of the curve above about 70 eV is linear as predicted by equation 3 or equation 13. The flux below ~70 eV/q is depleted due to a strong negative surface potential existing at the time of this event, i.e. the energy spectrum has been "shifted" by an amount approximately equal to  $q\phi_o$ . The SIDE mass analyzer shows the ions in this event to have mass 20 amu/q (see inset of figure 1). This event occurred at a solar zenith angle of  $\approx 71^\circ$  where the surface temp of  $\sim 284^\circ\text{K}$  gives

a scale height for neon of  $\sim 73$  km. The measured slope is  $\sim .011$  which gives a value of about 1.25 V/km for  $E_i$ . A typical solar wind velocity of 400 km/sec and typical  $\vec{B}_i$  of 5 $\gamma$  yields  $E_i = 2$  V/km. Other  $\vec{V}_{sw} \times \vec{B}_i$  events have been analyzed where  $\vec{E}_i$  was available from knowledge of the interplanetary magnetic field strength and solar wind velocity with the result that the calculated value of the scale height generally agrees with the theoretical value. Hence, the procedure of using the theoretical scale height and the measured slope to calculate  $\vec{E}_i$  is justified. The curve in figure 1 was obtained from eqs. 8 and 9 using  $\phi_0 = 50$  V,  $\lambda = 4.0$  km,  $E_i = 1.4$  V/km,  $h = 73$  km and  $pn_0 = .006 \text{ cm}^{-3} \text{ sec}^{-1}$ .

Using the value  $p = 1.1 \times 10^{-7} \text{ sec}^{-1}$ , the total ionization rate from photoionization, solar wind impact ionization and solar wind charge exchange (Siscoe and Mukherjee, 1972) for neon gives

$$n_0 \approx 5.4 \times 10^4 \text{ cm}^{-3} \quad (14)$$

This value of  $n_0$  is consistent with the results of Hoffman et al. 1973 who report data from the Lunar Atmospheric Composition Experiment indicating  $8.7 \times 10^4 \text{ cm}^{-3}$  near the terminator.

A second event of this type observed on day 43 of 1974 is shown in figure 2. The exponential nature of the ionosphere is again clearly shown by the linear portion of the curve above  $\sim 60$  eV/q. A strong negative surface potential is also evident in the spectrum; the flux is depleted below about 50 eV/q. This event occurred at a solar zenith angle of  $\sim 68^\circ$  which implies a scale height for  $\text{Ne}^{20}$  of  $\sim 75$  km. The



scale height coupled with the slope gives a value of 1.3 V/km for  $E_i$ . The smooth curve in figure 3<sup>n</sup> was computed from eqs. 8 and 9 with  $\phi_0 = 50$  V,  $\lambda = 1700$  m,  $E_i = 1.3$  V/km,  $h = 75$  km and  $pn_0 = .011 \text{ cm}^{-3}\text{sec}^{-1}$ . The simultaneous mass spectrum for this event showed the dominant mass to be 20 amu/q so that if the value of  $p$  given above for  $\text{Ne}^{20}$  is used with the fitted  $pn_0$  product, the surface number density of the neutrals is

$$n_0 \approx 1.0 \times 10^5 \text{ cm}^{-3} \quad (15)$$

When the interplanetary electric field strengthens, the slope of this type of spectrum becomes flatter for the same value of the scale height. Figure 3 shows an event observed on day 289 of 1973 at a solar zenith angle of  $\sim 64^\circ$  where the  $\text{Ne}^{20}$  scale height is  $\sim 78$  km. The calculated value of  $E_i$  for this event is 3.8 V/km which is somewhat larger than the previous events and is due to the flatter slope of this spectrum. The curve in figure 3 was obtained with  $\phi_0 = 45$  V,  $\lambda = 1370$  m,  $E_i = 3.8$  V/km,  $h = 78$  km and  $pn_0 = .015 \text{ cm}^{-3}\text{sec}^{-1}$ . The resulting value of the surface neutral number density is then

$$n_0 \approx 1.4 \times 10^5 \text{ cm}^{-3} \quad (16)$$

Other  $\vec{V}_{sw} \times \vec{B}_i$  events have been observed by the Apollo 15 instrument in 1973 and 1974 that give similar results. That is, a surface number density for neon of the order of  $10^5 \text{ cm}^{-3}$ ,  $\phi_0$  a few tens of volts negative and  $\lambda$  of the order of a kilometer. The detailed analysis of all of the data is not complete at this writing, but the events presented here may be considered representative of the data set.

All of the sunset terminator regions (beginning ~3 days before local sunset and continuing to sunset) in 1973 and through day 251 of 1974 for Apollo 15 have been searched for  $\vec{V}_{sw} \times \vec{B}_i$  events with the result that 14 events have been found for which simultaneous mass spectra exist. These are considered to be "high quality" events. Many other events exist in these regions that appear to be  $\vec{V}_{sw} \times \vec{B}_i$  events but for which no simultaneous mass spectrum exists. These "no-mass" spectrum events will be used in future analyses to enlarge the data base on the assumption that the principal component of the mass spectrum is neon. Not all of the high quality events have been analyzed to determine the parameters but an estimate of the surface number density for neon has been made from these spectra. The events presented in this paper are predominantly neon but many of the other observed spectra indicate that more than one gas is contributing to the spectrum. Work is presently in progress to determine if these spectra can be fit adequately assuming a multicomponent atmosphere.

The value of the surface number density of the neutral neon atoms ( $\sim 10^5 \text{ cm}^{-3}$ ) determined from the present analysis is about a factor of 10 less than reported from earlier SIDE data. The data discussed by Vondrak et al. [1974] were taken less than 6 months after deployment of the Apollo 15 instrument while the present data were taken more than 2 years after deployment. At present we do not understand the reason for this discrepancy. We hope to resolve this problem by examining data from the period between the earlier and the later data.

The investigation of the electric potential distribution versus height using this technique is a separate line of research and will not be discussed in detail here.

The other type of ionospheric ion event observed in the terminator regions is due to acceleration by the lunar surface potential alone. A typical example of one of these events is shown in figure 4. These monoenergetic low-energy ions provide good mass spectra which aid in determining the composition of the ionosphere and the magnitude of the lunar surface potential. However, the narrow peaks of the spectra make an analytical representation of these events difficult.

An analysis of nine terminator regions in 1973 and 1974 shows that the only consistently present components of the mass spectra in lunar surface potential type events are 20-28, 28-40, 40-44 amu/q ions (the SIDE mass analyzers are not well suited for the detection of masses below 10 amu/q).

### Summary

The results contained in this description of the lunar terminator ion environment may be summarized as follows:

A model is proposed to explain the dominant features of the  $\vec{V}_{sw} \times \vec{B}_i$  spectra that are observed in the terminator regions. This model uses an exponential atmosphere, the vertical  $\vec{V}_{sw} \times \vec{B}_i$  electric field, and an exponentially decreasing potential distribution near the surface. A reasonable fit to the  $\vec{V}_{sw} \times \vec{B}_i$  spectrum can be obtained which yields the parameters  $pn_0$ ,  $E_i$ ,  $\phi_0$  and  $\lambda$ . The form of the observed spectra confirm the exponential distribution of the neutral atmosphere in the observed mass range. The lunar surface potential as determined from the  $\vec{V}_{sw} \times \vec{B}_i$  spectra is often found to be a few tens of volts negative

at a solar zenith angle of  $\sim 70^\circ$  and the scale size  $\lambda$  of the distribution is of the order of 1 km. The analysis of several  $\vec{V}_{sw} \times \vec{B}_i$  spectra with a dominant mass of 20 amu/q shows that the neutral number density  $n_0$  is of the order of  $10^5 \text{ cm}^{-3}$ . Earlier SIDE data indicate a higher value.

The lunar surface potential events provide good mass spectra which show that the dominant constituents of the lunar ionosphere which are observable by the SIDE are ions of mass 20-28, 28-40, and 40-44 amu/q.

#### Acknowledgements

We acknowledge helpful discussions with R. H. Manka.

This research was supported by NASA contract NAS9-5911.

References

- Hoffman, J.H., Hodges, R. R., Jr., Johnson, F. S., Evans, D. E., (1973), Lunar atmospheric composition results from Apollo 17, Proc. Fourth Lunar Sci. Conference, Geochim. Cosmochim. Acta., Suppl. 4, Vol. 3, pp. 2865-2875. Pergamon.
- Lindeman, R. A., (1973a), Observation of Ions from the Lunar Ionosphere, PH.D. Thesis, Rice U., Houston, Texas.
- Lindeman, R. A., Freeman, J. W., Vondrak, R. R., (1973b), Ions from the lunar atmosphere, Proc. Fourth Lunar Sci. Conference, Geochim. Cosmochim. Acta., Suppl. 4, Vol. 3, pp. 2889-2896.
- Manka, R. H., and Michel, F. C., (1973), Lunar ion energy spectra and surface potential, Proc. Fourth Lunar Sci. Conference, Geochim. Cosmochim. Acta., Suppl. 4, Vol. 3, pp. 2897-2908.
- Siscoe, G. L., and Mukherjee, N. R., (1972), Upper limits on the Lunar Atmosphere determined from solar wind measurements, J. Geophys. Res., 77, 6042.
- Vondrak, R. R., Freeman, J. W., and Lindeman, R. A., (1974), Measurements of lunar atmospheric loss rate, Proc. Fifth Lunar Sci. Conference, Geochim. Cosmochim. Acta., Suppl. 5, Vol. 3, pp. 2945-2954. Pergamon.

### Figure Captions

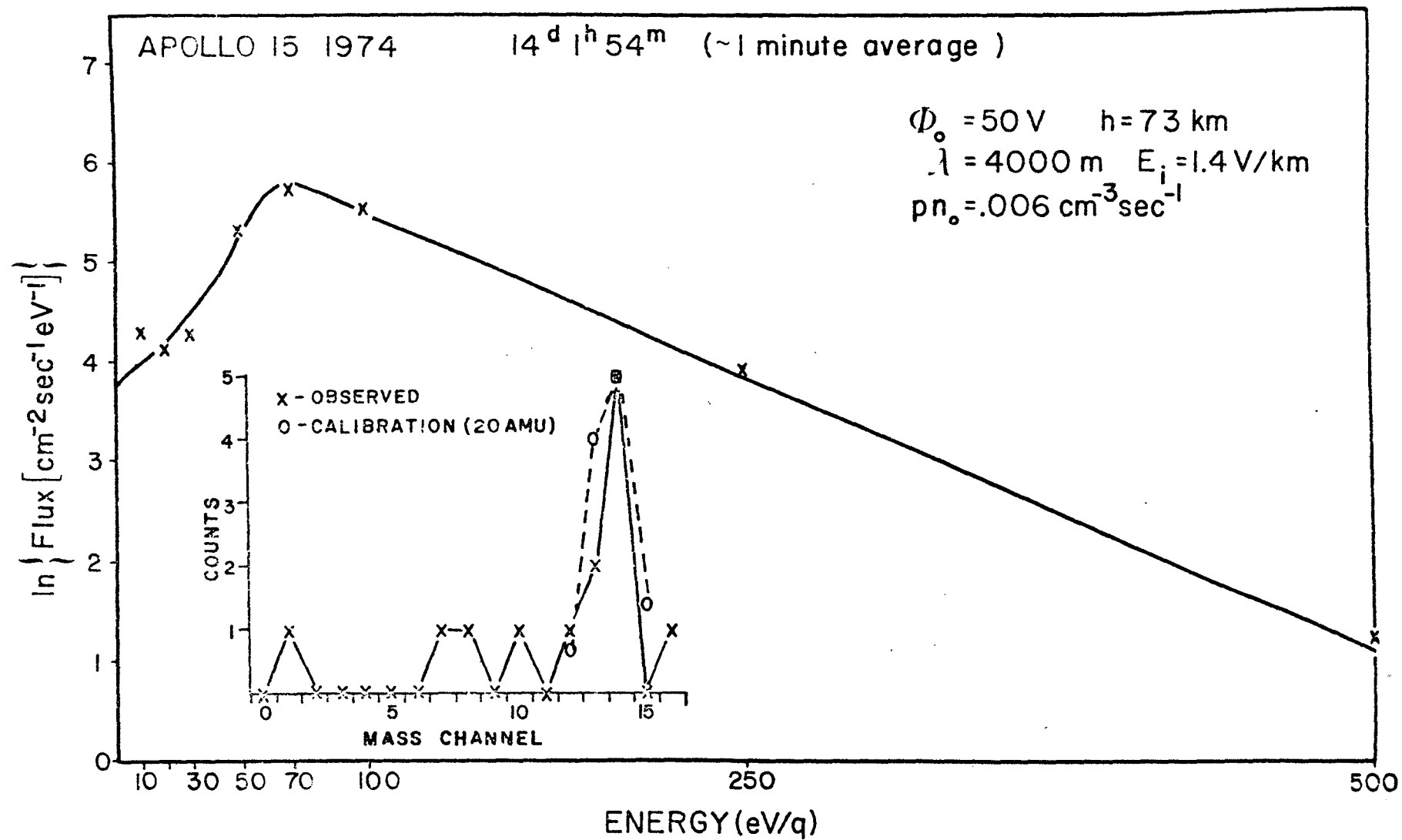
Figure 1. Fit of the theory to an observed  $\vec{V}_{sw} \times \vec{B}_i$  spectrum.

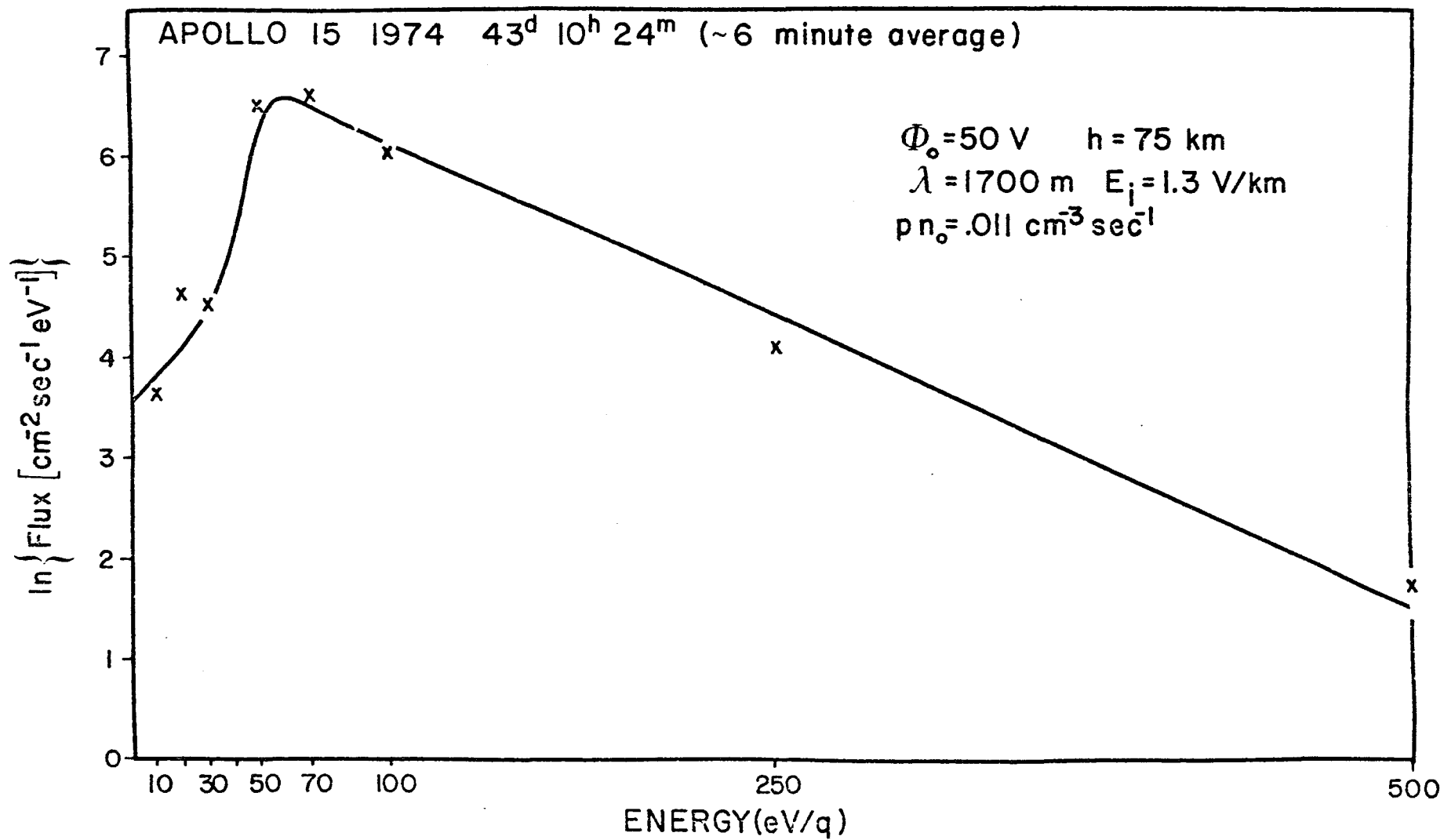
The inset shows that the dominant mass for this event is 20 amu/q. The circles connected by a dashed line represent the results of the calibration for 20 amu/q particles normalized to the observed counts.

Figure 2.  $\vec{V}_{sw} \times \vec{B}_i$  event observed on day 43 in 1974 by the Apollo 15 SIDE. The smooth curve is a fit to the data with  $\phi_0 = 50$  V,  $h = 75$  km,  $\lambda = 1700$  m  $E_i = 1.3$  V/km and  $pn_0 = .011 \text{ cm}^{-3}$ .

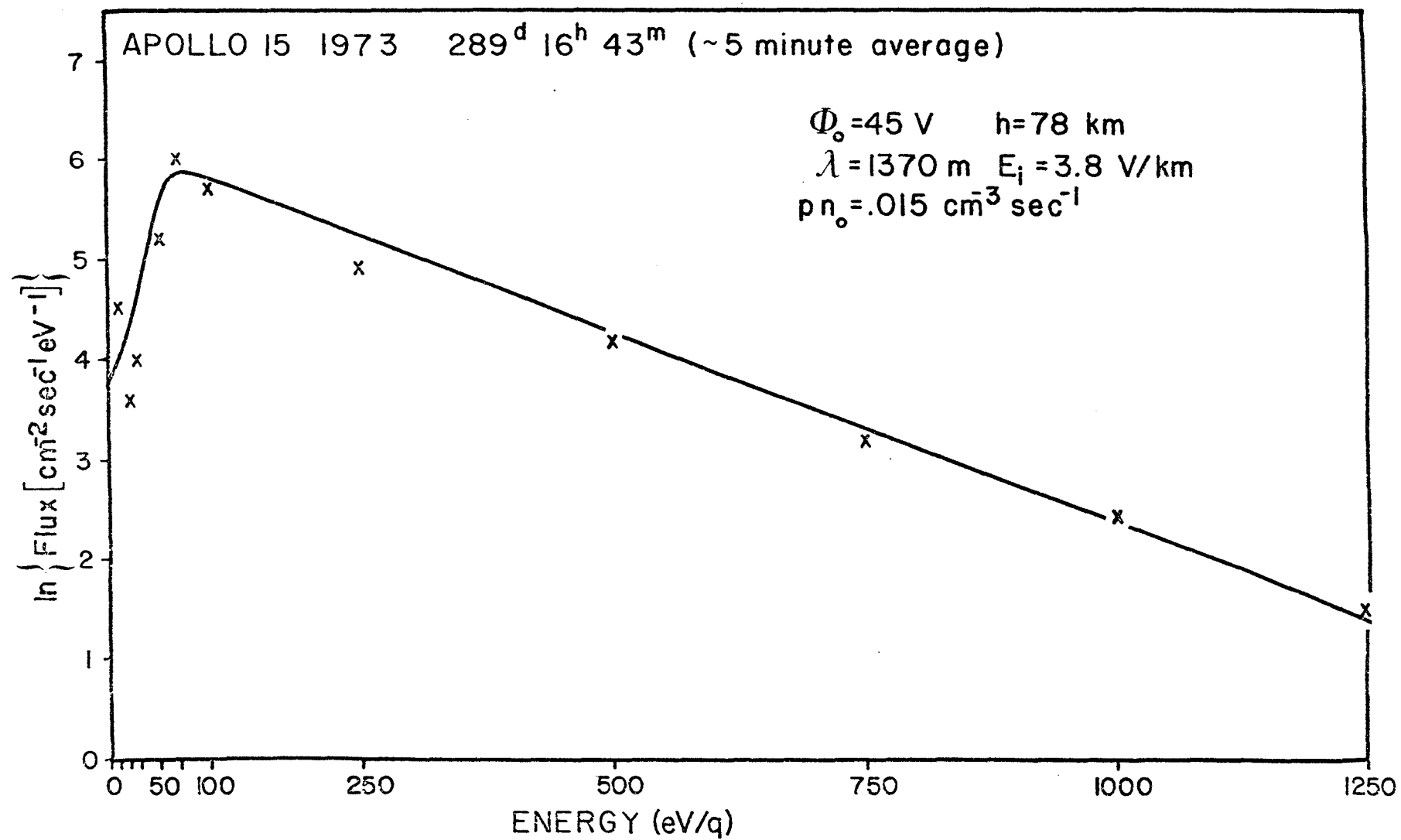
Figure 3.  $\vec{V}_{sw} \times \vec{B}_i$  event with stronger interplanetary field. The fit to this spectrum was made with  $\phi_0 = 45$  V,  $h = 78$  km,  $\lambda = 1370$  m  $E_i = 3.8$  V/km and  $pn_0 = .015 \text{ cm}^{-3}$ .

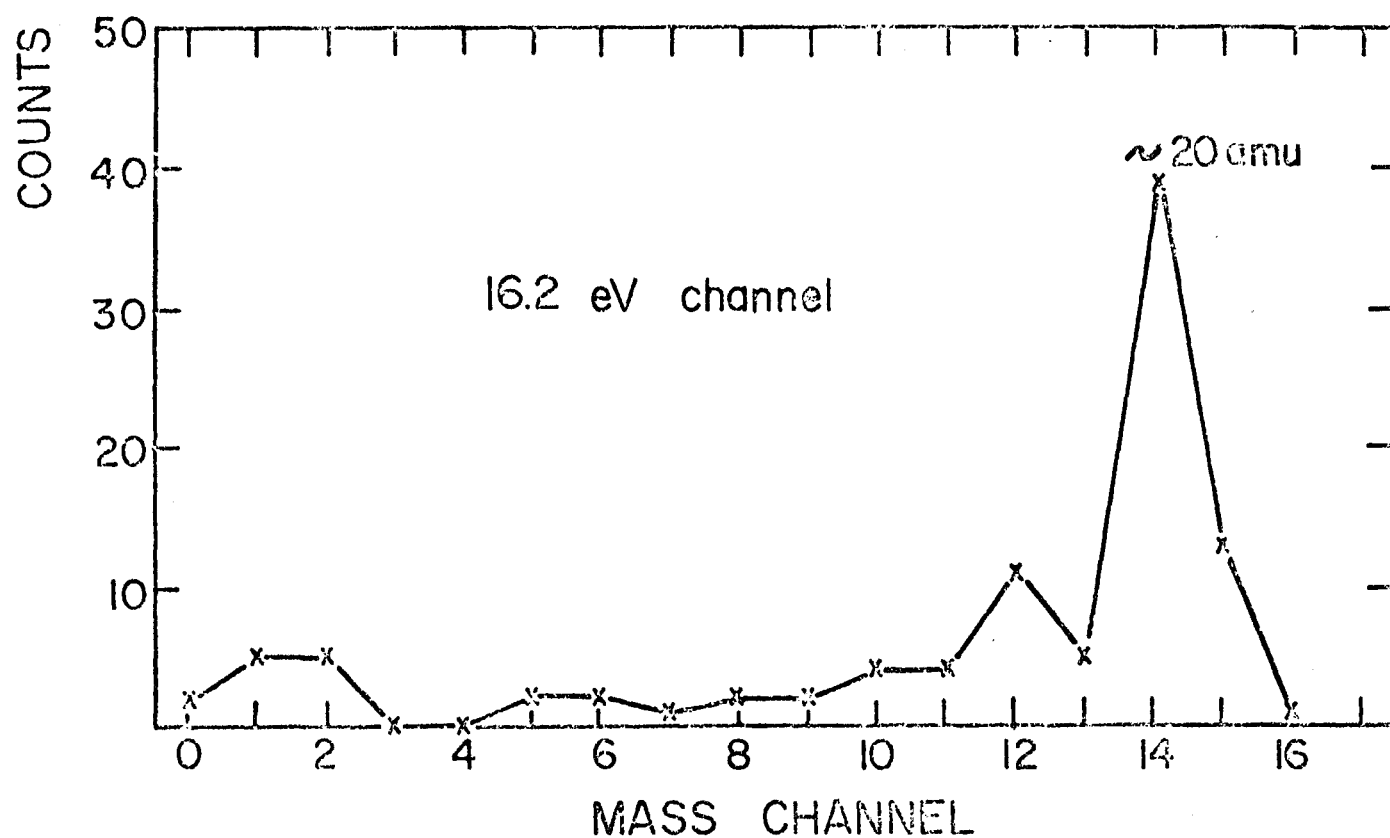
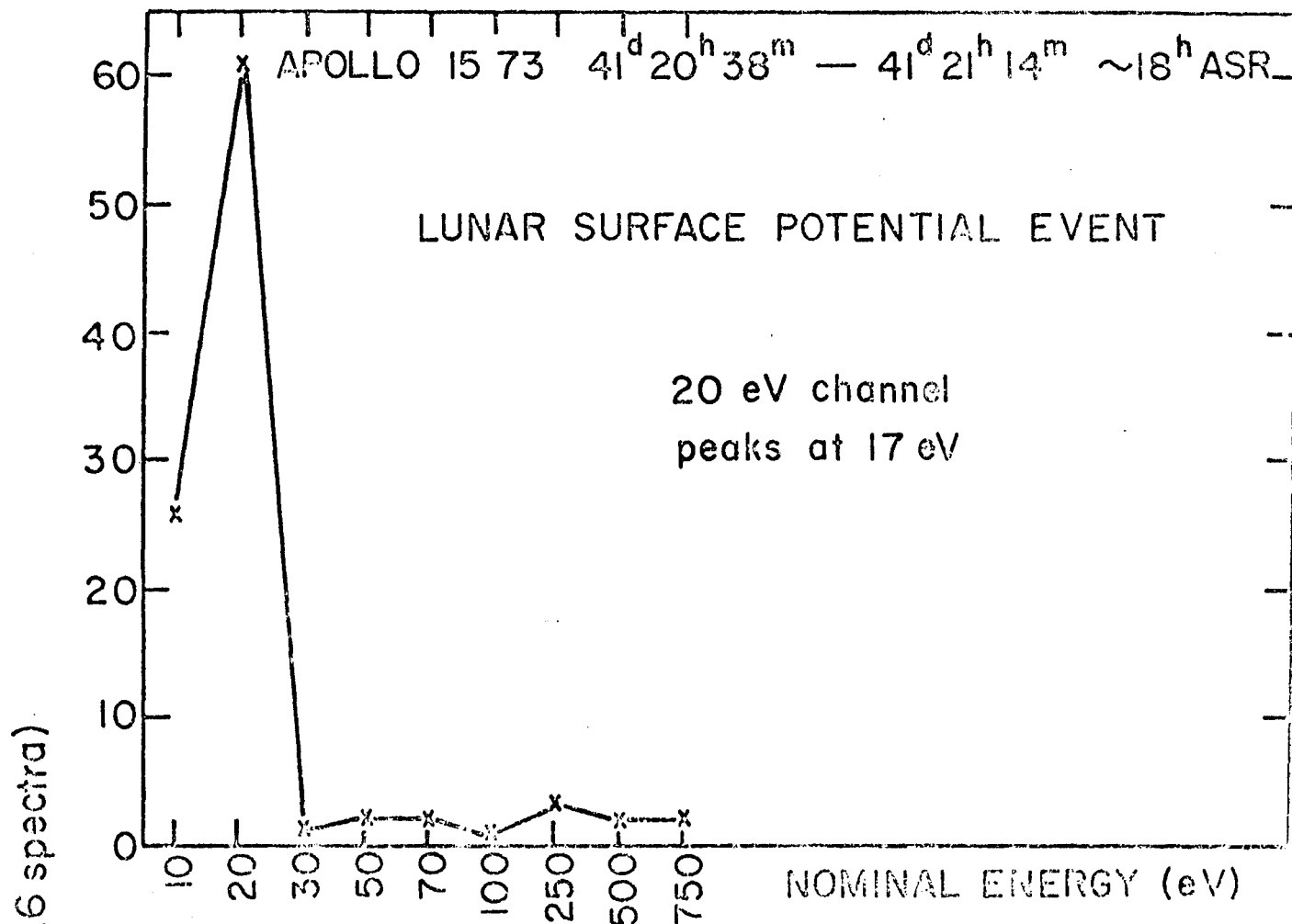
Figure 4. Typical lunar surface potential event showing simultaneous energy and mass spectra. The appearance of the counts in the 20 eV/q channel is interpreted to mean that the magnitude of the negative lunar surface potential is 20 V. The counts are summed over 16 spectra taken over  $\sim 1/2$  hr.













GEOCHIMICA ET COSMOCHIMICA ACTA  
Journal of The Geochemical Society and The Meteoritical Society  
SUPPLEMENT 4

**PROCEEDINGS  
OF THE  
FOURTH LUNAR SCIENCE CONFERENCE  
Houston, Texas, March 5-8, 1973**

Sponsored by  
The NASA Johnson Space Center  
and  
The Lunar Science Institute



PERGAMON PRESS

Printed in the U.S.A.

## The electric potential of the lunar surface

M. A. FENNER, J. W. FREEMAN, JR., and H. K. HILLS

Department of Space Science  
Rice University  
Houston, Texas 77001

**Abstract**—Acceleration and detection of the lunar thermal ionosphere in the presence of the lunar electric field yields a value of at least +10 volts for the lunar electric potential for solar zenith angles between approximately 20° and 45° and in the magnetosheath or solar wind. An enhanced positive ion flux is observed with the ALSEP Suprathermal Ion Detector when a pre-acceleration voltage attains certain values. This enhancement is greater when the moon is in the solar wind as opposed to the magnetosheath.

### INTRODUCTION

THEORETICAL STUDIES of the electric potential of the sunlit lunar surface in the presence of the solar wind have predicted values ranging from +20 volts down to a few volts positive. Originally, Öpik and Singer (1960) proposed a value of about +20 volts. More recently Grobman and Blank (1969) revised this estimate downward by about an order of magnitude and finally Manka (1972) has estimated a value near +10 volts. In the absence of the solar wind, Reasoner and Burke (1972) have reported potentials as high as +200 volts as the moon crosses the magnetospheric tail.

In this paper we discuss evidence for a sunlit potential in the magnetosheath and solar wind of about +10 volts. This evidence comes from the analysis of the energy spectra of lunar ionosphere thermal ions accelerated toward the moon by an artificial electric field. The data are provided by the Apollo Lunar Surface Experiment Package (ALSEP) Suprathermal Ion Detector Experiment (SIDE) deployed at the Apollo 14 and 15 sites.

### THE SIDE

The Suprathermal Ion Detector Experiment (SIDE) contains a total ion detector curved plate analyzer and ion mass analyzer designed to measure positive ions down to a few electron volts. To accomplish this in the face of possible lunar surface potentials of the order of several tens of volts, the instrument is equipped with a ground plane electrode (in contact with the lunar surface) whose potential with respect to a wire grid above the ion entrance apertures is stepped through a series of 24 voltages (*see* Fig. 1b). For certain negative (accelerating) voltages, the imposed electric field is able to overcome a positive surface potential allowing thermal ions to be measured by the instrument.

The ground plane electrode is a circular wire grid 65 cm in diameter. Close-up

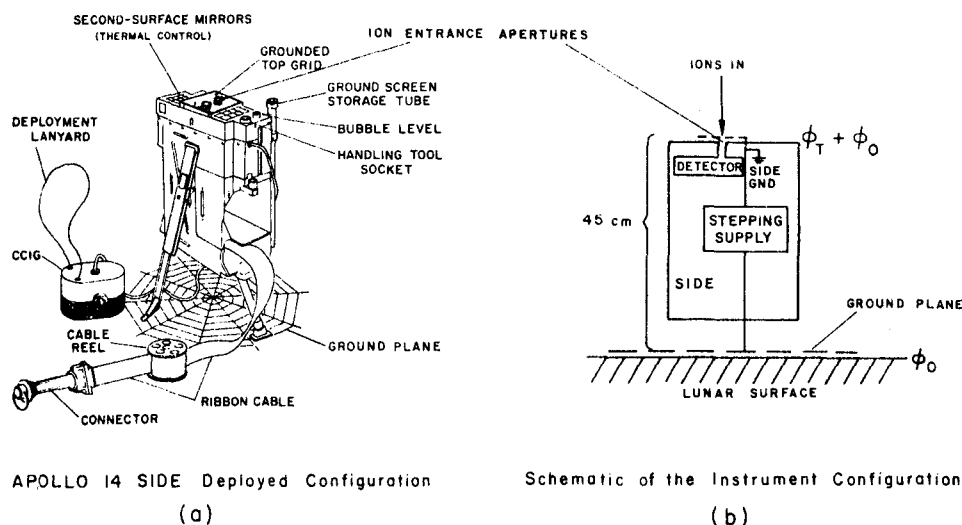


Fig. 1. The Suprathermal Ion Detector Experiment (a) as deployed on the lunar surface, and (b) showing the ground plane and top wire grid configuration schematically. Thermal ions are attracted to or repelled from the top of the instrument by the top grid.  $\phi_T$  is the voltage produced by the stepping supply. The ground plane is in actual contact with the lunar surface.

photographs show that the grid makes contact with the surface at many points, so good electrical contact will be assumed (*see* Appendix A). The SIDE is D.C. isolated from the ALSEP central station and other experiments.

These features of the SIDE allow the determination of the electric potential of the lunar surface under certain conditions. This is accomplished by examination of the energy spectra of thermal ions accelerated into the SIDE by the ground plane voltage in the presence of the electric field due to the surface charge of the moon.

Figure 1a shows the instrument and the ground plane in the deployed configuration. Further details of the experiment can be found in Freeman *et al.* (1972).

#### INSTRUMENT FUNCTION

Assuming good electrical coupling between the ground plane and the lunar surface the instrument would be expected to function as follows:

- (a) In the case of a near-zero lunar surface potential a negative ground plane stepper voltage accelerates thermal positive ions into the instrument with an energy approximately that of the stepper voltage.
- (b) When the lunar surface is substantially positive and the stepper voltage negative, but larger in absolute value, the energy of the detected ions is less than the stepper voltage by an amount equal to the lunar surface po-

tential. When the stepper voltage exactly matches but is of opposite sign from the lunar surface potential, the ions are seen unaccelerated.

- (c) When the lunar surface is negative the ions may be repelled by a sufficiently large positive stepper voltage.

We can assume that the ions seen are principally ionized neutral gas in thermal equilibrium with the lunar surface ( $T \approx 400^\circ\text{K}$ ) and further that most of the ions appear to have come from infinity so far as the energy acquired from the surface electric fields is concerned. Under these conditions, the foregoing can be made more explicit by expressing the ion energy,  $E$ , seen at the detector by

$$E = E_i - (\varphi_t + \varphi_0)q \quad (1)$$

where  $E_i$  is the initial ion energy (the neutral thermal energy),  $\varphi_t$  the potential of the top wire grid of the SIDE relative to the ground plane and hence to the lunar surface,  $\varphi_0$  the lunar surface potential, and  $q$  the ion charge (assumed to be  $+1$ ). We will be concerned with cases in which  $\varphi_t$  is negative and for which we assume  $q|\varphi_t + \varphi_0| \gg E_i$  so that (1) becomes

$$E \approx -(\varphi_t + \varphi_0)q \quad (2)$$

Using this equation observable values of  $\varphi_0 q$  are displayed in Table 1 for the differential energy channels,  $E$ , and stepper voltages,  $\varphi_t$ , of the Apollo 14 instrument. If the initial energy of the ions is not negligible then the tabular values represent  $(\varphi_0 q - E_i)$  and hence provide a lower limit on the surface potential; a situation that we consider unlikely (see Appendix B).

#### OBSERVATIONS

A feature of the data when the solar zenith angle is between approximately  $20^\circ$  and  $45^\circ$  is the frequent appearance of narrow low-energy ion flux spectra which show a correlation with the ground plane stepper voltage. That is, ions at certain peak energies recur with specific ground plane stepper voltages. We will refer to this occurrence as a resonance. There is often a complete absence of ions in any energy channel except at the resonant ground plane stepper voltage.

This phenomenon has been seen with the Apollo 14 and 15 SIDEs and exclusively in the solar wind or magnetosheath. Figure 2 shows the location in lunar orbit of these observations. Only one such observation has been made on the dawn side of the tail. It was seen at a time of high local gas pressure following the Apollo 15 LM impact. Each lunar cycle for which Apollo 14 data are available shows the resonance in the afternoon or dusk side magnetosheath and solar wind and some cycles of Apollo 15 data show this resonance in this quadrant as well.

Figure 3 shows an extended set of data from the Apollo 14 SIDE. Here the count rates from the two lowest energy channels have been grouped according to the ground plane stepper voltage. The energies that stand out near the center of the figure are 7 eV at ground plane voltage  $-16.2$  and 17 eV at ground

Table 1. Apollo 14 SIDE—Observable values of ( $\phi_0$   $q$ ).

0267	$\phi_i$ (volts)	E	
		Total ion detector Energy Channels	
		7 eV/q	17 eV/q
Ground Plane Stepper Voltage			
	- 0.6	- 6.4	- 16.4
	- 1.2	- 5.8	- 15.8
	- 1.8	- 5.2	- 15.2
	- 2.4	- 4.6	- 14.6
	- 3.6	- 3.4	- 13.4
	- 5.4	- 1.6	- 11.6
	- 7.8	+ 0.8	- 9.2
	- 10.2	+ 3.2	- 6.8
	- 16.2	+ 9.2	- 0.8
	- 19.8	+ 12.8	+ 2.8
	- 27.6	+ 20.6	+ 10.6
	0.0	- 7.0	- 17.0
	+ 0.6	- 7.6	- 17.6
	+ 1.2	- 8.2	- 18.2
	+ 1.8	- 8.8	- 18.8
	+ 2.4	- 9.4	- 19.4
	+ 3.6	- 10.6	- 20.6
	+ 5.4	- 12.4	- 22.4
	+ 7.8	- 14.8	- 24.8
	+ 10.2	- 17.2	- 27.2
	+ 16.2	- 23.2	- 33.2
	+ 19.8	- 26.8	- 36.8
	+ 27.6	- 34.6	- 44.6

plane voltage  $-27.6$ . From Equation (2) and Table 1 these examples yield a lunar surface potential,  $\phi_0$ , of approximately  $+10$  volts.

Ten months of Apollo 14 data have been scanned. Each lunation shows resonances similar to Fig. 3 indicating a surface potential of  $\sim +10$  volts for zenith angles between approximately  $20^\circ$  and  $45^\circ$ . A typical segment of data for this region is shown in Fig. 4. Here the counting rates in the 17 eV channel are plotted each time the ground plane stepper reads  $-27.6$  volts. The counting rates for the same energy channel are plotted when the ground plane stepper is at 0.0 volts as a measure of the background when particles cannot be accelerated into the detector by the stepper potential. This plot clearly shows the increase in the counting rate for the resonant step as the detector moves out into the free-flowing solar wind. The maximum rate, although not sharply defined, usually occurs near a zenith angle of  $35^\circ$ . In all the data that have been scanned, the resonance ends at about  $45^\circ$ . This suggests that at that point the lunar surface potential decreases below the energy level required to produce a resonance in our differential energy passbands.



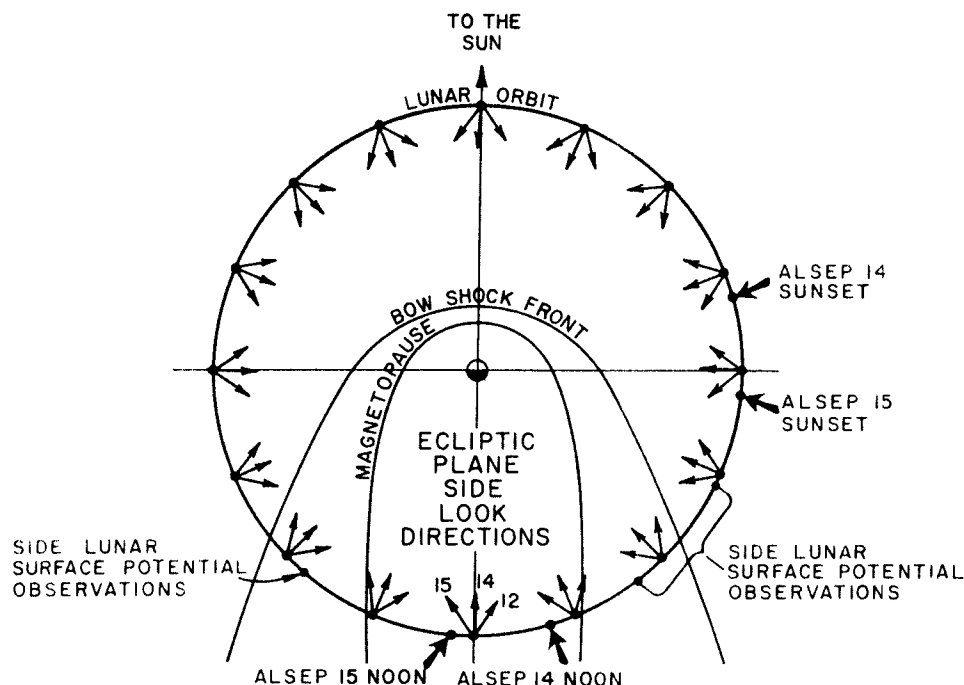


Fig. 2. Location in lunar orbit of the lunar surface potential observations.

These passbands are narrow ( $\pm 5\%$  FWHM) and not contiguous, so it is possible for the ion peak to disappear between them. Hence the disappearance of the resonance does not imply a discontinuity in the lunar surface potential. In fact it is important to note that the resonance shown here indicates that the surface potential does not change greatly over a large portion of the sunlit surface. At the equatorial site (Apollo 14) the potential remains  $+10 \text{ v} \pm 2 \text{ v}$  over the solar zenith angle range  $20^\circ$  to  $45^\circ$ . The same potential has been observed at least once within the same zenith angle range at the Apollo 15 site  $26.1^\circ$  north of the equator.

That the magnitude of the counting rate at resonance is related to the solar wind is further seen in Fig. 5. The solar wind velocity is relatively constant over the seven month interval shown; however, the solar wind number density varies by an order of magnitude. In November an unusually high number density in the solar wind was reflected in a very intense resonance. This observation is consistent with the source of ions considered below.

#### THE THERMAL LUNAR EXOSPHERE

The foregoing assumes that the thermal lunar ionosphere is being accelerated into the instrument in the presence of a lunar surface electric field and an artificial electric field arising from the SIDE. This hypothesis is not only supported by the

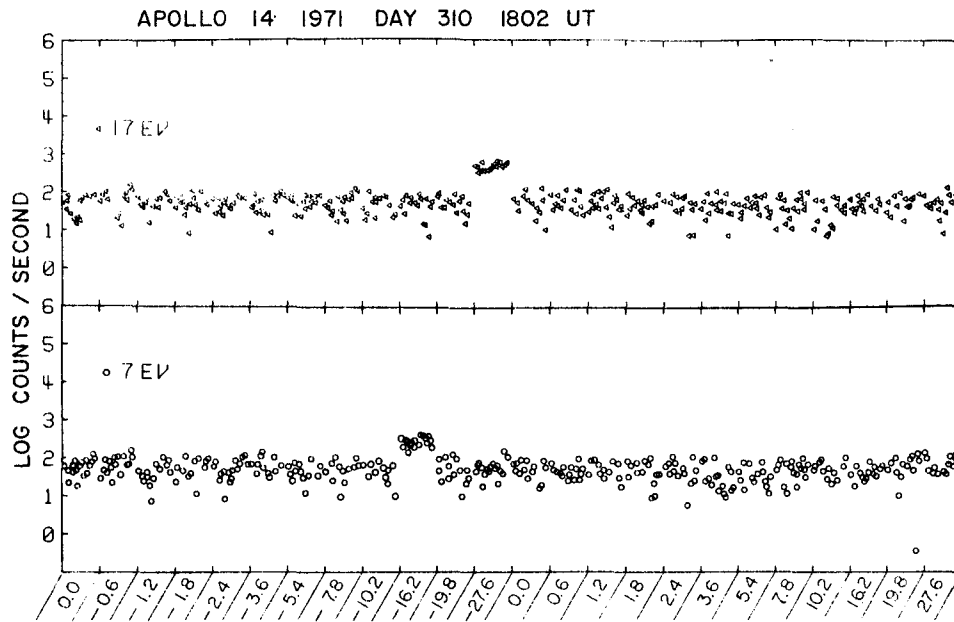


Fig. 3. SIDE total ion detector count rates in two energy channels for a three hour time interval grouped by ground plane stepper voltage. The time given is the start time of the interval.

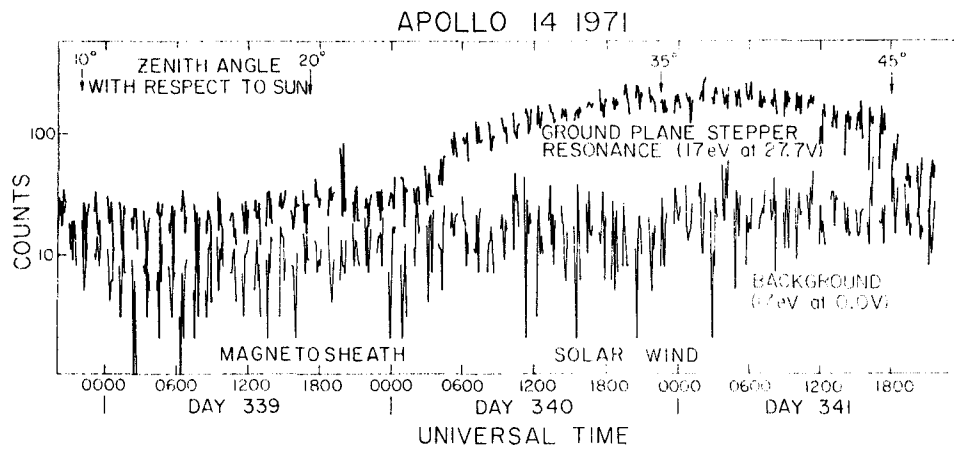


Fig. 4. Typical ground plane stepper resonance seen by Apollo 14 in the lunar afternoon. The counting rates in the resonant channel are compared with those in the 0.0 volt step which were used as a measure of background, i.e., ions not affected by the ground plane voltage. The six data points from  $\frac{1}{4}$ th of the stepper cycle are plotted on an expanded scale in each period of approximately one hour. Note that on this lunation the resonance begins at a solar zenith angle of 10°.

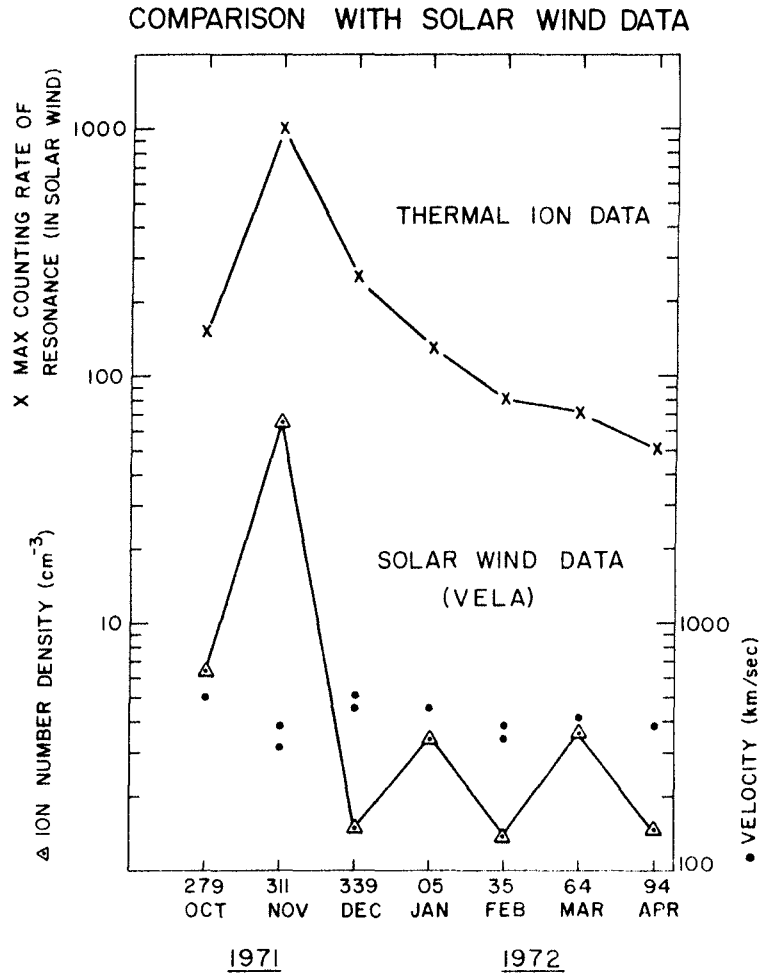


Fig. 5. Comparison of thermal ion data and solar wind data. The maximum counting rate in the resonant step is plotted for each month. Vela data is from *Solar-Geophysical Data*, U.S. Department of Commerce, Boulder, Colorado.

ground plane stepper resonance but also qualitatively by the observed narrow energy spectrum. This spectrum is typically less than the width between detector differential energy channels or  $10 \text{ eV}/q$ . There is an absence of a low energy tail.

Consider the electric field region to be confined to a screening length,  $L$ , analogous to the conventional Debye length. For the solar wind  $L$  is of the order of a few meters. At the lunar surface it is probably much less than this due to photoelectrons and electrons from the ionized neutrals. In any event,  $L \ll H$ , where  $H$  is the scale height of the neutral atmosphere to be ionized. As a result the volume above the detector within 1 screening length is very small compared to

that within the scale height  $H$ . The ions produced in the atmosphere within or above height  $H$  of the detector greatly predominate over those produced within height  $L$ . A large fraction of these will drift thermally or ballistically into the field region. The ion distribution function in energy space will then peak sharply at the potential of the instrument relative to infinity; as is actually observed. (In reality the drift of the thermal ions will also be somewhat influenced by the interplanetary electric field, however, this must be a second order effect because of the high stability of the resonance fluxes despite major changes in the interplanetary magnetic field.)

Assuming focusing to the detector of about 1 steradian we can use the observed ion flux to obtain an order of magnitude estimate of the requisite neutral number density in the lunar atmosphere. Following a treatment given by Manka (1972), for an exponential atmosphere, the omnidirectional ion flux seen by the detector,  $F$ , is related to the neutral surface number density,  $N_0$ , by

$$F \cong \frac{PN_0H}{2} \quad (3)$$

where  $P$  is the total production rate for ions, and  $H$  the scale height for neutrals. Referring to Fig. 3 we take 300 counts/second as typical of the 17 eV ions and calculate a flux of  $3 \times 10^6$  ions/cm<sup>2</sup>sec.

We must now make a choice regarding the composition of the atmosphere. Johnson (1971) has shown that the atmosphere is expected to consist largely of neon. Freeman *et al.* (1971) quote an afternoon surface temperature of 360°K yielding an  $H$  of 100 km for mass 20. Siscoe and Mukherjee (1972) estimate a total ion production rate of  $1.1 \times 10^{-7}$  ions/sec atom for neon. The requisite surface number density is then  $N_0 \sim 5 \times 10^6$  atoms/cm<sup>3</sup>. This is in reasonable agreement with the daytime surface number density reported by the ALSEP cold cathode gauges (Johnson, F. S., private communication).

Although the resonance phenomenon has been seen with the SIDE mass analyzer we have not been able to determine directly the ambient ion masses. Statistics are generally poor and the resonance mass analyzer data often fall in a very low energy channel where mass calibration is uncertain. The only occasion to date on which a well defined mass spectrum has been seen due to the ground plane stepper resonance followed shortly after the Apollo 15 mission. At that time the spectrum was typical of an exhaust gas spectrum. Lindeman, however, has found non-resonance SIDE mass analyzer spectra peaking near mass 20, 36, and 40 believed to represent the ambient lunar atmosphere [Lindeman *et al.*, 1973]. The mass 20  $N_0$  calculation is given here only for illustrative purposes since a correct calculation would require taking into account all of the masses present in their proper abundances.

The enhanced resonance peak in November 1971 (Fig. 5) can be explained by the increased solar wind flux. Bernstein *et al.* (1963) give the charge-exchange cross-section of solar wind protons on neon as  $5 \times 10^{-16}$  cm<sup>2</sup>. As seen from Fig. 5 the solar wind flux reached  $\sim 2 \times 10^9$  ions/cm<sup>2</sup>sec for a production rate of

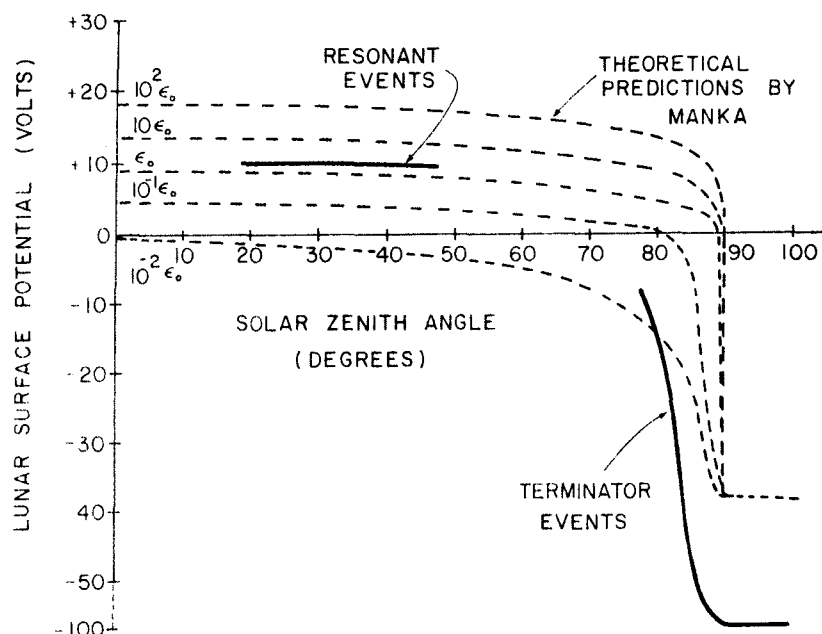
$10^6$  ions/sec atom; easily enough to account for the enhanced resonance during November.

#### DISCUSSION AND SUMMARY

Acceleration of the lunar thermal ionosphere with known voltages has led to the value of at least +10 volts for the dayside lunar surface potential. It should be emphasized this value holds only in the solar wind or magnetosheath plasma. Reasoner and Burke (1972) have reported evidence for potentials as high as +200 volts in the greater vacuum of the magnetospheric tail.

This +10 volt value appears to hold at least between solar zenith angles of  $20^\circ$  and  $45^\circ$ . The increase in intensity of the resonance during passage from the magnetosheath to the free streaming solar wind may be due to a slight change in the lunar surface potential such that the accelerated ions are more nearly centered on an energy passband. This shift in potential might arise from a changing electron temperature. On the other hand, the solar wind may enhance the ionization process itself since it is clear from Fig. 5 that the solar wind does play a key role in the magnitude of the resonance phenomena.

From SIDE data, Lindeman *et al.* (1973) have found that the potential of the lunar surface near the terminator goes from positive to negative as one approaches the lunar night. Figure 6 shows the composite data on the lunar surface



potential together with theoretical calculations by Manka (1972) for typical solar wind conditions. The general shape of the experimental curve is in good agreement with prediction. As pointed out by Manka (private communication), the point at which the potential goes negative and the ultimate night side potential are very sensitive to the assumed solar wind electron temperature.

*Acknowledgment*—We have profited from discussions with several Rice University scientists; particularly Dr. Richard Vondrak and Dr. Robert Manka. The Rice research was supported by NASA contract NAS 9-5911.

A portion of the research reported in this paper was done while one of us (J. W. F.) was a Visiting Scientist at The Lunar Science Institute which is operated by the Universities Space Research Association under Contract No. NSR 09-051-001 with the National Aeronautics and Space Administration.

## REFERENCES

- Bernstein W., Fredricks R. W., Vogl J. L., and Fowler W. A. (1963) The lunar atmosphere and the solar wind. *Icarus* **2**, 233.
- Freeman J. W. Jr., Hills H. K., and Fenner M. A. (1971) Some results from the Apollo 12 suprathermal ion detector. *Proc. Second Lunar Sci. Conf., Geochim. Cosmochim. Acta*, Suppl. 2, Vol. 3, pp. 2093. MIT Press.
- Freeman J. W. Jr., Fenner M. A., Hills H. K., Lindeman R. A., Medrano R., and Meister J., Suprathermal Ions Near the Moon. *Icarus* **16**, 328.
- Grobman W. D. and Blank J. L. (1969) Electrostatic potential distribution of the sunlit lunar surface. *J. Geophys. Res.* **74**, 3943.
- Johnson F. S. (1971) Lunar atmosphere. *Rev. Geophys. Space Phys.* **9**, 813.
- Lindeman R. A., Freeman J. W. Jr., and Vondrak R. (1973) Ions from the lunar atmosphere. *Proc. Fourth Lunar Sci. Conf., Geochim. Cosmochim. Acta*. In press.
- Manka, R. H. (1972) Lunar atmosphere and ionosphere. Ph.D. Thesis, Rice University.
- Manka R. H. and Michel F. C. (1970) Lunar atmosphere as a source of Argon-40 and other lunar surface elements. *Science* **169**, 278.
- Opik E. J. (1962) The lunar atmosphere. *Planet Space Sci.* **9**, 221.
- Opik E. J. and Singer S. F. (1960) Escape of gases from the moon. *J. Geophys. Res.* **65**, 3065.
- Reasoner D. L. and Burke W. J. (1972) Characteristics of the lunar photoelectron layer while in the geomagnetic tail. Paper presented at the *Sixth ESLAB Symposium*, 26–29 September 1972, Noordwijk, Holland.
- Siscoe G. L., and Mukherjee M. R. (1972) Upper limits on the lunar atmosphere determined from solar wind measurements. *J. Geophys. Res.* **77**, 6042.
- Strangway D. W., Chapman W. B., Olhoeft G. R., and Carnes J. (1972) Electrical properties of lunar soil dependence on frequency, temperature and moisture. *Earth and Planet. Sci. Lett.* **16**, 275.

## APPENDIX A

The question of the D.C. coupling between the ground plane and the lunar surface will be examined.

Close-up photographs show that the grid makes contact with the lunar soil at many points and where there is not direct contact the wires are rarely more than a few centimeters from the surface. Strangway *et al.* (1972) have measured the D.C. conductivity of lunar soil samples and found values below  $10^{-11}$  mhos/m in the temperature range of interest. This is sufficiently low that the soil may be considered a perfect insulator and we can direct our attention to conductivity via the plasma only.

The problem can be recast by considering the relative importance of two impedances  $R_i$  and  $R_{LS}$

and thinking of the SIDE as the center terminal in a voltage divider network.  $R_{\infty}$  represents the impedance between the SIDE top wire grid and infinity.  $R_{LS}$  represents the impedance between the ground plane and the lunar surface. In either case the impedance,  $R$  is approximated by

$$R \approx \frac{L}{\sigma A}$$

where  $L$  is the screening length for the plasma,  $\sigma$  its conductivity and  $A$  the effective area of the electrode. (Where the ground plane wire is less than  $L$  from the surface then some mean distance to the surface might replace  $L$ .) We assume that  $L$  and  $\sigma$  are the same at both electrodes and find that the relative impedances are determined by the areas of the two electrodes. The condition of small relative potential difference between the ground plane and the lunar surface, which is

$$R_{\infty} \gg R_{LS}$$

now becomes

$$A_{TG} \ll A_{GP}$$

where  $A_{TG}$  and  $A_{GP}$  are the effective areas of the top grid and ground plane respectively. The ground plane is approximately 65 cm in diameter and contains over 1300 cm of wire. The top is approximately  $10 \times 12$  cm and consists of knit wire mesh. We estimate

$$\frac{A_{TG}}{A_{GP}} \approx 0.01$$

and hence conclude that the potential difference between the ground plane and the lunar surface is a small fraction of the lunar surface potential relative to infinity.

## APPENDIX B

In the case of a screening length long compared to the dimension of the SIDE above the lunar surface ( $\sim 50$  cm) the lunar surface potential field may overwhelm the SIDE top grid field some distance out and set up a positive potential barrier for positive ions attempting to reach the SIDE. This suggests the possibility of non-negligible initial ion energies,  $E_i$ . One must then ask what the initial energy source might be since the resonance is clearly the result of lunar atmospheric ions as is demonstrated by the observed number density and the mass spectra seen on at least one occasion. Ion acceleration by the interplanetary electric field as discussed by Manka and Michel [1970] is frequently seen in the SIDE ion data, however, this leads to a sporadic highly directional and energy varying flux unlike the stable monochromatic flux associated with this resonance phenomenon. No other ion acceleration mechanisms are known that are appropriate to this zenith angle regime, hence we prefer the assumption of a smaller screening length and negligible  $E_i$ . In any event, our value for the lunar surface potential stands as a lower limit.





Lunar Electric Fields, Surface  
Potential and Associated Plasma Sheaths+

by

J. W. Freeman and M. Ibrahim

Department of Space Physics and Astronomy

Rice University

Houston, Texas

77001

U.S.A.

~~Submitted~~ Accepted by The Moon 3, 368-379, 1975.

- + Presented at the Conference of Interactions of the Interplanetary Plasma with the Ancient and Modern Moon, Lake Geneva, Wisconsin, October, 1974.

## Abstract

This paper reviews the electric field environment of the moon. Lunar surface electric potentials are reported as follows:

Solar Wind Dayside:  $\phi_0$  +10 to +18V

Solar Wind Terminator:  $\phi_0 \sim -10$  to  $-100$  V

Electron and ion densities in the plasma sheath adjacent to each surface potential regime are evaluated and the corresponding Debye length estimated. The electric fields are then approximated by the surface potential over the Debye length. The results are:

Solar Wind - Dayside:  $E_0 > 10$  V/m outward

Solar Wind - Terminator:  $E_0 \sim 1$  to  $10$  V/m inward

These fields are all at least 3 orders of magnitude higher than the pervasive solar wind electric field however they are confined to within a few tens of meters of the lunar surface.

## Lunar Electric Fields, Surface Potential, and Associated Plasma Sheaths

Any body emersed in a plasma acquires a net negative charge. A body exposed to intense ultra-violet radiation is inclined to acquire a positive charge. The Moon enjoys both of these environments simultaneously. As a result one expects a complicated surface charge distribution on the lunar surface.

Figure 1 shows the general environment of the Moon. On the left hand side is shown the continuous flux of photons from the sun, as well as solar wind protons and electrons. The photon flux dominates the solar wind proton flux and results in the ejection of photoelectrons from the sunlit lunar surface. We expect therefore that the dayside will exhibit a positive lunar surface potential. As one progresses towards the terminator regions where the solar wind proton and photons impact the surface at more oblique angles, the solar wind electrons, which have high random velocities, still have free access to the lunar surface with normal incidence. One therefore expects the potential to grow more and more negative as the terminator region is approached. A negative potential at the terminator is predicted.

Figure 2 illustrates these speculations more completely. We see here the positive potential on the dayside surface of the Moon and immediately adjacent to this positive potential, the regions of negative potential generated by the photoelectrons ejected from the lunar surface by the solar ultraviolet photons. This photoelectron sheath contains electron number densities on the order of several thousands to tens of thousands of electrons per cubic centimeters. It is confined to a region within a few meters of the lunar surface.

The surface potential becomes smaller and eventually goes negative as one approaches the terminator region. Above the negative surface potential in the terminator region we find a positive ion sheath made up of atmospheric ions. The positive charge regions above the surface may result in part from electron depletion, however, positive ions are seen.

This distribution of charges will give rise to electric fields in the vicinity of the Moon. These electric fields will be superimposed on the interplanetary electric field generated by the motion of the solar wind magnetic field past the Moon (The so-called  $\vec{v} \times \vec{B}$  or solar wind electric field). This electric field is approximately 3 orders of magnitude weaker but much more extensive than the electric field associated with the lunar surface potentials. The interplanetary electric field has received considerable

attention and will be the subject of several other papers at this conference so the balance of this paper will concentrate on the electric fields associated with the lunar surface potential.

Table 1 illustrates previous theoretical calculations aimed at determining the dayside lunar electric potential. Öpik and Singer [1960] were the first workers to attempt to estimate the electric potential of the dayside of the Moon. Their results, based on energy balance considerations, indicated potentials on the order of +20 to +25 volts. More recently, Grobman and Blank [1969] using collisionless probe theory estimated a range of potentials from approximately +10 volts down to practically zero depending on the assumed values for the photoelectric electron yield function and the work function of the lunar surface materials. Manka [1973] carried out similar calculations based on current balance. He found potentials ranging from approximately +4 volts to +9 volts positive depending again on assumptions about the photoelectron yield function. In a more elaborate calculation, Walbridge [1973] divided the photon flux from the Sun into 3 energy ranges. He found three corresponding electron energy distributions giving a surface potential on the order of +3.5 volts or greater for the dayside of the Moon.

Since all of these theories depend explicitly on the photoelectric yield function and the work function of the surface, Feuerbacher et al. [1972] undertook to make measurements of these functions on actual lunar soil materials. Their results indicated .07 for the photoelectron yield function and 5 eV for the work function. Reasoner and Burke [1972] using data from the CPLEE experiment were able to make in situ estimates of the work function and the photoelectric yield. Their data, which were taken when the moon was in the geomagnetic tail, indicate values for both of these numbers, in rough agreement with those of Feuerbacher et al. Based on this, the lower limit for the surface potential given by Grobman and Blank is inapplicable and the predicted lunar surface potentials range in value from few volts to 25 volts positive.

Experimental values for the lunar surface potential have been obtained by the apollo lunar surface suprathreshold ion detector experiment (SIDE) [Freeman et. al., 1973]. Figure 3 illustrates the configuration of the SIDE as deployed on the lunar surface. Immediately beneath the SIDE instrument is a ground plane electrode. This ground plane electrode is wired to a stepping supply inside the SIDE detector, which is in turn referenced to the SIDE ground. A small wire mesh grid immediately above the input aperture for the ion detectors is also wired to SIDE ground. Through

this stepping supply it is possible to alter the electric potential of the SIDE instrument relative to the lunar surface. When the stepping supply is negative, ions generated in the lunar atmosphere by solar ultraviolet and ionization from the solar wind can be accelerated directly into the instrument and the energy with which they are detected will be given by equation 1; assuming of course that the lunar surface is positive.

$$\epsilon/q = \epsilon_i/q - (\phi_o + \phi_s). \quad (1)$$

$\epsilon$  is the detection energy,  $\epsilon_i$  the ion initial energy,  $\phi_o$  and  $\phi_s$  the lunar surface potential and stepping supply potentials respectively, and  $q$  is the ion charge (assumed to be unity). The SIDE actually measures energy per unit charge in 20 discrete differential steps from 10 ev/q to 3500 ev/q for positive ions. The ground plane stepper has 23 discrete voltage levels. See Freeman et al. [1973] for a table of measurable lunar surface potentials.

We note the assumption that the initial energy of the ions is negligible compared to the energy acquired by acceleration by the instrument and the lunar surface potential. The initial energy of the ions is the thermal energy of the neutral atoms from which they originated. The assumption of negligible energy is therefore justified. However, if the initial energy is nonnegligible the calculated values for the lunar surface potential represent lower limits.

As the SIDE steps through various energy channels and ground plane stepping voltages "resonances" occur which consist of enhanced detector response in the energy channels appropriate to the instantaneous lunar surface potential for each ground plane stepping voltage. Figure 4 illustrates an example of these resonances in the actual raw SIDE count rate data. One can see a resonance in the 7 eV/q channel at the -16.2 ground plane stepping voltage, and another in the 17 eV/q channel, at the -27.6 ground plane stepping voltage. These two numbers taken together indicate a lunar surface potential of approximately +10 volts at this particular time.

The overall results of the SIDE instrument lunar surface potential measurements are illustrated in Figure 5. Here we have plotted the electric potential on the lunar surface as a function of the solar zenith angle. For most of the late morning and early afternoon the lunar surface potential is in the vicinity of +10 volts. A new result, reported here for the first time, is an asymmetry in this curve in the form of a small ear in the late lunar afternoon. Here the lunar surface potential rises to approximately +18 volts. This effect is seen at the Apollo 15 site but not at the Apollo 14 site due to an instrumental effect.

Notice from Figure 5, in early morning and late afternoon the surface potential goes to negative values as the terminator is approached. The potential measurements



in these regimes are not made by the technique just described, but rather are derived from a set of data which will be described.

Goldstein [1974] has analyzed electron data from the ALSEP Solar Wind Spectrometer experiment and computed a lunar surface potential of the subsolar point in the solar wind of +5 to -3 volts. The discrepancy between this result and the SIDE data has not yet been resolved.

Manka [1973] has investigated the lunar surface potential in the vicinity of the terminator regions. Figure 6 shows his theoretical curves indicating an asymptotic potential at the terminator of about -35 volts. This value is highly dependent on the solar wind electron temperature and could in fact be considerably more negative at times. These theoretical curves bear a strong similarity to the observed potential curves shown in figure 5.

Actual data on the lunar surface potential in the vicinity of the terminator can be obtained by the SIDE instrument through the observations of the atmospheric ions associated with the ion sheath adjacent to the lunar surface [Lindeman et al., 1973]. These ions reach the surface with peak energies corresponding to the lunar surface potential. As the SIDE approaches the terminator region very low energy ions are seen first. These energies increase gradually as the instrument passes the terminator. This phenomena is illustrated in figure 7. Here we see ions of approximately

10 electron volts about 1.5 days prior to the terminator. About 0.5 days before terminator crossing the ion energies begin to climb until they reach values of 70 electron volts approximately 0.5 days after the terminator crossing. This is believed to be a direct observation of the ambient lunar ions generated in the atmosphere by ultraviolet ionization and accelerated to the lunar surface by the negative surface potential. The energy in the ions is therefore a measurement of the lunar surface potential itself. Lindeman et al. [1973] have shown these potentials to go as low as -100 volts on some terminator crossings. It is interesting to note that -70 volts is about the potential expected for a stationary plasma whose ion and electron temperatures are  $10^5$  and  $2 \times 10^5$ °K, the temperatures appropriate to the solar wind. This calculation uses the potential expression given by Chopra [1961] for a body in a stationary plasma.

The fact that these ions are indeed ambient atmospheric ions is verified by some sample ion mass spectra also taken by the SIDE as shown in figure 8.

The terminator electric potentials measured in this manner can be verified independently by the energy spectra of ions accelerated toward the moon by the interplanetary electric field. These ions show the expected exponential spectra [Manka and Michel, 1973] offset by an amount of energy equal to that obtained in falling through the surface potential field. We thus have two independent determinations

of the terminator surface potentials.

No theoretical studies have been published on the electric potential of the lunar nightside and because of the absence of a strong ionizing mechanism our experimental techniques for the day and terminator regions are of no value here. A complete analysis of the problem involves a detailed study of the solar wind electron temperature and the ways, if any, in which it might be modified on the night side of the moon. Reasoner [private communication] has CPLEE electron data which may prove helpful in this regard.

Schneider and Freeman [1974] and Freeman [1972] have reported ions of slightly less than solar wind energy whose flux is 2 orders of magnitude below that of the solar wind appearing on the night side of the moon. These ions tend to occur most frequently several days before local sunrise and several days after sunset, however, they have been seen throughout the entire lunar night. Whether or not these ions constitute a component of the lunar ionosphere remains to be seen. Certain  $\vec{E}_{sw} \times \vec{B}_{sw}$  ion trajectories do allow transfer of atmospheric ions from the dayside to the nightside [Manka, private communication]. The energy of the ions however suggests solar wind that has been diverted to the night side of the moon by some mechanism. One conceivable approach is to consider these ions to form the positive ion sheath for a negative nightside surface potential; in which case the deflecting force is electrostatic and the surface

potentials required would be negative several hundred volts. We recall that the terminator nightside potential is indicated to be of the order of -100 volts. Alternatively, these ions may arise from a turbulence or solar wind thermalizing process associated with limb shocks or the passage of the moon through the solar wind.

Next we direct our attention to the lunar surface potential in the geomagnetic tail.

Knott [1973] has pointed out that energetic electrons found in the plasma sheet can be expected to drive the nightside of the moon to several kilovolts negative on occasions. Such large potentials are found on satellites in the tail during eclipses [DeForest, 1972].

Regarding the day side potential for the moon in the geomagnetic tail, Reasoner and Burke [1972] have reported observations of photoelectrons in the photoelectron sheath whose cut-off energy indicate dayside potentials ranging up to approximately +200 volts. Furthermore, they saw these potentials depressed to below their limit of detectability, +40 volts, when the moon entered the plasma sheet during an intense magnetic storm. The SIDE data show resonances, similar to those described above, in some regimes in the geomagnetic tail and indicates at those times potentials +10 volts or greater. A detailed comparison of the SIDE and CPLEE data has not yet been made for periods of simultaneous

data. It appears that the lunar surface potential can have a wide range of values in the tail depending on local plasma conditions. We expect more complete reports on tail potentials in the future. For completeness, the currently reported or predicted tail potentials are summarized in Table 2.

Finally we discuss the electric fields associated with these surface potentials. For the photoelectron layer Walbridge [1973] calculates a field of the order of 10 to 15 volts/meter. This is consistent with our surface potential of 10 volts if the effective screening length is 1 meter. Feuerbacher et al. [1972] calculate 78 cm for the screening length.

In the terminator region we assume the Debye length to be that of the solar wind or approximately 10 meters. Therefore, the electric field over the region where the surface potential can be determined by the SIDE is of the order of 1 to 10 volts/meter and directed radially inward.

The situation is much less certain on the far night-side. For the sake of completeness in this review we will speculate that the energetic ions ( $N_0 \sim 0.05 \text{ ion/cm}^3$ ) form an ion sheath for a surface potential of the order of -100 volts, and that their effective temperature is that of the solar wind or  $\sim 10^5 \text{ K}$ . In this case, the Debye length is of the order of 100 meters and the electric field is 1 volt/meter directed radially inward.

Figure 2 summarizes the electric charge distribution around the moon. The ion number densities shown,  $N_0$ , are those measured by the SIDE at the lunar surface. The ions forming the atmospheric ion sheath at the terminator are those illustrated in Figure 7. The nightside ions are those reported by Schneider and Freeman [1974].

Superimposed on the surface electric fields is the electric field of the solar wind whose value is of the order of  $2 \times 10^{-3}$  volts/meter. This field dominates any ion trajectory calculations at distances from the Moon greater than the Debye screening length.

Figure 9 illustrates these electric field configurations. The electric fields considered in this paper are only large scale fields. As Criswell [1972, 1973] has pointed out small scale fields may be very intense.

Given these electric fields, it is possible to make calculations on the ion trajectories for ions arising from ionization of the lunar atmosphere. The results of these calculations are the subject of the paper by Vondrak and Freeman [1974]. Similar calculations are also presented by Manka and Michel [1973].

In summary, the gross electric field distribution in the vicinity of the Moon is understood. The next task before us is to determine the effect of this electric field distribution on the lunar ionosphere. In this connection we

note that only a small fraction of the lunar atmosphere is found above the lunar surface at any time. The lunar atmosphere is essentially a solid state atmosphere residing beneath the lunar surface in the soil fines. This remarkable type of atmosphere is sustained, in part, by the ability of these electric fields to return ions to the surface with high velocities. We might say that the lunar atmosphere (at least for some gases) is recycled. Having established the electric field environment, it is now possible to proceed to consider quantitatively its effect on the ion return or reimplantation rates.

### Acknowledgement

We gratefully acknowledge helpful discussions with many numbers of the Rice Space Physics and Astronomy Department, in particular Dr. H. K. Hills. This research was supported by NASA contract NAS9-5911.



## References

- Criswell, D. R., Lunar Dust Motion, Suppl. 3, Geochim. et. Cosmochim. Acta. B, 2671, 1972.
- Criswell, D. R., Photoelectrons and the Solar Wind Lunar Limb Interaction, The Moon, 7, 202, 1973.
- Chopra, K. P., Interactions of Rapidly Moving Bodies In Terrestrial Atmosphere, Rev. Mod. Phys., 33, 153, 1961.
- DeForest, S. E., Spacecraft Charging at Synchronous Orbit, J. Geophys. Res., 77, 651, 1972.
- Feuerbacher, B., M. Anderegg, B. Fitton, L. D. Laude and R. F. Willis, Photoemission from Lunar Fines and the Lunar Photoelectron sheath, Suppl. 3, Geochim. et. Cosmochim. Acta., 3, 2655, 1972.
- Freeman, J. W. Jr., Energetic Ion Bursts on the Nightside of the Moon, J. Geophys. Res., 77, 239, 1972.
- Freeman, J. W., M. A. Fenner and H. K. Hills, The Electric Potential of the Moon in the Solar Wind, Photon and Particles Interactions with Surfaces in Space, R. J. L. Garard (ed.) D. Reidel Pub. Co., 1973. Also see J. Geophys. Res., 78, 4560, 1973
- Goldstein, Bruce E., Observations of Electrons of the Lunar Surface, J. Geophys. Res., 79, 23, 1974.
- Grobman, W. D. and J. L. Blank, Electrostatic Potential Distribution of the Sunlit Lunar Surface, J. Geophys. Res., 74 3943, 1969.

- Knott, K., Electrostatic Charging of the Lunar Surface and Possible Consequences, J. Geophys. Res., 78, 3172, 1973.
- Lindeman, R. A., J. W. Freeman and R. Vondrak, Ions from the Lunar Ionosphere, Geochim. et. Cosmochim. Acta. Supplement 3, 3, 2889, 1973.
- Manka, Robert H., Plasma and Potential at the Lunar Surface; Photon and Particle Interactions with Surfaces in Space, R. J. L. Grard (ed) D. Reidel Publishing Co. 1973. Also see R. H. Manka, Lunar Ion Energy Spectra and Surface Potential, Supplement 4, Geochim. et. Cosmochim. Acta., 3, 2897, 1973.
- Manka, R. H., F. C. Michel, Lunar Ion Energy Spectra and Surface Potential, Supplement 4, Geochim. et. Cosmochim. Acta., 3, 2897, 1973.
- Opik, E. J. and S. F. Singer, Escape of Gases From the Moon, J. Geophys. Res., 65, 3068, 1960.
- Reasoner, D. L. and W. J. Burke, Characteristics of the Lunar Photoelectron Layer in the Geomagnetic Tail, J. Geophys. Res., 77, 6671, 1972. Also see J. Geophys. Res., 78, 5844, 1973.
- Schneider, H. E. and J. W. Freeman, Energetic Lunar Night-time Ion Events, Conference of Interactions of the Interplanetary Plasma with the Modern and Ancient Moon, Lake Geneva, Wisconsin, 1974. Abstract volume available from the Lunar Science Institute, Houston, Texas, 77058.

Vondrak, R. R. and J. W. Freeman, The Lunar Ionosphere,  
Conference on Interaction of the Interplanetary Plasma  
with the Modern and Ancient Moon, Lake Geneva, Wisconsin,  
1974. Abstract volume available from the Lunar Science  
Institute, Houston, Texas 77058.

Walbridge, E., The Lunar Photoelectron Layer 1: The  
Steady State, J. Geophys. Res., 78, 3668, 1973.

### Figure Captions

1. The solar wind plasma and solar photon environment of the moon.
2. The electric charge distribution on and near the moon.
3. The mechanical and schematic details of the deployed SIDE.
4. Raw data from the SIDE differential energy channels as a function of ground plane stepper voltage (voltage of the SIDE relative to the ground plane).
5. The measured lunar surface potential,  $\phi_0$ , as a function of solar zenith angle.
6. Theoretical predictions of the lunar surface potential versus solar zenith angle prepared by Manka [1973].
7. SIDE total ion detector 20 minute average count rate energy spectra versus time. The short time is at the bottom of the figure and increases along the y axis. The vertical log count scales are 24 hours apart. Energy along the x axis is in eV/q. The differential energy channels are as follows: 10, 20, 30, 50, 70, 100, 250, then increasing by 250 up to 3500 eV/q. Shortly after the start time at least three energy peaks are apparent. The lowest energy peak is due to ambient ions accelerated by the lunar surface potential. The peak at around 1000 eV/q may be turbulent solar wind whose flow has been disrupted by a limb shock.

The higher energy peak, whose upper limit is outside our energy range, is due to protons escaping from the bow shock front of the earth. These protons are seen on and off throughout this time period.

8. A mass per unit charge spectrum from the SIDE mass analyzer showing three peaks tentatively attributed to helium, neon and argon. This spectrum, taken during a terminator crossing verifies that the low energy ions seen are from the lunar atmosphere and not accelerated solar wind ions.
9. The electric field environment of the moon.

TABLE 1

## SUNLIT LUNAR SURFACE IN THE SOLAR WIND

WORKERS	METHOD	$\gamma$	W(ev)	$\phi_0$ (volts)	No ( $\frac{\text{elect}}{\text{cm}^3}$ )	$\lambda_D$ (M)
Opik and Singer (1960)	Energy Balance			+20 to 25		
Grobman and Blank (1969)	Probe Theory	0.001	4	+0.6		
		0.01	6	+10.2		
Manka (1973)	Current Balance	$I_p \sim 5 \times 10^{-9} \text{ amp cm}^{-2}$		+9		
		$I/10 I_p$		+4		
Walbridge (1973)	3 Ranges of Energy	0.2	6	$\geq +3.5$	$5 \times 10^3$ $10^5$	0.6 0.04
Feuerbacher et al. (1972)	Lunar Soils	0.07	5		130	0.78
Reasoner and Burke (1972)	CPLEE Photoelectron Data	0.05	6	Tail Data Only		

TABLE 2

## LUNAR SURFACE POTENTIAL IN THE TAIL

WORKERS	METHOD	NIGHTSIDE	DAYSIDE
Knott (1973)	From plasmashet electron spectra	~several kv in plasmashet	
Reasoner and Burke (1972)	CPLEE photoelectron data		$\leq +40$ to $+200$ v
Freeman and Ibrahim	SIDE ion resonance data		$\geq +10$ v

THE  
SOLAR  
WIND

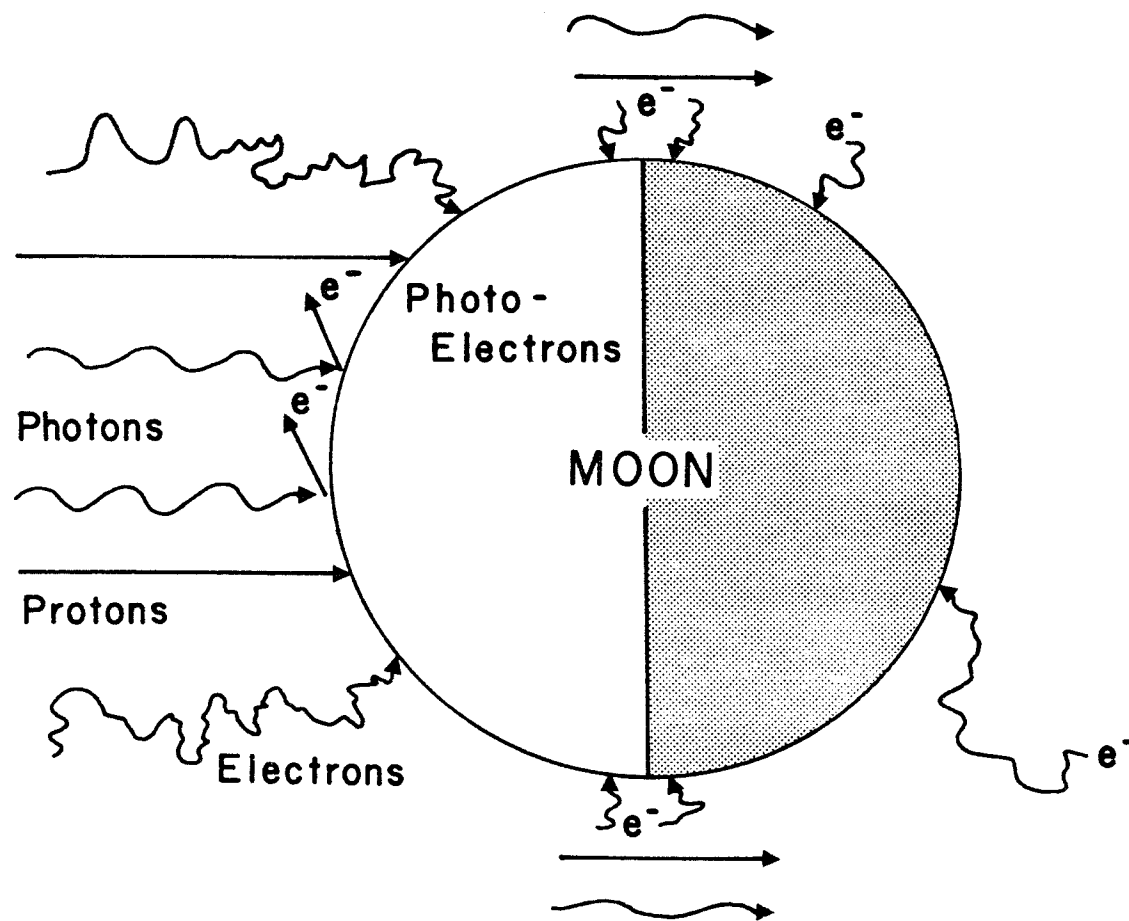


Figure 1



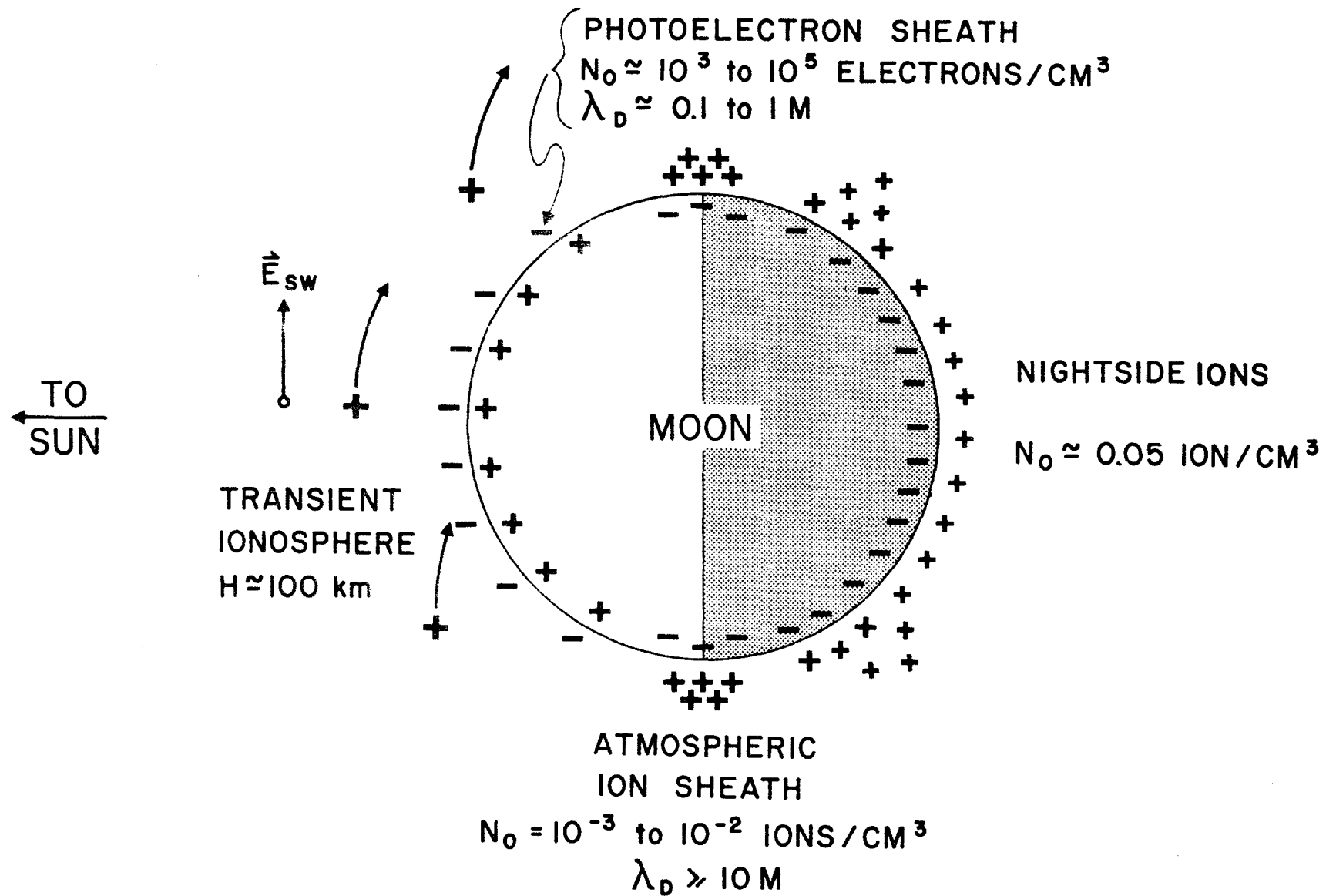
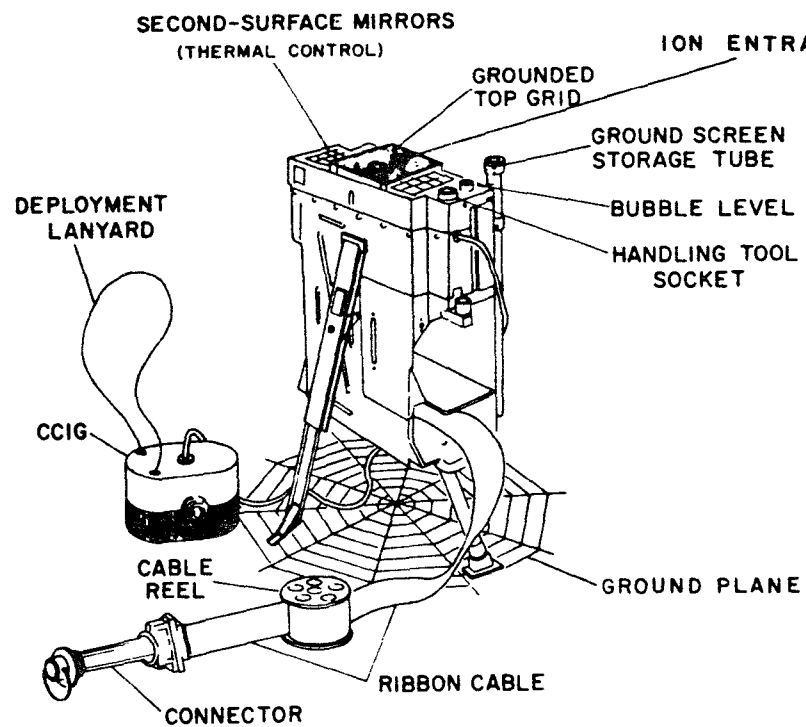
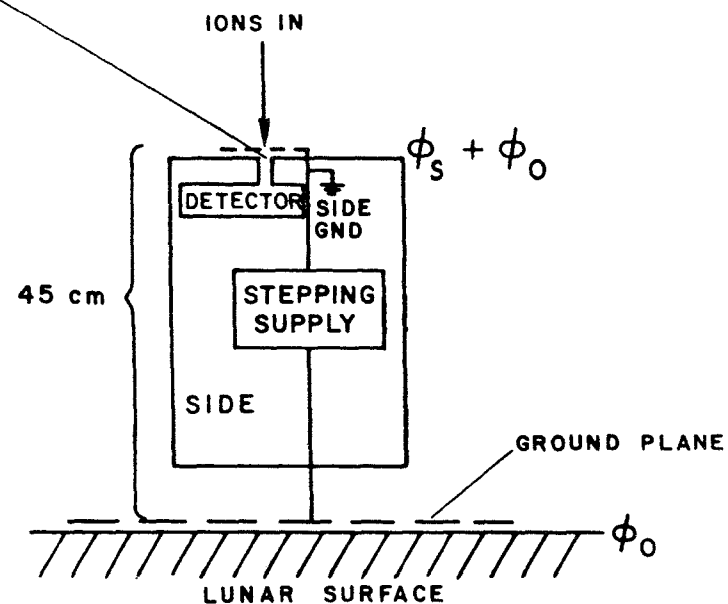


Figure 2



APOLLO 14 SIDE Deployed Configuration  
(a)



Schematic of the Instrument Configuration  
(b)

Figure 3

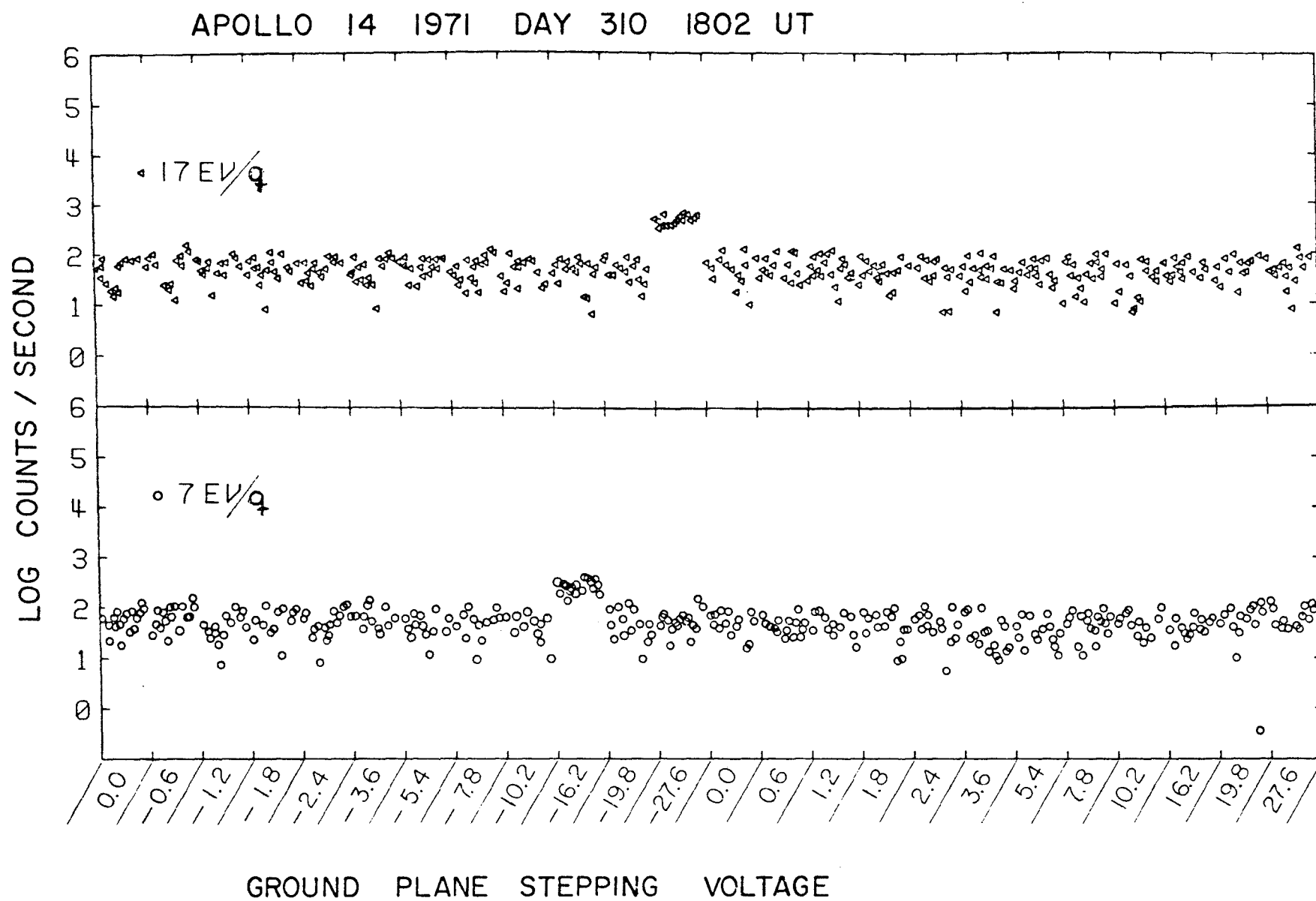
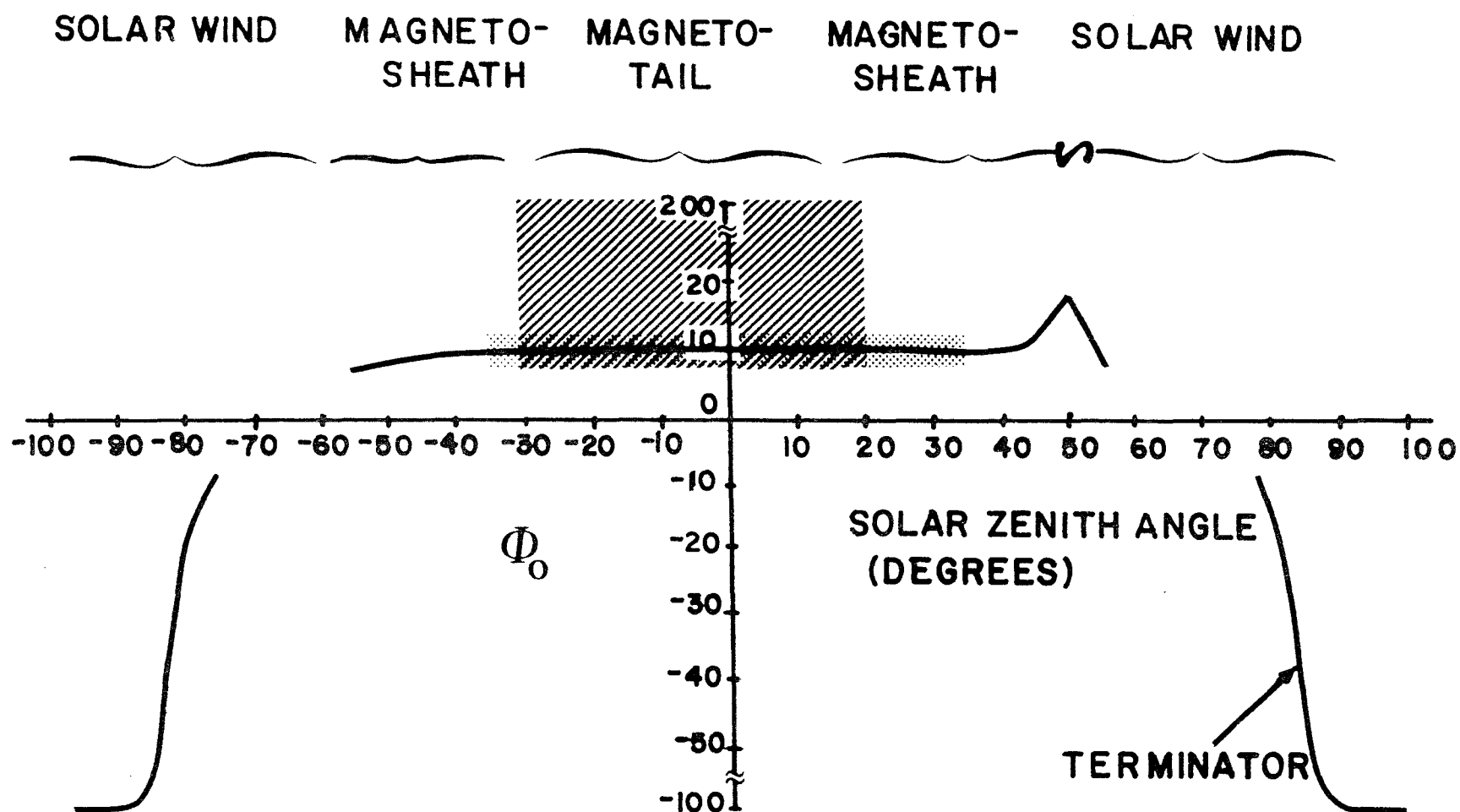


Figure 4



$\Phi_0$  = LUNAR SURFACE POTENTIAL (VOLTS)

▒ = RANGE OF UNCERTAINTY

/// = RANGE OF POSSIBLE POTENTIALS

Figure 5

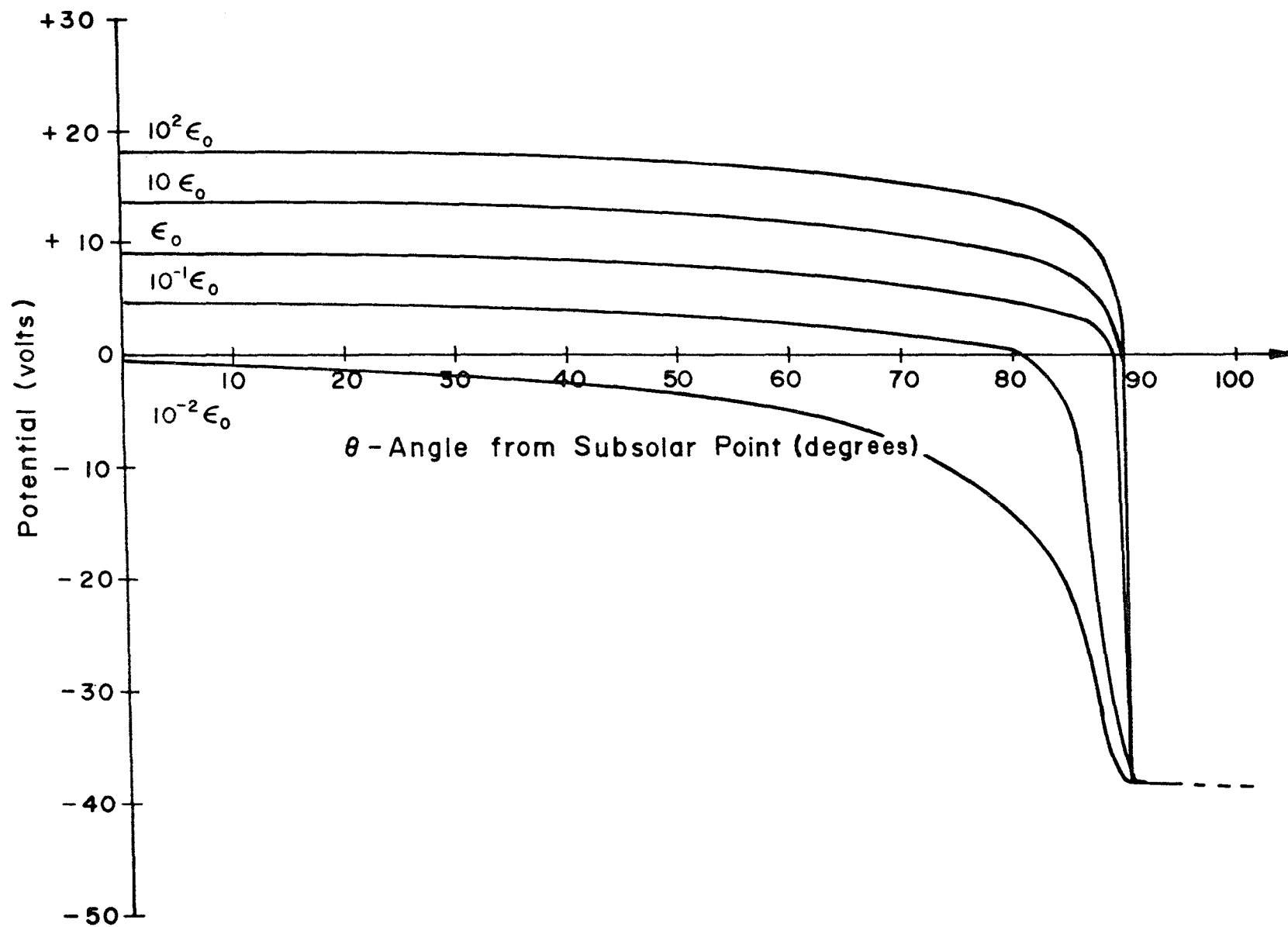


Figure 6

APOLLO 14 71  
START TIME 137 8 26  
20 MIN AV  
24.00HR/DIV

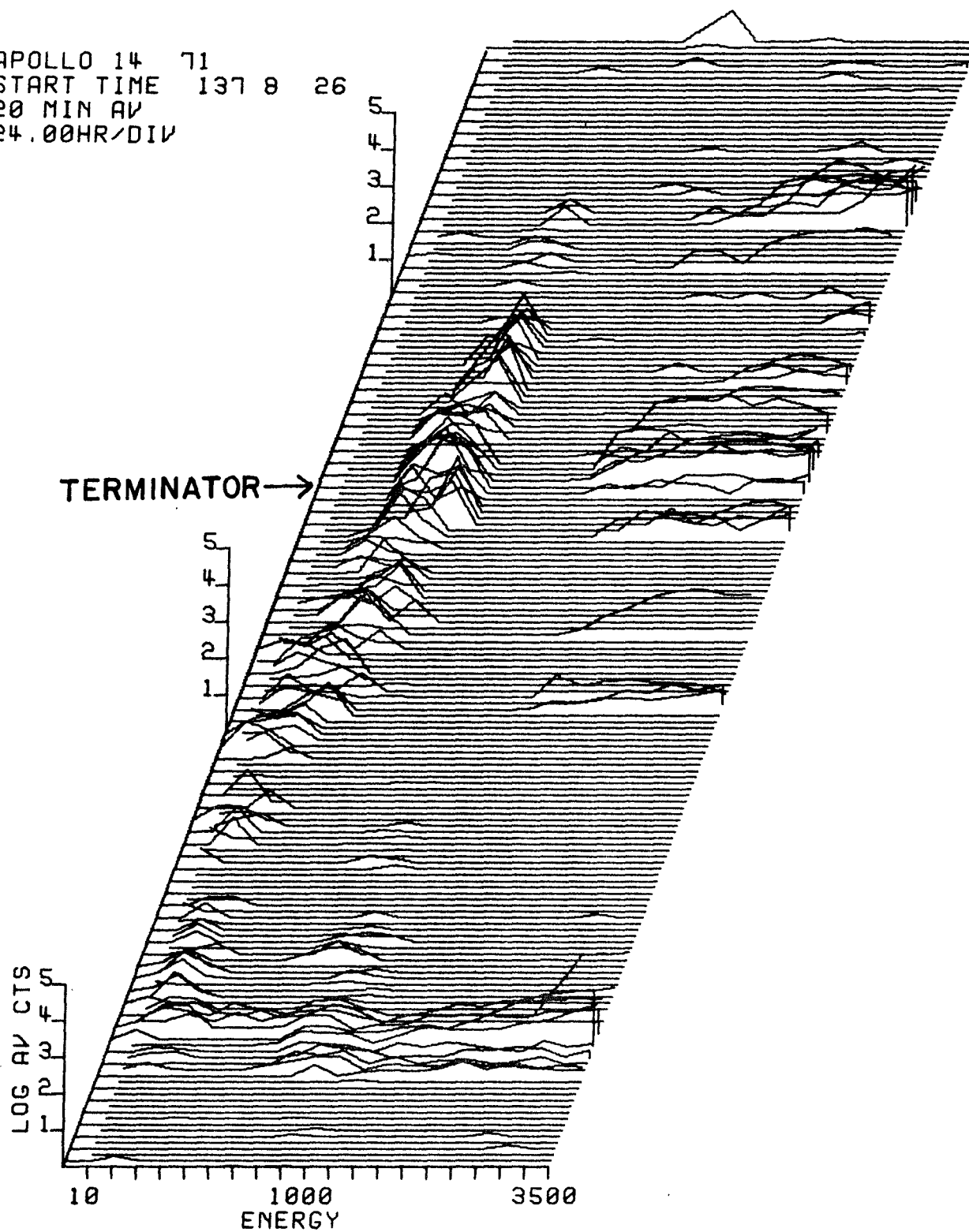


Figure 7

# Event 14

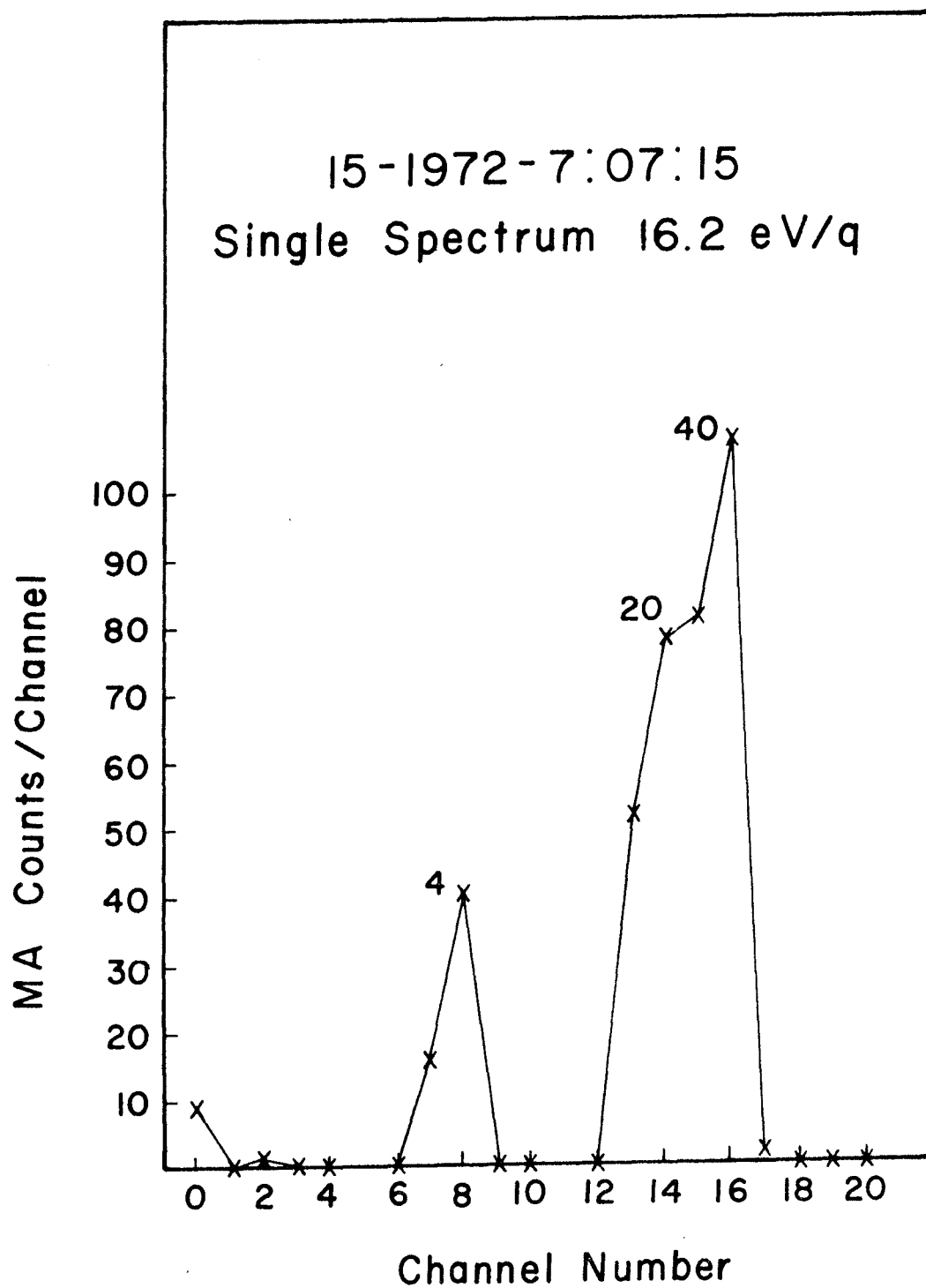


Figure 8

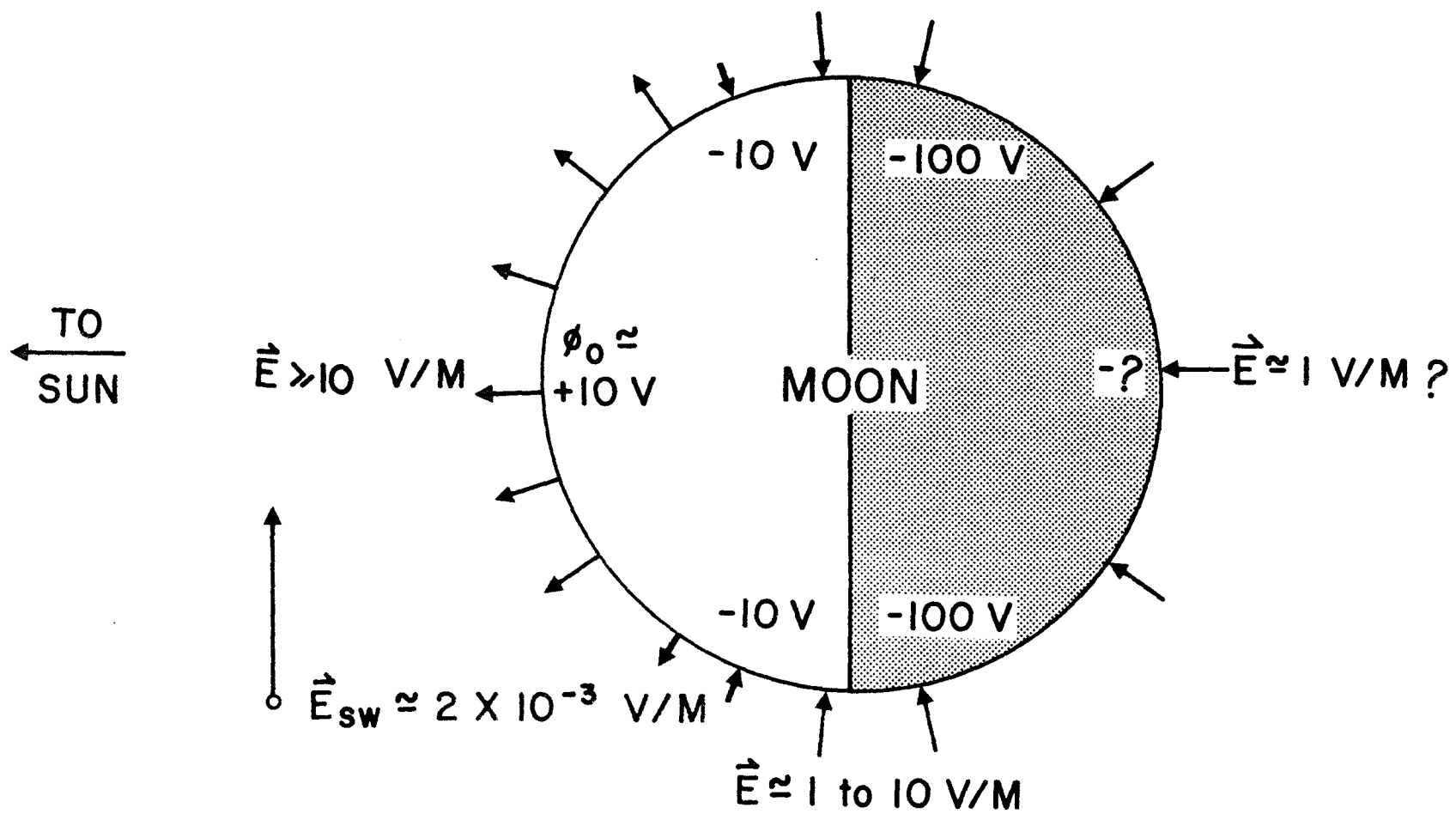


Figure 9





RICE UNIVERSITY

An Observation of Lunar Nighttime Ions

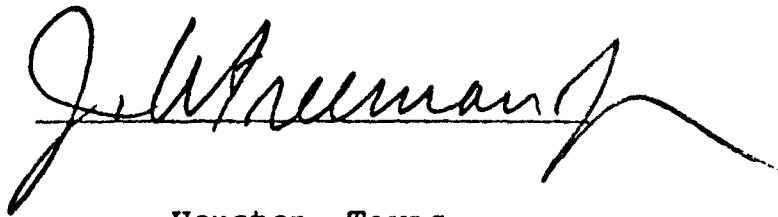
by

Henry Emil Schneider

A THESIS SUBMITTED  
IN PARTIAL FULFILLMENT OF THE  
REQUIREMENTS FOR THE DEGREE OF

Master of Science

Thesis Director's Signature:

A handwritten signature in dark ink, appearing to read "J. A. Freeman", is written over a horizontal line. The signature is fluid and cursive, with a long, sweeping tail that extends to the right.

Houston, Texas

April 28, 1975

Are there frogs on the moon?



## ABSTRACT

### An Observation of Lunar Nighttime Ions

by

Henry Emil Schneider

The Rice University Suprathermal Ion Detector Experiment deployed on Apollo missions 12, 14, and 15 regularly observes ion events all through the lunar night.

The ion events are most often less than 4 hours in duration, and usually less than one hour.

The energy spectra of the events vary from mono-energetic at 250 eV/q to 500 eV/q to fairly broad. The energy represented may range from 250 eV/q to 1500 eV/q. There is some indication that the peak energy of the events increases from 500 eV/q at local sunset to 750 eV/q at about 3 days before local sunrise and then decreases to 250 eV/q 1 day before the sunrise terminator crossing.

The ion energies are generally less than the solar wind and the ion flux ( $\approx 10^6$  ions/cm<sup>2</sup>-sec-ster) is down by 2 orders of magnitude from the solar wind.

Ion activity increases in the period 1 to 6 days prior to local sunrise with a peak at 2 to 3 days before sunrise. There is also a weak secondary activity peak 3 to 4 days after local sunset.

Data from the Apollo 12 SIDE has not been looked at yet. The Apollo 14 and Apollo 15 SIDE's both exhibit the same activity profile. This fact suggests a local lunar time dependence rather than a position in orbit for the occurrence of these events.

## ACKNOWLEDGEMENTS

I wish to thank my thesis advisor, Dr. John W. Freeman, Jr., for his help and encouragement in the preparation of this work. Without his support and suggestions, this thesis would not have been possible.

My thanks go also to John Benson and Mohammed Ibrahim for many helpful discussions about this work. I would also like to thank Dr. H. Kent Hills, Dave Nystrom, and Lynne Mutchler, all of whom aided in my understanding of the SIDE data and in the operation of the SDS 920 computer system.

My very special thanks and love go to my wife Donna for the encouragement and moral support that she gave me.

This research was supported by NASA contract NAS 9-5911.

## CHAPTER 1 - INTRODUCTION

This thesis is concerned with the study of the plasma interaction with the moon when the moon is outside the earth's magnetosphere and in the interplanetary medium.

### 1.1 INTRODUCTION TO THE SIDE

The six Apollo lunar missions placed a number of particles and fields experiments directly on the lunar surface as a part of the Apollo Lunar Surface Experiment Package (ALSEP). These experiments study the lunar plasma environment. The results reported in this thesis come from the data reduction of one such experiment, the Rice University Suprathermal Ion Detector Experiment (SIDE). The SIDE is an ion spectrometer.

The scientific objectives of the SIDE were summarized by Freeman et al. [1970] as follows:

1. Provide information on the energy and mass spectra of positive ions close to the lunar surface resulting from solar UV or solar wind ionization of gases from any of the following sources:
  - a. A residual primordial atmosphere of heavy gases.
  - b. Sporadic outgassing such as volcanic activity.
  - c. Evaporation of solar wind gases accreted on the lunar surface.
  - d. Exhaust gases from the LM ascent and descent motors and the astronaut portable life support equipment.
2. Measure the flux and energy spectrum of positive ions in the earth's magnetotail and magnetosheath during those periods when the moon passes through the magnetic tail of the earth.

## TABLE OF CONTENTS

CHAPTER 1 - INTRODUCTION	1
1.1 INTRODUCTION TO THE SIDE	1
1.2 GENERAL BACKGROUND - EXPERIMENTAL RESULTS	2
1.3 GENERAL BACKGROUND - THEORY	4
1.4 RESEARCH OBJECTIVES	6
 CHAPTER 2 - INSTRUMENT	 7
2.1 BASIC PHYSICS OF OPERATION	7
2.2 INSTRUMENT DESIGN	11
2.3 CALIBRATION	13
2.4 DEPLOYMENT AND ORIENTATION IN SPACE	16
 CHAPTER 3 - DATA	 19
3.1 INTRODUCTION	19
3.2 OBSERVATIONS	20
3.3 CORRELATION WITH K <sub>p</sub>	25
3.4 OBSERVATIONAL CONCLUSIONS	29
3.5 DISCUSSION	31
3.6 TOPICS FOR FURTHER INVESTIGATION	34
 REFERENCE LIST	 36

3. Provide data on the plasma interaction between the solar wind and the moon.
4. Determine a preliminary value for the electric potential of the surface.

In order to understand the ion data observed on the dark side of the moon, one must be familiar with the theories concerning solar wind interaction with the moon. The following sections briefly discuss the current knowledge concerning this area.

## 1.2 GENERAL BACKGROUND - EXPERIMENTAL RESULTS

The solar wind is a tenuous plasma that continually streams radially outwards from the sun. The solar wind consists primarily of equal numbers of protons and electrons. Typical number densities of the solar wind are of the order of 5 particles/cm<sup>3</sup>. The solar wind velocity is supersonic in that it is greater than the Alfvén velocity of the medium. Table 1-1 and figure 1-1 summarize the solar wind parameters.

The conductivity of the solar wind is essentially infinite. Therefore, the interplanetary magnetic field lines are "frozen" into the plasma and thus dragged along by the solar wind. The interplanetary magnetic field lines intersect the earth's orbit at approximately a 45° angle to the earth - sun line.

When the solar wind reaches the earth, the solar wind plasma is unable to penetrate the earth's dipolar field. The solar wind compresses the field thus giving rise to the earth's magnetosphere (figure 1-2).

The solar wind interaction with the moon is entirely different from the interaction with the earth because the moon has an extremely small intrinsic magnetic field. The solar



TABLE 1-1

## OBSERVED PROPERTIES OF THE SOLAR WIND

<u>QUANTITY</u>	<u>MINIMUM</u>	<u>MAXIMUM</u>	<u>AVERAGE</u>
flux $N_p v$ (ions/cm <sup>2</sup> -sec)	$10^8$	$10^{10}$	$2-3 \times 10^8$
velocity $v$ (km/sec)	200	900	400-500
density $N_e \approx N_p$ (ions/cm <sup>3</sup> )	0.4	80	5
temperature $T_p$ (°K)	$5 \times 10^3$	$1 \times 10^6$	$2 \times 10^5$
thermal anisotropy ( $T_{\max}/T_{\text{avg}}$ ) (isotropic)	1.0	2.5	1.4
helium abundance $N(\text{He})/N(p)$	0	0.25	0.05
flow direction	$\pm 15^\circ$ of radius vector; average from $\approx 2^\circ$ east		
magnetic field $B(\gamma)$	0.25	40	6
B direction	Polar component variable, average in plane of ecliptic-solar equator; planar component variable, near the earth, average spiral angle $\varphi \approx 45^\circ$		
Alfvén speed (km/sec)	30	150	60

SOURCE: Brandt [1970]

Figure 1-1. Satellite Vela 3A measurements of the solar wind conducted in July 1965. The energy spectrum and directions are shown (180° corresponds to particles moving radially away from the sun, viewed from the spacecraft). The small hump in the energy spectrum curve may be due to  $\text{He}^{2+}$  ions (Hundhausen et al. [1967]).

Figure 1-2. A summary of the configuration of the magnetosphere in the noon - midnight plane (Ness[1965]).

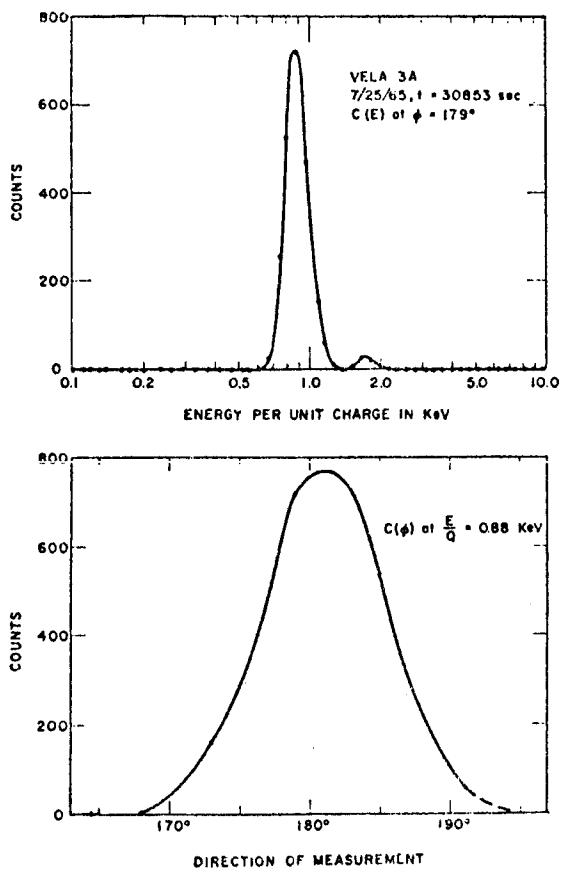


FIGURE 1-1

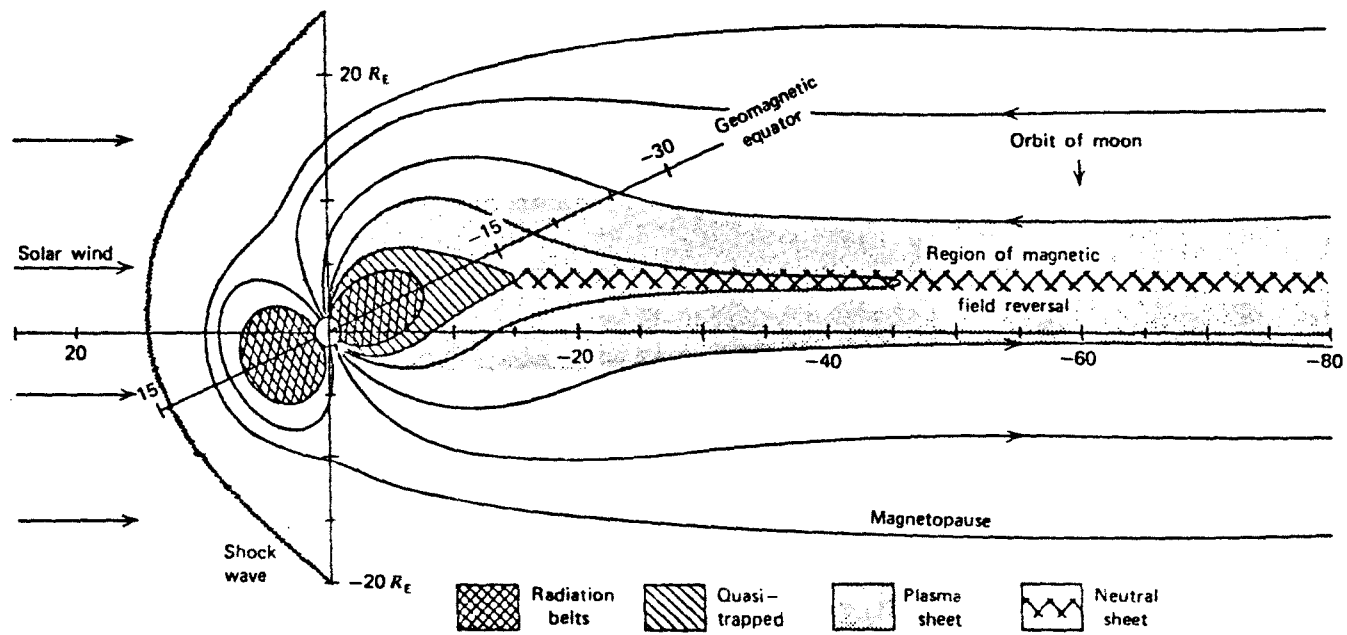


FIGURE 1-2

wind is directly incident on the lunar surface and the particles are absorbed there. The absorption of the solar wind on the dayside lunar surface creates a cavity in the solar wind on the night side of the moon.

Explorer 35, an United States satellite that was placed in lunar orbit on July 22, 1967, provided the first accurate measurements of the solar wind interaction with the moon.

Lyon et al. [1967], upon reduction of data obtained by the M. I. T. plasma probe flown on Explorer 35, established the clear existence of a plasma void on the dark side of the moon (figure 1-3).

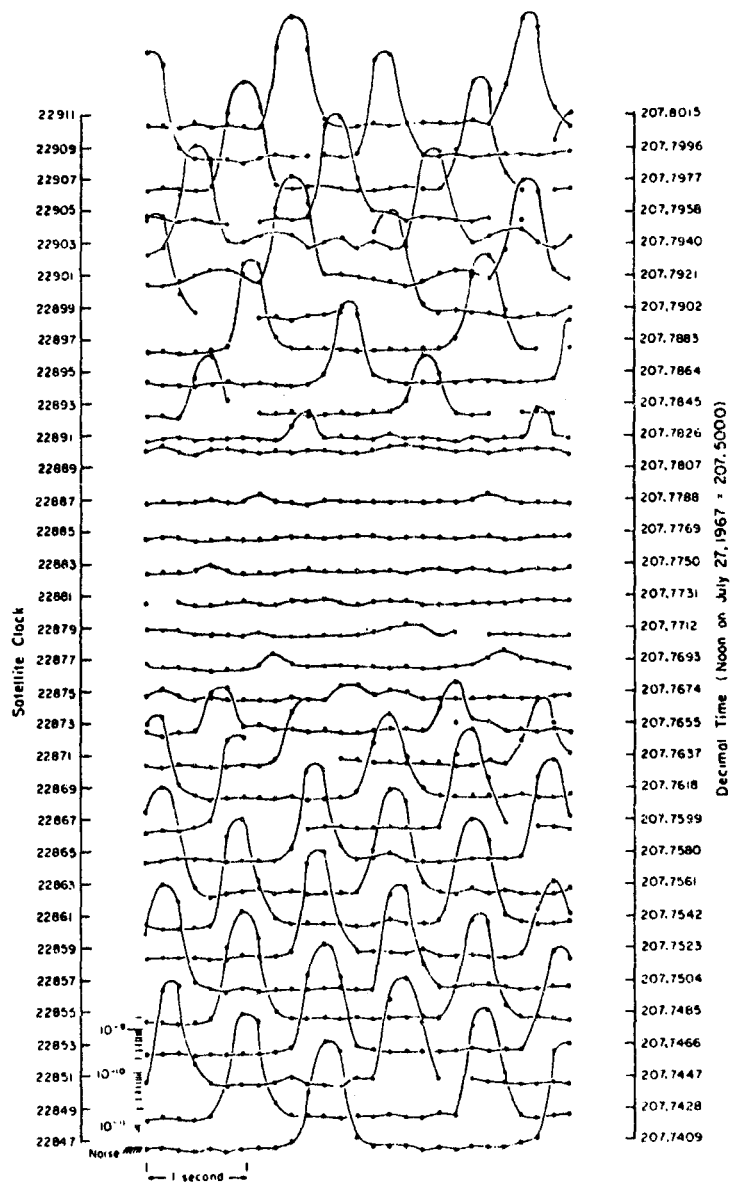
Other results obtained by Explorer 35 of the solar wind-moon interaction are summarized by Ness [1972] as follows:

1. The absence of a lunar magnetic field (at least none greater than  $2\gamma$ ) at satellite periselene when the moon was in the geomagnetic tail.
2. The absence of a bow shock wave or magnetosheath (similar to the earth's) surrounding the moon, when it was in the interplanetary field.
3. The existence of a plasma cavity or void region behind the moon when in the solar wind flow.

The only effect noted in the interplanetary field was the existence of:

4. Field magnitude increase in the region corresponding to the plasma umbra, and
5. Field magnitude decreases on either side, in the plasma penumbra.
6. The field direction is only slightly perturbed ( $<20^\circ$ ) in the lunar wake from that in the undisturbed solar wind.
7. Sometimes there exist increased field magnitudes in the penumbral regions in addition to the penumbral

Figure 1-3. Early Explorer 35 studies of the integral solar wind plasma flux ( $50 < E_p < 2850$  eV) on the downwind side of the moon. A logarithmic scale, used for the amplitude of the plasma current, is shown at lower left. Note the absence of counts in the middle of the plot. The spacecraft is now in the plasma void (Lyon et al. [1967]).



EXPLORER 35 PLASMA CURRENT SAMPLES (July 27, 1967)

FIGURE 1-3

decreases and umbral increase. These magnitude perturbations are generally small ( $< 30\%$ ).

In summary, the moon appears to behave like a spherical obstacle in the solar wind flow. The moon absorbs the plasma flux incident on its surface but permits the interplanetary field to be convectively carried past it without significant distortion or the formation of a pseudo-magnetosphere or shock waves.

### 1.3 GENERAL BACKGROUND - THEORY

In order to formulate an effective model of solar wind interaction, one must be aware of the important fundamental physical quantities. These parameters are summarized in figure 1-4. It is seen from figure 1-4 that the cyclotron radius for both ions and electrons is less than one lunar radii. Therefore, a guiding center approximation would be valid to first order in treating the problem.

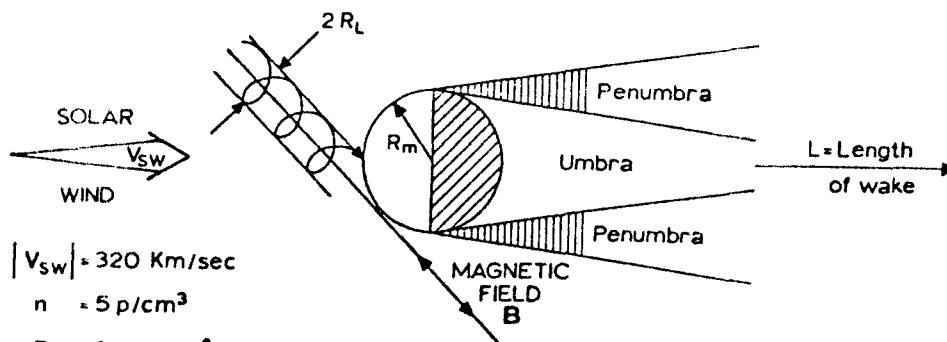
Michel [1964] first suggested two possible solar wind interactions with the moon. He examined the plasma flow in two limiting cases. The first case was the undeviated flow of the solar wind past the moon. The solar wind is completely absorbed and neutralized upon impact with the lunar surface. The other case was the potential flow of the solar wind about the moon. The plasma flow would be deflected around the moon by a magnetic field induced as the interplanetary magnetic field is dragged past a lunar interior that has a finite conductivity. The development of a bow shock would lead to a subsonic flow behind it (figure 1-5).

So little was known about the solar wind and its interactions at the time of this writing that Michel did not develop his models any further. Present Explorer 35 measurements



Figure 1-4. Summary of physical considerations for theoretical analysis of solar wind flow past the moon, using the most probable values of plasma and magnetic field parameters (Ness [1972]).

Figure 1-5. The upper figure indicates flow of solar wind plasma onto the moon in the undeviated flow model. Slanting lines indicate plasma. The lower figure indicates flow of solar wind plasma around the moon in the potential flow model. Dotted lines indicate the effect of the shock wake (Michel [1964]).



$$|V_{sw}| = 320 \text{ Km/sec}$$

$$n = 5 \text{ p/cm}^3$$

$$B = 6 \gamma @ 135^\circ / 315^\circ$$

	ions	electrons	Notes
T (K)	$4 \times 10^4$	$10^5$	$T_{  }/T_{\perp} > 1$
$V_T$ (Km/sec)	25	1700	
$R_L$ (Km)	44	1.6	$R_m = 1738$
$\tau_L$ (sec)	11	$6 \times 10^{-3}$	

$$L \propto \frac{V_{sw}}{V_{Ti}} R_m = 13$$

$$\tau \propto \frac{2 R_m}{V_{sw}} = 11 \text{ sec}$$

$$\beta = \frac{nK(T_e + T_i)}{H^2/8\pi} \approx 1$$

$$V_A = \frac{H}{\sqrt{4\pi n m_i}} = 60 \text{ Km/sec}$$

- $V_{sw}$  - Velocity of the solar wind
- $n$  - Number density of ions (electric neutrality assumed)
- $B_o$  - Interplanetary magnetic field angle  $\Phi_o$  to moon-sun line
- $T$  - Temperature (parallel,  $T_{||}$ , and perpendicular,  $T_{\perp}$ , to the magnetic field)
- $V_T$  - Thermal velocity of particles (root-mean-square value)
- $L$  - Characteristic scale length of the wake
- $R_L$  - Cyclotron radius
- $\tau_L$  - Cyclotron period
- $\tau$  - Characteristic time scale required to convect past the moon
- $\beta$  - Ratio of plasma pressure (perpendicular to field lines) to perpendicular magnetic field pressure
- $V_A$  - Alfvén velocity

FIGURE 1-4

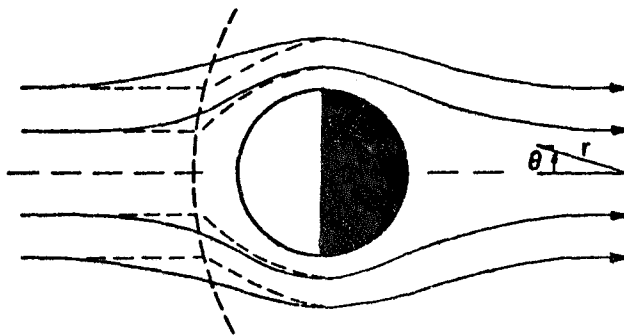
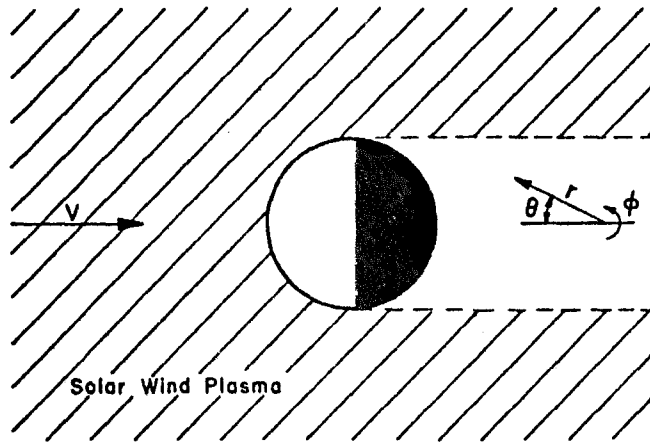


FIGURE 1-5

indicate now that Michel's model of undeviated flow past the moon most closely resembles the actual mechanism in operation.

Michel [1967], using the early results of Explorer 35, proposed that the solar wind closed in behind the moon causing a shock wave when the collapse of the plasma was halted (figure 1-6). Michel [1968] extended this study to include the effect of different directions of the interplanetary magnetic field. It was determined that the formation of the shock wave downstream from the moon was independent of the direction of the magnetic field (see figure 1-6).

Johnson and Midgley [1968] studied the closure of the plasma cavity. They determined that the rate at which the void behind the moon is filled depends on the orientation and the relative strength of the interplanetary magnetic field.

Using the guiding center approximation, Whang [1968] studied the ion flow in the vicinity of the moon. He assumed that the directional and magnitude perturbations of the interplanetary magnetic field were negligible. His results showed that the wake was confined to a region behind the moon and it was not axially symmetric about the x-axis (figure 1-7).

Wolf [1968] extended the work of Michel and of Johnson and Midgley using the continuum fluid approach and a cylinder to approximate the moon. He studied the problem for the case where the interplanetary magnetic field is aligned with the plasma flow velocity and for an isotropic pressure of the magnetized plasma. From his analysis, Wolf arrived at the same results as Michel (see figure 1-8).

Using the kinetic theory approach and neglecting the interplanetary magnetic field, Wu and Dryer [1972] arrived at number density contours and flow patterns about the moon (see figures 1-9 and 1-10). They predict that on the dark side of the moon there is a probability of a very low, but finite,

Figure 1-6. Sketch of the development of a trailing shock wave in the lunar wake (Michel [1968]).

Figure 1-7. The distribution of ion flux in the X - Y coordinate plane for varying direction angle  $\varphi$  (Whang [1968]).

Figure 1-8. Diagram developing further geometry and flow characteristics behind the moon leading to the formation of a trailing shock wave. The upper figure refers to the plane of symmetry while the lower figure refers to a plane perpendicular to this (Wolf [1968]).

Figure 1-9. Constant density contours with a non-central force field potential in the vicinity of a "small" spherical obstacle. Note the development of a continuum-like "Mach cone" at the limb, compression near the subsolar point, and expansion immediately beyond the limb.  $n_{\infty}$  is the number density of the incident solar wind. The x-axis scale is in units of obstacle radii (Wu and Dryer [1972]).

Figure 1-10. Velocity vectors with a non-central force field potential in the vicinity of a "small" spherical obstacle. Note the turning of the plasma flow on the sunlit hemisphere and the acceleration of particles around the limb. The x-axis scale is in units of obstacle radii (Wu and Dryer [1972]).

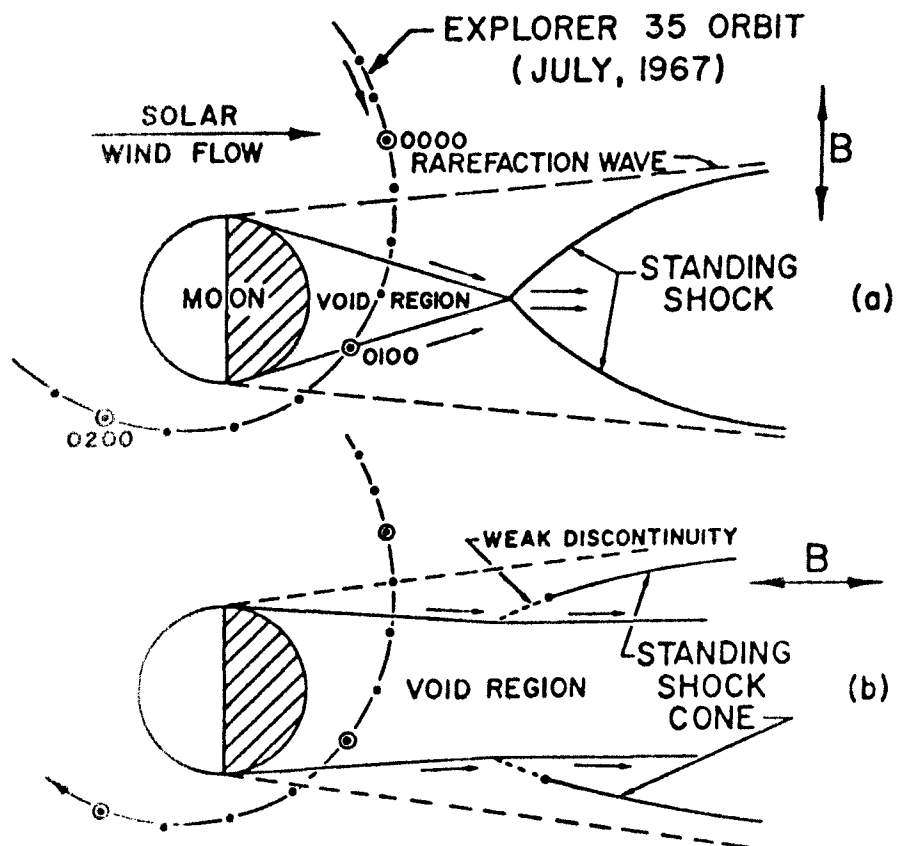


FIGURE 1-6

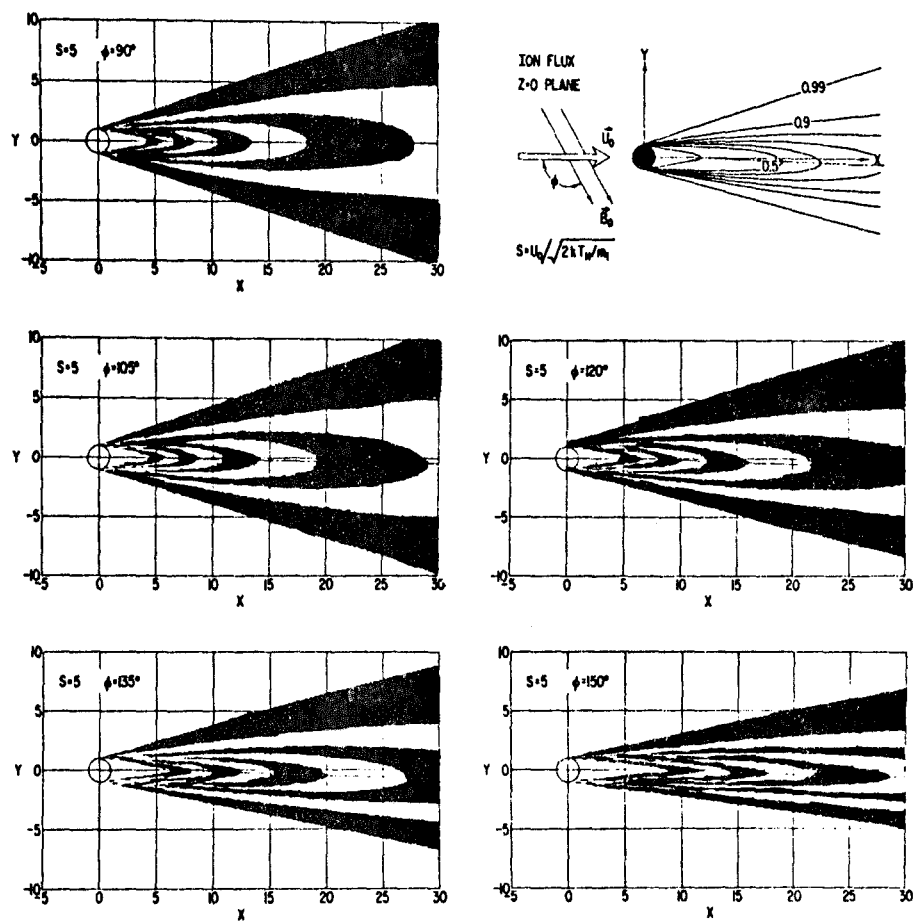


FIGURE 1-7

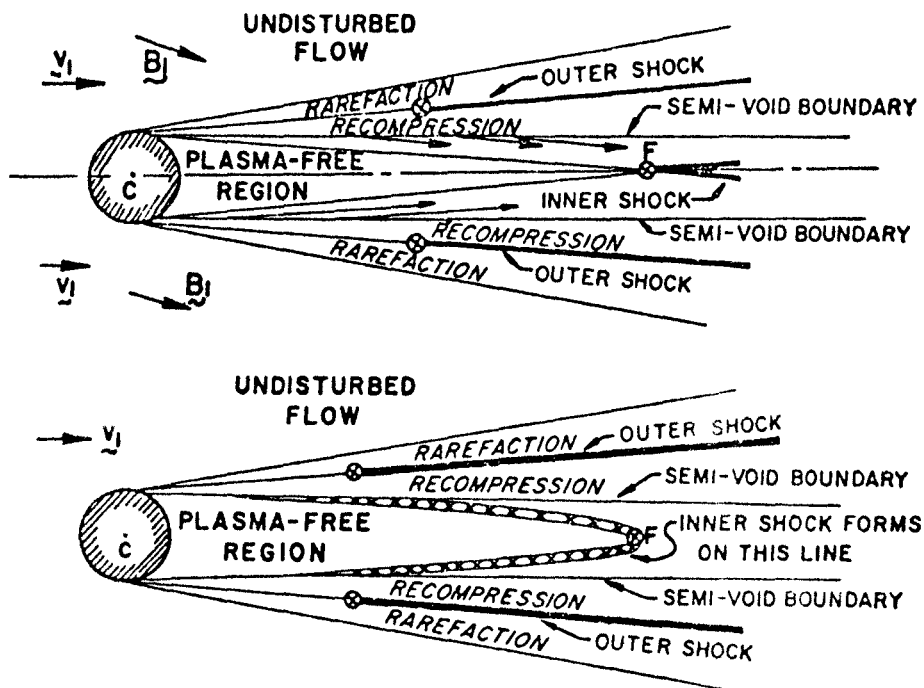


FIGURE 1-8



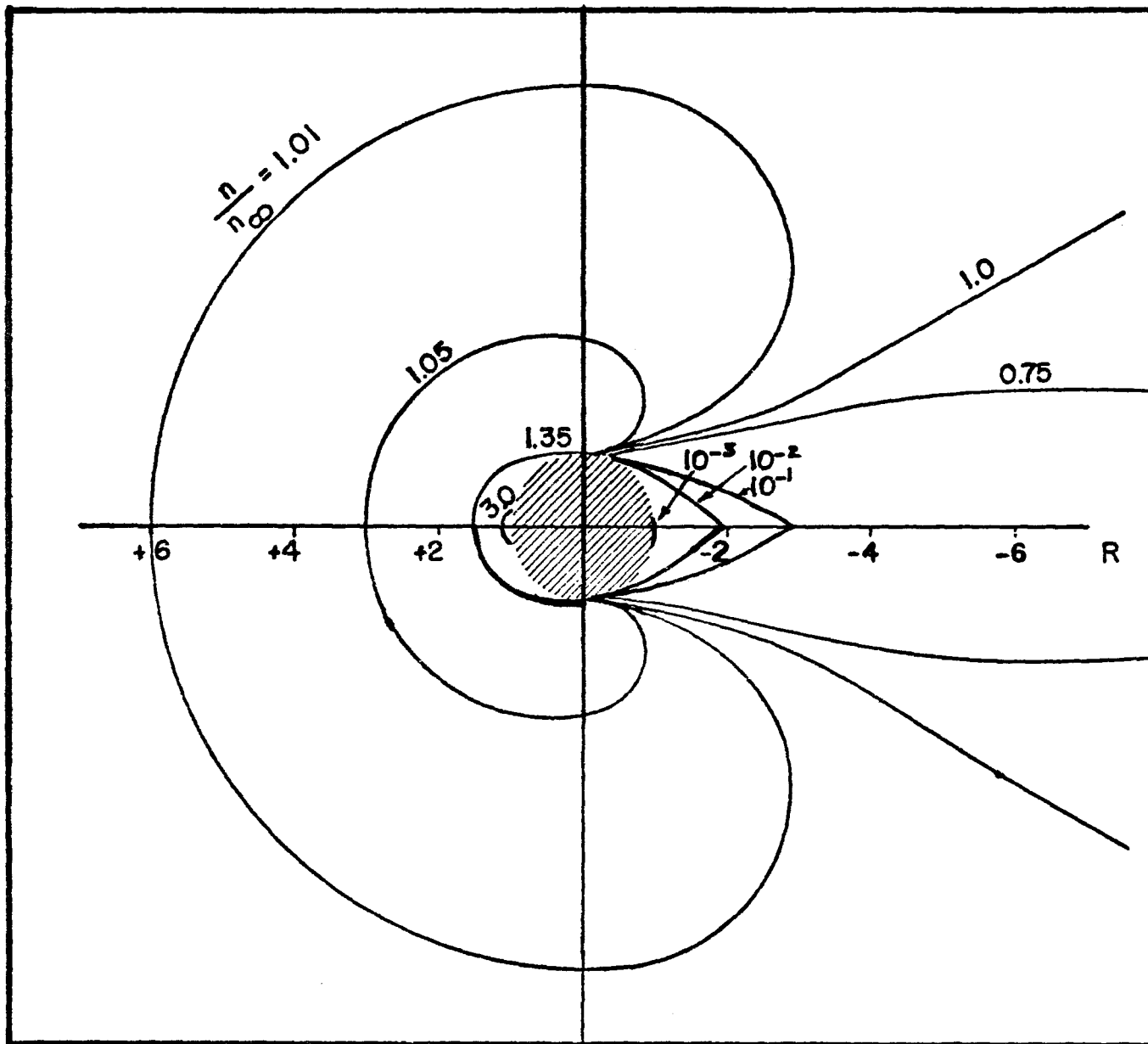


FIGURE 1-9

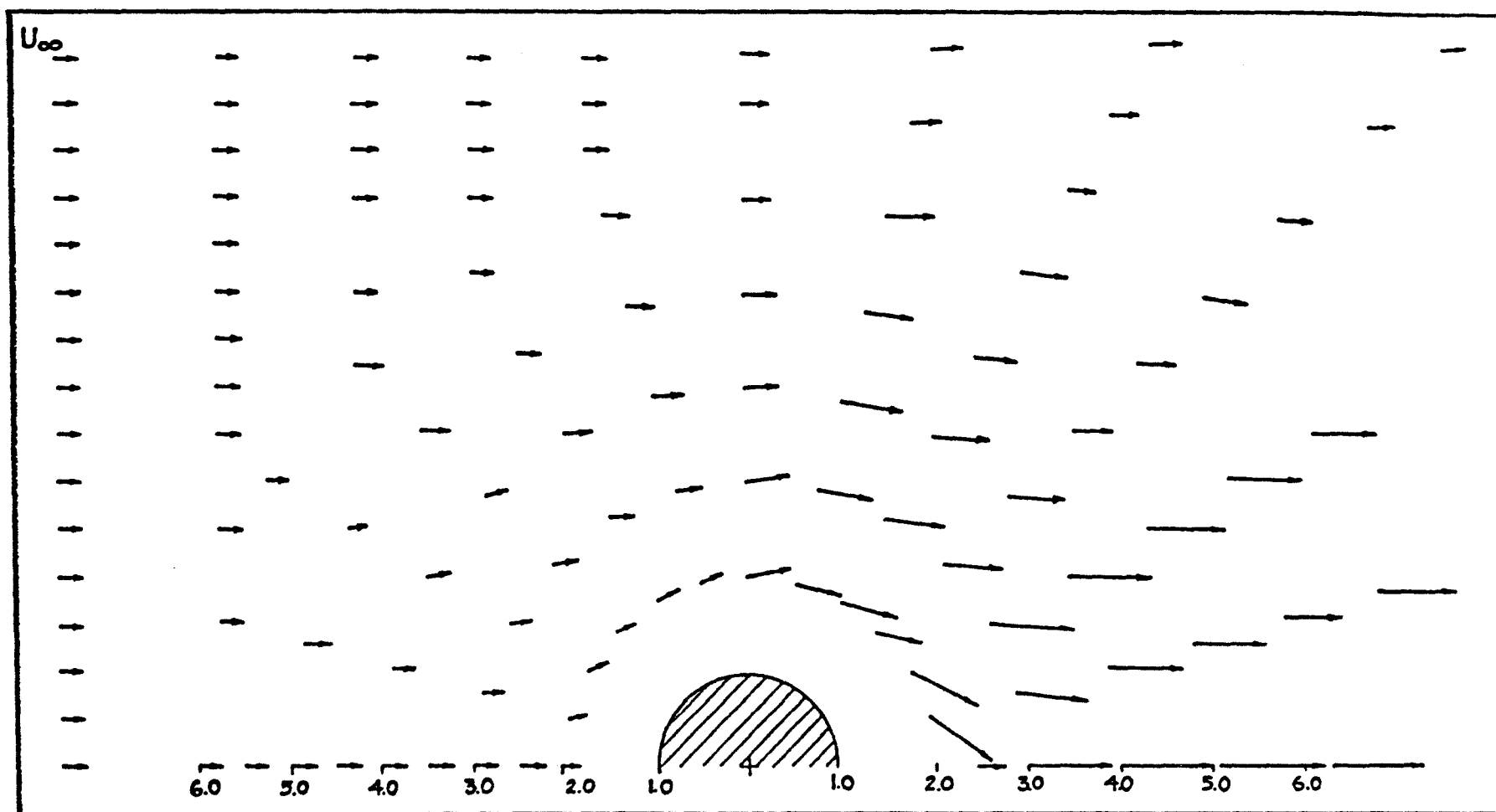


FIGURE 1-10

density of particles.

#### 1.4 RESEARCH OBJECTIVES

The SIDE observes ion fluxes of a narrow energy range sporadically from local lunar sunset to local lunar sunrise. The lack of a complete understanding of this ion data and the fact that very little analysis has been performed on this data so far leads to the following research objectives:

- a. To determine if the ion bursts occur randomly or are correlated with Kp.
- b. To determine if there is a dependence on the occurrence of the events on position in lunar orbit or lunar local time.
- c. To determine the characteristics of the ion spectra.
- d. To suggest some possible explanations for the presence of these ions in the plasma cavity behind the moon.

## CHAPTER 2 - INSTRUMENT

2.1 BASIC PHYSICS OF OPERATION

The SIDE, like most other particle detectors with an energy discrimination capability, determines the energy of a charged particle by observing how its trajectory is changed on entering a region where an electric exists. Normally this electric field is created by applying a constant potential difference across two parallel plates. If the applied electric field is perpendicular to the trajectory of the particle, then the amount of deflection from the initial trajectory is a function of the energy of the charged particle and the strength of the deflecting field.

The simplest configuration is shown in figure 2-1. The velocity in the direction of the deflected particle is:

$$v_y = \sqrt{\frac{2\xi_p}{m}} \quad 2-1$$

where  $\xi_p$  is the energy of the particle and  $m$  is the mass of the particle.

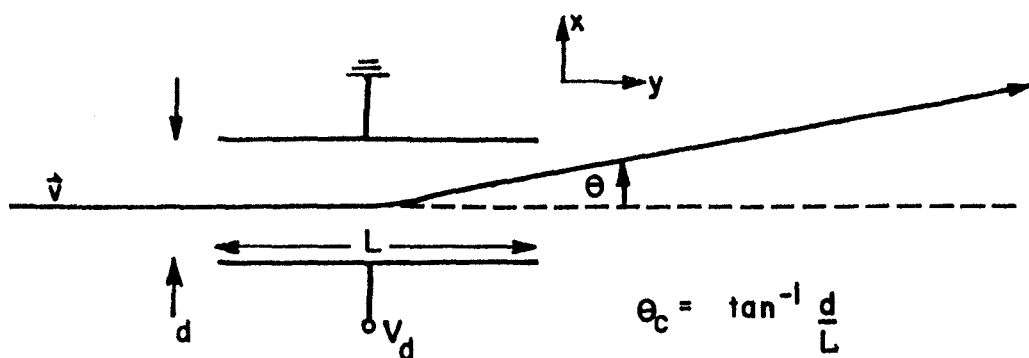
If  $V_d$  is the voltage across the plates, separated by a distance  $d$ , then the electric field will be:

$$E_x = \frac{V_d}{d} \quad 2-2$$

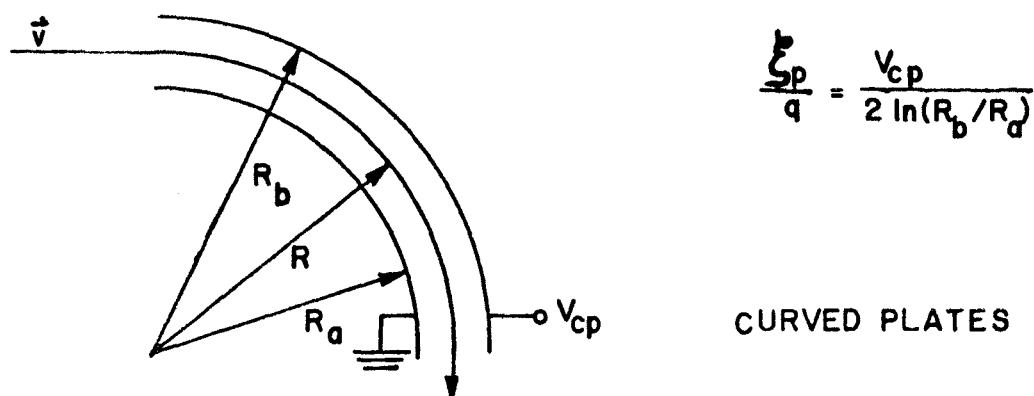
The particle will experience a transverse force resulting in a transverse velocity  $v_x$  given by:

$$v_x = \frac{qE}{m} \Delta t = \frac{q}{m} \frac{V_d}{d} \Delta t$$

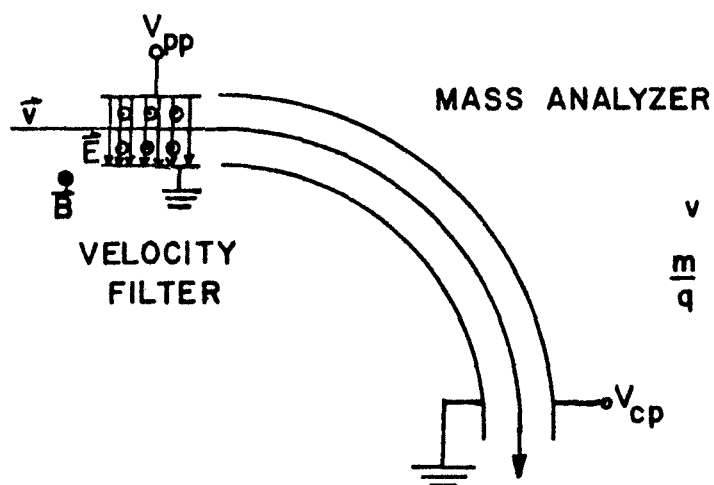
Figure 2-1. Schematic diagram of plane and curved plate electrostatic analyzers. The Wein velocity filter preceeds the curved plat analyzer to form the Mass Analyzer.



PLANE PLATES



CURVED PLATES



$$v = E/B$$

$$\frac{m}{q} = \frac{B^2 d^2}{\ln(R_b/R_a)} \frac{V_{cp}}{V_{pp}^2}$$

FIGURE 2-1

where  $q$  is the charge of the particle and  $\Delta t$  is the time spent by the particle in the electric field.

Thus

$$\Delta t = \frac{L}{v_y}$$

and

$$v_x = \frac{q}{m} \frac{V_d}{d} \frac{L}{v_y} \quad 2-3$$

where  $L$  is the length of the plates.

The angle of deflection of the particle is then given by:

$$\tan \theta = \frac{v_x}{v_y} = \frac{q}{m} \frac{V_d}{d} \frac{L}{v_y^2} = q \frac{V_d}{d} \frac{L}{2\xi_p} \quad 2-4$$

where  $v_y$  is given by equation 2-1. So

$$\frac{\xi_p}{q} = \frac{L V_d}{2d \tan \theta} \quad 2-5$$

The critical energy to just pass through the plates is:

$$\frac{\xi_c}{q} = \frac{L V_d}{2d \tan \theta_c}$$

where  $\tan \theta_c = d/L$ . Therefore

$$\frac{\xi_c}{q} = \frac{L^2 V_d}{2d^2} \quad 2-6$$

This method of energy determination is not very useful since it only provides a lower limit to the energy of the particle. Thus, for  $\xi_p \geq \xi_c$ , all particles will pass through

the plates. An upper cutoff for the particle energy may be provided if curved plates are used to generate the electrostatic field. Now the energies of the particles that make it through the plates are confined to a narrow range. Both detectors in the SIDE instrument, the Total Ion Detector (TID) and the Mass Aalyzer (MA), use such a set of curved plates for energy discrimination.

The potential, as a function of  $R$ , between the curved plates is:

$$\phi(R) = \frac{V_{cp} \ln(R/R_a)}{\ln(R_b/R_a)} \quad 2-7$$

where  $R_b$  is the radius of curvature of the outer plate, and  $R_a$  is the radius of curvature of the inner plate (figure 2-1).  $V_{cp}$  is the total potential difference that is applied between the two curved plates.

The electric field is given by:

$$\vec{E} = -\vec{\nabla}\phi \quad 2-8$$

so

$$|\vec{E}| = E = \frac{V_{cp}}{\ln(R_b/R_a)} \frac{1}{R} \quad 2-9$$

Performing a similar derivation as for the parallel plates, one gets for the particle energy that makes it through the plates:

$$\frac{\xi_p}{q} = \frac{mv^2}{2q} = \frac{V_{cp}}{2\ln(R_b/R_a)} \quad 2-10$$



It can be seen from equation 2-10 and the geometry of the system that only a narrow range of energies may pass safely through the apparatus.

The curved plates described above may be used in conjunction with a velocity filter for mass discrimination of charged particles. The Wein velocity filter used in the MA consists of perpendicular electric and magnetic fields. The electric field is again a result of two parallel plane plates and the magnetic field is produced by a permanent magnet.

The velocity of the particles is first determined by the velocity filter and then it is allowed to pass through the curved plates to determine its energy.

On entering the velocity filter, the charged particle experiences two forces. One force due to  $\vec{E}$  and one due to  $\vec{B}$ .

$$\begin{aligned}\vec{F}_E &= q\vec{E} \\ \vec{F}_B &= q\vec{v} \times \vec{B}\end{aligned}\tag{2-11}$$

In order for the particle to pass through the filter without a change in trajectory, the total force must be zero.

$$\vec{F}_T = \vec{F}_E + \vec{F}_B = 0\tag{2-12}$$

The particular velocity required for this condition to hold is:

$$\begin{aligned}v &= E/B \\ &= \frac{V_{pp}}{Bd}\end{aligned}\tag{2-13}$$

where  $V_{pp}$  is the potential applied across the parallel plates and  $d$  is the separation of the plates. Thus, by varying  $V_{pp}$ , the allowed value of  $v$  may be changed.

Combining equations 2-10 and 2-13, yields

$$\frac{m}{q} = \frac{V_{cp}}{2 \ln(R_b/R_a)} \frac{2}{v^2} = \frac{B^2 d^2}{\ln(R_b/R_a)} \frac{V_{cp}}{V_{pp}^2} \quad 2-14$$

So, from equation 2-14, we see that for a certain value of  $v$  or  $V_{pp}$  we can determine the mass spectrum of the incoming particles by varying  $V_{cp}$ .

Figure 2-1 also shows the basic idea behind the operation of the MA.

## 2.2 INSTRUMENT DESIGN

Figure 2-2 shows schematically how the two detectors are arranged in the SIDE. The SIDE consists of two positive particle detectors. The MA is indicated at the top and the TID at the bottom of the figure. The ions are incident from the right in the diagram. The entrance aperture for the TID measures 8 mm x 3 mm. The field of view for the TID is a square solid angle of approximately  $6^\circ$  on a side. The two concentric curved plates have radii 4.25 and 3.75 cm both covering an arc of  $127^\circ 17'$  ( $\pi/\sqrt{2}$  radians). The plates of the TID are stepped through twenty voltage increments resulting in the following energy channels: 10, 20, 30, 50, 70, 100, 250, 500, 750, 1000, 1250, 1500, 1750, 2000, 2250, 2500, 2750, 3000, 3250, and 3500 eV/q. This energy range covers solar wind energies down to the energy range expected for ions formed in the lunar atmosphere.

After passing through the curved plates, an ion is detected

Figure 2-2. Schematic diagram of the TID and MA in the plane of the ion trajectories (Hills et al. [1971]).

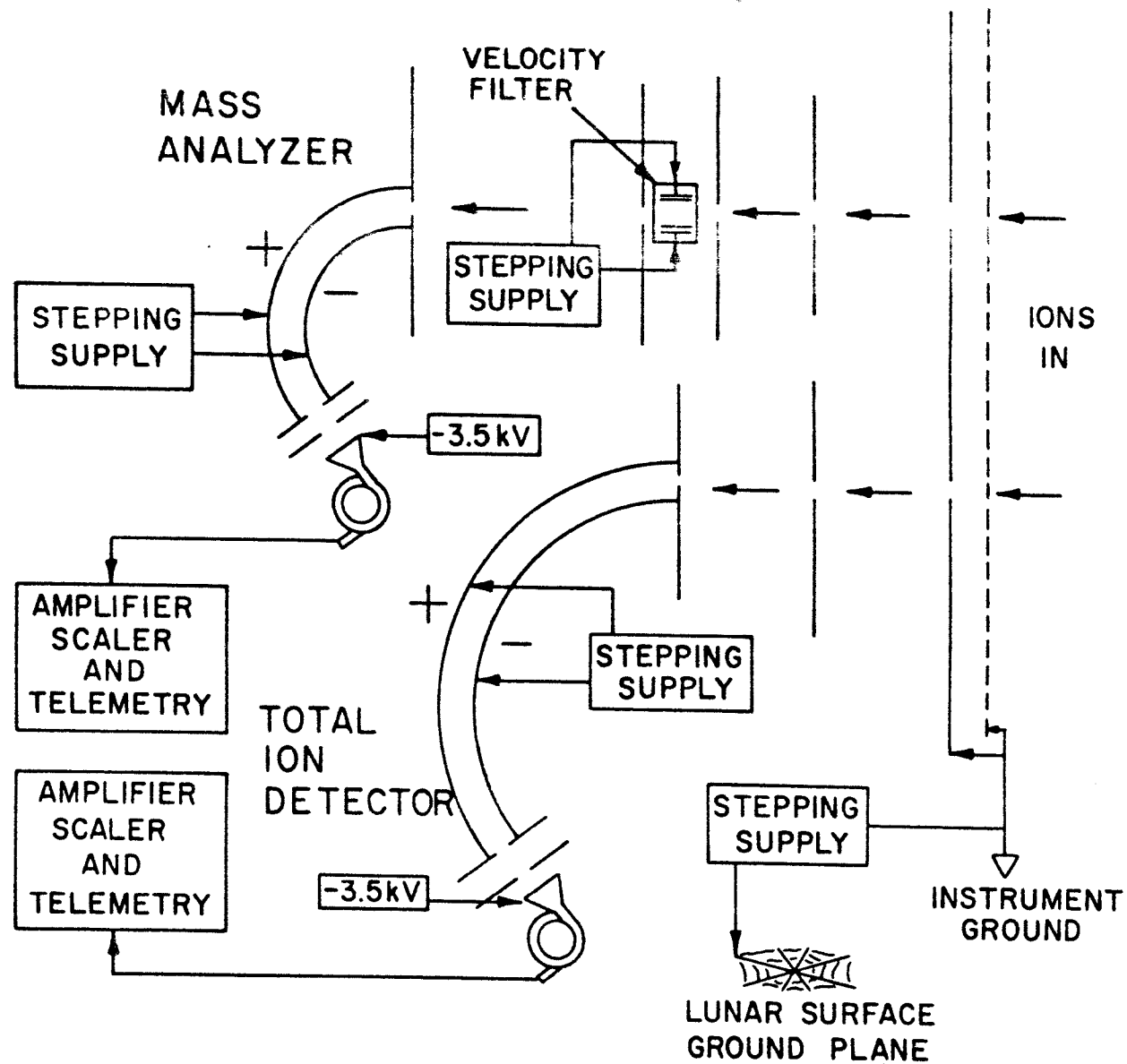


FIGURE 2-2

by a Bendix 4028 Channeltron<sup>(R)</sup>. This channel electron multiplier is held at a potential of -3.6 kV to accelerate the particles into the detector, thereby enhancing the collection efficiency. The detector is operated in the pulse saturated mode so that the response of the counter is independent of the energy of the incoming particle.

The curved plate electrostatic analyzer of the MA is similar in design to the TID. These plates are stepped through six voltage increments that correspond to the following energy steps: 48.6, 16.2, 5.4, 1.8, 0.6, and 0.2 eV/q.

The Wein velocity filter is composed of two parallel plates each measuring 8 mm x 2 mm and separated by a distance of 0.8 cm. The magnetic field of the filter is provided by a permanent magnet that has a strength of  $850 \pm 10$  gauss.

The particle detector for the MA is another Bendix Channeltron<sup>(R)</sup> and it is also at a potential of -3.5 kV.

The field of view for the MA is a square solid angle of  $4^\circ$  on a side.

The mode of operation of the SIDE is as follows. The SIDE executes one complete cycle every 2.55 minutes. Each cycle consists of 128 frames, 1.2 seconds per frame. The TID cycles through all twenty energy channels in twenty frames, thus obtaining six complete spectra each SIDE cycle. During this same 120 frames, the MA cycles through the twenty ion channels for each of the six energy steps. The remaining eight frames contain calibration data (figure 2-3). The accumulation interval for each step in both the MA and the TID is  $1.13 \text{ sec} \pm 0.025 \text{ sec}$ . In order to allow time for data read-out and for transients to die out between frames, this time interval is less than the 1.2 seconds allowed per frame.

The Wein velocity filter for each SIDE is different. The three SIDE's therefore measure different mass ranges. Table

Figure 2-3. Normal operating mode for the TID and MA (Lindeman [1973]).

SIDE FRAME	TID	MA
0	4*	Mass Spectrum 48.6 eV/q
1-19	Energy Spectrum	Mass Spectrum 16.2 eV/q
20		
21-39	Energy Spectrum	Mass Spectrum 5.4 eV/q
40		
41-59	Energy Spectrum	Mass Spectrum 1.8 eV/q
60		
61-79	Energy Spectrum	Mass Spectrum 0.6 eV/q
80		
81-99	Energy Spectrum	Mass Spectrum 0.2 eV/q
100		
101-119	Energy Spectrum	1*
120		
121	1*	2*
122	2*	3*
123	3*	4*
124	4*	1*
125	1*	2*
126	2*	3*
127	3*	4*

1\* Background Reading Taken; Curved Plates Grounded

2\* Counting Electronics Calibrated at 137 Hz.

3\* Counting Electronics Calibrated at 17.5 kHz.

4\* Counting Electronics Calibrated at 560 kHz.

FIGURE 2-3

2-1 summarizes the characteristics of the SIDE's deployed on Apollo missions 12, 14, and 15. The physical configuration of the SIDE is shown in figure 2-4.

In order to measure the lunar surface potential, a wire spider web-like screen is placed under each SIDE on the moon. This screen connects the SIDE directly to the lunar surface assuming that there is good electrical contact between the screen and the lunar surface (see figures 2-5 and 2-6). The wire screen is connected to a stepping voltage supply. This stepping voltage is also connected to a wire grid above the ion apertures (figure 2-6). The stepping voltage cycles through 24 voltage steps from 27.6 volts to -27.6 volts (see Table 2-1). In the normal mode of operation, this voltage is stepped once every SIDE cycle. Therefore, one complete cycle of all 24 voltage steps requires 61.2 minutes.

Analysis of lunar surface potential measurements by Fenner et al. [1973] and Freeman and Ibrahim [1974] has yielded a value of +10 volts for the dayside lunar surface potential. The surface potential becomes negative at the terminators and possibly -100 volts on the night side of the moon (figure 2-7).

### 2.3 CALIBRATION

The quantity that is directly available from the SIDE data is the counting rate  $R$ .  $R$  may be converted in to a more useful quantity known as the unidirectional differential flux  $j(E, \Omega)$ .

The counting rate at an energy  $E$  may be calculated as follows:

$$R = \int_E \int_{\Omega} g(E, \theta, \varphi) j(E, \theta, \varphi) d\theta d\varphi dE \quad 2-15$$



TABLE 2-1

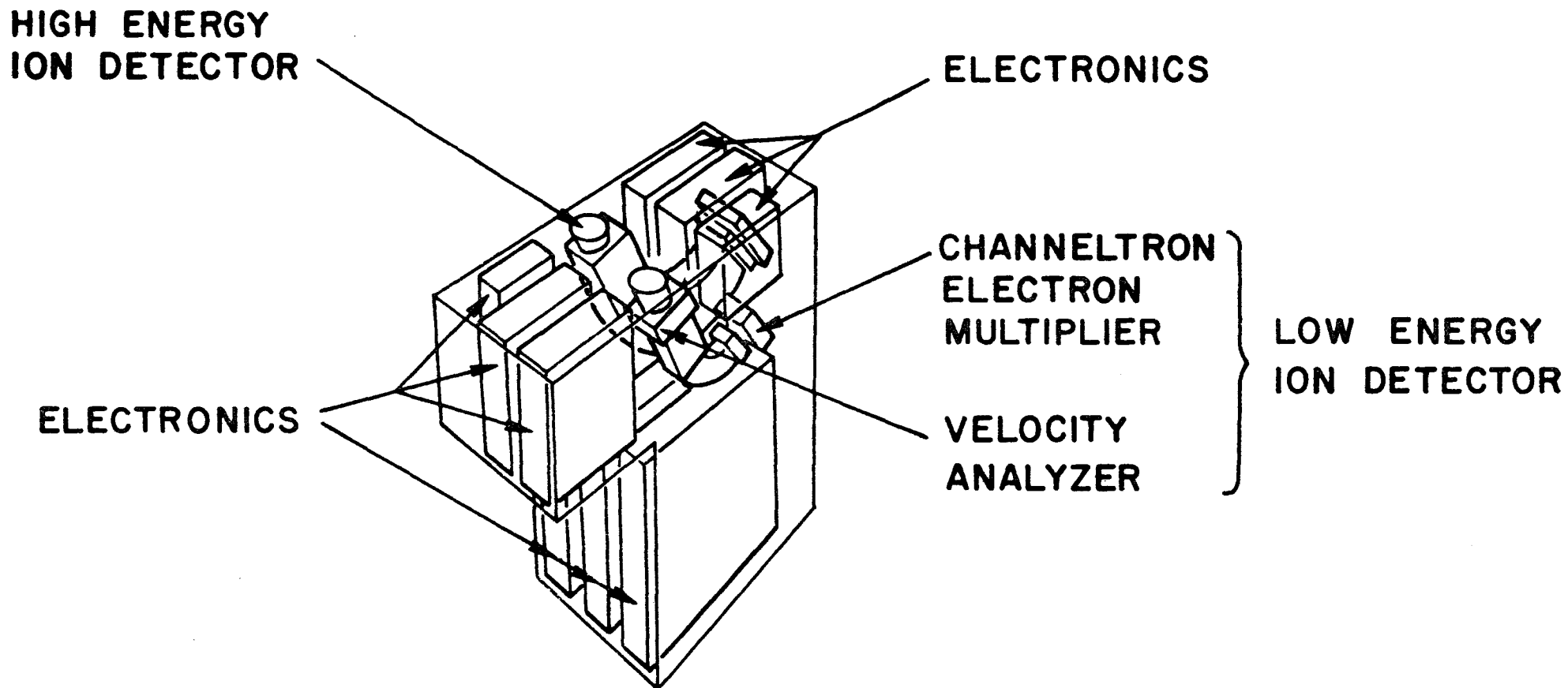
<u>ENERGY STEPS (eV/q)</u>		<u>APPROX. MASS RANGES (AMU)</u>			<u>GROUND PLANE STEPPER (volts)</u>
<u>TID</u>	<u>MA</u>	Apollo <u>12</u>	Apollo <u>14</u>	Apollo <u>15</u>	
10	48.6	10-1500	6-750	1-90	0.0
20	16.2				0.6
30	5.4				1.2
50	1.8				1.8
70	0.6				2.4
100	0.2				3.6
250					5.4
500					7.8
750					10.2
1000					16.2
1250					19.8
1500					27.6
1750					0.0
2000					-0.6
2250					-1.2
2500					-1.8
2750					-2.4
3000					-3.6
3250					-5.4
3500					-7.8
					-10.2
					-16.2
					-19.8
					-27.6

Figure 2-4. Schematic diagram depicting the location of the electronics and the two analyzers in the experiment package (Freeman et al. [1969]).

Figure 2-5. Deployed configuration of the SIDE showing the ground plane grid and the grid over the entrance apertures (Freeman et al. [1969]).

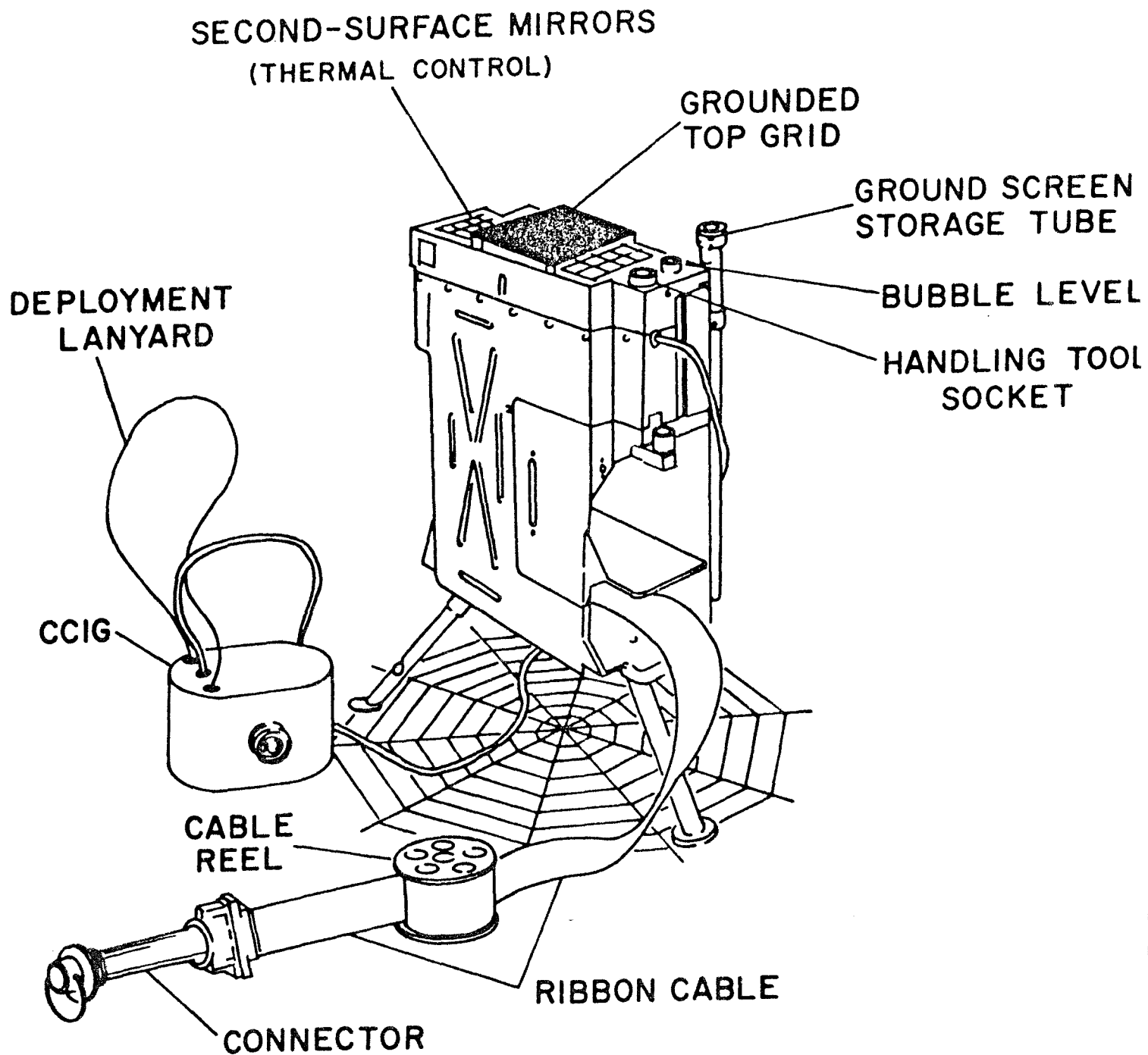
Figure 2-6. Schematic diagram illustrating the relationship between the entrance grid and the ground plane grid. The two grids are connected with each other by a stepping voltage supply.

Figure 2-7. Results of the determination of the lunar surface potential (Freeman and Ibrahim [1974]).



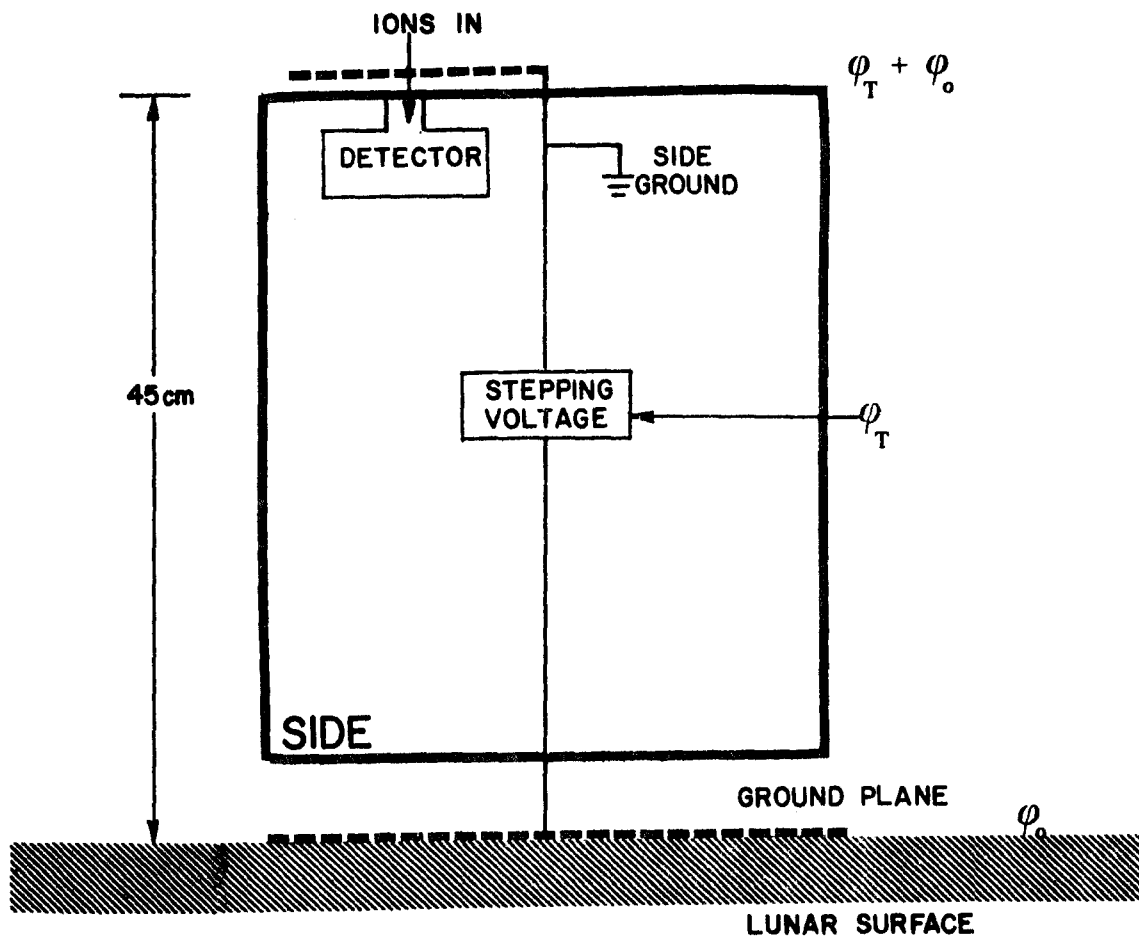
INTERNAL DIAGRAM OF THE  
SUPRATHERMAL ION DETECTOR EXPERIMENT

FIGURE 2-4



## DEPLOYED CONFIGURATION

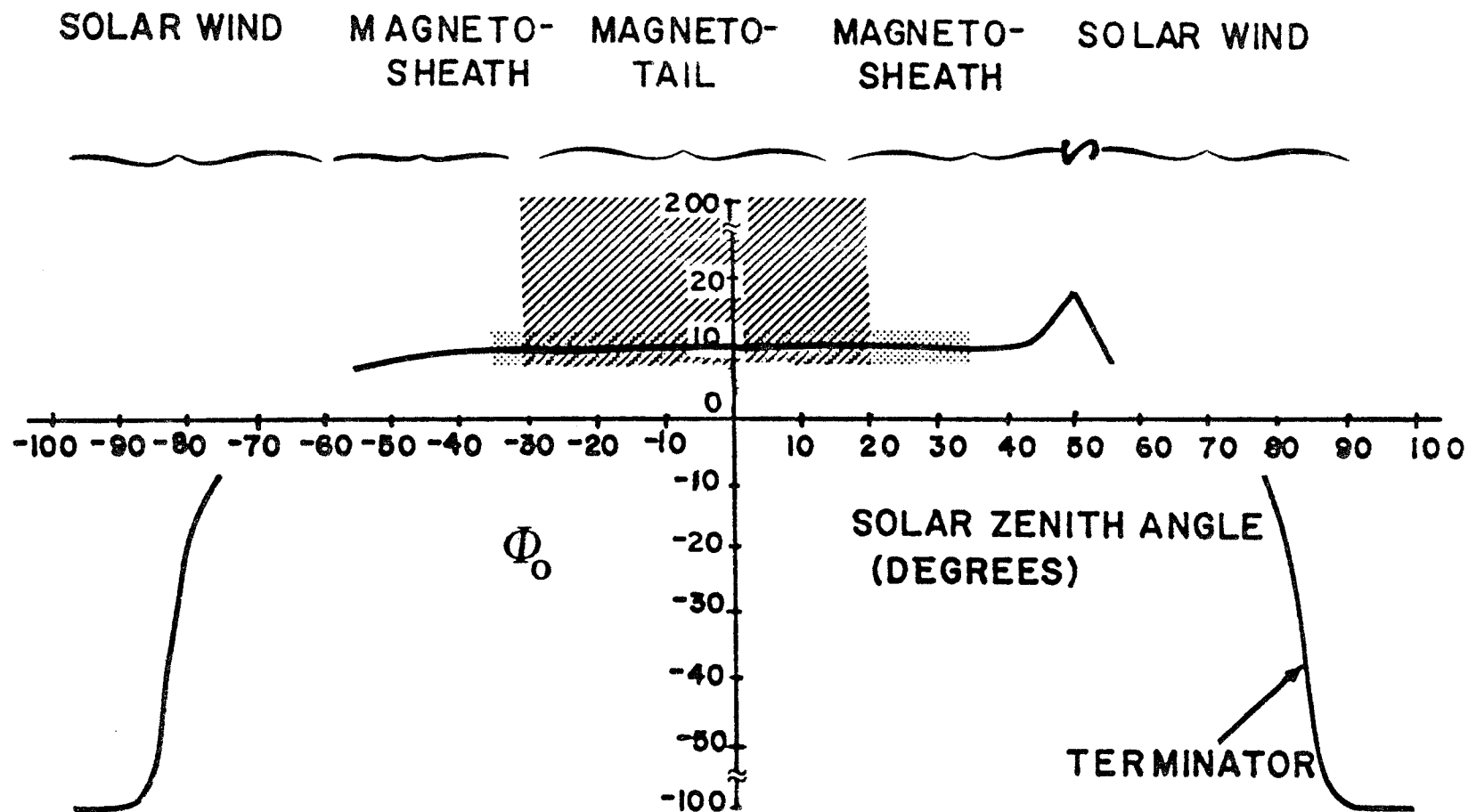
FIGURE 2-5



$\phi_o$  = POTENTIAL OF SURFACE

$\phi_T$  = STEPPER POTENTIAL

FIGURE 2-6



$\Phi_0$  = LUNAR SURFACE POTENTIAL (VOLTS)

▨ = RANGE OF UNCERTAINTY

▨ = RANGE OF POSSIBLE POTENTIALS

FIGURE 2-7

where

$g(E, \theta, \varphi)$  = unidirectional geometric factor at  
energy  $E$

If we assume that the flux of particles is isotropic over the field of view of the detector, then  $j(E, \theta, \varphi)$  is approximately independent of  $\theta$  and  $\varphi$ . Then,

$$R = \int_E j(E, \Omega) \int_{\Omega} g(E, \theta, \varphi) d\theta d\varphi dE \quad 2-16$$

The only quantity that may be experimentally determined in the laboratory is:

$$G(E) = A(E) \Omega(E) \epsilon(E) = \int_{\Omega} g(E, \theta, \varphi) d\theta d\varphi \quad 2-17$$

where,

$A(E)$  = effective area of the detector seen by the  
particle

$\Omega(E)$  = effective solid angle seen by the incoming  
particle

$\epsilon(E)$  = efficiency of the detector for a particle of  
energy  $E$

If we make the second assumption that the flux is also constant over the bandwidth of the detector, then,

$$R = j(E, \Omega) \int_E G(E) dE$$

$$R = G_0 j(E, \Omega) \quad 2-18$$

where

$$G_o = \int_E G(E) dE \quad (\text{cm}^2\text{-ster-eV})$$

$G(E)$  is integrated over the bandwidth of the detector. Therefore,

$$j(E, \Omega) = \frac{R}{G_o} \left( \frac{\text{particles}}{\text{cm}^2\text{-ster-sec-eV}} \right) \quad 2-19$$

The omnidirectional flux is obtained by integrating  $j(E, \Omega)$  over  $\Omega_{\text{space}}$ .

$$j_{\text{omni}} = \int_{\Omega} j(E, \Omega) d\Omega \quad \left( \frac{\text{particles}}{\text{cm}^2\text{-sec-eV}} \right) \quad 2-20$$

The corresponding integral fluxes are obtained by integrating over the entire energy spectrum.

$$J_{\text{uni}} = \int_E j(E, \Omega) dE \quad \left( \frac{\text{particles}}{\text{cm}^2\text{-ster-sec}} \right) \quad 2-21$$

and

$$J_{\text{omni}} = \int_{\Omega} \int_E j(E, \Omega) dE d\Omega \quad \left( \frac{\text{particles}}{\text{cm}^2\text{-sec}} \right) \quad 2-22$$

All three SIDE instruments have been calibrated in the laboratory. Lindeman [1973] gives an extensive discussion of the calibration and the analysis of the results of both the MA and the TID. The calibration results for the MA and the TID are shown in figures 2-8 to 2-10.



Figure 2-8. TID calibration results of the Apollo 14 instrument. The upper graph shows the unidirectional geometric factor as a function of the nominal center energy. The middle graph shows the parallel beam geometric factor as a function of the nominal center energy. The lower graph shows the energy bandpass (full width at half maximum) as a function of the nominal center energy. Note that the bandpass is approximately 8% of the center energy (plotted from data compiled by Lindeman [1973]).

Figure 2-9. The energy response of the SIDE for a typical calibration run using a single energy channel (Fenner [1974]).

Figure 2-10. Summary of the results of the MA calibration (plotted from data compiled by Lindeman [1973]).

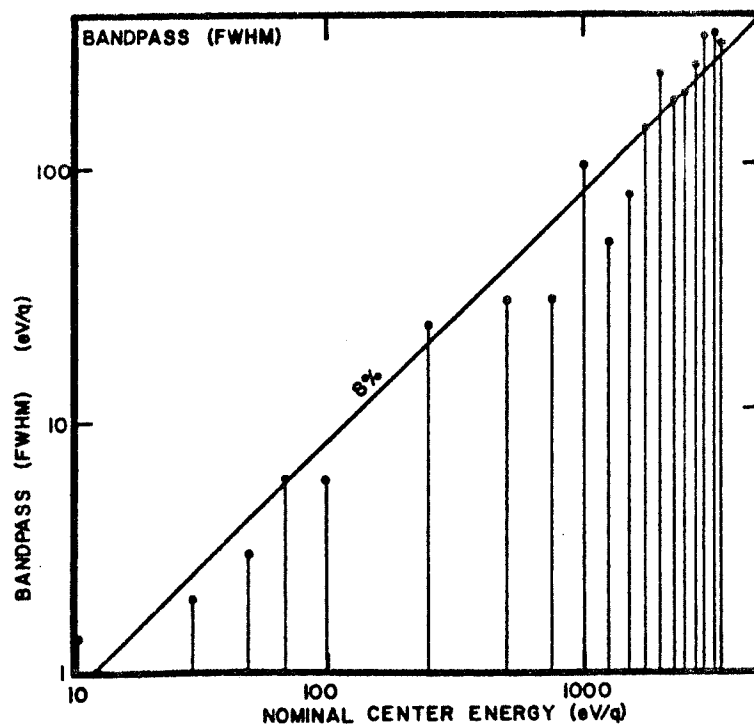
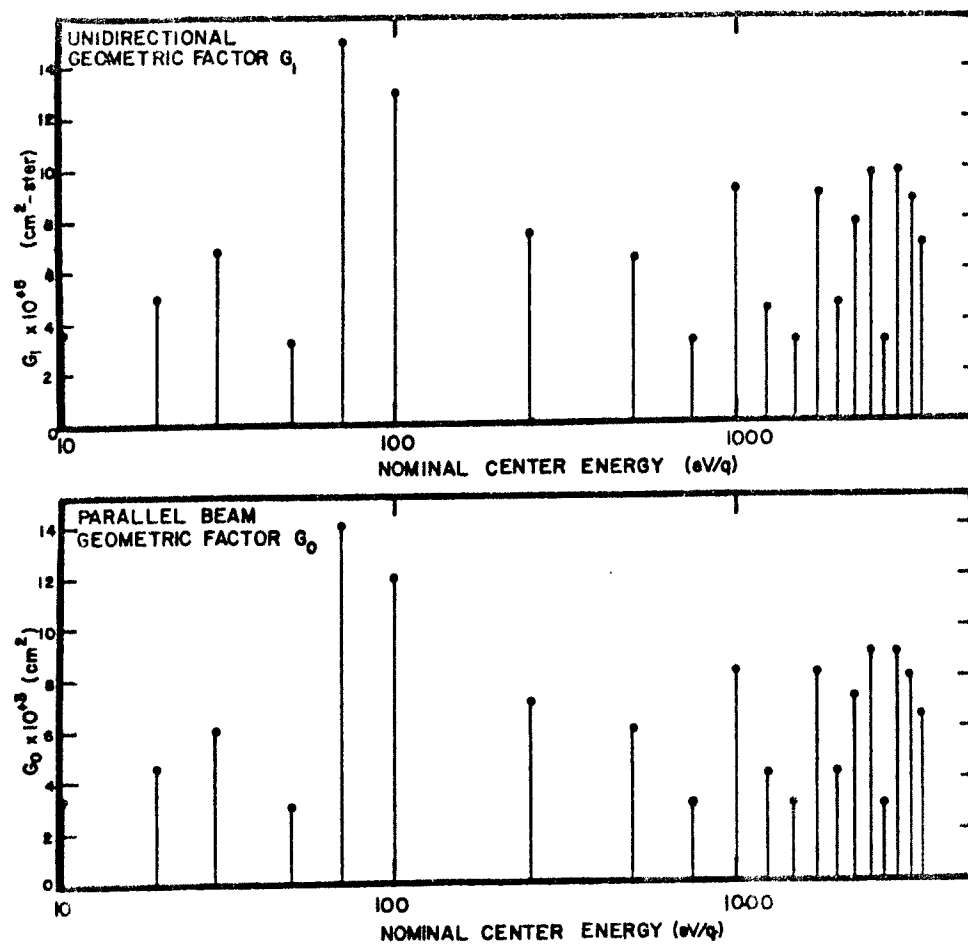


FIGURE 2-8

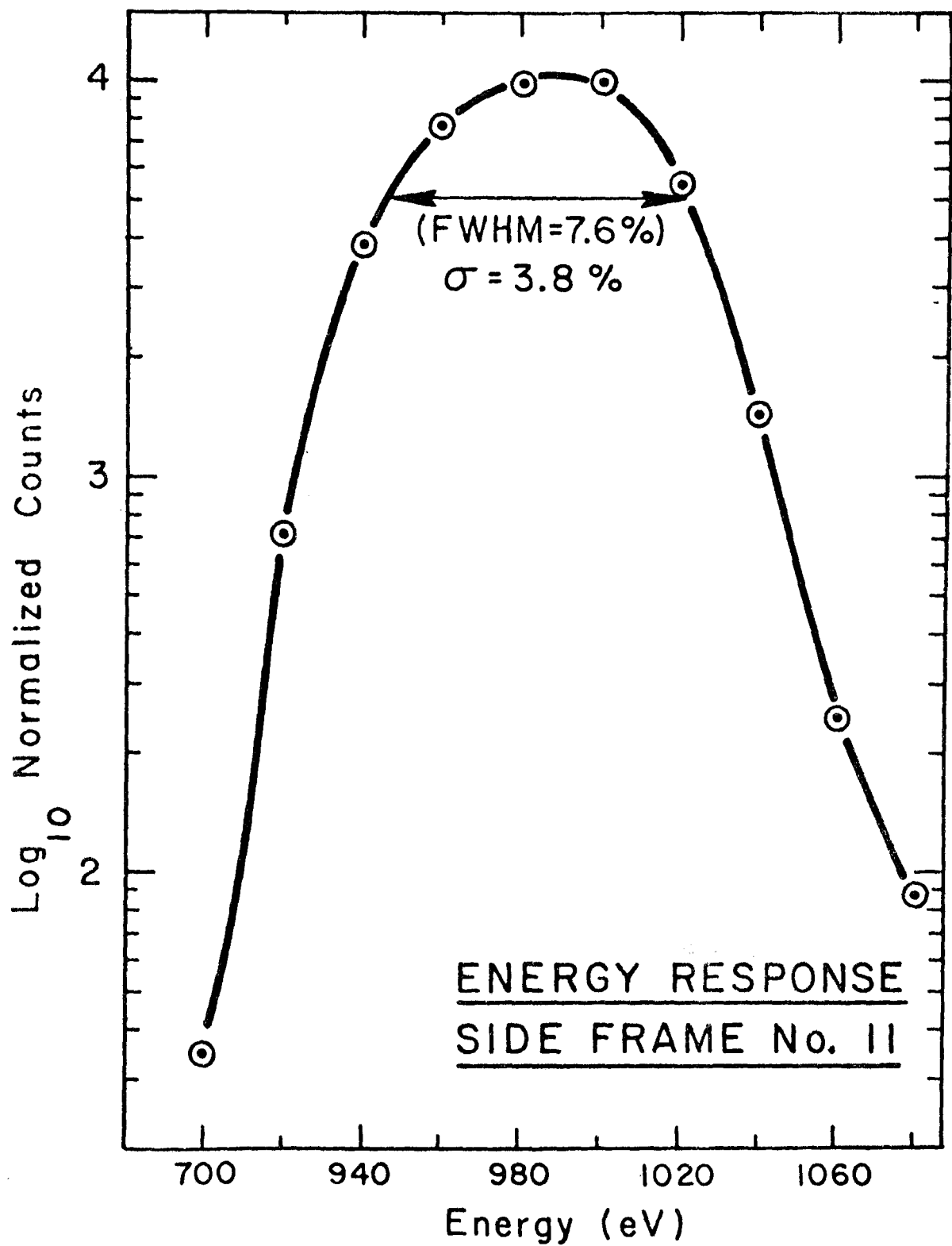


FIGURE 2-9

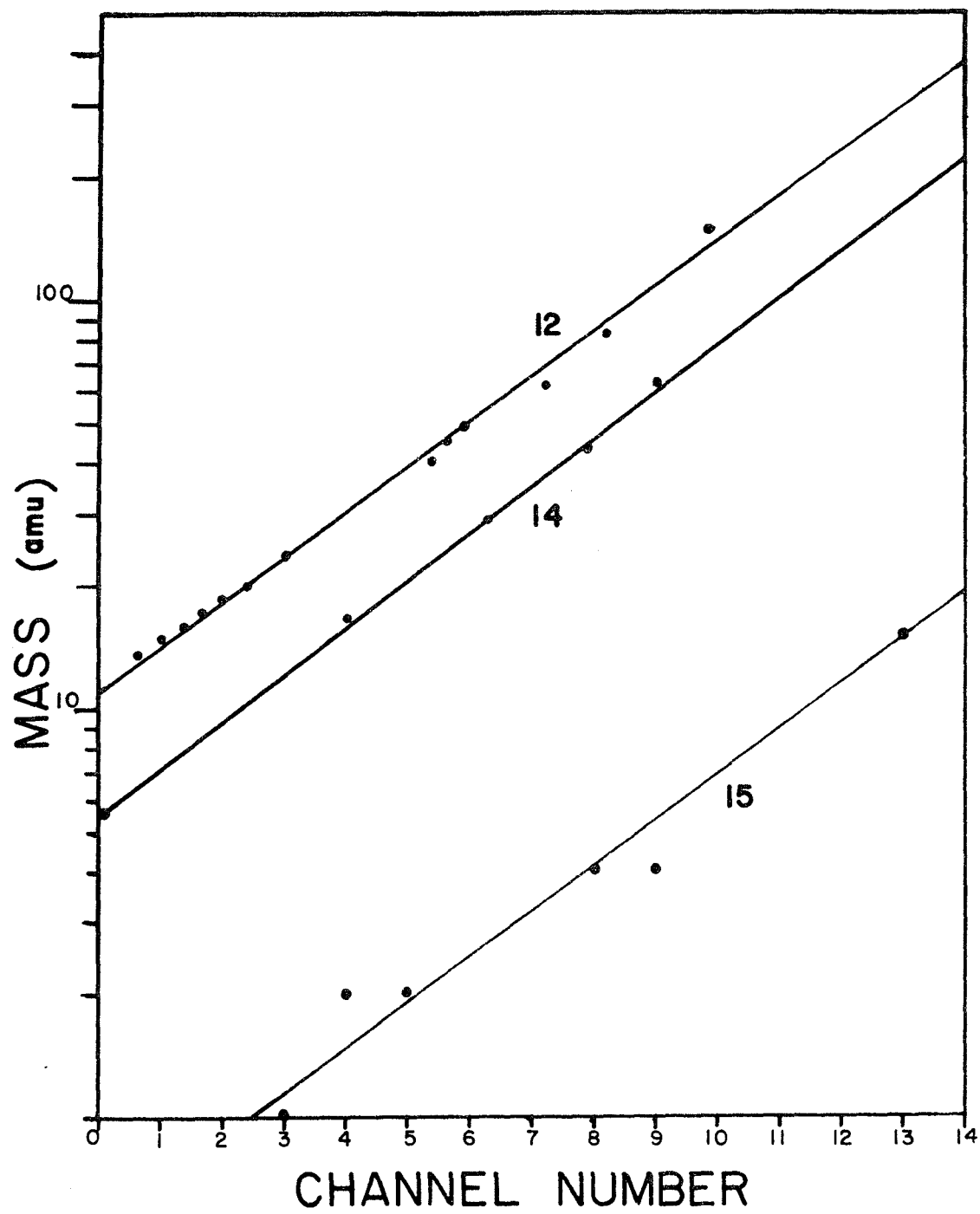


FIGURE 2-10

## 2.4 DEPLOYMENT AND ORIENTATION IN SPACE

The SIDE was deployed in three separate locations on the moon by Apollo missions 12, 14, and 15. All three SIDE's were successfully deployed and only the Apollo 12 and 15 instruments are still functioning at the time of this writing. The Apollo 14 SIDE stopped transmitting reliable data near the end of 1974.

The Apollo 12 SIDE was deployed by Alan Bean and Pete Conrad during their first lunar excursion (EVA) on November 19, 1969. The Apollo 12 site is located in the Ocean of Storms at  $23.4^{\circ}$  W longitude and  $3.04^{\circ}$  S latitude (all locations are in selenographic coordinates).

The second instrument, the Apollo 14 SIDE, was placed on the moon by Alan Shepard and Ed Mitchell on their first EVA in the Fra Mauro Highlands ( $17.48^{\circ}$  W,  $3.65^{\circ}$  S) on February 5, 1971.

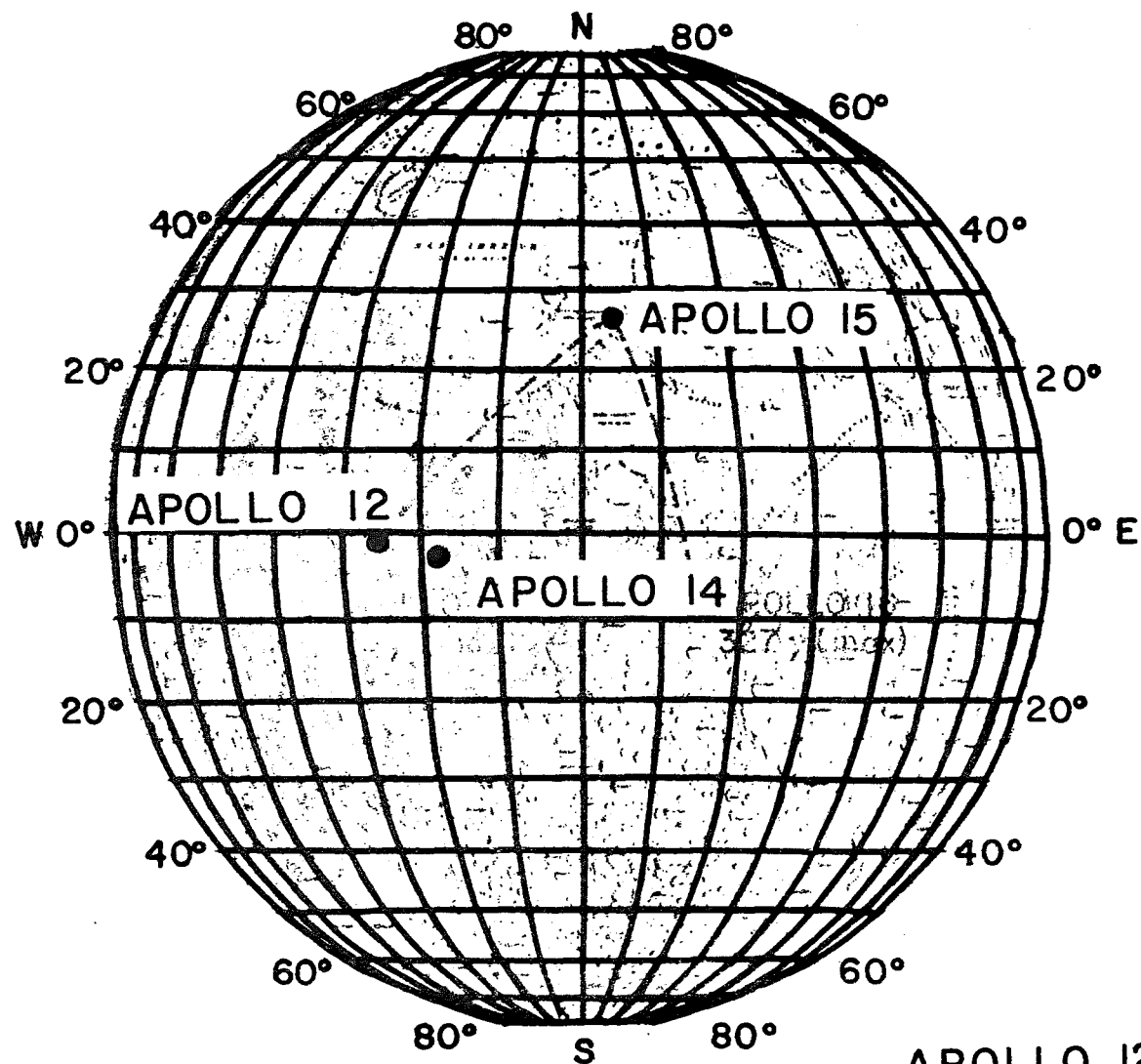
Almost six months later, the Apollo 15 SIDE was deployed in the Hadley - Appenine area ( $3.7^{\circ}$  E,  $26.2^{\circ}$  N) on July 31, 1971 by Dave Scott and James Irwin.

Figure 2-11 shows the location of each SIDE instrument on the lunar surface and their corresponding selenographic coordinates. Figure 2-12 is a collection of photographs showing the SIDE's in the deployed configuration in the laboratory and on the moon.

In order to assure the proper alignment of the Apollo 12 and 14 SIDE's, each SIDE was equipped with a bubble leveling device attached to the top of the instrument. The bubble level allows the astronaut to align the SIDE within  $5^{\circ}$  of local vertical, thus permitting the look direction of the Apollo 12 and 14 SIDE's to be approximately in the ecliptic plane. Due to its high latitude, the Apollo 15 SIDE was equip-

Figure 2-11. The location on the moon of the Apollo 12, 14, and 15 ALSEP sites along with their respective selenographic coordinates.

Figure 2-12. Photographs of the Apollo 12 and Apollo 14 SIDE's deployed on the lunar surface. The photograph of the Apollo 15 SIDE was taken in the laboratory prior to flight (after Medrano [1973]).



	LONG	LAT
APOLLO 12	23.4°W	3.04°S
APOLLO 14	17.48°W	3.65°S
APOLLO 15	3.7°E	26.2°N

FIGURE 2-11

ped with an adjustable leg permitting its look direction to be also approximately in the ecliptic plane (figure 2-13). The whole instrument is thus tilted  $26^\circ$  south with respect to the local vertical at the ALSEP site.

The look direction of the detector in each SIDE is  $15^\circ$  from the body axis of the SIDE (figure 2-14). The selenographic longitude of each instrument plus this  $15^\circ$  offset yields the correct longitude of the look direction of each instrument.

The three different look directions of the three SIDE's provides a directional sampling of magnetosphere and solar wind particles at any given time. The look directions of the three detectors are shown for various positions in lunar orbit in figure 2-15. The magnetosphere and the bow shock front are drawn in for reference.

The moon, and therefore the three SIDE instruments, moves through a number of different plasma regimes in the course of one lunation. In this thesis we will be concerned with only ions observed during the lunar night. Nighttime ions may be observed at any time between local sunset and local sunrise for each of the three SIDE instruments. It can be seen in figure 2-15 that during local lunar night for each SIDE, the detector is looking away from the sun, and thus into the so-called plasma void. This "void" is caused by the moon blocking the solar wind.

Figure 2-16 illustrates the look directions of the Apollo 12, Apollo 14, and Apollo 15 instruments at local sunset, local midnight, and local sunrise. It is interesting to note that at local sunset, the Apollo 12 SIDE looks  $15^\circ$  towards the plasma flow, whereas the Apollo 14 and Apollo 15 instruments look  $15^\circ$  away from the plasma flow. At local sunrise, the situation is reversed.

Only data from the Apollo 14 and 15 instruments have been



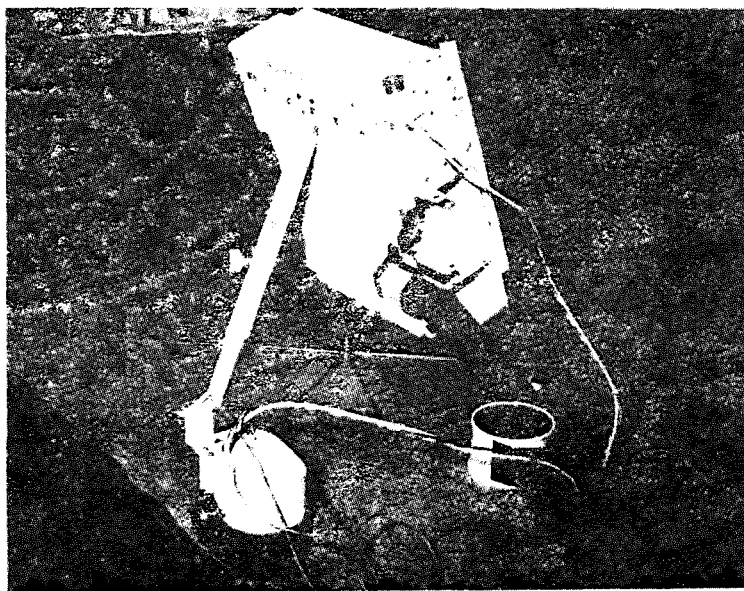
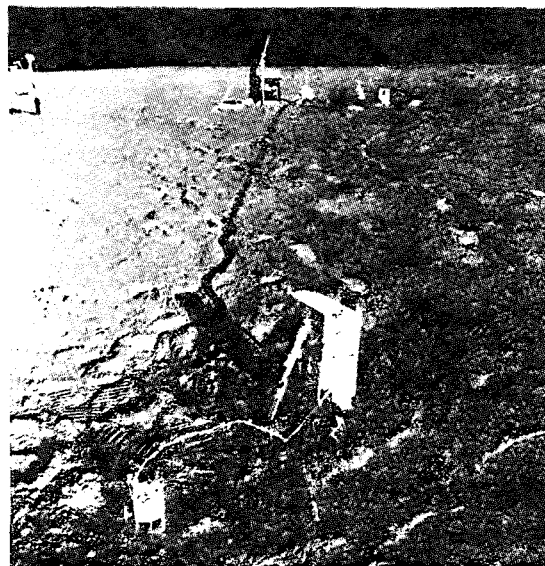


FIGURE 2-12

Figure 2-13. The upper figure shows the location in latitude of the three SIDE instruments. Apollo 12 and Apollo 14 are at approximately the same latitude. The lower figure shows the longitudinal location of the three SIDE's. The Apollo 14 SIDE looks almost directly back at the earth at all times (Benson [1974]).

Figure 2-14. Relationship of the look directions of the three detectors to their respective body axes (Benson [1974]).

Figure 2-15. The look directions of the three detectors at various positions in lunar orbit. Local noon, sunset, midnight, and sunrise are indicated for each instrument. The positions of the bow shock front and the magnetopause are shown for reference.

Figure 2-16. Look directions of the Apollo 12, Apollo 14, and Apollo 15 instruments at local sunset, local midnight, and local sunrise. The look direction of the Apollo 12 SIDE is separated by  $30^\circ$  from the Apollo 14 and Apollo 15 SIDE's at the same local time. The spacing between each set of look directions is one day. Note that at local sunset the Apollo 12 instrument looks  $15^\circ$  towards the plasma flow and the Apollo 14 and Apollo 15 instruments look  $15^\circ$  away from the flow. The situation is reversed at local sunrise.

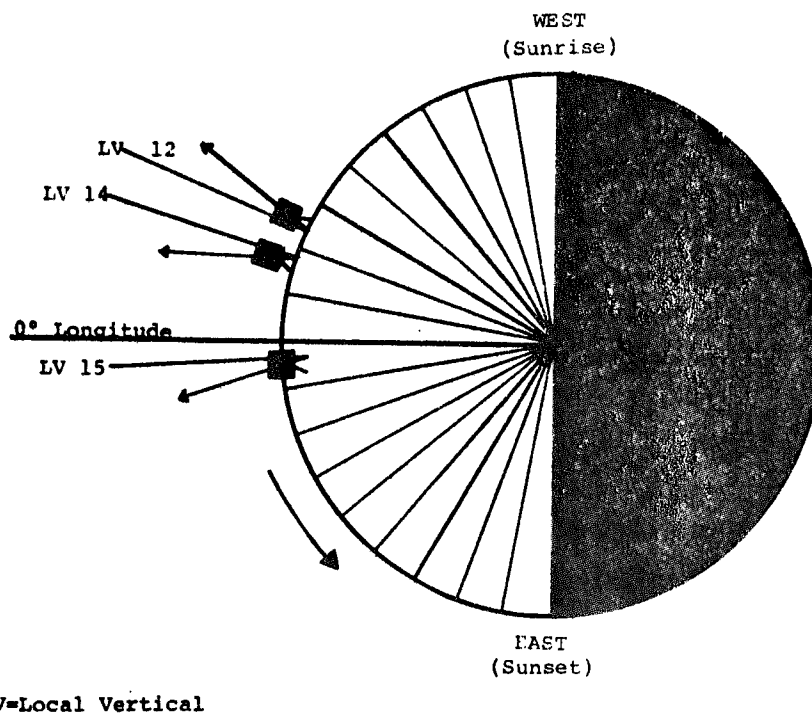
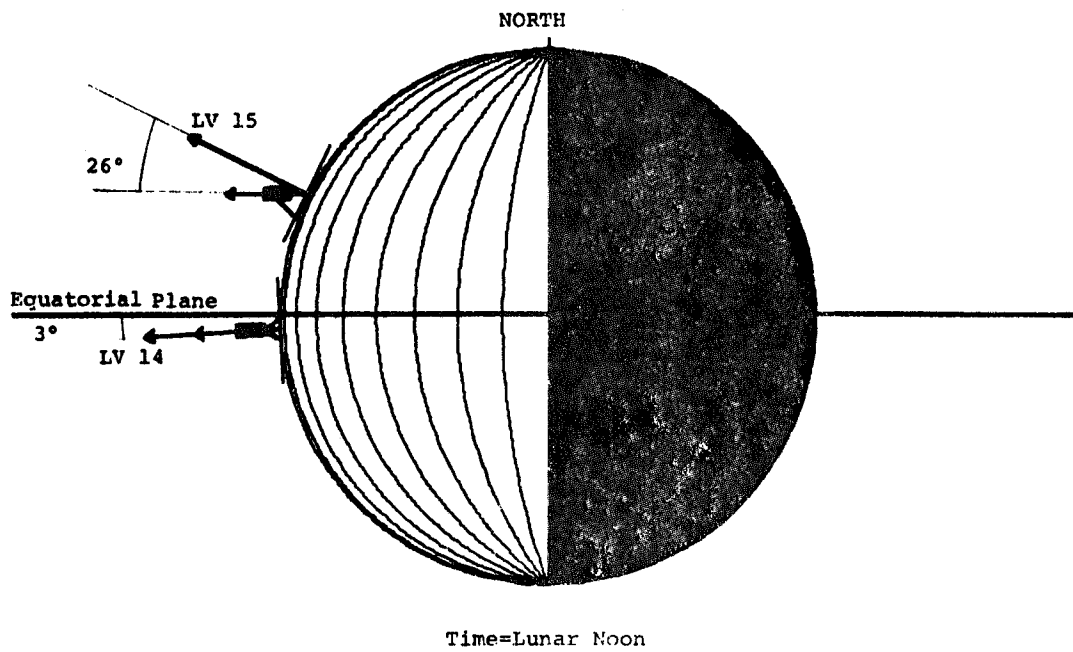
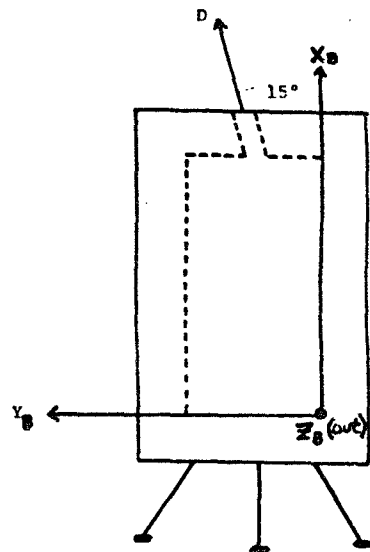
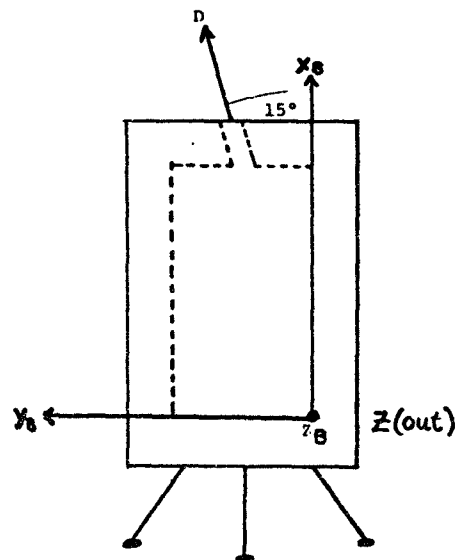


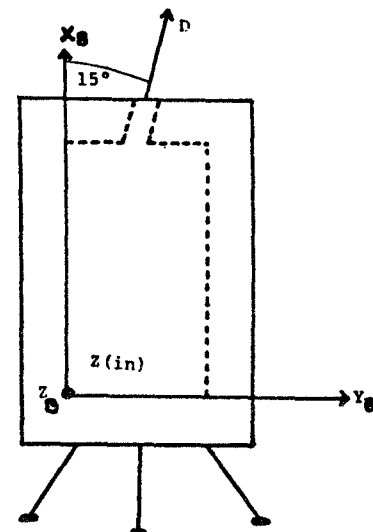
FIGURE 2-13



Apollo 15



Apollo 14



Apollo 12

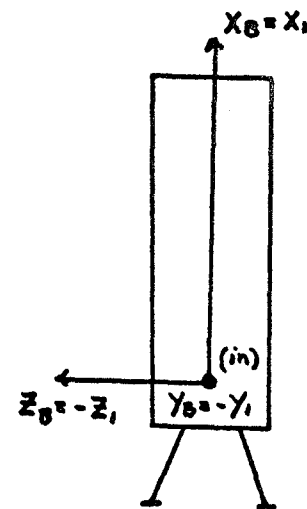
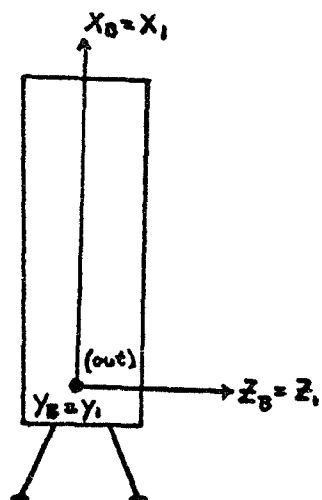
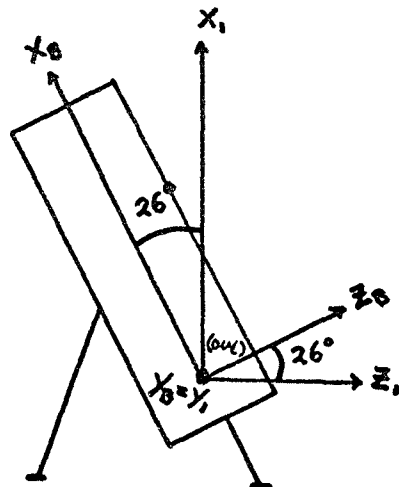


FIGURE 2-14

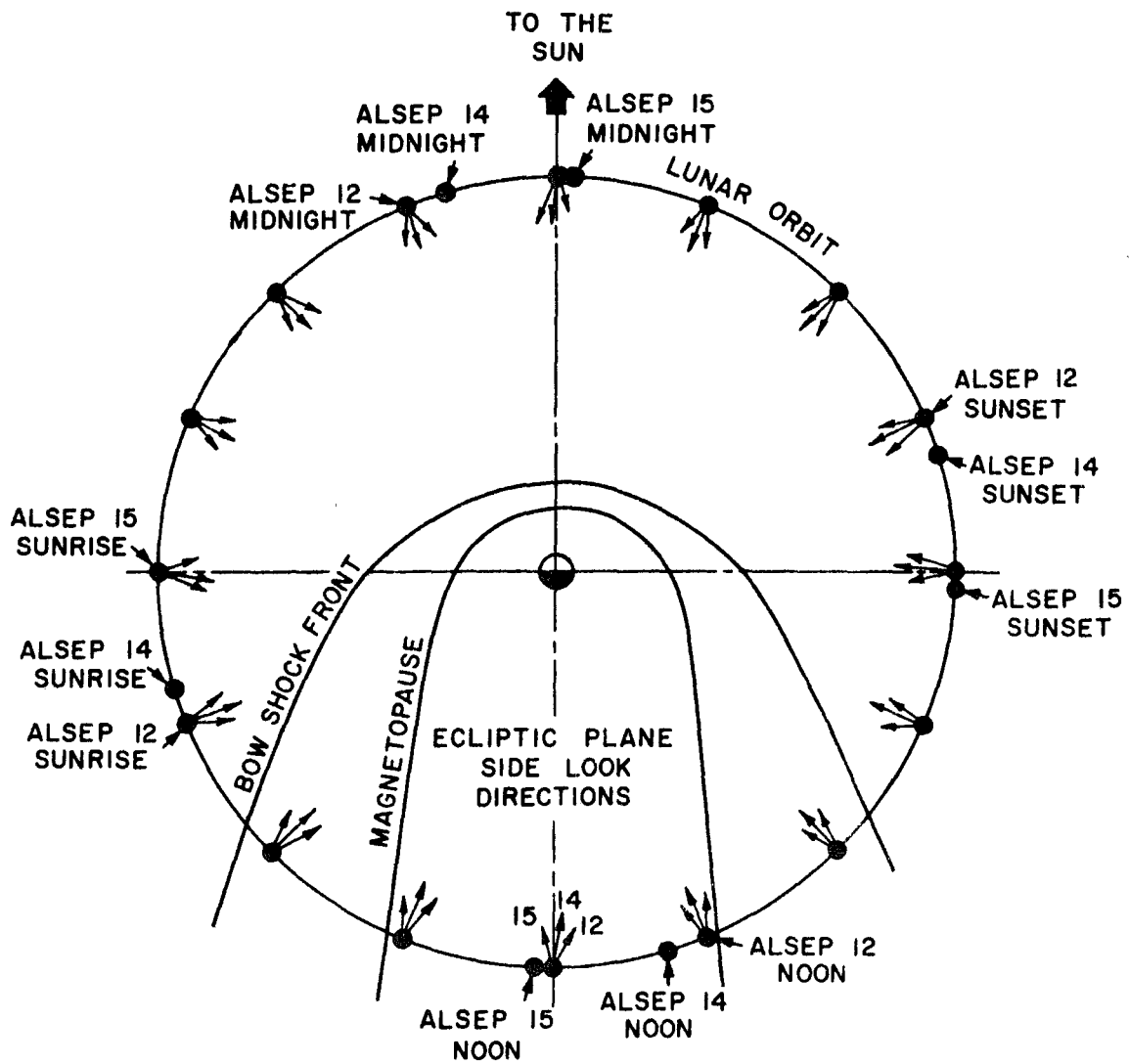
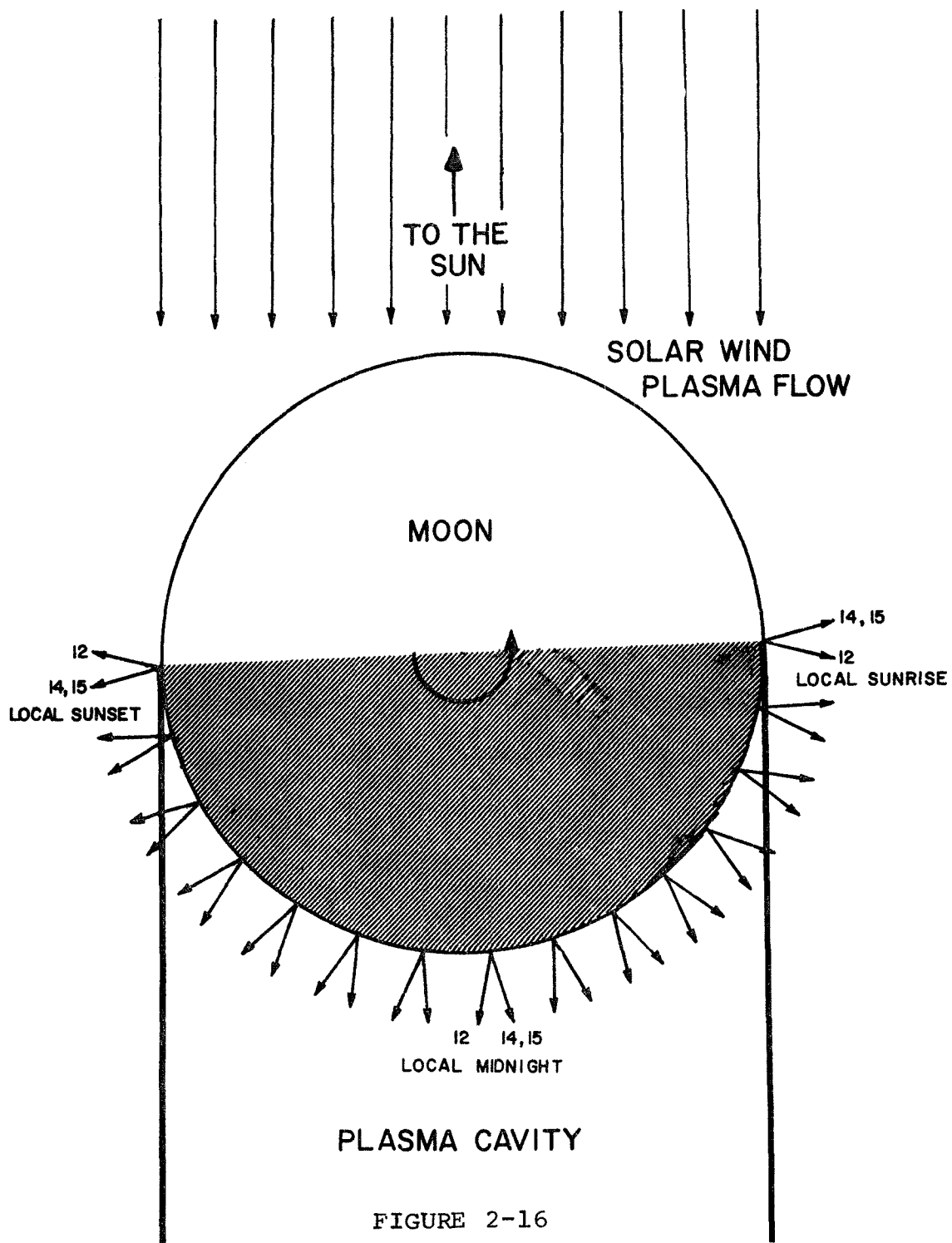


FIGURE 2-15



used in this study. Data from Apollo 12 has not been looked at as of this time.

## CHAPTER 3 - DATA

3.1 INTRODUCTION

The three SIDE's located at the Apollo 12, 14, and 15 ALSEP sites regularly observe ion fluxes at any time during the local lunar night (figure 3-1). Freeman [1972] reported on one particular ion event seen by the Apollo 12 SIDE 4.7 days prior to local sunrise. This ion event and the ion events reported in this thesis are the Type III ion events seen by Lindeman [1971]. This thesis reports on the preliminary findings of a detailed study begun on this particular subject.

Only data from the Apollo 14 and Apollo 15 SIDE's is discussed in this thesis. The data from the Apollo 12 SIDE has not been analyzed yet.

In the present analysis, the first twenty seven lunations of the Apollo 14 instrument (February 1971 - April 1973) and the first twenty one lunations (excluding lunations 16, 17, and 18) of the Apollo 15 instrument (August 1971 - April 1973) were examined. Since the Apollo 15 SIDE was deployed approximately six months after the Apollo 14 SIDE, only the latter twenty one lunations of the Apollo 14 data are coincident in time with the data from the Apollo 15 instrument.

No mass analysis of the nighttime ion events is possible since their respective energies are too high to be detected by the Mass Analyzer. The highest particle energy that the MA can observe is 48.6 eV/q and the lowest energy of the nighttime ion events is 250 eV/q. Therefore, only data from the TID was analyzed. Consequently, one has to assume a mass composition for these ion events.



Figure 3-1. Diagram showing one complete lunation (from local midnight to local midnight) of ion data collected by the SIDE. The lunation plotted is lunation 20 for the Apollo 15 SIDE. Nighttime ion events (NIE) are seen in the first panel. The x-axis represents the 20 energy channels of the SIDE which are: 10, 20, 30, 50, 70, 100, 250, 500, 750, 1000, 1250, 1500, 1750, 2000, 2250, 2500, 2750, 3000, 3250, and 3500 eV/q. The y-axis proceeds up the page and each unit is equal to 24 hours. The z-axis is the log of the average counting rate in each energy channel and one counting rate energy spectrum corresponds to a twenty minute average of the data. The whole lunation is divided into 4 panels. The first panel runs in time from local midnight to local sunrise, the second from local sunrise to local noon, the third from local noon to local sunset, and the fourth from local sunset to local midnight. Each panel is approximately 7 1/2 days of data. Mid, s r, noon, and s s correspond to midnight, sunrise, noon, and sunset respectively.

APOLLO 15  
1973  
LUN 20

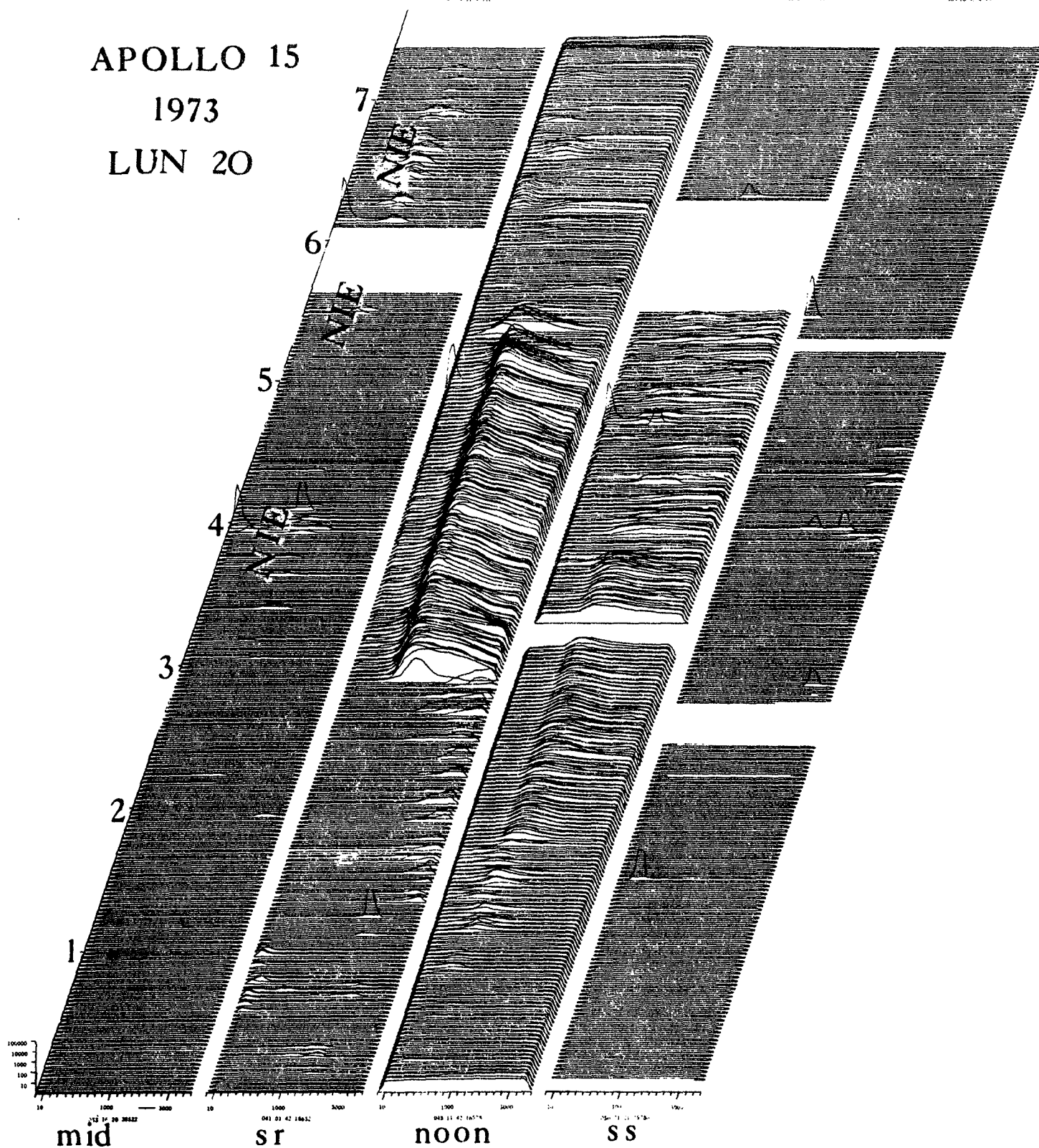


FIGURE 3-1

### 3.2 OBSERVATIONS

Nighttime ion events occur sporadically throughout the local lunar night and are not observed on every lunation. Some lunations show very little activity whereas other lunations are extremely active. There is, however, a definite period just before local lunar midnight where nighttime ions are never observed (figures 3-2 and 3-3). It can be seen from figures 3-2 and 3-3 that the activity increases after local midnight and that the Apollo 15 instrument is much more active than the Apollo 14 instrument for the same period of time.

The increased activity at the Apollo 15 ALSEP site over the Apollo 14 ALSEP site may be due to the fact that the local magnetic field at the Apollo 14 site is much stronger than at the Apollo 15 ALSEP site. Burke and Moore [1975] calculated that the magnetic field at the Apollo 14 site strongly influences the flux of photoelectrons that they observe. This local magnetic field tends to screen the detectors at the Apollo 14 ALSEP site from incoming particles. Since there is a very small local magnetic field at the Apollo 15 ALSEP site, it would not effect the particle fluxes incident there at the lunar surface.

The observed energies of nighttime ion events range from 250 to 1000 eV/q. These ion energies are slightly less than the average solar wind energy of 800 eV. The nighttime ion events differential flux energy spectra normally peak in the 500 eV/q energy channel (figure 3-4). However, the peak energy of the differential flux energy spectra statistically shifts as the moon rotates. The Apollo 14 SIDE observes nighttime ion events peaking in the 500 eV/q energy channel up to 3 days past local midnight. The peak energy then shifts up to the 750 eV/q energy channel for about one day. Approximately 48

Figure 3-2. Chart depicting the time of occurrence and duration of nighttime ion events for the Apollo 14 SIDE. The x-axis is in units of hours after local sunset with local midnight at 180 hours and local sunrise at 360 hours (based on a 15 day lunar night). The y-axis is the lunation number of the 27 consecutive lunations progressing down the page. The strength of the nighttime ion events is not indicated, but the peak energy present in the counting rate spectrum for each event is shown.

Figure 3-3. Same format as for figure 3-2 except that the data plotted is for Apollo 15.

Figure 3-4. Twenty minute averaged differential flux energy spectrum for an event in the 500 eV/q energy channel. The background flux represents an average counting rate of 0.18 counts per energy channel. This event occurred 4 days before local sunrise (Schneider and Freeman [1975]).

# TIME OF OCCURENCE AND DURATION OF NIGHTTIME ION EVENTS FOR APOLLO 14

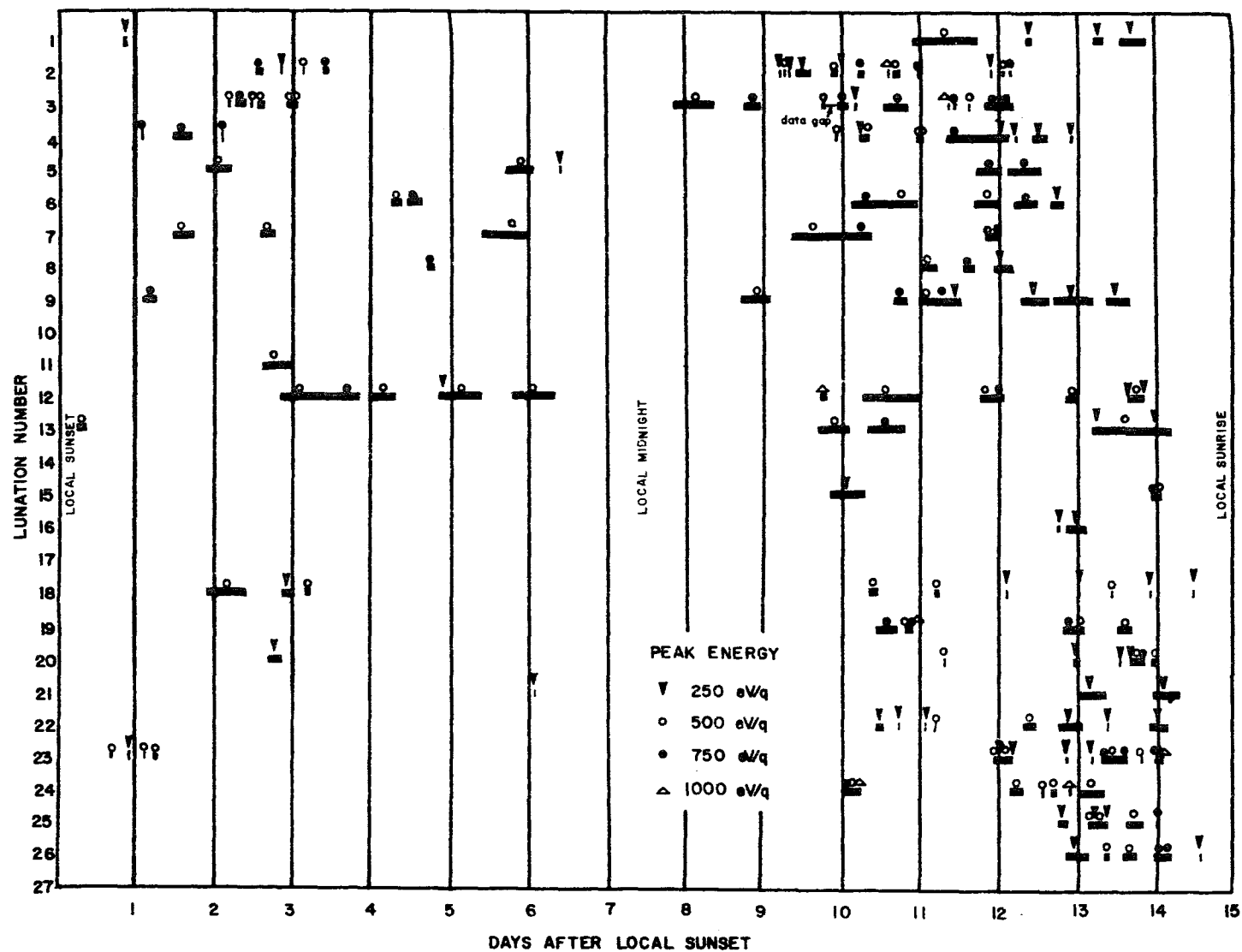


FIGURE 3-2

# TIME OF OCCURENCE AND DURATION OF NIGHTTIME ION EVENTS FOR APOLLO 15

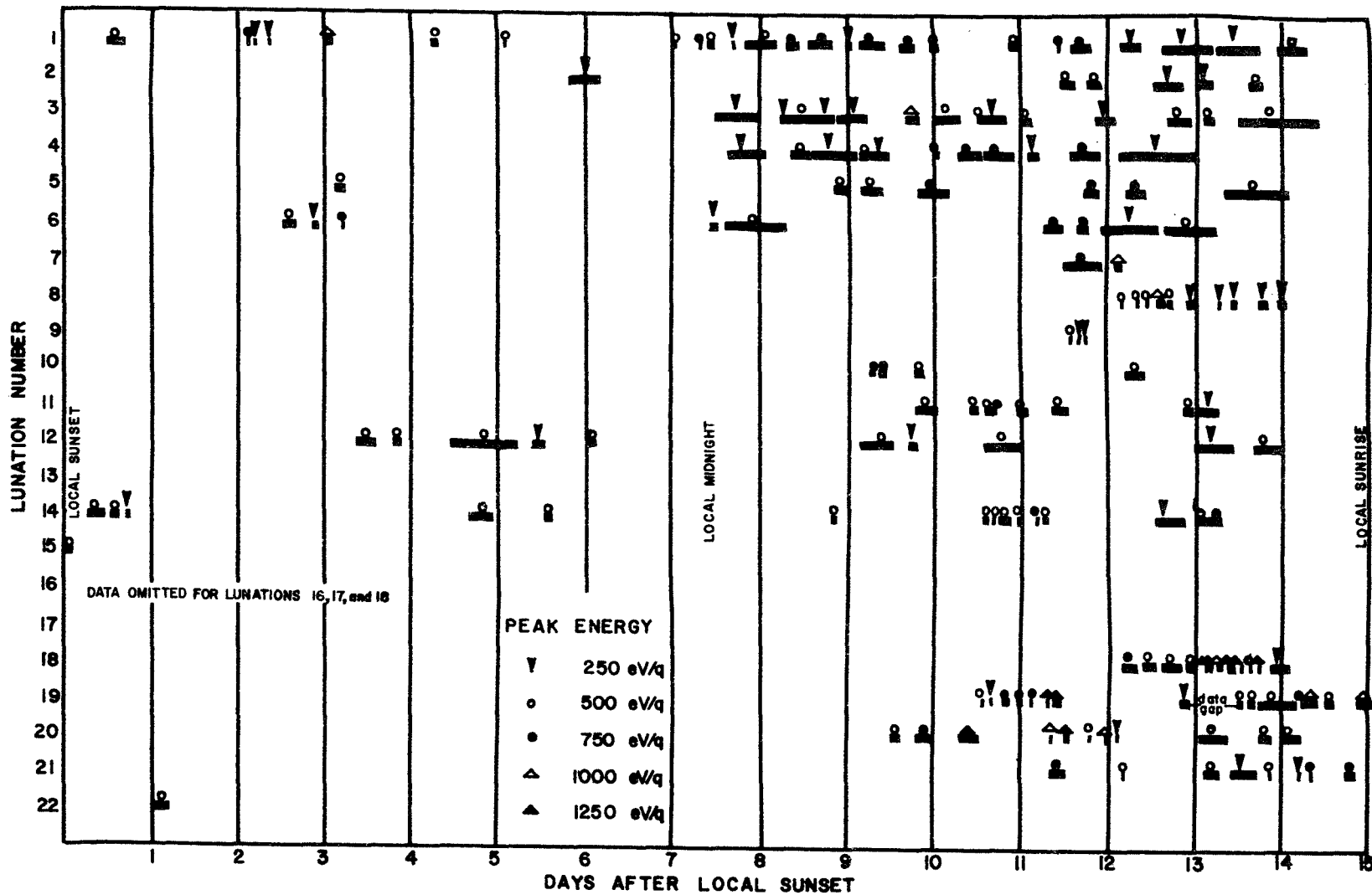


FIGURE 3-3

APOLLO 14 1971

61<sup>d</sup> 9<sup>h</sup> 5<sup>m</sup>

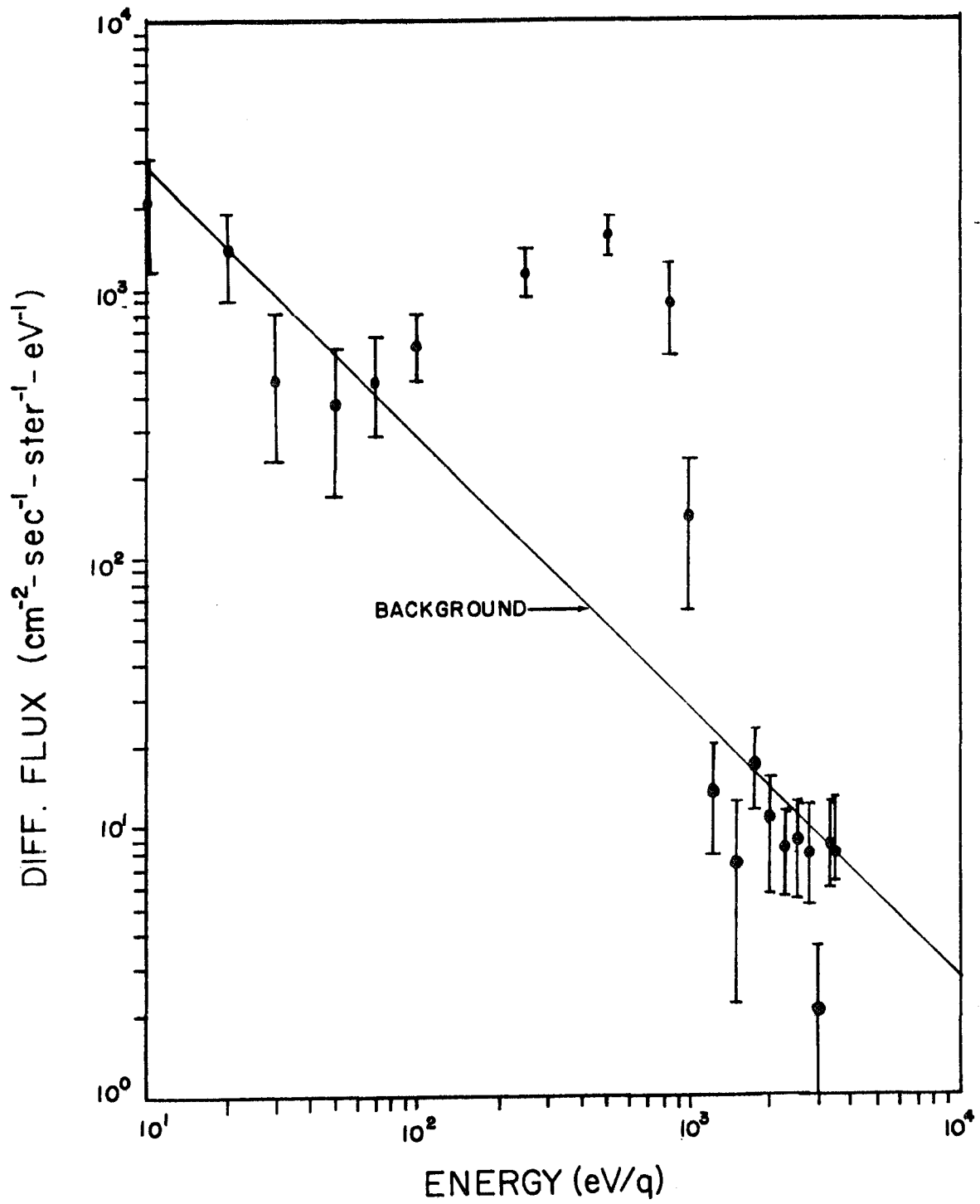


FIGURE 3-4

hours prior to local sunrise, the energy spectrum shifts down to 250 eV/q and this peak energy is observed up to the sunrise terminator (figure 3-5).

The Apollo 15 SIDE observes qualitatively the same behavior. The peak energy is seen to shift between the 250 and 500 eV/q energy channels for ten days past local sunset, most often peaking in the 500 eV/q energy channel. The nighttime ion spectra are then observed to peak in either the 500 or 750 eV/q energy channels for approximately two days. Again, prior to local sunrise, the peak energy of the nighttime ion spectra shifts down to the 250 eV/q energy channel (figure 3-6).

One notices from figures 3-2, 3-3, 3-5, and 3-6 that nighttime ion events do occur with peak energies of 1000 and 1250 eV/q. It can also be seen that these higher peaked energy events occur most often after local midnight. This phenomenon is probably a result of the fact that more nighttime ion events are observed after local midnight than before.

Figures 3-7, 3-8, and 3-9 show twenty minute averaged nighttime ion differential flux energy spectra peaking respectively in the 250, 750, and 1000 eV/q energy channels. One notices from figures 3-4, 3-7, 3-8, and 3-9 that the differential flux of the ions is sharply peaked about the peak energy. The background differential flux line in each figure represents an average counting rate in all energy channels that is very small (0.11 to 0.23 counts). The average background flux is computed for the corresponding twenty minute time interval that is averaged over for each individual event. The nighttime background flux is very stable and it is always within the above limits for a twenty minute average of nighttime data. One must keep in mind, however, that the background differential flux that is plotted is indeed a time average and



Figure 3-5. Diagram displaying the peak energy shift of nighttime ion events for the Apollo 14 SIDE from local sunset to local sunrise. Time progresses down the page in 12 hour segments and energy increases to the right. The third dimension is the number of events per lunation with a particular peak energy. A scale to measure this number from the plot is given in the lower right hand corner.

Figure 3-6. Diagram displaying the peak energy shift of nighttime ion events for the Apollo 15 SIDE from local sunset to local sunrise. Same format as figure 3-5.

Figure 3-7. Twenty minute averaged differential flux energy spectrum for a nighttime ion event peaking in the 250 eV/q energy channel. The background flux represents an average counting rate of 0.19 counts per energy channel. This particular event occurred 4 days after local sunset.

Figure 3-8. Twenty minute averaged differential flux energy spectrum for an event in the 750 eV/q energy channel. The background flux represents an average counting rate of 0.11 counts per energy channel. This event occurred 4 days before local sunrise.

Figure 3-9. Twenty minute averaged differential flux energy spectrum for an event peaking in the 1000 eV/q energy channel. The background flux represents an average counting rate of 0.23 counts per energy channel. This event occurred 4 days before local sunrise.

# FREQUENCY OF OCCURENCE OF A PEAK ENERGY FOR APOLLO 14

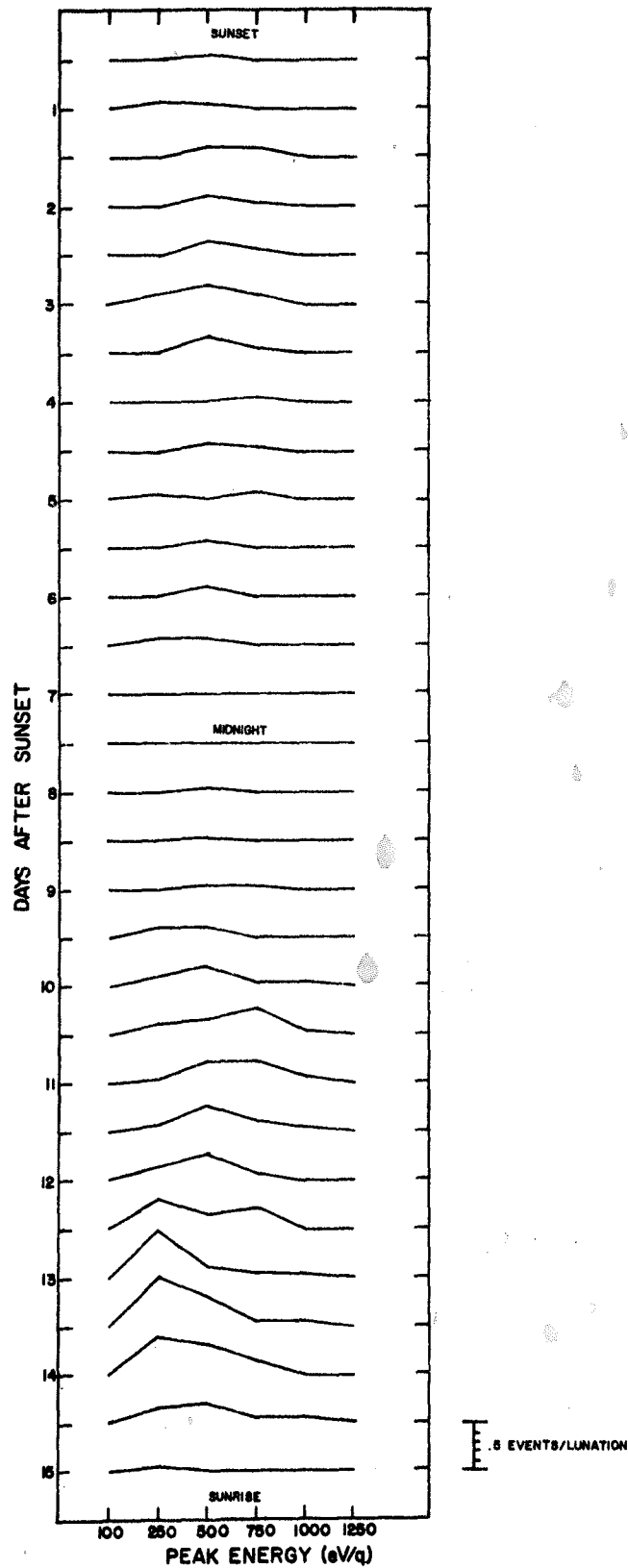


FIGURE 3-5

FREQUENCY OF OCCURENCE OF A PEAK ENERGY  
FOR APOLLO 15

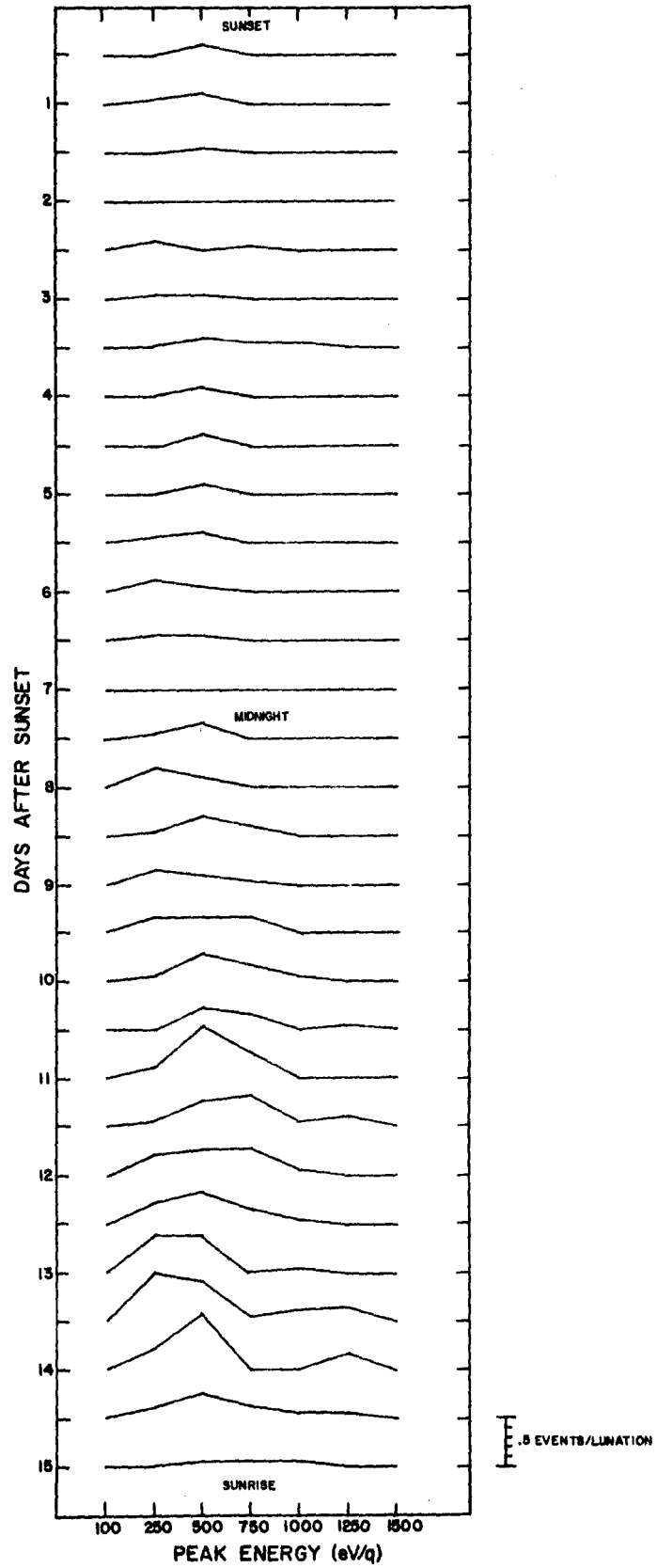


FIGURE 3-6

APOLLO 14 1971

$83^d 1^h 12^m$

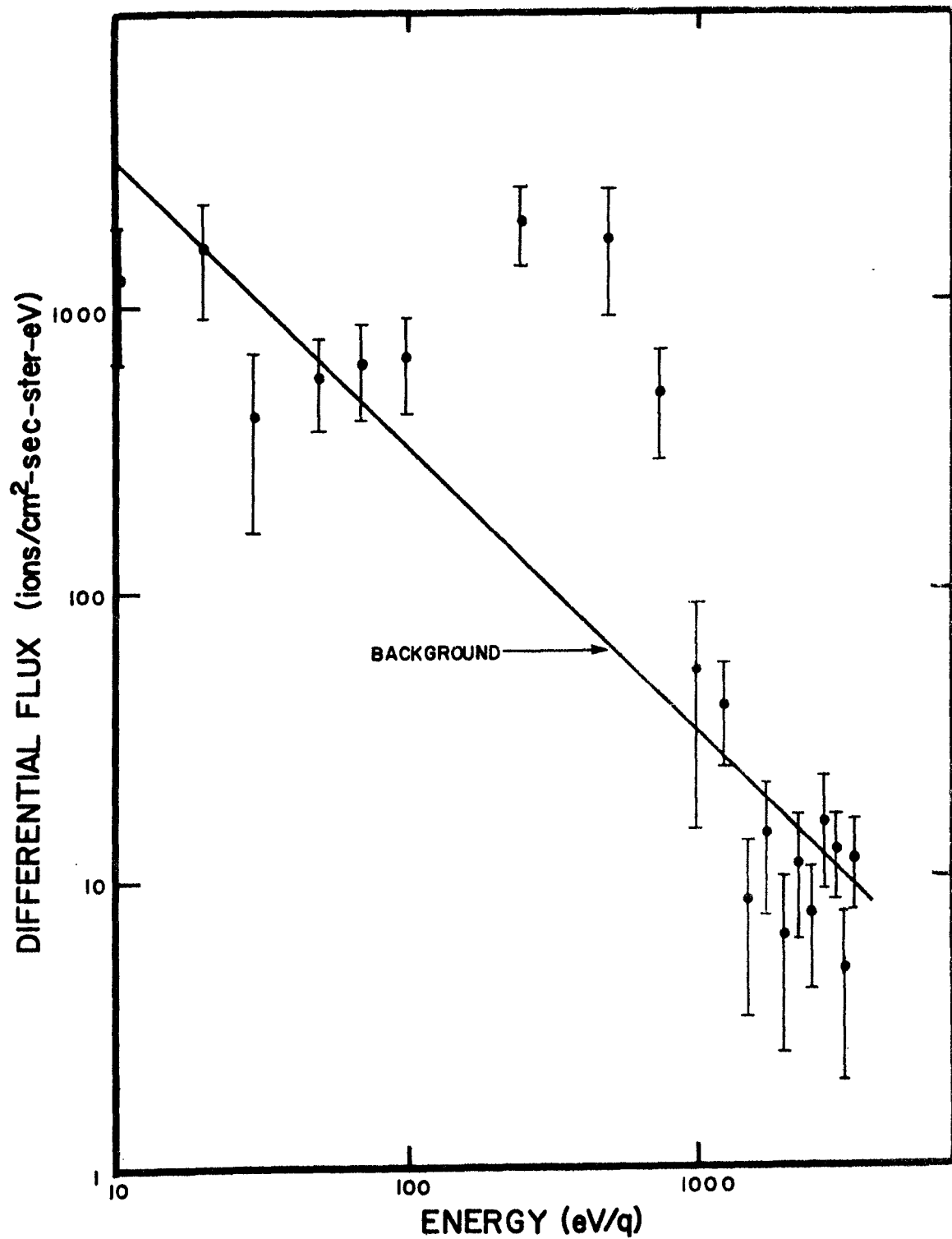


FIGURE 3-7

APOLLO 15 1971

237<sup>d</sup> 9<sup>h</sup> 0<sup>m</sup>

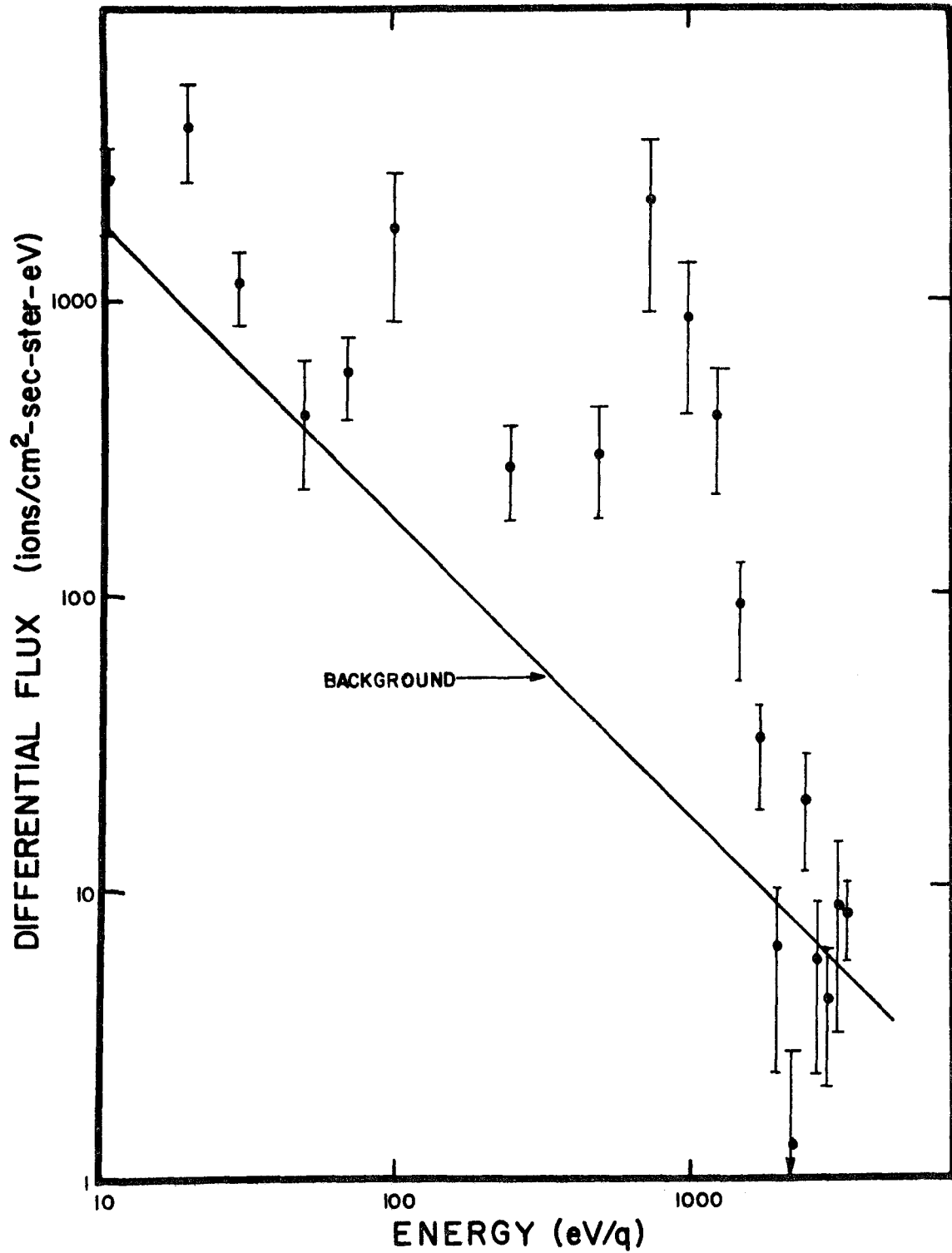


FIGURE 3-8

APOLLO 15 1971

237<sup>d</sup> 8<sup>h</sup> 29<sup>m</sup>

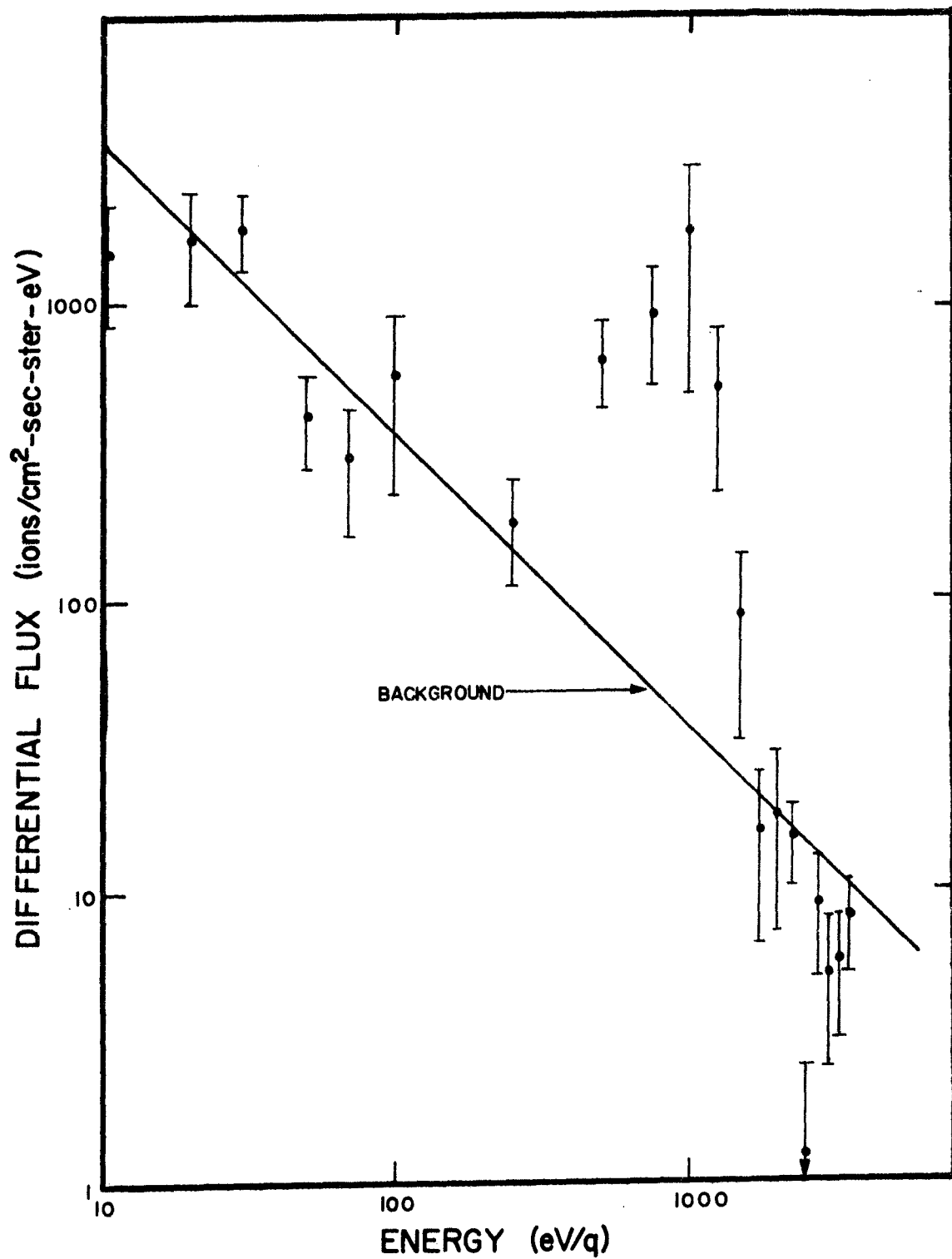


FIGURE 3-9

not necessarily the same in each energy channel. Figure 3-8 shows what appears to be a double peaked spectrum with energy peaks in the 100 and 750 eV/q energy channels. What is actually the case is that the background differential flux computed from the background channels is in all probability too low. If the real background flux represented an average counting rate of 0.23 counts instead of 0.11 counts, then the spectrum above the background would not be double peaked.

One notices from figures 3-4, 3-7, 3-8, and 3-9 that, when an event occurs, the differential flux in the energy channels where an event is present is of the order of  $10^3$  ions/cm<sup>2</sup>-sec-ster-eV. Integration over the entire spectrum above the background for an event yields an integral flux on the order of  $10^6$  ions/cm<sup>2</sup>-sec-ster. This flux is less than the solar wind flux by 2 orders of magnitude.

There are a few scattered cases when either the Apollo 14 or Apollo 15 SIDE observes a mono-energetic nighttime ion spectrum in either the 250 or 500 eV/q energy channel (figure 3-10). These events always occur 2 to 3 days prior to local sunrise. The error bars on the peak in figure 3-10 are so small because this particular event was continuous at the same flux throughout almost the entire twenty minutes the event was averaged over.

The occurrence of a nighttime ion event is characterized by a sharp increase in the counting rate, in the characteristic energy channels, at the onset and a sharp decrease in the counting rate at the end. There is no noticeable rise or decay of the counting rate. Figure 3-11 displays the ten minute averaged counting rate for twenty four hours in the 250, 500, 750, 1000, and 1250 eV/q energy channels. The particular events plotted were seen by the Apollo 15 instrument on day 65 of 1973. These ion events occurred six days prior to local

Figure 3-10. Twenty minute averaged differential flux energy spectrum for a mono-energetic nighttime ion event in the 250 eV/q energy channel. The background flux represents an average counting rate of 0.21 counts per energy channel. This event occurred 3 days before local sunrise.

Figure 3-11. A plot of the ten minute averaged counting rate for 24 hours in the 250, 500, 750, 1000, and 1250 eV/q energy channels. Shaded regions indicate the time and duration of the events. These particular events occurred at the Apollo 15 ALSEP site 6 days before local sunrise.



APOLLO 15 1971

238<sup>d</sup> 8<sup>h</sup> 6<sup>m</sup>

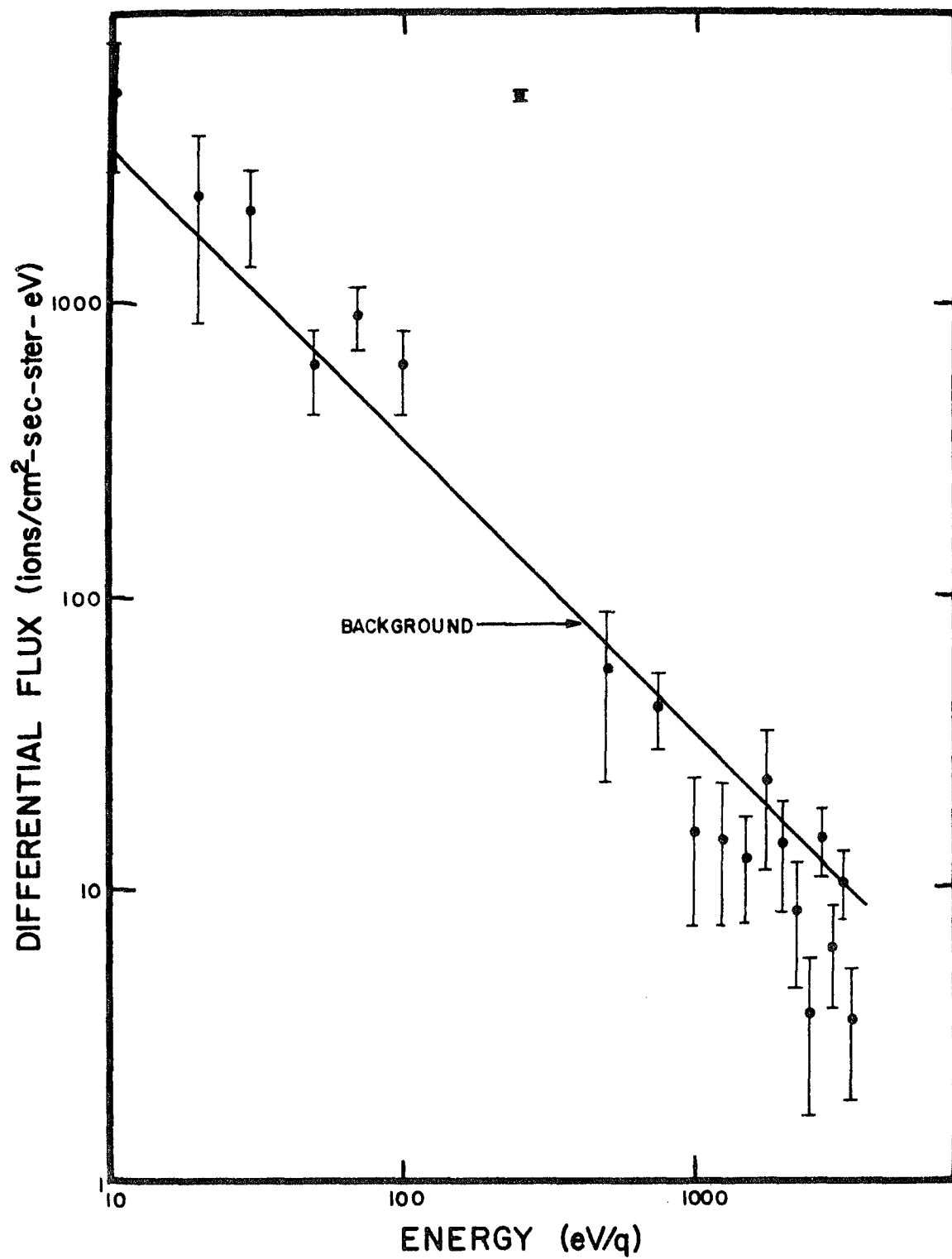


FIGURE 3-10

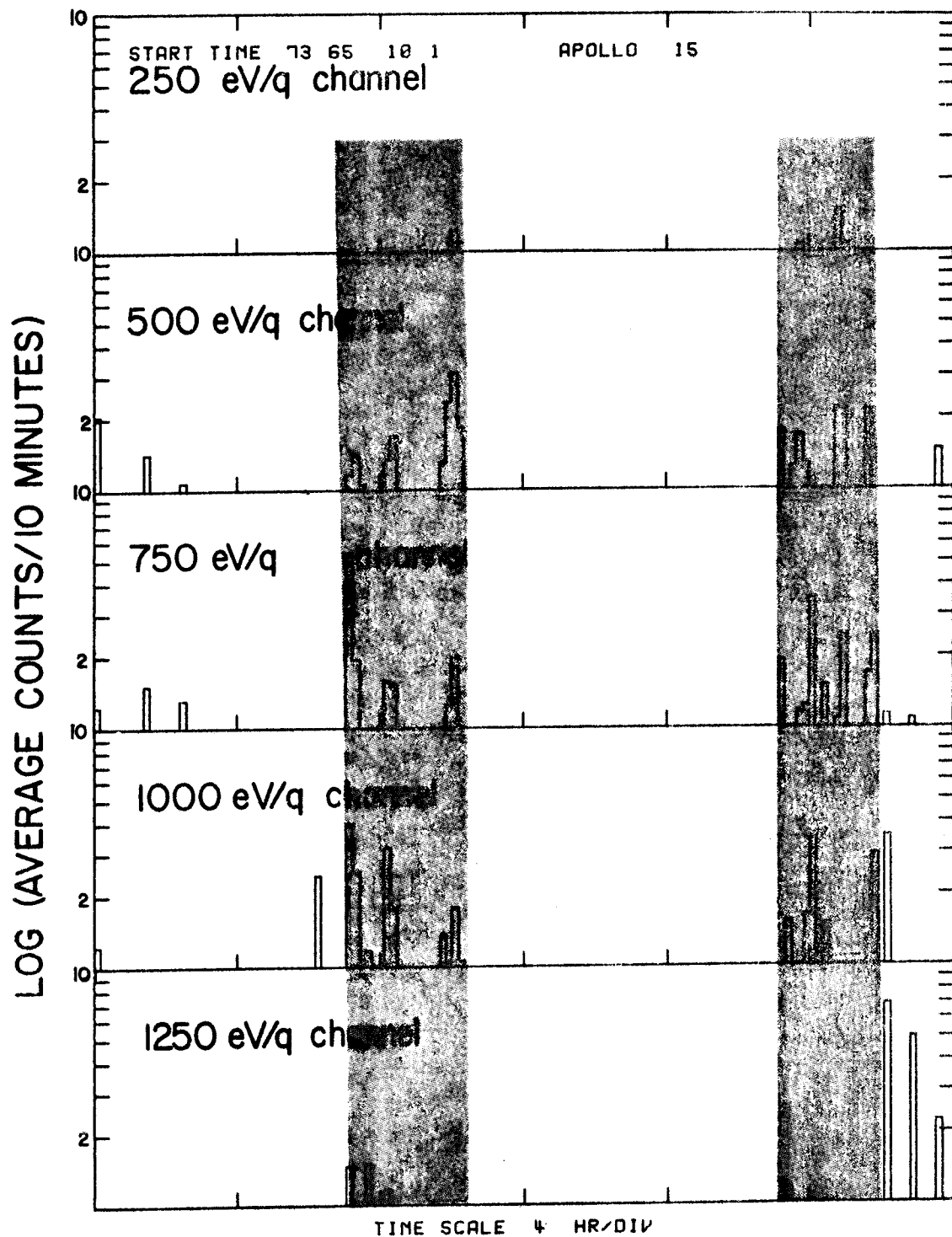


FIGURE 3-11

sunrise.

Figure 3-11 also demonstrates the fact that the nighttime ion events are short lived. The duration of nighttime ion events is most often 4 hours or less and normally on the order of minutes. Table 3-1 tabulates the number of events of a particular duration for both the Apollo 14 and Apollo 15 instruments. The long lived ion events listed in Table 3-1 are normally a superposition of a number of shorter events.

The lunar night is very quiet except for the occurrence of a nighttime ion event. It is therefore extremely easy to detect the presence of an event. Near the terminator regions, the SIDE also observes bow shock protons (Benson [1974]). The energy spectrum of nighttime ions is entirely different from bow shock protons (figure 3-12). We can safely state, therefore, that the source mechanism for these two types of ion events is different. Figure 3-13 gives a clear indication of the difference between nighttime ions and bow shock protons. The bow shock protons are seen in figure 3-13 as the high energy shoulder that starts just before sunrise. Also seen in figure 3-13, starting at about sunrise, are low energy ions. These ions are a result of the negative surface potential near the terminator (Lindeman et al. [1973]).

As mentioned earlier, nighttime ion events may occur at any time between local lunar sunset and local lunar sunrise. Nighttime ion events are not just confined to the lunar nighttime. There are a few rare cases where the SIDE observes a monoenergetic 500 eV/q ion peak that begins prior to the sunrise terminator crossing and persists until the moon enters the earth's magnetosheath. This phenomenon will be discussed further in a later section.

There is a preference for nighttime ion events to occur

TABLE 3-1  
NUMBER OF EVENTS OF A PARTICULAR DURATION

<u>DURATION</u>	<u>APOLLO 14</u>	<u>APOLLO 15</u>
0 to 1 hours	50	49
1 to 2	27	31
2 to 3	9	21
3 to 4	18	17
4 to 5	9	13
5 to 6	8	7
6 to 7	7	4
7 to 8	11	9
8 to 9	2	6
9 to 10	0	4
10 to 11	1	0
11 to 12	4	2
12 to 13	0	1
13 to 14	2	1
14 to 15	0	2
15 to 16	0	0
16 to 17	0	1
17 to 18	0	2
18 to 19	2	0
19 to 20	2	0
20 to 21	0	0
21 to 22	0	2
22 to 23	0	0
23 to 24	0	0

Figure 3-12. Two bow shock proton spectra averaged over twenty minutes. These bow shock proton spectra occurred about 1 day from the bow shock on either side of the magnetosphere. Dusk and dawn refer to a terrestrial coordinate system. The integral fluxes were obtained by integrating over the spectrum that is above background. Note the obvious difference between these spectra and the nighttime ion spectra (Benson et al. [1974]).

Figure 3-13. A three-dimensional plot illustrating the positive nighttime ion events and bow shock proton events. The energy channel scale is not a linear scale, the corresponding energy channels measure the following energies: 10, 20, 30, 50, 70, 100, 250, 500, 750, 1000, 1250, 1500, 1750, 2000, 2250, 2500, 2750, 3000, 3250, and 3500 eV/q. The z-axis is the logarithm of the average counting rate over a twenty minute time interval. The y-axis is the time axis proceeding positively up the page. One unit on the y-scale is 24 hours and one spectrum represents a twenty minute average of the data. This particular plot starts about 13 days after local sunset. The low energy ions seen near the end of the plot are terminator ions and are only seen at the terminators. BSP, NIE, and TI are abbreviations for bow shock protons, nighttime ion events, and terminator ions respectively (after Schneider and Freeman [1975]).

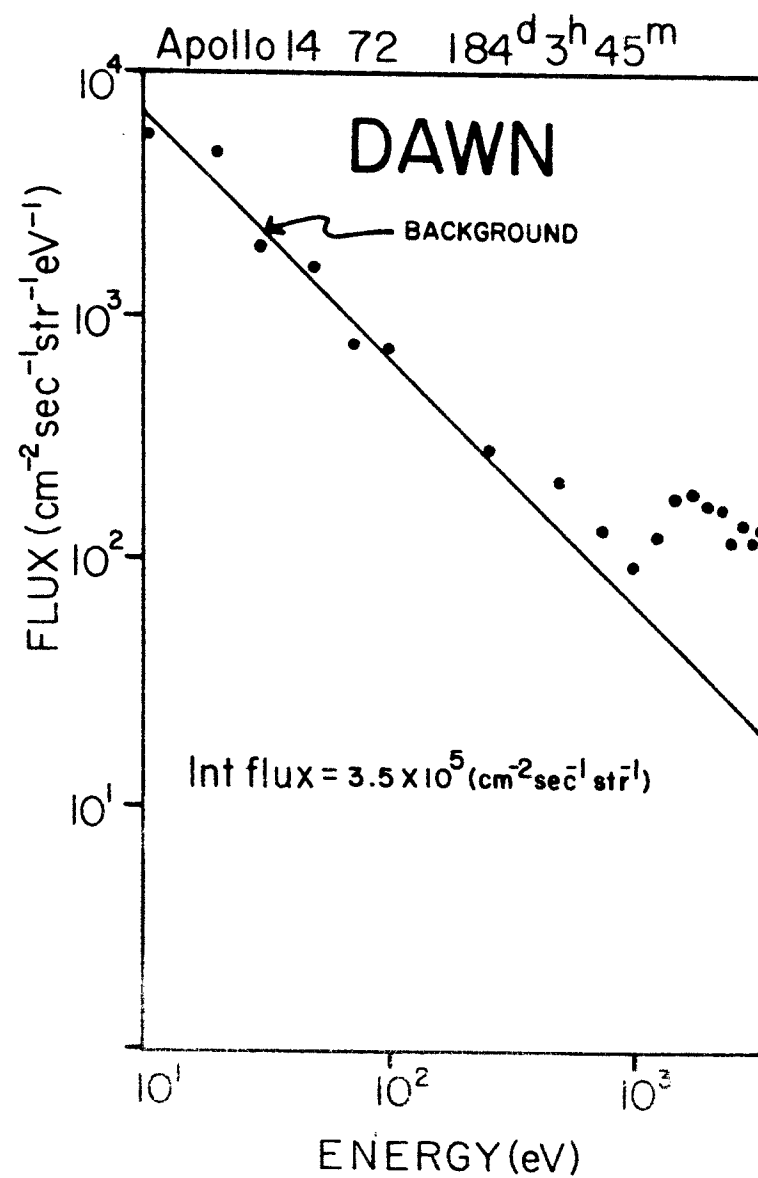
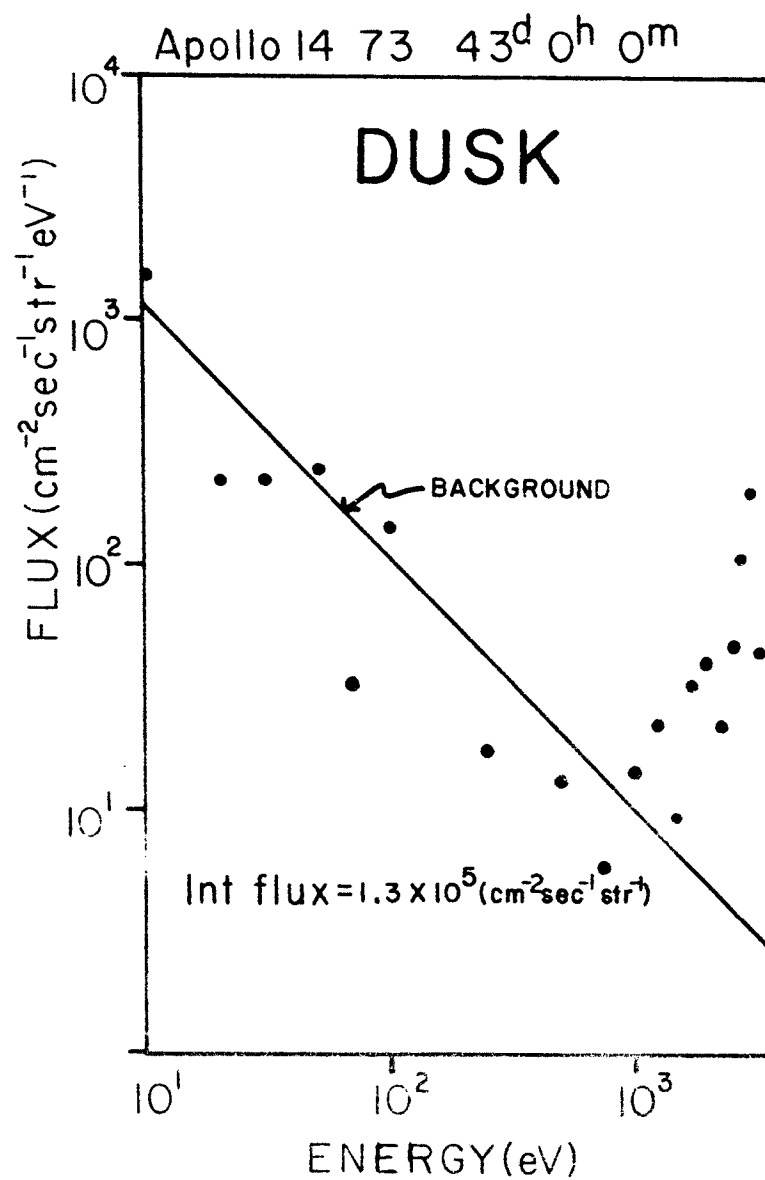


FIGURE 3-12

APOLLO 14 1971  
 START TIME 63 0 1  
 20 MIN AV  
 24.00HR/DIV

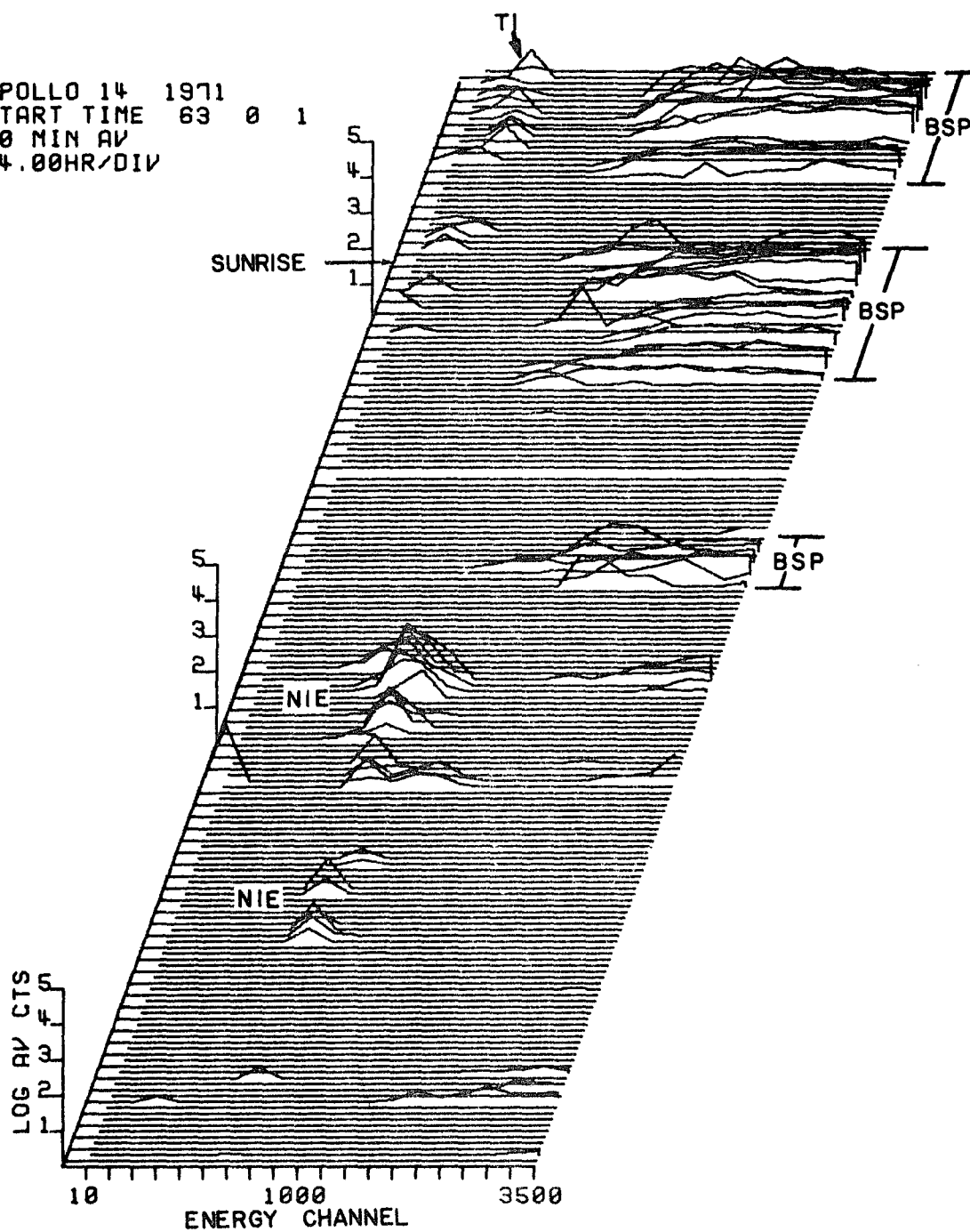


FIGURE 3-13

most often 1 to 6 days before local sunrise with a peak 2 to 3 days before local sunrise. There is also a secondary peak 3 to 4 days after local sunset (figure 3-14). The time scales for the data from the Apollo 14 and Apollo 15 SIDE's are adjusted in figure 3-14 such that local sunset for both instruments coincides. It can be seen from figure 3-14 that both the Apollo 14 and Apollo 15 SIDE's exhibit roughly identical frequency of occurrence profiles.

One noticeable feature of figure 3-14 is the minimum of zero activity just before local midnight for both SIDE's. At this position, the SIDE is looking in the anti-solar direction and right in to the middle of the plasma "cavity".

The peak counting rate of the nighttime ion events also has a profile that is a function of time after sunset (figure 3-15). The error bars are large on the data points, but the peak counting rate profile has a similar shape as the frequency of occurrence profile. The two peaks in the counting rate profile coincide with the two peaks in the activity profile at 2 days before sunrise and 3 days after sunset.

It is interesting to note that near the local sunset terminator, the Apollo 14 and Apollo 15 SIDE's look  $15^\circ$  away from the plasma flow. At the local sunrise terminator, the two instruments look  $15^\circ$  towards the plasma flow (figure 3-16). From figure 3-14 one sees that the secondary activity peak at 3 days after local sunset is very much smaller than the primary activity peak at 2 days prior to local sunrise. These factors suggest that there is a greater probability of observing an event by the SIDE when the look direction of the SIDE is perpendicular to the plasma flow than when it is not. If this hypothesis is indeed the case, then the Apollo 12 SIDE would be expected to exhibit a frequency of occurrence profile with the primary peak at 3 to 4 days after local sunset and the



Figure 3-14. The average number of nighttime ion events per lunation for a 12 hour segment as a function of time after local sunset. The data is adjusted to local sunset for both the Apollo 14 and Apollo 15 SIDE's. This adjustment was performed because sunset occurs 2 days earlier at the Apollo 15 ALSEP site than at the Apollo 14 ALSEP site. Activity increases outward from the center. Note that the primary activity peak is much stronger than the secondary peak. Note also that the Apollo 15 SIDE is more active than the Apollo 14 SIDE.

Figure 3-15. The average counting rate per lunation for a 12 hour period as a function of time after local sunset for the Apollo 14 SIDE. Note that this graph exhibits the same behavior as figure 3-14.

Figure 3-16. Look directions of the Apollo 12, Apollo 14, and Apollo 15 instruments at local sunset, local midnight, and local sunrise. Note that at local sunset the Apollo 12 instrument looks  $15^\circ$  towards the plasma flow and the Apollo 14 and Apollo 15 SIDE's look  $15^\circ$  away from the flow. The situation is reversed at local sunrise. The separation between each set of look directions is one day.

# NUMBER OF EVENTS PER LUNATION

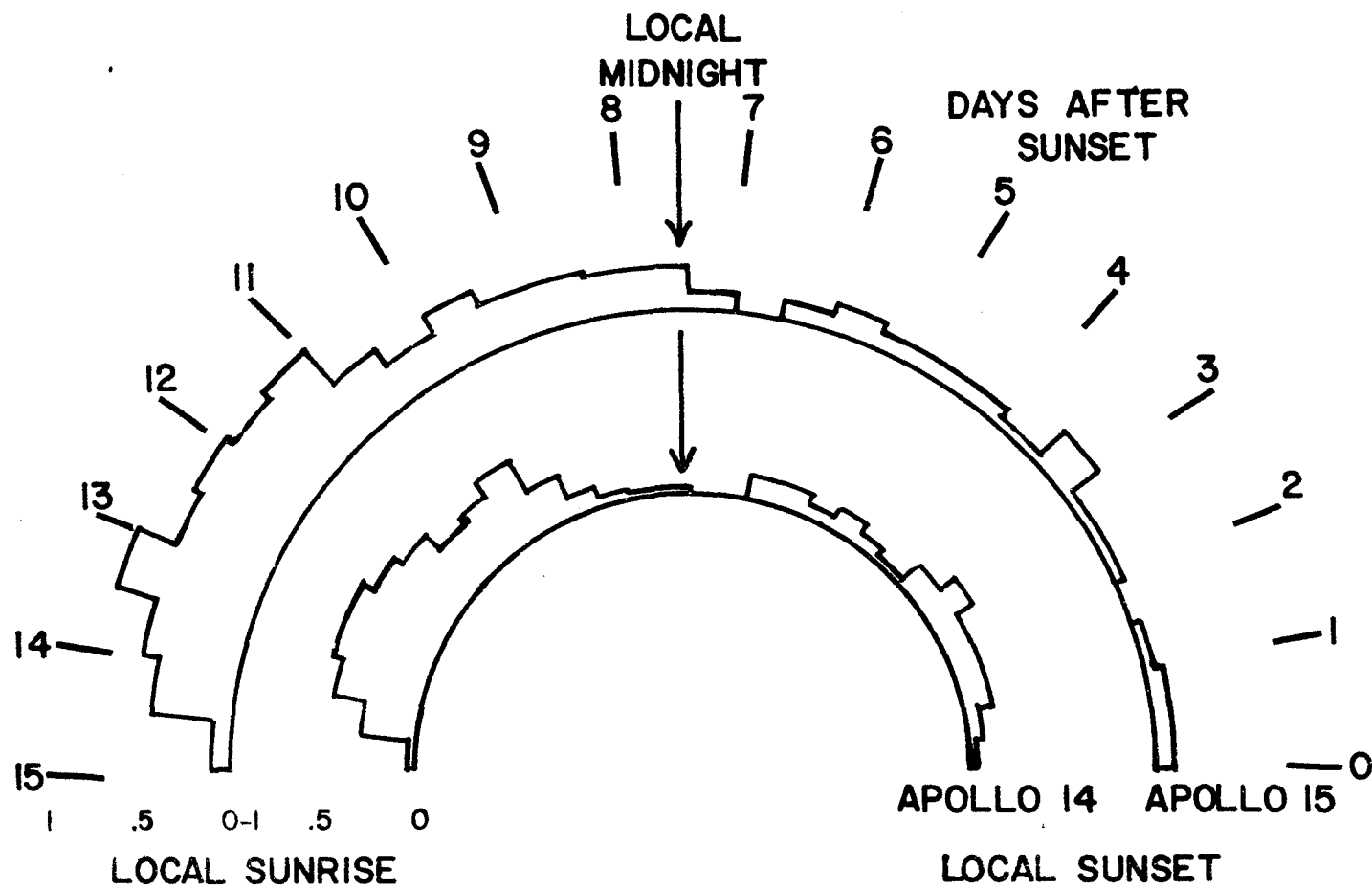


FIGURE 3-14

# APOLLO 14

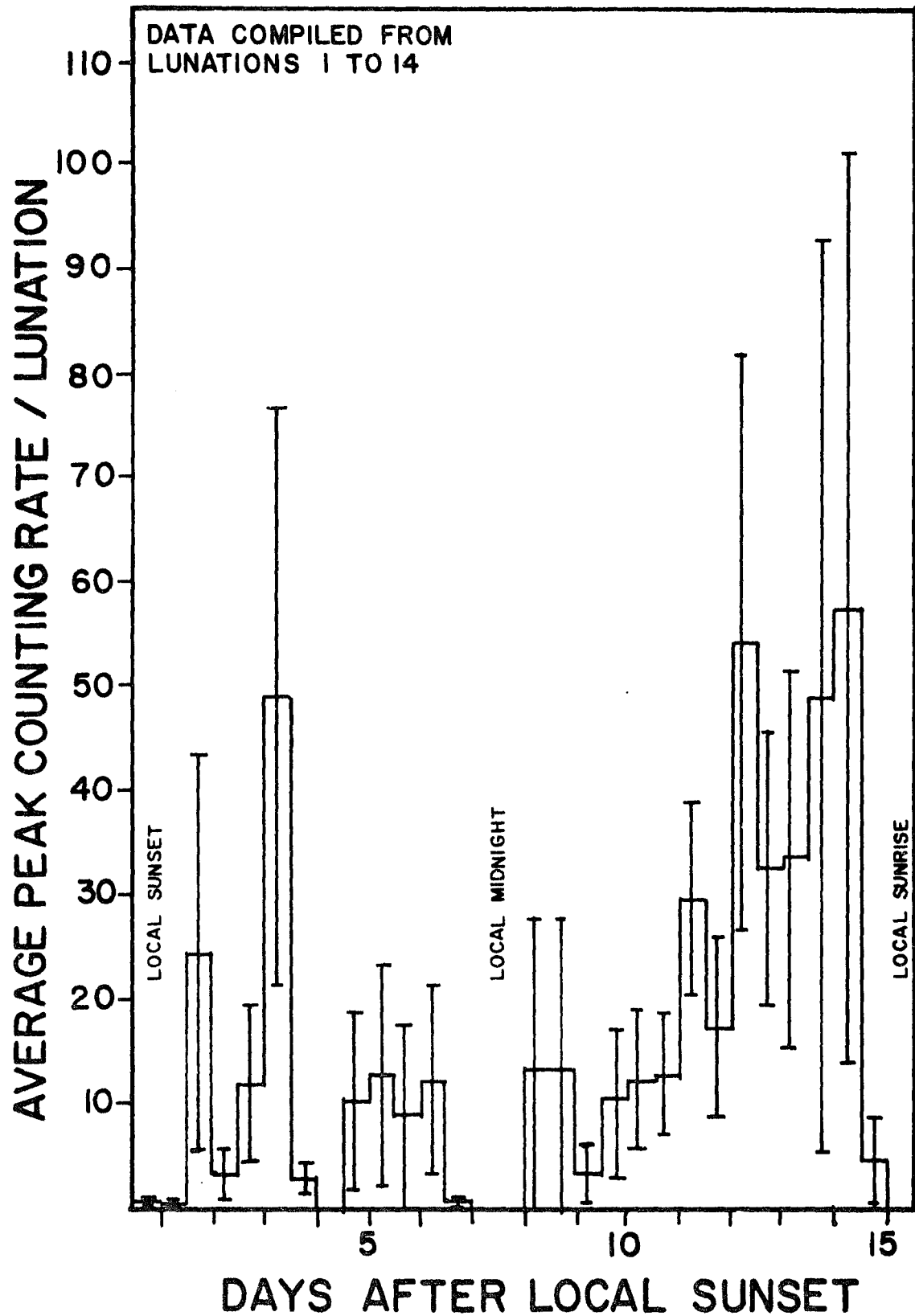


FIGURE 3-15

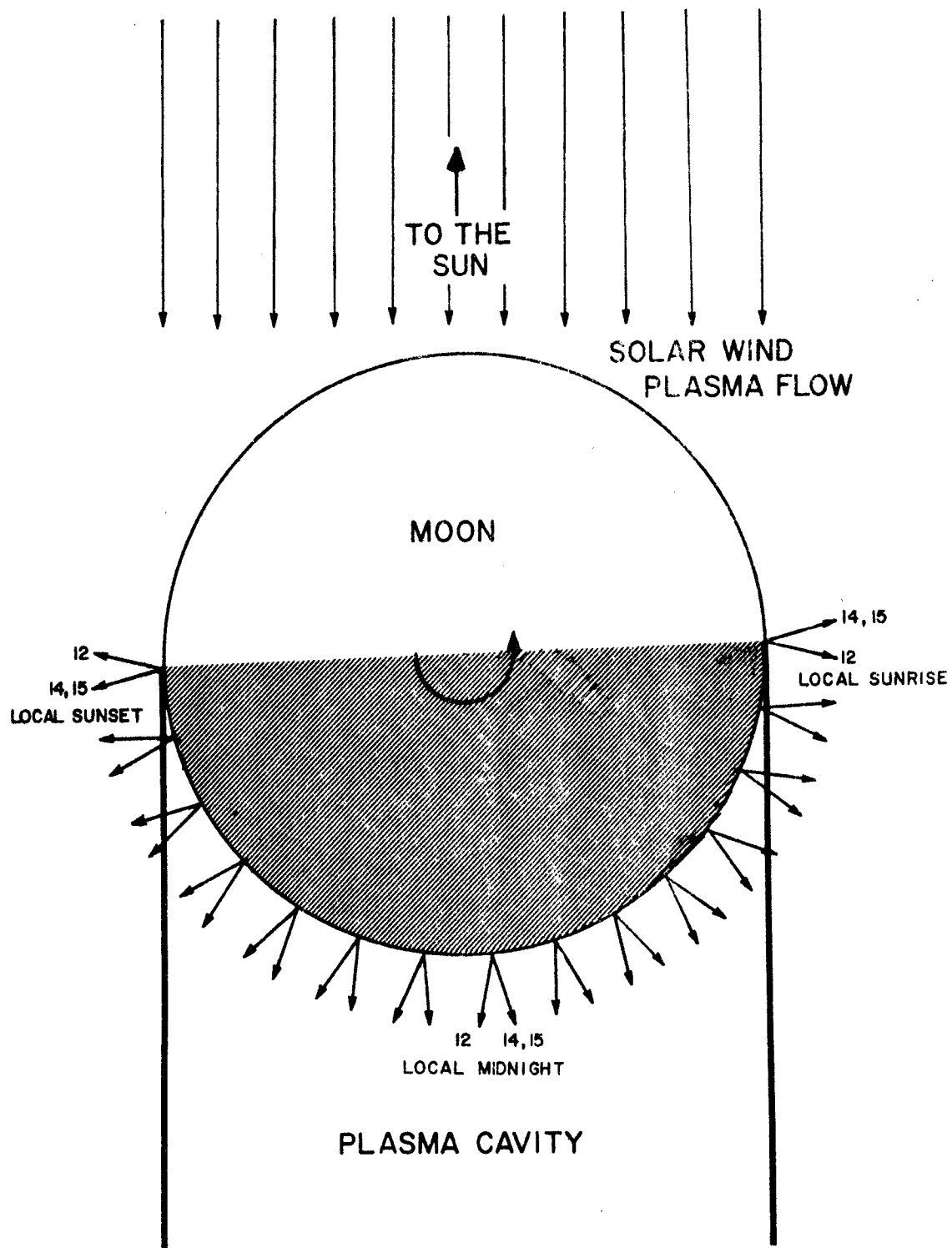


FIGURE 3-16

secondary peak 2 to 3 days prior to local sunrise. This behavior would be expected since that at the same lunar local time, the look direction of the Apollo 12 SIDE points  $30^\circ$  away from the look directions of the Apollo 14 and Apollo 15 SIDE's. Figure 3-16 clearly illustrates this point.

The selenographic coordinates of each ALSEP site were given in section 2.4. One notices that the Apollo 14 site is separated from the Apollo 15 ALSEP site by approximately  $20^\circ$  of longitude. Twenty four hours corresponds to  $12.2^\circ$  of lunar rotation. Therefore, any particular lunar local time at the Apollo 15 ALSEP site occurs almost two days before the same lunar local time at the Apollo 14 ALSEP site. Combining this fact and similarity in the frequency of occurrence profiles (figure 3-14) leads directly to the conclusion that the occurrence of nighttime ion events depends on lunar local time rather than on a position in lunar orbit.

### 3.3 CORRELATION WITH Kp

One possible explanation for the source of nighttime ions is that they are deviated solar wind particles. One method of checking this hypothesis is to see if there is any correlation of nighttime ion events with solar wind parameters. Since solar wind data is not readily available, an alternative value to use is the geomagnetic activity index Kp.

Scientists have recently confirmed a direct correlation of the following solar wind parameters with an increase in Kp (reviewed by Hundhausen [1970]):

1. An increase in the solar wind speed (Ballif et al. [1969]).
2. An increase in the magnitude of the interplanetary magnetic field (Schatten and Wilcox [1967]).

3. Fluctuations in the interplanetary magnetic field (Rostoker and Fälthammer [1967]).
4. An increase in the southward component of the interplanetary magnetic field (Schatten and Wilcox [1967]).

However, the mechanism by which the solar wind influences and changes Kp is not generally agreed upon (Brandt [1970]).

There are two major limiting factors in using Kp to study the solar wind interaction problem. Firstly, the only values of Kp available are three hour averages, where a time resolution of a few minutes is really needed. Secondly, Kp only gives an average value for the level of geomagnetic activity and it does not distinguish between types of geomagnetic events.

If it is possible to correlate nighttime ion events with Kp, then one would be able to state that nighttime ions are in some way correlated with the solar wind or geomagnetic activity.

A thorough study of the Kp correlation problem was only carried out for the first eleven lunations of the Apollo 14 SIDE (February 1971 to December 1971). A cursory examination of Kp and the Apollo 15 data indicate that the behavior was the same for both instruments.

The first attempt at Kp correlation was to determine if Kp was correlated with the activity profile of Apollo 14 (figure 3-14). The fifteen days of lunar night were divided into 12 hour periods and then the average Kp for each 12 hour period was calculated. The total Kp for a particular period was then compared with the average number of nighttime ion events per lunation for that period. Figure 3-17 gives the results and shows that there is little or no Kp correlation.

The next attempt at Kp correlation was to see if Kp was correlated with the duration or the peak energy of the nighttime ion events. Again, the results were negative (see figures

Figure 3-17. The average number of events per lunation vs.  
Kp. The correlation coefficient  $r = 0,1588$ .

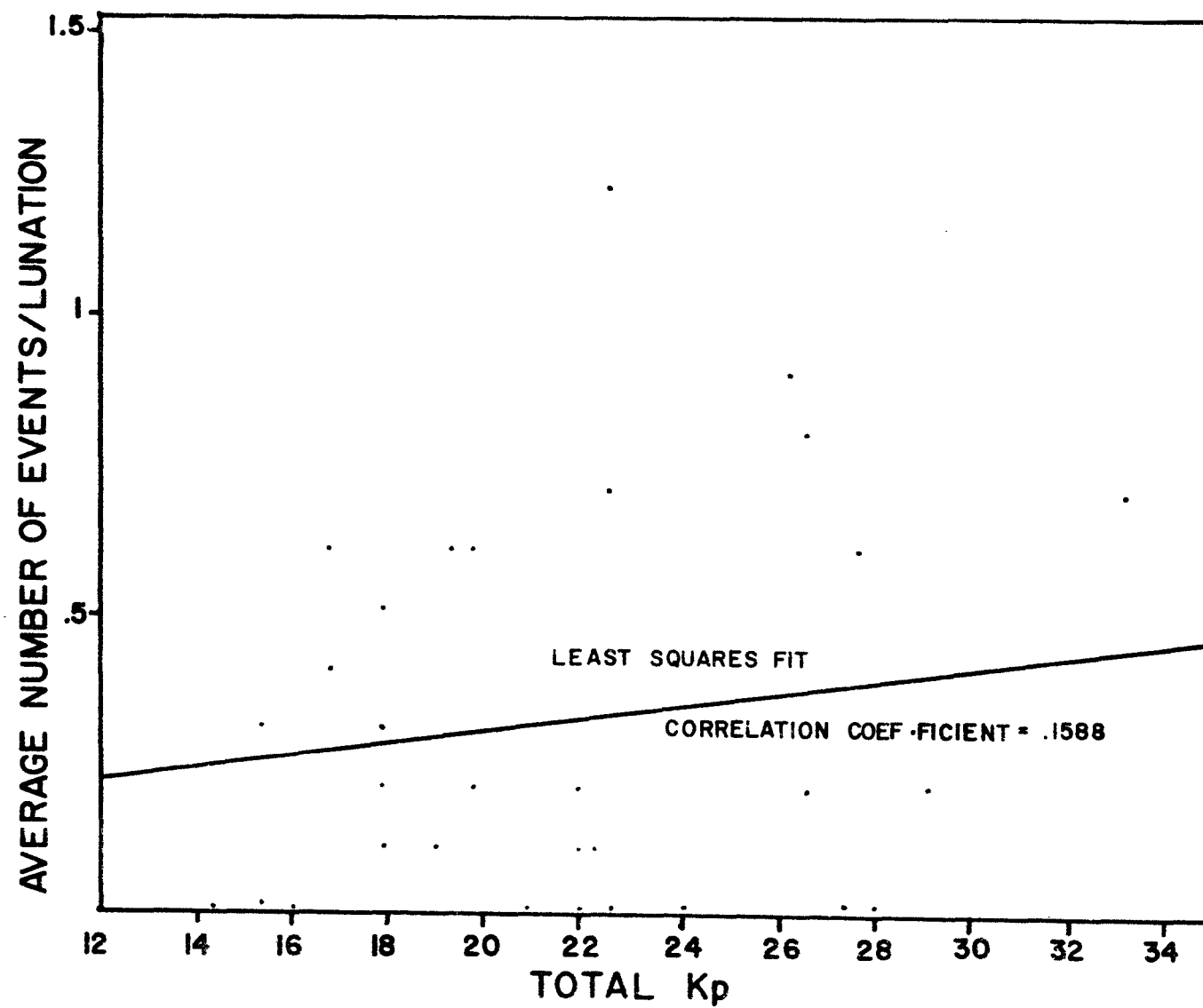


FIGURE 3-17



3-18 and 3-19).

A final attempt at ascertaining if there is a correlation with Kp was to check on the relationship between the total counting rate and Kp. Total counting rate is directly related to the integral flux, so this attempt is also a check on integral flux as a function of Kp. First the total counting rate, for a twenty minute average, was checked as a function of Kp for the entire lunar night (see figure 3-20). Little or no correlation with Kp was found. The next step was to take out the effect of the orbital position of the moon from the data. The orbital effect was removed by looking at a particular period in the orbit. The time interval 2 to 3 days prior to local sunrise (i. e. the most active time period in the lunar night) was divided in to 3 hour time segments to coincide with the 3 hour averages of Kp. The total counting rate observed by the Apollo 14 SIDE was then compared with the Kp for the same 3 hour period in the 11 consecutive lunations (figure 3-21). Again, as in the other cases, there was found to be little or no correlation with Kp.

As was mentioned earlier in this chapter, the SIDE sometimes observes a mono-energetic spectrum centered in the 500 eV/q energy channel that is observed to continue through the sunrise terminator region and on up to the magnetosheath crossing (figure 3-22). This particular event is only observed with the Apollo 15 SIDE and it only occurred in 4 lunations out of the 19 lunations that were studied.

This 500 eV/q "ridge" is different in appearance from nighttime ion events in that it is not burst of ions that characterizes nighttime ion events and its differential flux is constant over a relatively long period of time (figure 3-22).

A cursory comparison of the occurrence of this phenomenon and Kp indicates that this type of ion event is absent during

Figure 3-18. The duration of an event vs. Kp. The correlation coefficient  $r = -0.084$ .

Figure 3-19. The peak energy of an event vs. the average Kp. There appears to be no correlation.

Figure 3-20. Total average counting rate per 20 minutes for a 3 hour Kp interval vs. Kp. The correlation coefficient  $r = 0.0732$ .

Figure 3-21. Total average counting rate per 20 minutes for a 3 hour Kp interval for a particular 3 hour interval during the lunar night vs. Kp. The correlation coefficient  $r = -0.0265$ .

Figure 3-22. Figure similar in format to figure 3-13. Note the steady mono-energetic 500 eV/q "ridge" that continues on up to the magnetosheath. BSP and MS are abbreviations for bow shock protons and magnetosheath respectively.

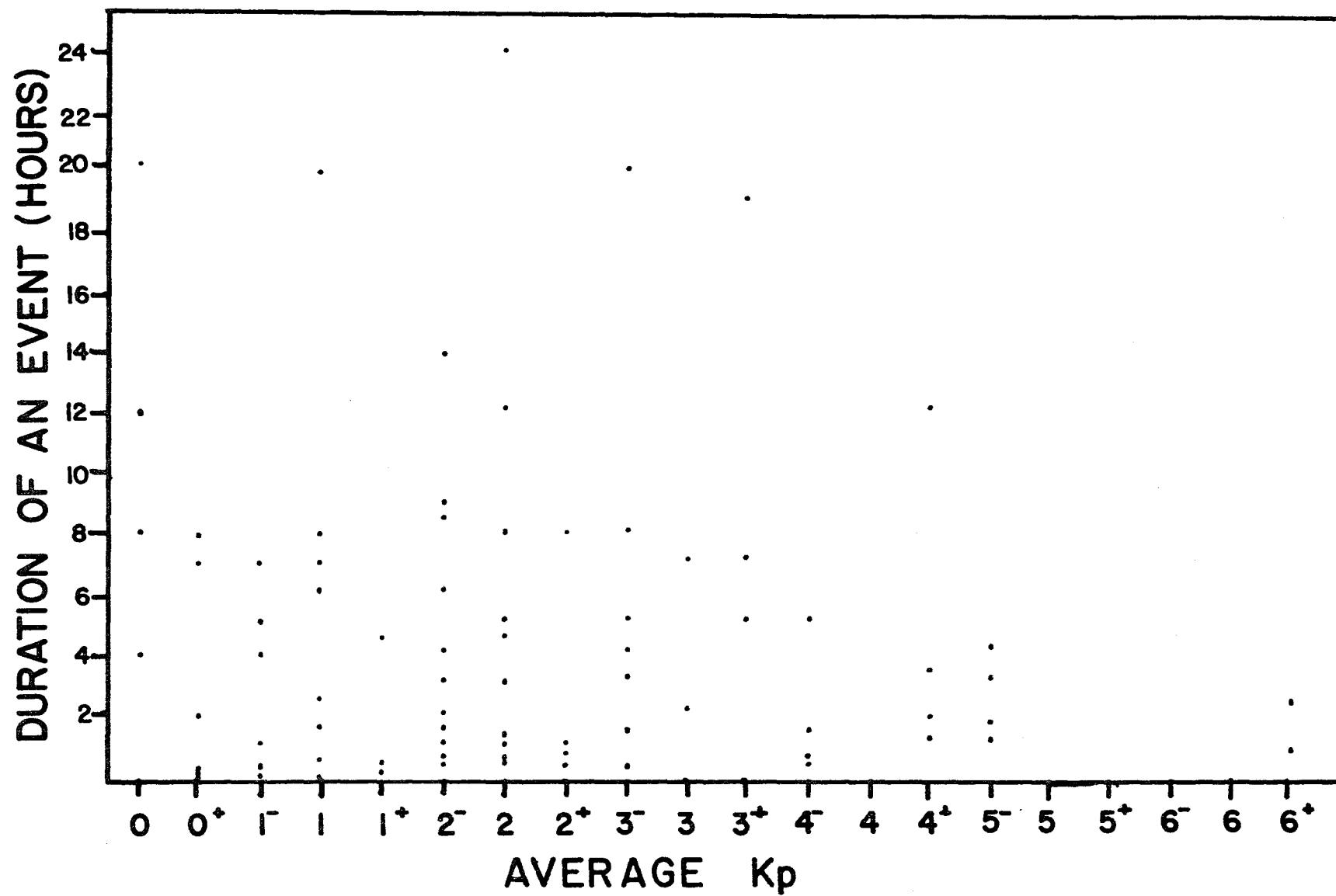


FIGURE 3-18

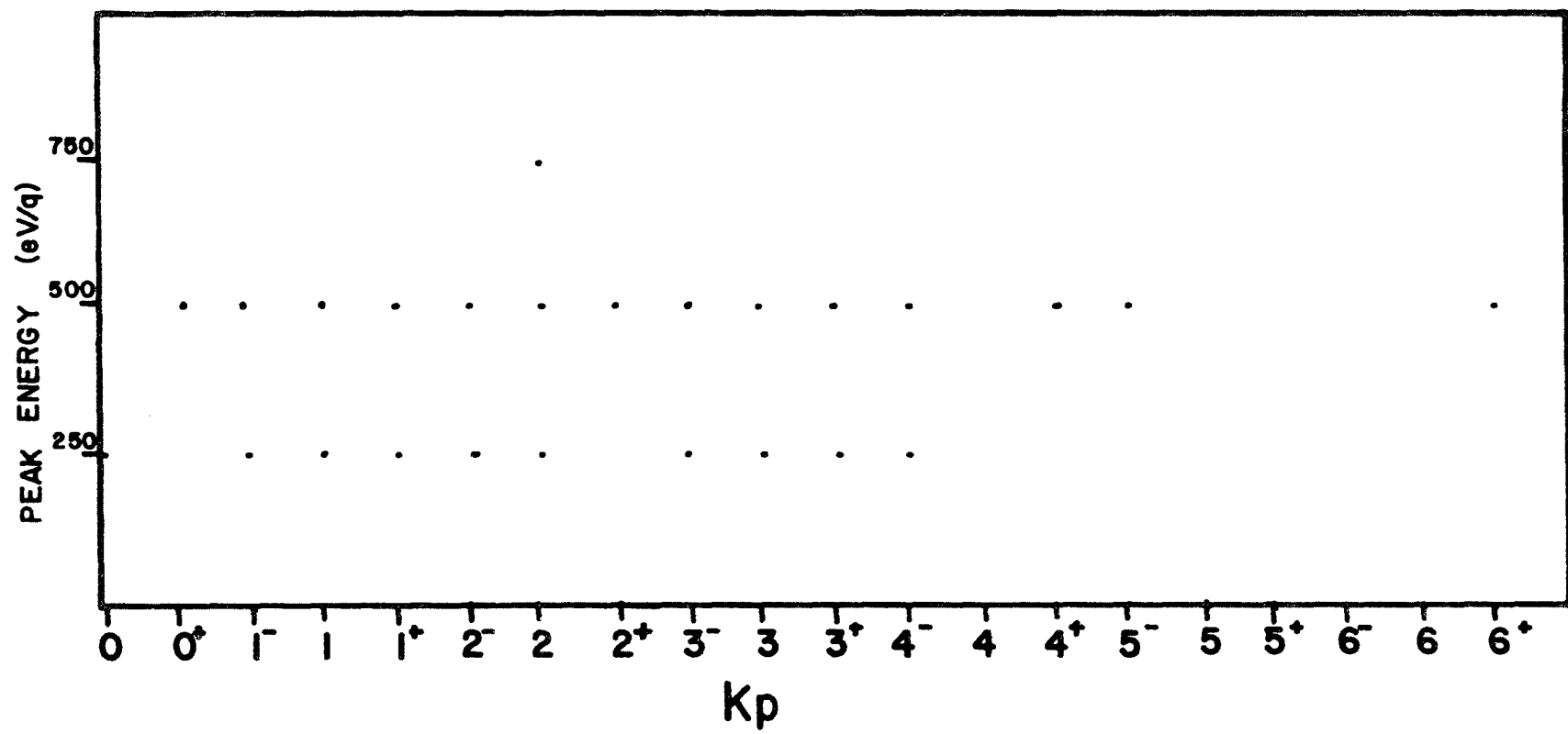


FIGURE 3-19

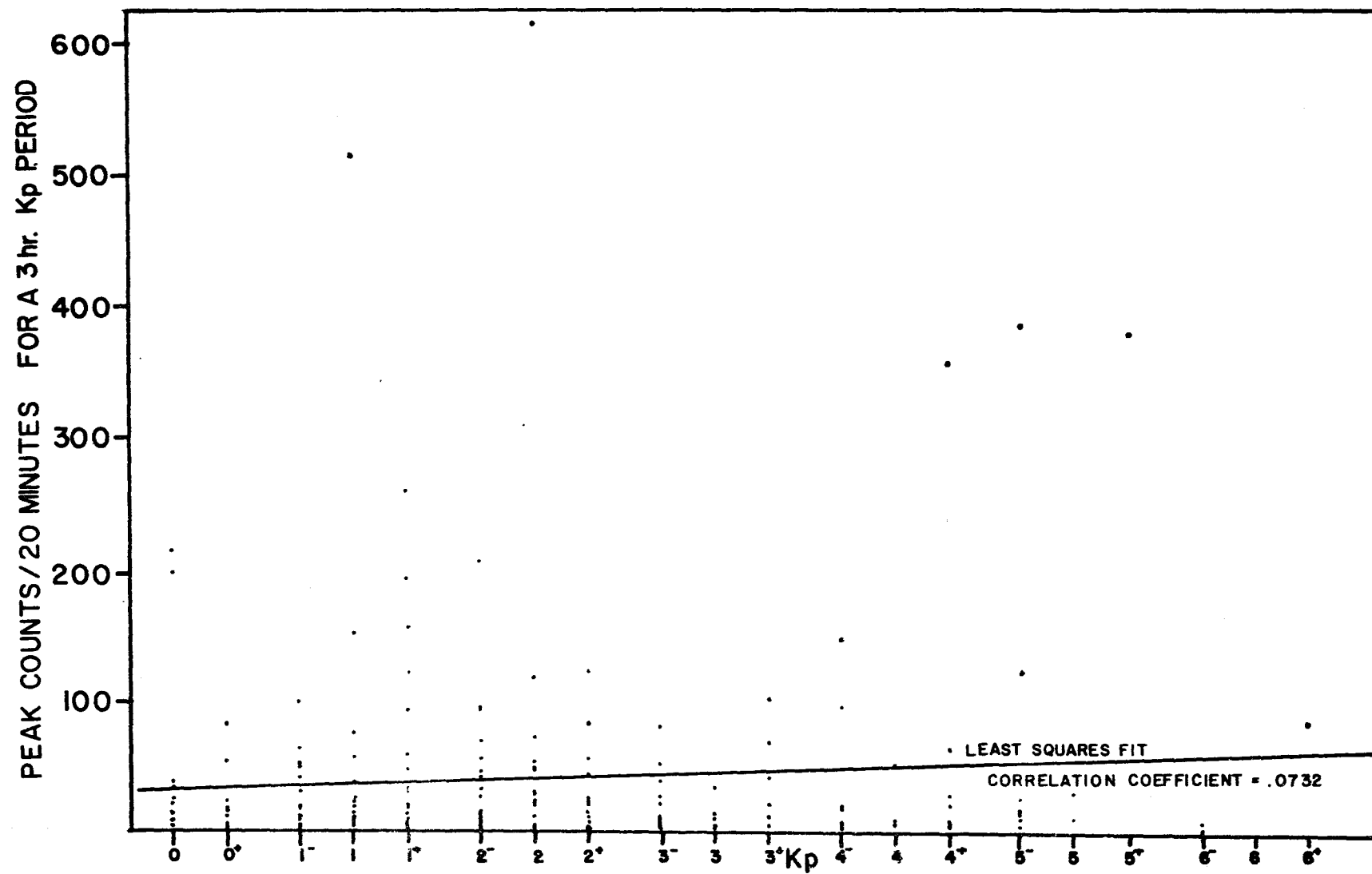


FIGURE 3-20

APOLLO 14

270-273 hours after sunset

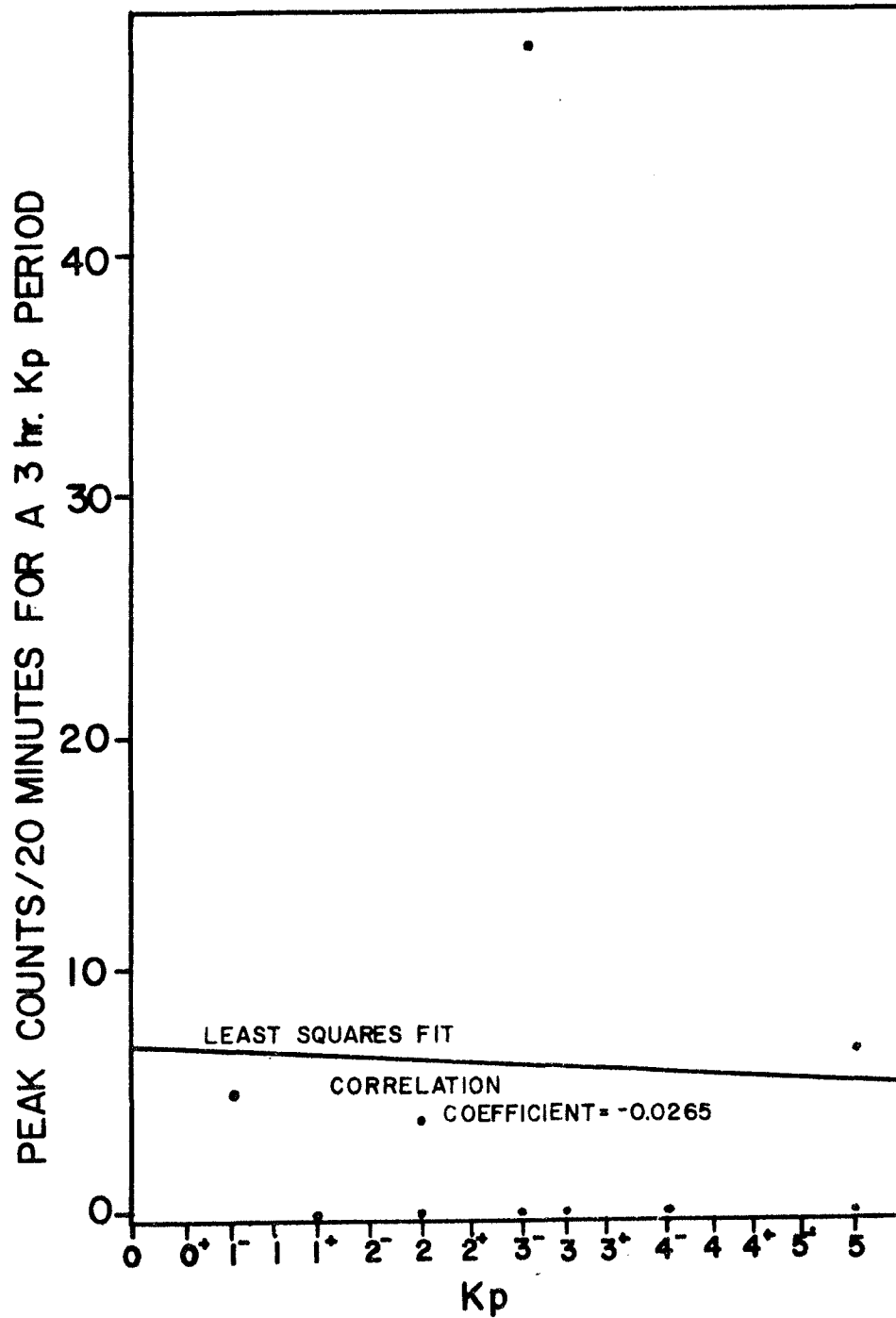


FIGURE 3-21

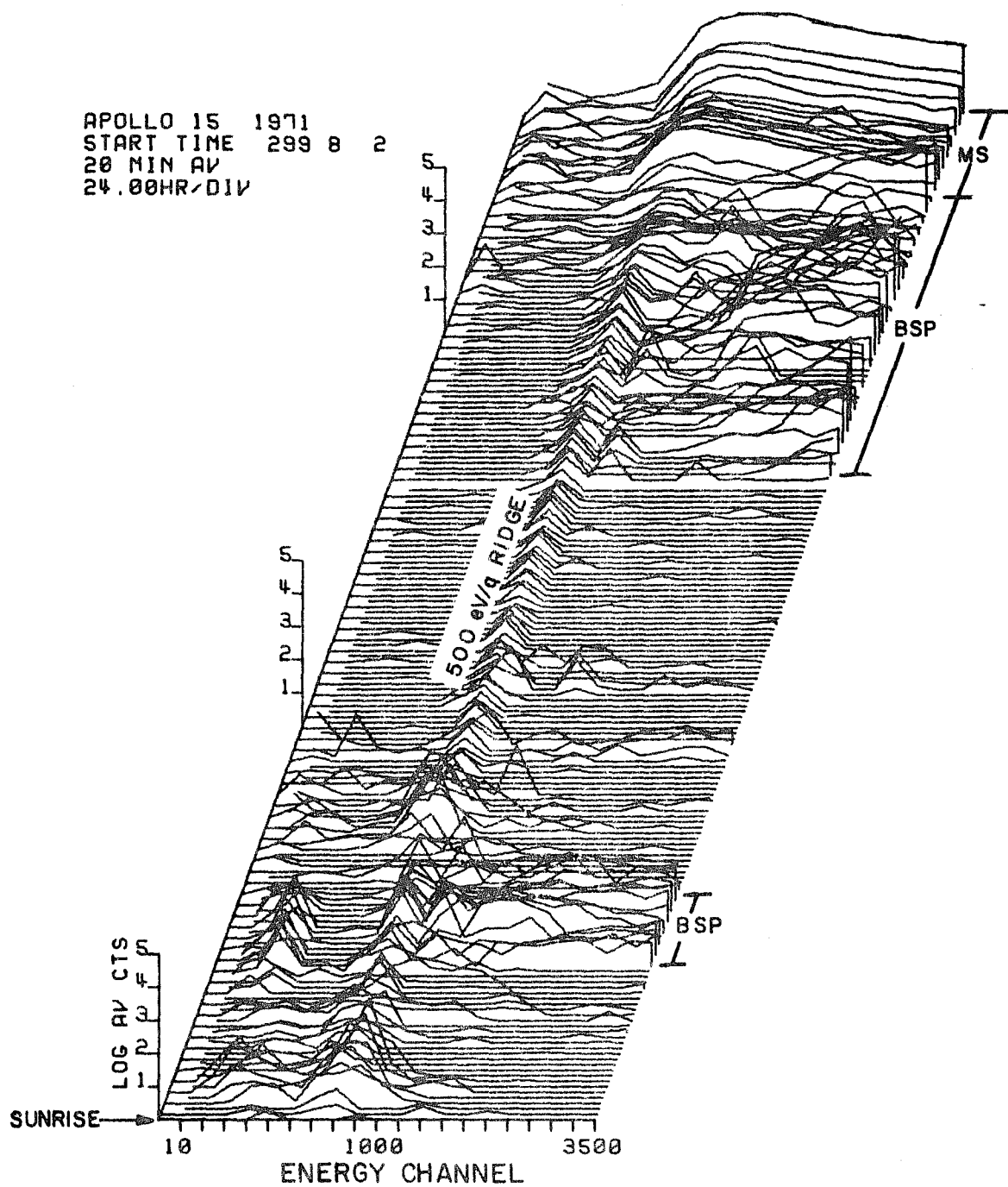


FIGURE 3-22

disturbed periods, i. e.  $K_p > 3$ . This information indicates that this type of ion event is of a different nature than the nighttime ion events.

In summary, the correlation with  $K_p$  was found to be extremely marginal for the following quantities:

1. The frequency of occurrence of an event.
2. The duration of an event.
3. The peak energy of the counting rate spectrum of an event.
4. The total counting rate or integral flux of an event.

Therefore, nighttime ion events are not related to geomagnetic activity, but they may be related to a single solar wind parameter. This fact has yet to be determined.

### 3.4 OBSERVATIONAL CONCLUSIONS

The characteristics of nighttime ion events may be summarized as follows:

1. Nighttime ion events occur more often at the Apollo 15 site than at the Apollo 14 site.
2. The range of energies of nighttime ion events is from 250 to 1000 eV/q peaking most often in the 500 eV/q energy channel. The average solar wind energy is 800 eV, which corresponds to a solar wind velocity of about 400 km/sec. It was mentioned in Chapter 1 that the velocity of the solar wind may vary from 200 to 900 km/sec. These velocities correspond to peak solar wind energies ranging from 200 eV to 4200 eV. This energy range is sufficient to overlap the energies of nighttime ion events. Figure 1-1 is a counting rate spectrum for the solar wind and thus it can not be compared to a differential flux energy spectrum of a



nighttime ion event without knowing the geometric factor of the Vela 3 detector. It will be interesting to compare concurrent differential flux energy spectra for the solar wind and nighttime ion events to see how far the peak energy is shifted, if at all.

3. The differential flux energy spectrum (figure 3-23) of a nighttime ion event is sharply peaked about the central energy like the solar wind. The integral flux of nighttime ions is also down by 2 orders of magnitude from the solar wind.
4. The peak energy of nighttime ion events statistically shifts from 500 eV/q at local sunset to 750 eV/q just after local midnight to 250 eV/q in the pre-dawn hours.
5. A nighttime ion event appears to be a burst of ions rather than a rising or decaying ion flux. Nighttime ion events last for only a short period of time, usually less than one hour. This behavior is indicative of highly directional ion fluxes. Therefore, an isotropic mixing of plasma in the plasma cavity near the lunar surface seems unlikely.
6. Nighttime ion events may be seen at any time during the lunar night except near local midnight. There are two activity peaks, a primary peak 2 to 3 days before local sunrise, and a very weak secondary peak 3 to 4 days after local sunset. Figure 3-24 shows the region where the primary peak occurs. This region is broadened in the figure because of the 2 day lag between lunar local times at the 2 ALSEP sites. Also, because of this time lag, there are never any simultaneous events observed by the Apollo 14 and Apollo 15 SIDE's.

The counting rate of the Apollo 14 SIDE also increases

Figure 3-23. Twenty minute averaged differential flux energy spectrum for an event where the differential flux spectrum peaks in the 500 eV/q energy channel. The background flux represents an average counting rate of 0.18 counts per energy channel. This event occurred 4 days after local sunset.

Figure 3-24. Lunar orbit showing the look directions of the three SIDE instruments with respect to the earth-moon system. The area of greatest activity of nighttime ion events is indicated. The region appears broad because it is a superposition of the data from the Apollo 14 and Apollo 15 SIDE's. The bow shock front and the magnetopause are drawn in for reference (Schneider and Freeman [1975]).

APOLLO 14 1971

83<sup>d</sup> 7<sup>h</sup> 49<sup>m</sup>

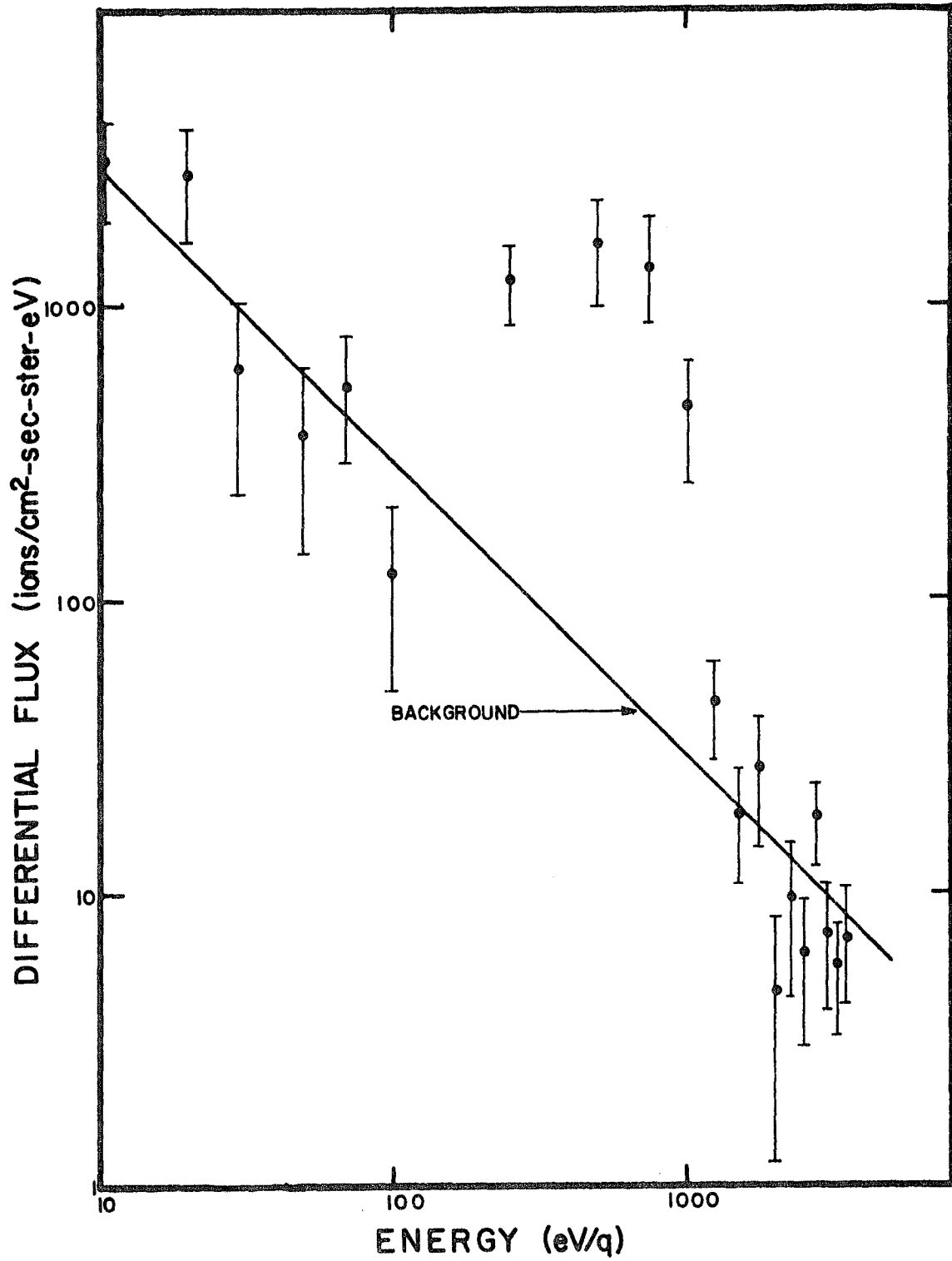


FIGURE 3-23

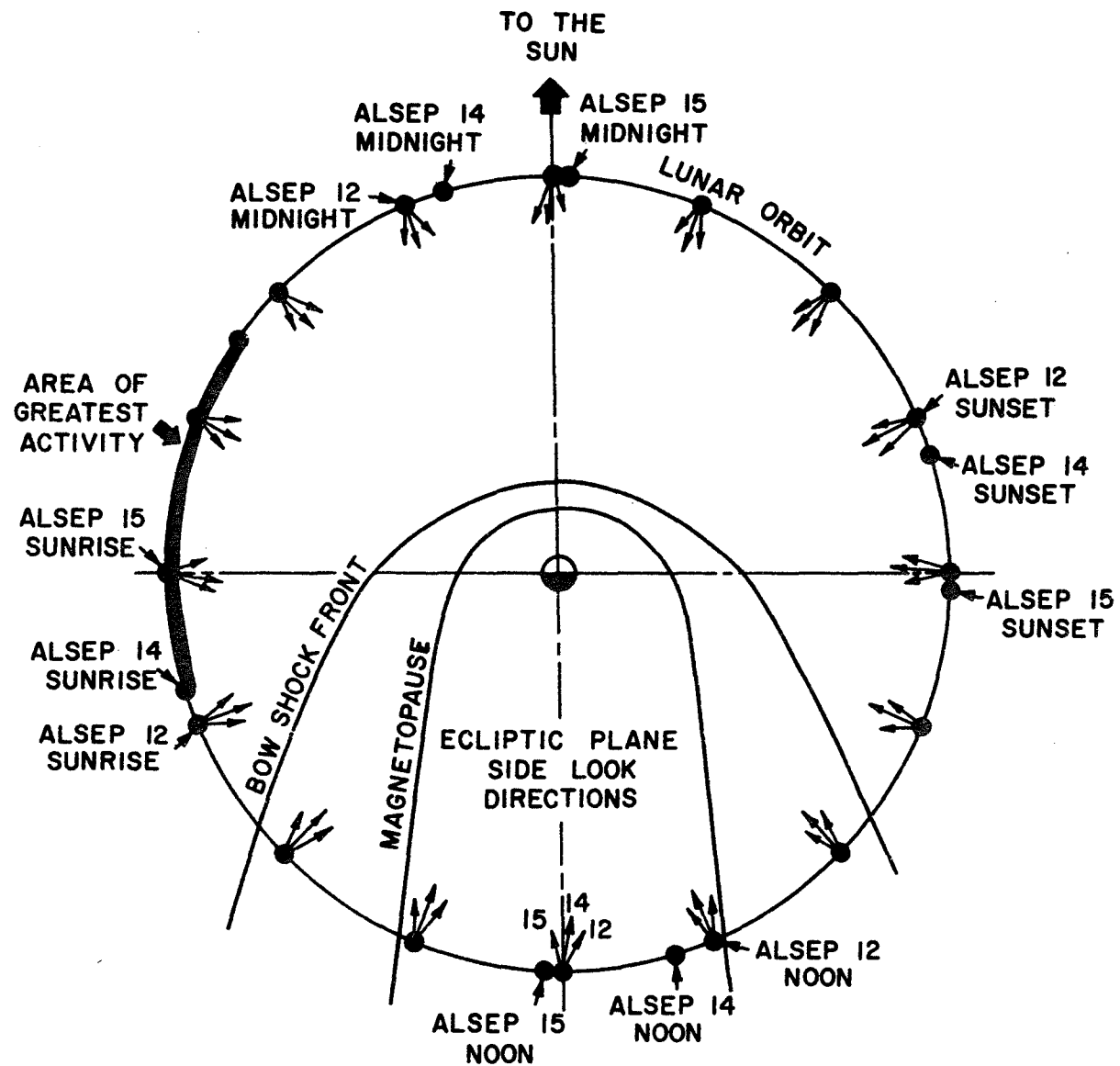


FIGURE 3-24

with increased activity resulting in a profile that has the same general shape as the frequency of occurrence profile.

These facts again argue that the occurrence of a nighttime ion event is a lunar local time dependent phenomenon.

7. There is little or no correlation of nighttime ion events with Kp. Hence, these events can not be related to the earth's magnetosphere.

### 3.5 DISCUSSION

Reasoner [1975] has observed electron fluxes on the night-side of the moon with the Charged Particle Lunar Environment Experiment (CPLEE) which he has classified into three types of events.

Type I electron events are only seen when an interplanetary magnetic field line connects the dark side of the moon with the earth's bow shock front. These electron events have been labeled as bow shock electrons.

Type II electron events are lower intensity than Type I and are uncorrelated with both the interplanetary magnetic field and Kp. Reasoner theorizes that the source of these electrons is the weak shock 4 to 5 lunar radii downstream from the moon that was first modeled by Michel [1968].

The third type of electron fluxes, Type III, are only observed in the lunar terminator regions and are absent when Kp is 1+ or less. Reasoner speculates that Type III electrons are due to solar wind electrons which have been thermalized and scattered to the lunar surface by lunar limb shocks.

Since Reasoner's Type II electron fluxes are uncorrelated with Kp and occur sporadically throughout the lunar night, they may be associated with nighttime ion events. However, the energies of Type II electrons range from 90 to 120 eV, which is

too low to match the energies of nighttime ions. Freeman and Ibrahim [1974] suggest that the lunar surface potential may be as negative as -100 volts on the nightside of the moon. If this is indeed the case, then any electrons in the vicinity of this potential will lose energy before reaching the moon, and any ions will gain energy before reaching the moon. A lunar surface potential of -100 volts would imply initial electron energies of 190 to 220 eV and initial nighttime ion energies of 150 to 900 eV/q. This potential is sufficient to cause an overlap of electron and ion energies. It is possible, therefore, that the source mechanism for Type II electrons and nighttime ions is the same. One problem in checking the validity of this statement is the fact that Reasoner has analyzed only six or seven months of nighttime electron data (private communication). Therefore, a statistical statement about Type II electrons can not be made.

Because the characteristic energies of nighttime ion events, even after being accelerated by a possible -100 volts lunar surface potential, are still close to the solar wind energies, the source of these ions is probably the solar wind. This source is further suggested by the lunar local time dependence of the phenomenon. These ions probably represent solar wind plasma that has moved in, perhaps by turbulence near the limbs, to partially fill the plasma void behind the moon.

As mentioned earlier in Chapter 1, Wu and Dryer [1972] predict a small but finite ion density in the plasma void behind the moon. Making the assumptions that the source of the nighttime ions is in the region of the number density contour  $n/n_{\infty} = 10^{-2}$  (figure 1-9), that nighttime ions are primarily protons, and that the most probable ion energy is 500 eV/q, then one arrives at an integral flux that could reach the moon on the order of  $10^6$  ions/cm<sup>2</sup>-sec. This number is fairly close

to the integral flux computed for nighttime ion events ( $\sim 10^6$  ions/cm<sup>2</sup>-sec-ster). The only problem encountered in trying to fit this theory to the data is that Wu and Dryer do not predict flow directions that would cause particles to be incident on the dark side of the moon (see figure 1-10).

One must keep in mind that the Wu and Dryer model used the kinetic theory approach and not fluid flow to arrive at the number density profiles and flow directions for the lunar interaction problem. Their predicted flow directions will change if a fluid flow approach is taken.

Supersonic flow past an obstacle creates a shock wave upstream of the obstacle. Since there is no detectable lunar bow shock, a subsonic fluid flow approach to the moon-solar wind interaction problem may be valid. Figure 3-24 illustrates subsonic fluid flow past a smooth and a rough circular cylinder. In both cases, a wake is formed where the direction of fluid flow is reversed causing fluid to impact the back side of the obstacle. Since the moon is obviously not smooth, it most likely responds as the rough cylinder (Case 2) in figure 3-25.

It is interesting to note that these nighttime ions may form part of a positive ion sheath that is required by the highly negative lunar surface potential on the night side of the moon (figure 3-26). If this ion sheath is the only source of nighttime ions and assuming that their initial energies are small or zero, then the energies detected by the SIDE during lunar night may give an alternative measure of the negative lunar nighttime surface potential. This approach is only valid if the ionic charge composition of nighttime ions is known.

Summarizing, there is no satisfactory explanation of nighttime ion events as of yet. Further analysis of the data will determine in the Wu and Dryer model completely describes the SIDE's observations.

Figure 3-25. Diagram illustrating subsonic flow past a circular cylinder. Case 1 is for a smooth cylinder giving rise to laminar separation. Case 2 is for a rough cylinder giving rise to turbulent separation. The graphs under each figure plot the fluid pressure as one moves along the surface of the cylinder from A to S. Note that the pressure drag for a rough cylinder is less than for a smooth cylinder. Also note the reversal of the flow direction in the wake (John and Haberman [1971]).

Figure 3-26. The electric charge distribution on and near the moon. Note the positive ion sheath on the night side of the moon (Freeman and Ibrahim [1974]).



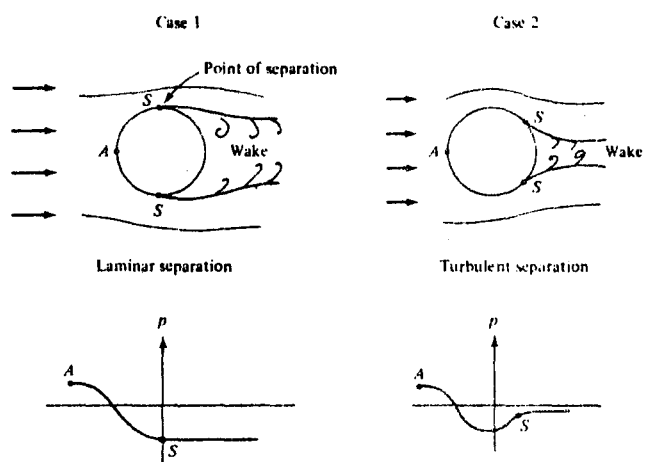


FIGURE 3-25

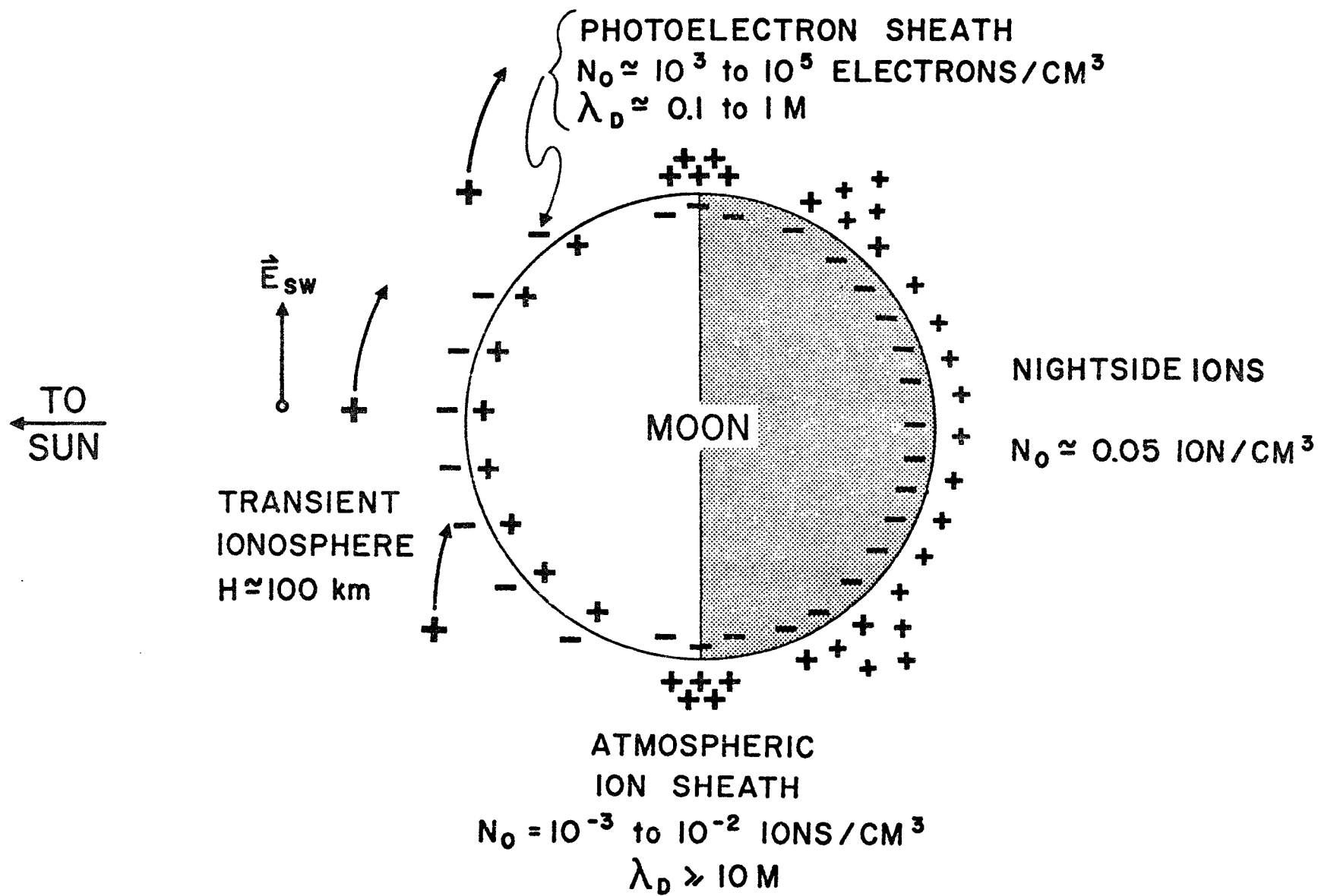


FIGURE 3-26

### 3.6 TOPICS FOR FURTHER INVESTIGATION

There are several avenues for further investigation of this phenomenon. They are summarized as follows:

1. The data from the Apollo 12 SIDE has been relatively untouched. It will be interesting to see if, in fact, the Apollo 12 SIDE data exhibits a mirror image of the frequency of occurrence profile observed by the Apollo 14 and Apollo 15 SIDE's. Since the Apollo 12 and the Apollo 14 ALSEP are relatively close to one another (138 km), there will, in all probability, be some nighttime ion events that are simultaneously observed by both the Apollo 12 and Apollo 14 SIDE's. This new data will give some information as to whether the nighttime ion flux is isotropic or anisotropic. If the flux is anisotropic, then the comparison of data from the Apollo 12 and Apollo 14 SIDE's will indicate if there is an east-west component to the ion flux.
2. An important comparison that has yet to be made is whether the nighttime ion events are in any way correlated with the either the magnitude or direction of the interplanetary magnetic field. The theoretical models mentioned in Chapter 1 indicate that the shape of the moon's wake is a function of the interplanetary magnetic field.
3. Some important questions that have yet to be answered are:
  - a. Why is there an asymmetry in the activity profile?
  - b. Why are some lunations more active than others?
  - c. Why are nighttime ion events short lived?
  - d. Why is there a peak energy shift as a function of lunar local time?

- e. Why is there a minimum in the activity profile prior to local midnight?
  - f. What causes the apparent shift towards local sunrise of the occurrence of the events exhibited in figures 3-1 and 3-2?
4. Finally, a model must be chosen that adequately accounts for the observations.

## REFERENCE LIST

Ballif, J. R., Jones, D. E., and Coleman, P. J., Further Evidence on the Correlation Between Transverse Fluctuations in the Interplanetary Magnetic Field and Kp, J. Geophys. Res., 74, 2289, 1968.

Benson, J. L., Observations of Bow Shock Protons at the Lunar Orbit, M. S. Thesis. Rice U., 1974.

Benson, J., Hills, H. K., Freeman, J. W., and Vondrak, R. R., Bow Shock Protons in the Lunar Environment, presented at the Conference on Interactions of the Interplanetary Plasma with the Modern and Ancient Moon, George Williams College, Lake Geneva Campus, Williams Bay, Wisconsin, Sept., 1974.

Brandt, J. C., Introduction to the Solar Wind, W. H. Freeman and Company, San Francisco, 1970.

Burke, W. J. and Moore, P. R., The Effect of Local Magnetic Fields on the Lunar Photoelectron Layer While the Moon is in the Plasma Sheet, abstract submitted to the Sixth Lunar Science Conference, Lyndon B. Johnson Space Center, March, 1975.

Fenner, M. A., Freeman, J. W., Jr., and Hills, H. K., The Electric Potential of the Lunar Surface, Proceedings of the Fourth Lunar Science Conference, 3, 2877, 1973.

Fenner, M. A., Observations of Magnetosheath Plasma at the Lunar Orbit, Ph. D. Thesis, Rice U., 1974.

Freeman, J. W., Jr., Michel, F. C., and Hills, H. K., The ALSEP Lunar Ionosphere Detector, prepared for Project Apollo by Rice University, Houston, Texas, Sept., 1969.

Freeman, J. W., Jr., Balsiger, H., and Hills H. K., Suprathermal Ion Detector Experiment, Apollo 12 Pre. Sci. Rep., NASA SP-235, 83, 1970.

Freeman, J. W., Jr., Energetic Ion Bursts on the Nightside of the Moon, J. Geophys. Res., 77, 239, 1972.

Freeman, J. W. and Ibrahim, M. E., The Lunar Electric Potential and its Plasma Sheath Effect, presented at the Conference on Interactions of the Interplanetary Plasma with the Modern and Ancient Moon, George Williams College, Lake Geneva Campus, Willaims Bay, Wisconsin, Sept., 1974.

Hills, H. K., Meister, J., Vondrak, R. R., and Freeman, J. W., Jr., The Suprathermal Ion Detector Experiment, Apollo 15 Pre. Sci. Rep., 12-1, 1971.

Hundhausen, A. J., Asbridge, J. R., Bame, S. J., Gilbert, H. E., and Strong, I. B., Vela 3 Satellite Observations of Solar Wind Ions: A Preliminary Report, J. Geophys. Res., 72, 87, 1967.

Hundhausen, A. J., Solar Wind Properties and the State of the Magnetosphere, Ann. Geophys., 26, 427, 1970.

John, J. E. A. and Haberman, W., Introduction to Fluid Mechanics, Prentice-Hall, Inc., Englewood Cliffs, New Jersey, 190-196, 1971.

Johnson, F. S. and Midgley, J. E., Notes of the Lunar Magnetosphere, J. Geophys. Res., 73, 1523, 1968.

Lindeman, R. A., Recurring Ion Events at the Lunar Surface, M. S. Thesis, Rice U., 1971.

Lindeman, R. A., Observations of Ions from the Lunar Atmosphere, Ph. D. Thesis, Rice U., 1973.

Lindeman, R. A., Freeman, J. W., and Vondrak, R., Ions from the Lunar Ionosphere, Geochim. et. Cosmochim. Acta., Supplement 3, 3, 2889, 1973.

Lyon, E. F., Bridge, H. S., and Binsack, J. H., Explorer 35 Plasma Measurements in the Vicinity of the Moon, J. Geophys. Res., 72, 6113, 1967.

Medrano, R. A., Unusual Solar Wind and Solar Proton Events Observed on the Lunar Surface, Ph. D. Thesis, Rice U., 1973.

Michel, F. C., Interaction Between the Solar Wind and the Lunar Atmosphere, Planet. Space Sci., 12, 1075, 1964.

Michel, F. C., Shock Wave Trailing the Moon, J. Geophys. Res., 72, 5508, 1967.

Michel, F. C., Magnetic Field Structure Behind the Moon, J. Geophys. Res., 73, 1533, 1968.

Ness, N. F., The Earth's Magnetic Tail, J. Geophys. Res., 70, 2989, 1965.

Ness, N. F., Interaction of the Solar Wind with the Moon, Solar Terrestrial Physics/1970: Part II, Dyer ed., D. Reidel Pub. Co., Dordrecht-Holland, 159, 1972.

Reasoner, D. L., Lunar Nightside Electron Fluxes, abstract submitted to the Sixth Lunar Science Conference, Lyndon B. Johnson Space Center, March, 1975.

Rostoker, G. and Fälthammer, C. G., Relationship Between Changes in the Interplanetary Magnetic Field and Variations in the Magnetic Field at the Earth's Surface, J. Geophys. Res., 72, 5853, 1967.

Schatten, K. H., and Wilcox, J. M., Response of the Geomagnetic Activity Index  $K_p$  to the Interplanetary Magnetic Field, J. Geophys. Res., 72, 5185, 1967.

Schneider, H. E. and Freeman, J. W., Energetic Lunar Nighttime Ion Events, submitted for publication in The Moon, Jan., 1975.

Whang, Y. C., Interaction of the Magnetized Solar Wind with the Moon, The Physics of Fluids, 11, 969, 1968.

Wolf, R. A., Solar-Wind Flow Behind the Moon, J. Geophys. Res., 73, 4281, 1968.

Wu, S. T. and Dryer, M., Kinetic Theory Analysis of Solar Wind Interaction with Planetary Objects, presented at the Symposium on Photon and Particle Interactions with Surfaces in Space, Sixth ESLAB Symposium, Noordwijk, Holland, Sept., 1972.





BOW SHOCK PROTONS IN THE LUNAR ENVIRONMENT

J. Benson, J. W. Freeman, H. K. Hills  
Department of Space Physics and Astronomy  
Rice University  
Houston, Texas  
77001

R. R. Vondrak  
Radio Physics Laboratory  
Stanford Research Institute  
Menlo Park, California

Submitted for publication in The Moon  
January 1975

11 - pages, manuscript  
6 - pages figures

## ABSTRACT

Protons from the earth's bow shock are observed by the Suprathermal Ion detector Experiment (SIDE) in two regions of the lunar orbit. The dawn region begins at the dawn side bow shock crossing and ends ~5 days later and the dusk region begins at ~2 days prior to entering the dusk side magnetosheath and ends at the inbound bow shock crossing. Dusk and dawn refer to a terrestrial coordinate system. The dominant contribution to the ion spectra observed by the SIDE in these regions is from particles with energies between ~750 eV/q and 3500 eV/q. 3500 eV/q is the upper limit of the energy range of the detector. Analysis of simultaneous data from the Explorer 35 magnetometer and the SIDE indicates that the observability of bow shock protons at the lunar distance is dependent on the configuration of the interplanetary magnetic field.

## INTRODUCTION

Protons in the energy range of 4 to 7 keV were observed to be coming from the direction of the bow shock by Asbridge et al., [1968] using data from Vela satellites. The existence of suprathermal protons in the energy range of ~1 to 3.5 keV at the lunar orbit was confirmed by Freeman et al. [1970] and Hills et al. [1970]. More recently Lin et al. [1974] have reported protons at the lunar distance in the energy range of 30 to 100 keV. The behavior of the ~1 to 3.5 keV protons with respect to the interplanetary magnetic field has been studied by Benson [1974] and this paper reports some results from that study.

## OBSERVATIONS

Figure 1 shows typical time development of the SIDE count spectra for the two regions of the orbit in which the bow shock protons are observed. The "dusk" and "dawn" regions refer to the dusk and dawn sides of the magnetosphere when the moon is in the solar wind as indicated in figure 3. Note that the dusk side spectra show the onset of the flow coming at  $\sim 1.5$  days before the magnetosheath and that the spectra get progressively softer as the moon approaches the bow shock. The dawn side spectra show a gradual hardening as the moon moves away from the bow shock and a cessation of the flow  $\sim 5$  days after shock crossing. These examples of the ion spectra are "typical" and can vary considerably when interplanetary magnetic field and solar wind conditions change.

Figure 2 shows a single spectrum (20 minute average) for each of the two regions shown in Figure 1. These spectra were determined from data taken at  $\sim 1$  day from the bow shock on either side of the magnetosphere. The differences in the dusk and dawn spectra shown here are typical. The dusk spectrum is harder than the dawn spectrum for the same distance from the bow shock. The fluxes shown on these graphs were determined by integrating over the portions of the spectrum that contained counts above background.

## THEORY

The asymmetry of the ion spectra observed in the dusk and dawn regions can be explained by considering the configuration of the interplanetary  $\vec{B}$  field and its influence on the particle trajectory on the two sides of the magnetosphere.

The equation of motion that describes a charged particle's trajectory in the rest frame of the bow shock and in the interplanetary medium is,

$$\frac{m d\vec{V}_p}{dt} = q (\vec{E} + \vec{V}_p \times \vec{B}) \quad (1)$$

where  $\vec{E}$  is the interplanetary electric field,  $\vec{B}$  is the interplanetary magnetic field,  $m$ ,  $q$ , and  $\vec{V}_p$  are the particle's mass, charge and velocity respectively. The solution of equation 1 yields a helical trajectory for a particle released at the shock surface with some initial velocity  $\vec{V}_p$ . The motions parallel and perpendicular to the  $\vec{B}$  field are uncoupled and consequently the equation that describes the guiding center trajectory of the particle is

$$\vec{V}_r = \vec{V}_{p||} + \vec{V}_d \quad (2)$$

where  $\vec{V}_{p||}$  is the particle velocity parallel to  $\vec{B}$  and  $\vec{V}_d$  is the drift velocity.

Figure 3 illustrates the geometry associated with equation 2. When  $\vec{B}$  is at its average position, that is the garden hose angle, the field lines will contact the dawn

side bow shock at a more normal angle of incidence than will the field lines on the dusk side. If it is assumed that protons with sufficient energy to escape the bow shock are released to the solar wind along interplanetary field lines, as originally suggested by Asbridge et al., [1968] then the ones released on the dusk side will be swept downwind much closer to the shock surface than those on the dawn side. The absence of lower energy particles in the upstream spectra is therefore more pronounced on the dusk side than the dawn side at the same distance from the shock.

In addition to this longitudinal dependence, whether or not a particle is observed at the moon is influenced by the latitude of the field. It is clear that if the interplanetary  $\vec{B}$  field has a large latitude component, then  $\vec{V}_{p||}$  can cause the resultant guiding center trajectory to miss the moon entirely. A complete discussion of the three-dimensional nature of the problem can be found in Benson [1974].

#### SIMULTANEOUS DATA

Figure 4 is a plot of the latitude of the interplanetary  $\vec{B}$  field as measured by Explorer 35 and the simultaneous integral flux measured by the SIDE for three hours in a dawn region. This figure shows directly that the integral flux tends to increase as the value of the field latitude gets closer to zero and tends to decrease as the field latitude moves away from zero. In order to further determine the

dependence of the observed particles on the configuration of the field, three days of simultaneous magnetic field and ion data were analyzed. Figure 5 shows the total number of times a particular value of the field latitude was observed in the period versus the latitude and the average counts seen at that latitude. It can be seen from this distribution that the average number of particles observed is greater when the field latitude is nearer zero. Figure 6 shows an analagous distribution for the field longitude where it can be seen that there are two peaks separated by approximately  $180^\circ$ . One would expect this type of distribution if the guiding center picture is correct.

#### SUMMARY

Definite dusk-dawn asymmetries are observed in the suprathermal protons seen by the SIDE on the lunar surface. The dawn side proton flows are seen much deeper into lunar night than the dusk side flows. The low energy cutoff in the dusk spectra occurs at a higher energy than it does for the dawn spectra at the same distance from the bow shock. The appearance of these particles at the moon is dependent on the latitude and the longitude of the interplanetary magnetic field. These observations are consistent with the assumption that the protons follow  $\vec{E} \times \vec{B}$  drift trajectories from the bow shock to the moon.



## ACKNOWLEDGEMENTS

The authors would like to thank D. S. Colburn of the NASA Ames Research Center for providing the magnetic field data. The authors would also like to thank R. P. Lin of the Space Sciences Laboratory, University of California, Berkeley and D. R. Criswell of the Lunar Science Institute for their helpful comments.

This research was supported by NASA contract NAS9-5911.

## REFERENCES

- Asbridge, J. R., Bame, S. J., Strong, I. B., Outward Flow of Protons from the Earth's Bow Shock, J. Geophys. Res., 73, 5777.
- Benson, J., Observation of Bow Shock Protons at the Lunar Orbit, M. S. Thesis, Rice University, Houston, Texas 77001.
- Freeman, J. W., Jr., Balsiger, H., Hills, H. K., 1970, Suprathermal Ion Detector Experiment, Apollo 12 Preliminary Science Report, NASA SP-235, 83.
- Hills, H. K., Freeman, J. W., Jr., Balsiger, H., 1970, Energetic Protons Observed at the Lunar Surface on the Night Side of the Moon, Trans. Am. Geophys. Union, 51, 407.
- Lin, R. P., Meng, C. I., Anderson, K. A., 1974, 30 to 100 keV Protons Upstream from the Earth's Bow Shock, J. Geophys. Res., 79, 489.

## FIGURE CAPTIONS

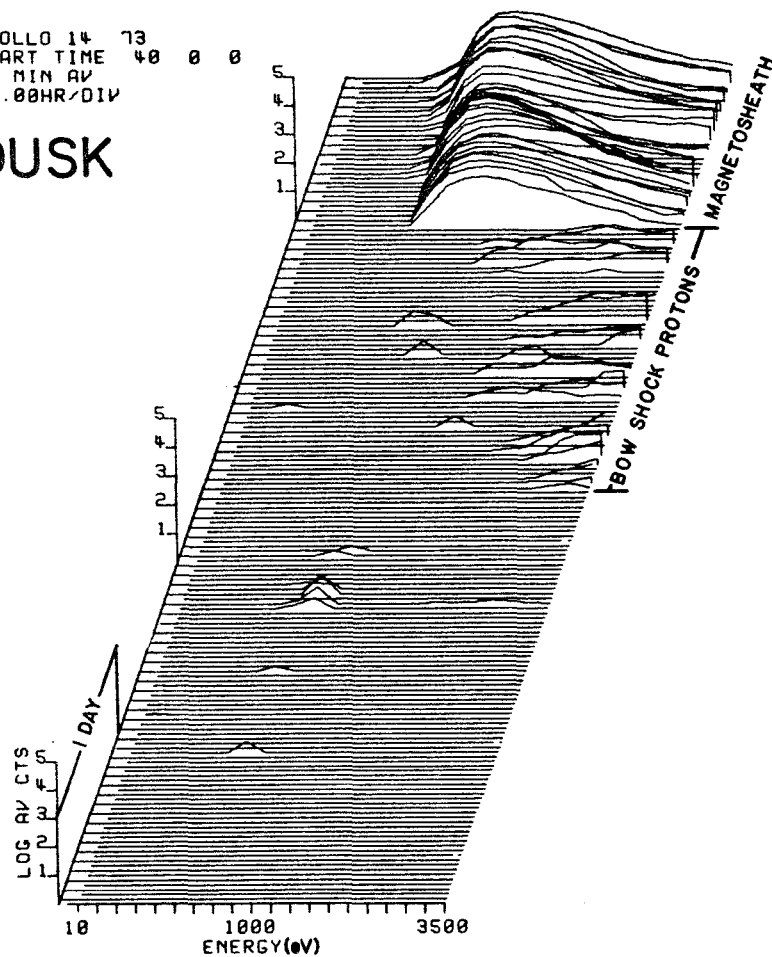
1. Typical counting rate spectra for the magnetospheric dusk and dawn bow shock regions. Time progresses along the diagonal axis. Each trace represents a 20 minute average of the counts in each energy channel. The small ridge of monoenergetic low energy particles seen on the dawn side ~4 days from the bow shock is due to locally accelerated lunar atmospheric ions.
2. Typical differential flux spectra taken from each bow shock region at ~1 day from the bow shock. The spectra are generated from a 20 minute average of the counts in each channel. Note the harder spectrum on the dusk side and lower total flux.
3. Ecliptic plane view of the vector diagram illustrating the resultant guiding center trajectory of a particle leaving the surface of the bow shock. Two special cases of the direction of the interplanetary  $\vec{E}$  field are also shown.
4. Time history of simultaneous data from Explorer 35 and SIDE for a short period in a dawn region. The top trace is the solar equatorial latitude of the interplanetary  $\vec{B}$  field and the bottom trace is the integral flux observed by the SIDE.

5. Distribution of the average number of particles observed at a particular solar equatorial latitude vs. the latitude. The average is computed by dividing the total number of counts accumulated at a particular latitude over the time period by the total number of times the field was at that latitude. Also shown is the frequency of occurrence of the latitude over the observation period. (1972 153<sup>d</sup> 19<sup>h</sup> 24<sup>m</sup> to 156<sup>d</sup> 19<sup>h</sup> 24<sup>m</sup>).

6. Same as for Figure 5 for the solar equatorial longitude of the field.

APOLLO 14 73  
 START TIME 40 0 0  
 40 MIN AV  
 48.00HR/DIV

DUSK



APOLLO 14 72  
 START TIME 193 0 1  
 40 MIN AV  
 48.00HR/DIV

DAWN

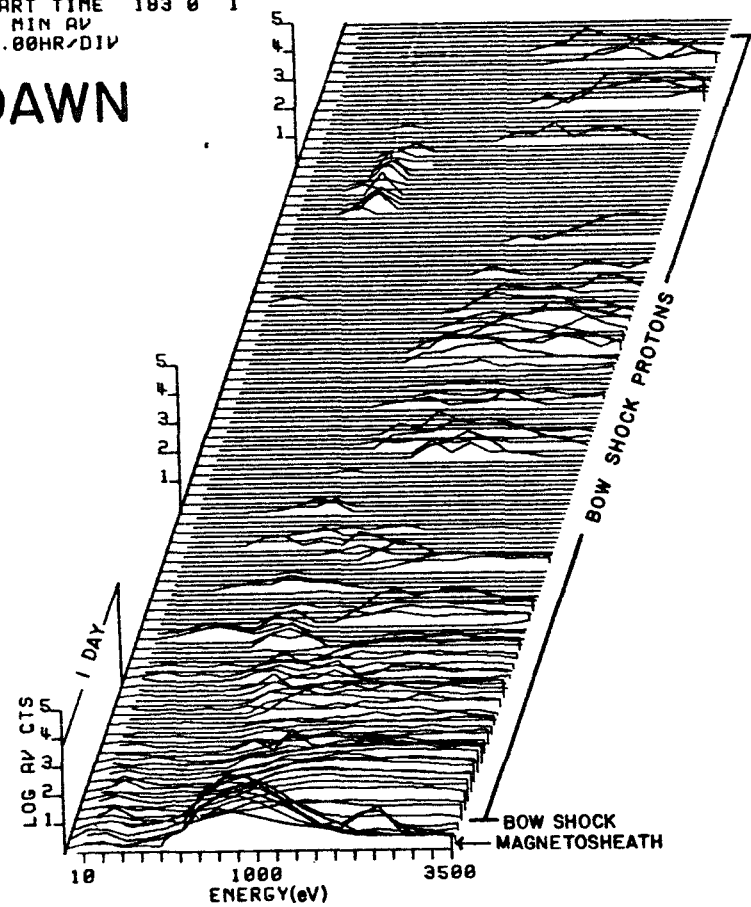


Figure 1

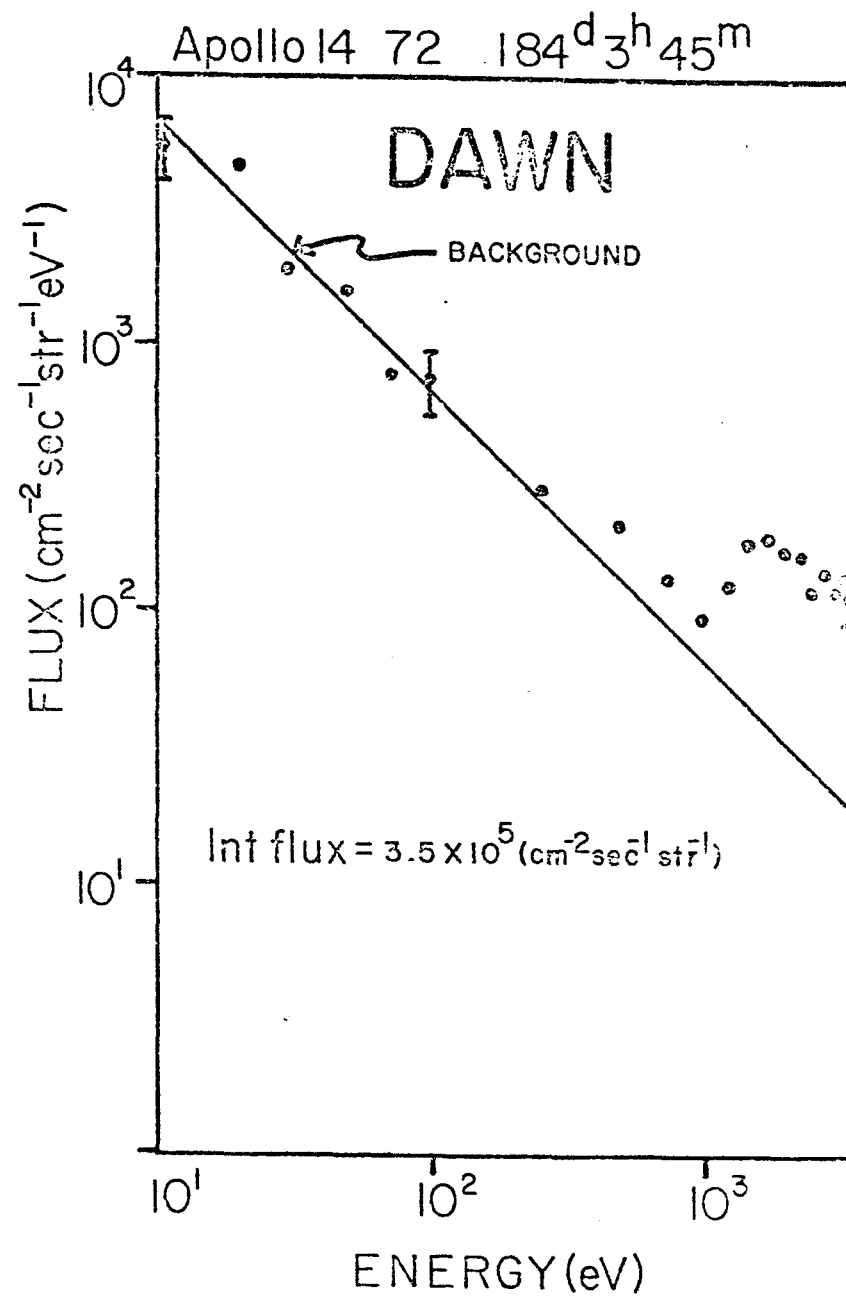
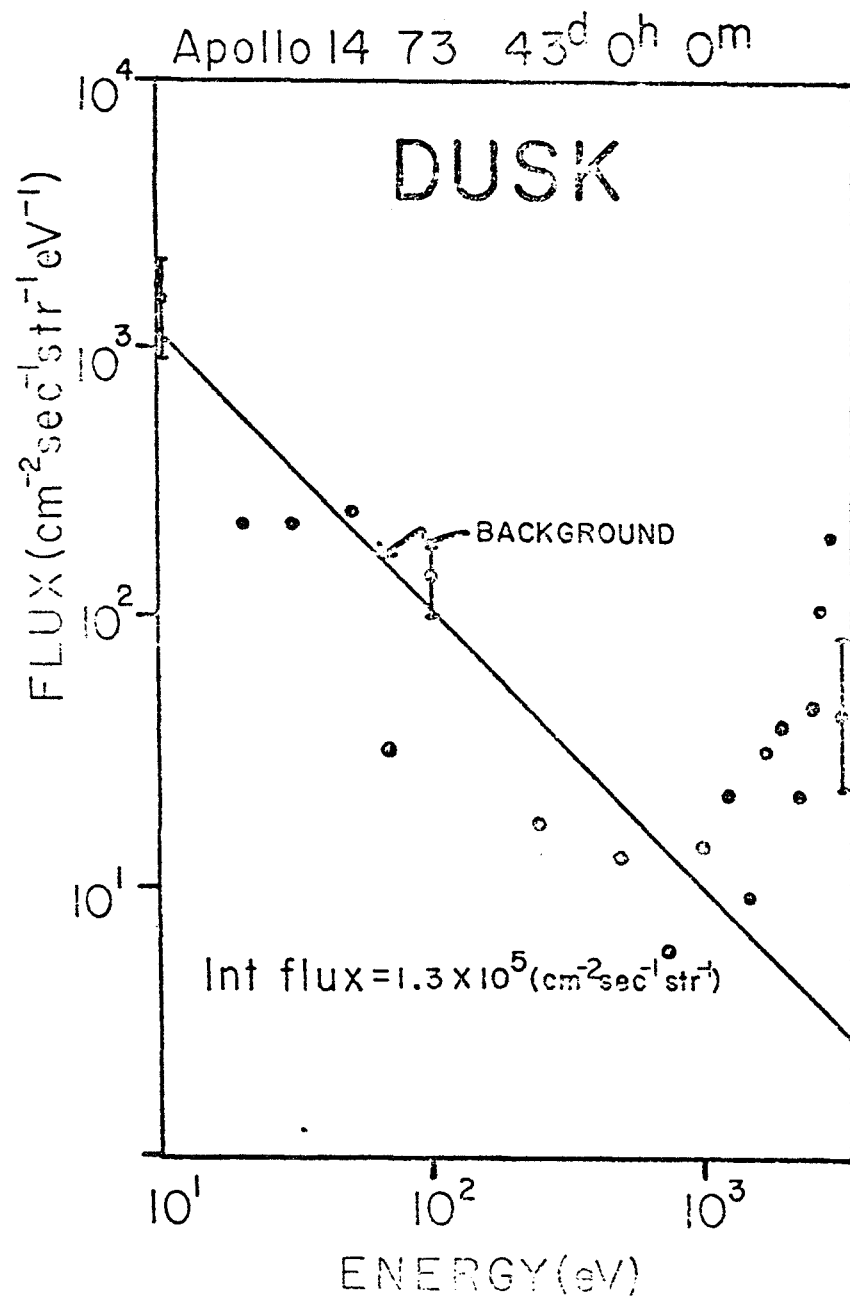


Figure 2

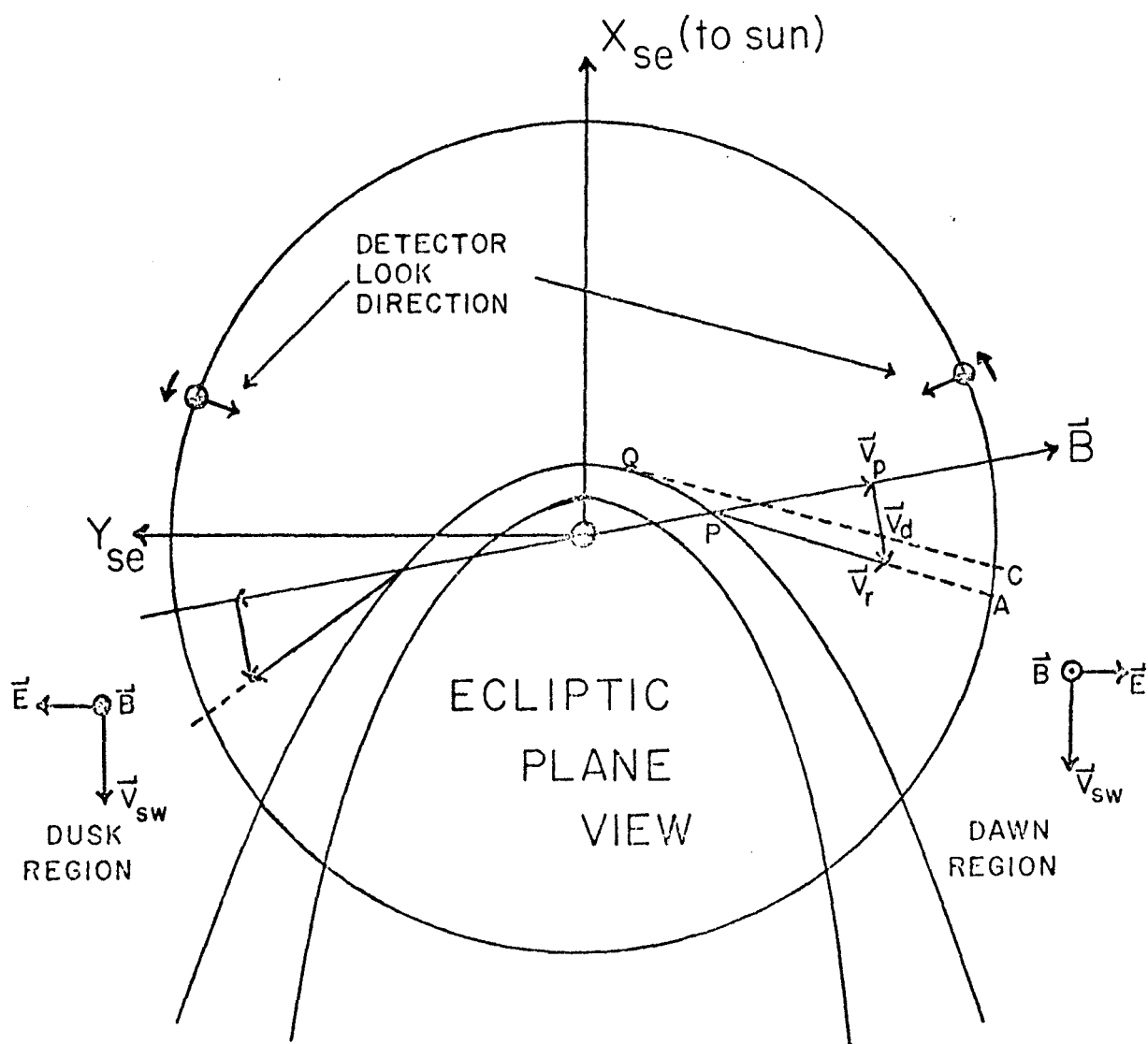


Figure 3

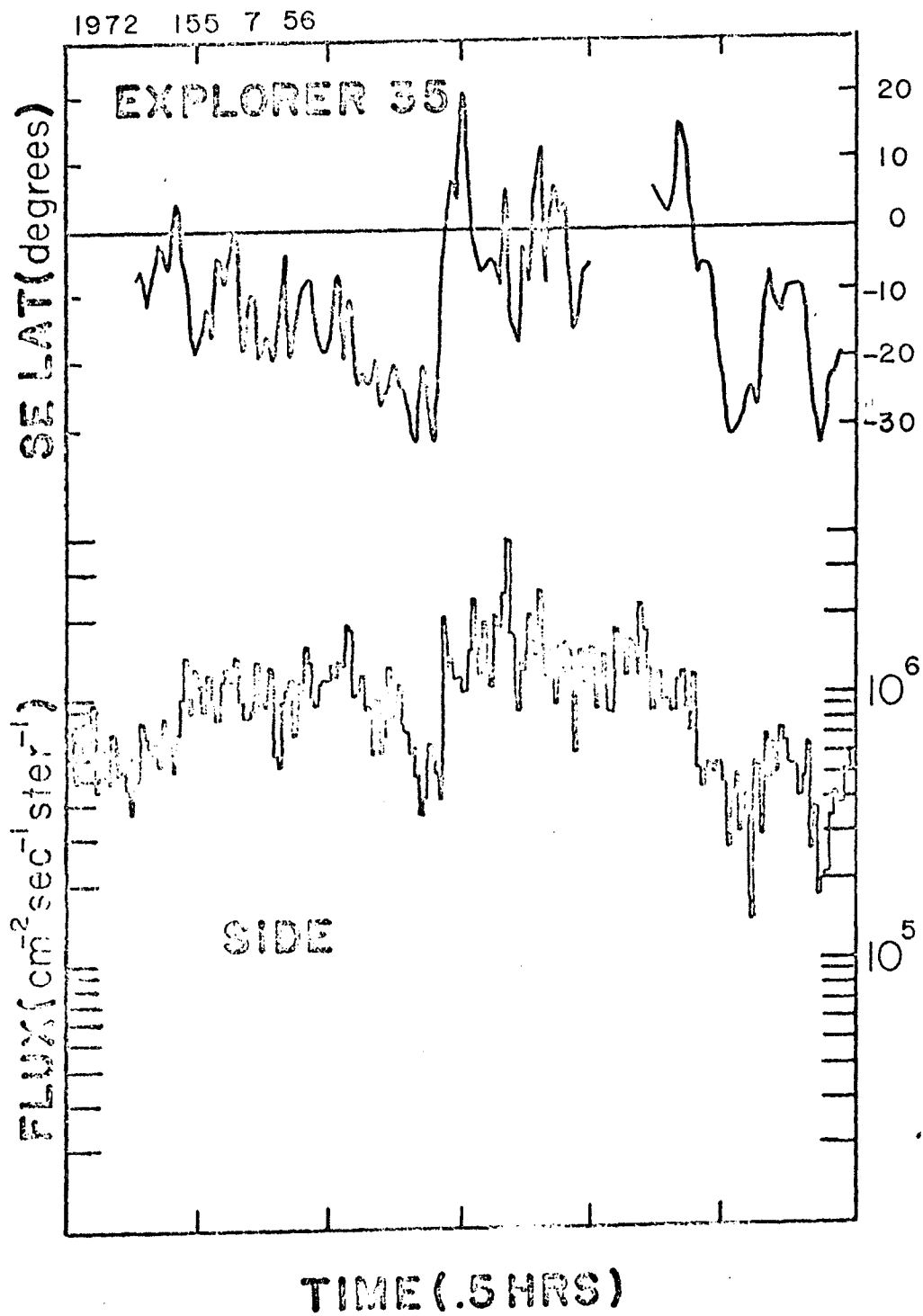


Figure 4



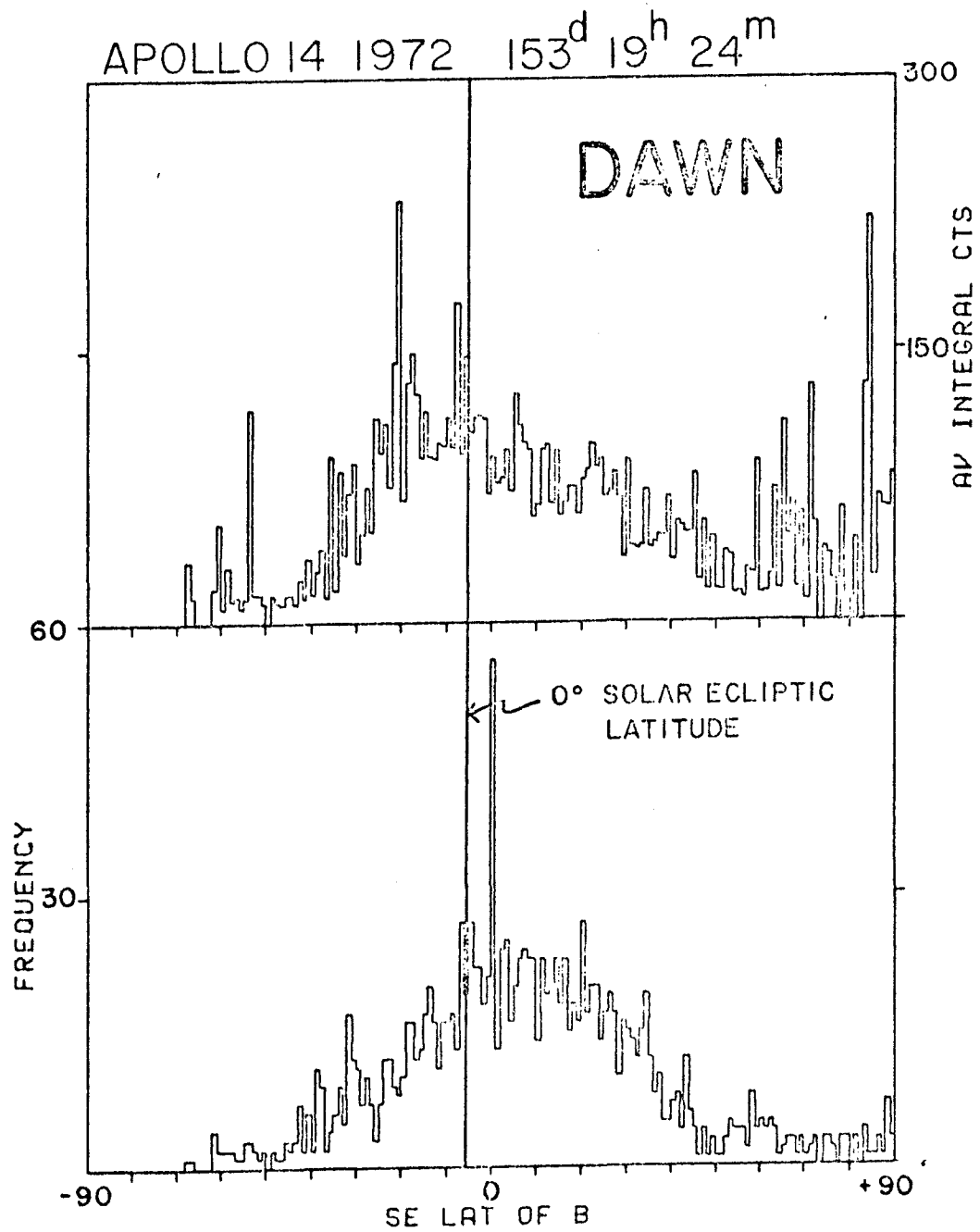


Figure 5

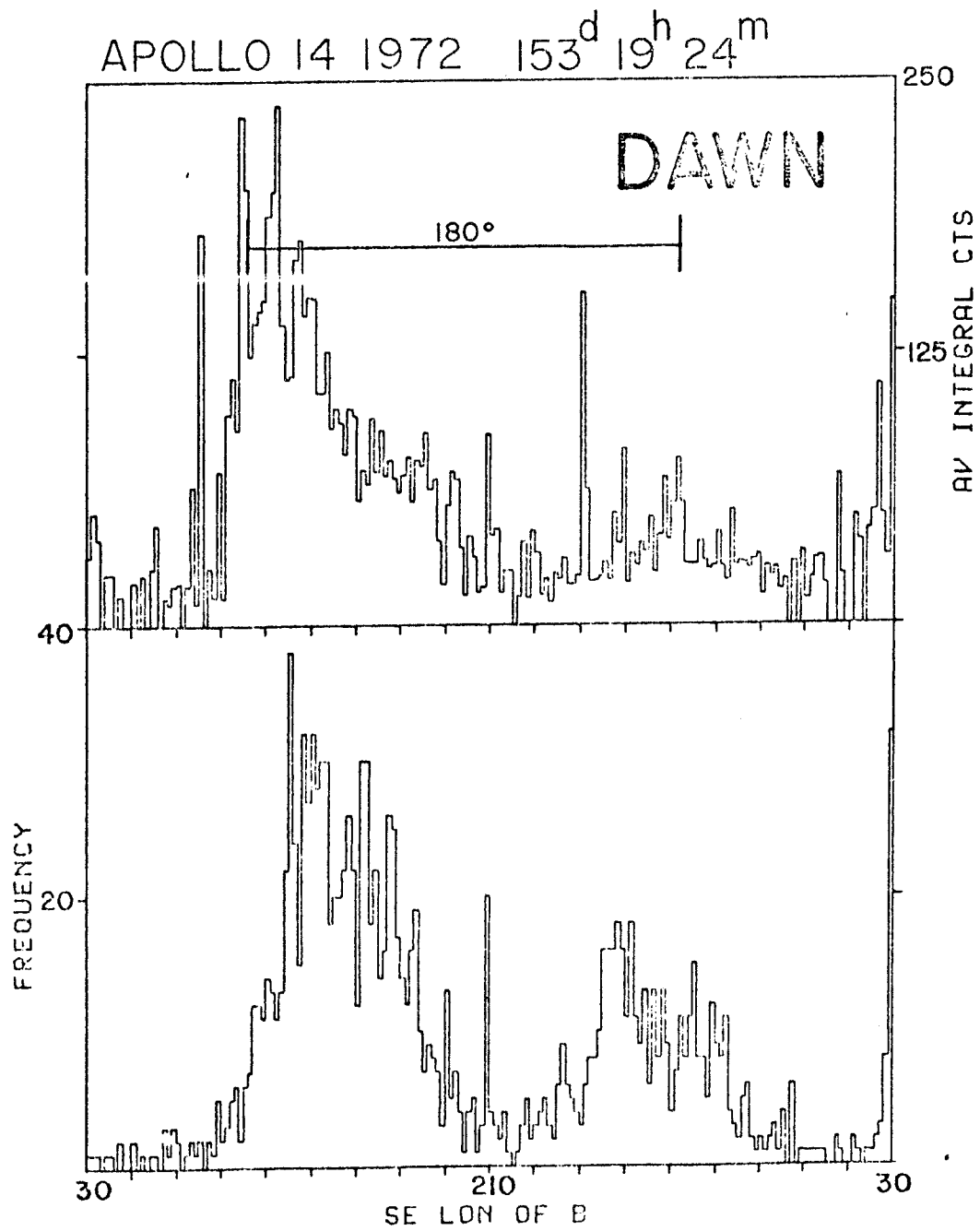


Figure 6



Dawn-Dusk Magnetosheath Plasma Asymmetries  
at  $60 R_e$

M. A. Fenner<sup>1</sup> and J. W. Freeman, Jr.

Department of Space Physics and Astronomy  
Rice University  
Houston, Texas 77001

February 1975

Accepted for Publication in the Journal  
of Geophysical Research

<sup>1</sup> Present address, Bell Laboratories, Whippany,  
New Jersey 07981.

6774R  
1/3

DAWN-DUSK MAGNETOSHEATH

PLASMA ASYMMETRIES AT  $60 R_e$

M. A. Fenner<sup>1</sup> and J. W. Freeman, Jr.

Department of Space Physics and Astronomy

Rice University

Houston, Texas 77001

ABSTRACT

A study of data from the Apollo Lunar Surface Suprathermal Ion Detector Experiment package shows that plasma flow and energy parameters in the dusk magnetosheath are much better correlated with geomagnetic activity than those in the dawn magnetosheath. This result is in agreement with a dawn-dusk asymmetry in the magnetosheath magnetic field and in the bow shock configuration. The different orientations between the mean interplanetary magnetic field direction and the shock normal for the magnetosheaths suggests an explanation of the difference in the plasma parameters on the two sides.

<sup>1</sup>Now at Bell Laboratories, Whippany, New Jersey 07981

## I. Introduction

This paper presents magnetosheath positive ion data taken at a distance of  $60 R_e$ , the lunar orbit. Velocity distribution functions have been determined from twenty minute averages of the data, an equivalent resolution of  $\sim 1000$  km. From these velocity distribution functions a study of the bulk flow parameters in the sheath was performed. Ten lunations of data were employed. These data were then compared with the geomagnetic activity index,  $K_p$ .

A unique advantage of the lunar orbit for magnetosheath studies is the coverage of both the dawn and dusk magnetosheaths in the same general time frame. The moon takes approximately eight days from the dusk to dawn bow shocks. In this paper we compare the dusk magnetosheath parameters with those of the dawn magnetosheath.

Previous workers have reported asymmetries in various aspects of magnetospheric structure. Fairfield (1971) observed the dawn magnetosheath field to be more disturbed than the dusk field. Explorer 35 data (Howe, 1971) showed twice as many bow shock crossings on the dawn side as on the dusk side. Greenstadt (1972) further observed an asymmetry in the types of shock crossings observed on the two sides.

He classified shock crossings as oblique or perpendicular according to the angle of the interplanetary field with respect to the direction of the propagation of the shock wave. Greenstadt (1973) estimated 50% more oblique shocks to occur on the dawn side. Oblique shocks are associated with fluctuating fields and rapidly varying proton spectra.

The evidence of asymmetries in the sides of the magnetosheath is important to the over-all view of energy transport from the interplanetary medium into the magnetosphere. The magnetohydrodynamic processes in the sheath are important in understanding the mechanism of energy transport. This paper presents evidence that the particle distribution function behaves differently in the two different sheaths. The explanation of this asymmetry is perhaps found in Greenstadt's picture of the field configuration producing different types of shock waves. It is suggested that the plasma behavior depends on the field configuration and different processes are present on the dawn side as opposed to the dusk side of the magnetosphere.

## II. Experiment and Data Analysis

The Suprathermal Ion Detector Experiment (SIDE) is designed to measure plasma near the moon. Identical SIDEs were deployed at the Apollo 12, 14 and 15 landing sites, Figure 1. The SIDE has been described in Freeman et al.,

(1972). The positive ion detector measures spectrum in velocity space by stepping through a range of 20 voltages on a curved plate analyzer. Velocities per unit charge, equivalent to proton energies per unit charge, are measured in a period of 24 seconds. The 20 steps cover a range from 10 eV/q to 3500 eV/q. The basic collector is a channel-electron-multiplier used in the pulse counting mode. The front end is biased at an accelerating voltage of -3.5 KV to collect the low energy ions.

The orientations of the three instruments on the moon's surface are such that the detector look axes lie approximately in the ecliptic. The look angle of each detector in the ecliptic is shown in Figure 2. The detectors were arranged so that the Apollo 15 instrument looks in the direction of plasma flow in the dusk magnetosheath and the Apollo 12 instrument does so in the dawn magnetosheath. On both sides the Apollo 14 instrument records a lower flux level of ions away from the bulk flow direction. The field of view of each detector is square and approximately  $6^\circ$  on a side.

Twenty minute averages of the differential energy spectra were calculated. The resulting spectra were converted to distribution function spectra in velocity space. Figure 3 shows these spectra plotted for part of a typical



crossing of the dusk magnetosheath. From these spectra, the plasma flow parameters of number density, bulk velocity and temperature were calculated by the method of moments, following Vasyliunas (1969). These parameters are plotted in Figure 4 for the data from Figure 3.

Pressure is calculated from the number density and temperature using the equation of state for the gas. Energy density is given by

$$\int_{E_1}^{E_2} E f(E) dE$$

where  $f(E)$  is the distribution function in energy space and the integral is taken from energy  $E_1$  to energy  $E_2$ .

$R$  is the ratio of the high energy density, obtained by integrating from 1250 eV to 3500 eV, to the total energy density, obtained by integrating from 100 eV to 3500 eV. Notice that this ratio can remain constant although the pressure and total energy density are increasing. This indicates that the shape of the spectrum may remain the same while the intensity increases. The energy density ratio,  $R$ , is used to indicate the presence of a high energy tail. The presence of these high energy particles is taken as an indication of a disturbance in the magnetosheath. A sharp peak in the energy density ratio (around 20 HR UT, Figure 4) merely indicates a boundary crossing where the directed sheath flow disappears. Horizontal lines on this plot indicate that the parameters were not calculated because magnetosheath spectra were not observed in the direction of the detector.

### III. Results

The plasma parameters across the magnetosheath, both dusk and dawn sides, for 10 lunations reveal the general trends predicted by laminar flow in the Spreiter and Alksne (1969) theory. The effects are less pronounced at  $60 R_e$  than closer to Earth (Wolfe, et al. 1968). This indicates greater mixing at greater distances in the sheath.

The parameter of particular interest is the energy density ratio. The energy density ratio is found to decrease from the bow shock to the magnetopause. This decrease of the energy density ratio away from the bow shock is observed more frequently during the dusk rather than the dawn sheath crossings. The high energy particles do not show as consistent a pattern on the dawn side as on the dusk side of the magnetosheath.

In order to study the relationship of sheath parameters to  $K_p$ ,  $K_p$  was averaged for an entire sheath crossing. The five calculated plasma parameters were averaged in the same manner. Plots of  $K_p$  and the parameters for the 10 inbound and outbound sheath crossings for each instrument are given in Figure 5. For the dusk sheath the curve of the energy density ratio seems to follow that of  $K_p$  quite well.

Velocity and temperature appear to be somewhat correlated but to a lesser degree. Pressure, which is directly related to the total energy density is not correlated with  $K_p$  at all. Number density is also apparently unrelated. The magnitude of the values for the three instruments with respect to each other is in agreement with their relative angles to the flow direction.

It is important to note that the detector farther from the flow direction (Apollo 14) reports a greater energy density ratio. A detailed examination of the energy spectra reveals that the intensity of the high energy particles was the same for all three instruments regardless of the direction-related variation in peak intensity. This is an indication that the dispersion of particles in velocity space may be isotropic. Howe (1971) reported double peaked ions at the bow shock to be in a different direction from the bulk flow. The SIDE detector also observes the sudden appearance and disappearance of multiple peaks in individual 20 second spectra. This might indicate a directional effect. However, the average over a longer time indicates isotropy.

A linear regression analysis was run on each of the curves in Figure 5 with respect to  $K_p$ . The correlation coefficient  $r$  for each of the variables is given in Table 1. Note the strong correlation of velocity and energy density ratio to  $K_p$  on the dusk side and almost no correlation on the dawn side.

To further emphasize this correlation the energy density ratio for Apollo 14 is plotted versus average  $K_p$  (Figure 6). A least squares fit was attempted on both the dusk and dawn data. The fit is plotted for the dusk data, but is meaningless for the dawn data since the correlation coefficient indicates random data. Thus the high energy particle population in the dawn sheath is not at all correlated with geomagnetic activity, while the dusk sheath particles shows a strong correlation.

Finally, we note from figure 5 that despite the asymmetry in the correlation between  $R$  and  $K_p$ , the values for  $R$  cover approximately the same range in both magnetosheaths.

It might be argued that an increase in  $R$  merely represents an increase in the bulk flow velocity. That this is not the case is demonstrated in the appendix.

#### IV. Discussion

To understand this result we must look at two problems: 1) what correlation with  $K_p$  means and 2) what is indicated by the asymmetry. At the same time we must bear in mind the significance of the similar absolute values for  $R$  in the dawn and dusk magnetosheath.

First we address the question of correlation with geomagnetic activity. It is well known that geomagnetic activity is correlated with interplanetary conditions. Both an increase in solar wind speed (Ballif et al. 1969) and an

increase in the magnitude of the interplanetary field (Schatten and Wilcox, 1967) are correlated with an increase in  $K_p$ . An increase in the momentum flux of the solar wind is known to compress the geomagnetic cavity and Freeman (1964) has shown that magnetopause boundary locations are related to  $K_p$ . It is obvious that solar wind energy must be transmitted through the magnetosheath to reach the magnetosphere and influence  $K_p$ , however, there have not been any previous correlations of sheath variations with geomagnetic activity.

The high correlation between  $R$  and  $K_p$  shown here indicates that the high energy tail of the magnetosheath spectrum is a direct result of the transfer of energy from the solar wind to the magnetosphere. It seems unlikely that the high energy particles carry the transferred energy themselves. For example, we note that the bulk flow velocity is also increased at times of excess high energy particles and so in the dusk magnetosheath bulk flow velocity is also correlated with  $K_p$ . We take the view that the high energy tail is the result of acceleration processes that are an intrinsic part of the energy transfer process. An alternative view which we are not inclined to accept is that high energy particles enter the magnetosheath from the plasma sheet at the cusps or along the flanks of the tail. In this case there might also be a correlation with  $K_p$ , but the high energy population would not be expected to increase toward the bow shock as is observed.

Regarding the asymmetry, we note that Formisano et al. (1973) have shown the magnetosheath high energy tail to be correlated with the absence of waves upstream of the bow shock. This suggests that waves have a tendency to diffuse particle concentrations in velocity space and hence reduce high energy particle intensities. The field configuration envisioned by Greenstadt (1972) shows that oblique shocks occur predominantly on the dawn side of the magnetosphere. The post-shock field is much more disturbed in the oblique shock case and wavelike disturbances are expected. We suggest that these disturbances influence the occurrence of particles in the high energy tail in the dawn magnetosheath. This masks the  $K_p$  correlation that would otherwise be present. In order to more fully understand the relationship between  $R$  and  $K_p$  it may be necessary to know if there is a statistical connection between the formation of oblique shocks and  $K_p$ .

The intrinsic asymmetry between the dawn and dusk magnetosheaths is thus not an asymmetry in the ion acceleration processes but rather in processes which tend to disperse the accelerated ions, namely magnetic noise. The dawn magnetosheath is a more complex region and the key to understanding it may lie in a better understanding of oblique shocks.

#### V. Acknowledgement

This research was supported in part by NASA contract NAS9-5911.

TABLE 1  
 LINEAR REGRESSION OF  $K_p$  VERSUS PARAMETERS

---

Gives values of the correlation coefficient  $0 < r < 1$

where  $r = \pm 1$  is a perfect correlation

$r = 0$  is random data

PARAMETERS	DUSK		DAWN	
	APOLLO 14	APOLLO 15	APOLLO 14	APOLLO 12
Energy density ratio	.88	.67	.05	.30
Velocity	.79	.77	.20	.13
Temperature	.76	.36	.36	-.41
Number density	-.36	.20	-.27	-.32
Pressure	.19	-.17	-.06	-.11

## APPENDIX

Since the energy density ratio is a new parameter, a further explanation of it is given here. In velocity space the expression for energy density (equation 1) becomes  $\Sigma \frac{1}{2} m^2 v_i^3 f(v_i) dv_i$ . Using a kappa = 2 distribution function (Olbert, 1969) for  $f(v)$ , the quantity  $v^3 f(v)$  is plotted (Figure 7) for three different values of bulk flow velocity  $v_B = 300, 400$  and  $500$  km/sec. For the two lower values, the shaded areas illustrate the energy density in the high energy region of the spectrum. For a change in bulk velocity from 300 km/sec to 400 km/sec the energy density ratio of a kappa = 2 distribution function changes from 1% to 10%. The velocity corresponding to the 1250 eV energy channel was arbitrarily chosen for the break point in calculating the ratio. Since the velocities observed in this data were less than 400 km/sec, the choice of a break point is adequate. That is, the large energy density ratios (>20%) are not the result of merely a change in bulk velocity, because the velocity is 400 km/sec or less.



## BIBLIOGRAPHY

- Ballif, J. R., D. E. Jones, and P. J. Coleman, Further evidence on the correlation between transverse fluctuations in the interplanetary magnetic field and  $K_p$ , J. Geophys. Res., 74, 2289, 1969.
- Fairfield, Donald H., Average and unusual locations of the earth's magnetopause and bow shock, J. Geophys. Res. 76, 28, 6700, 1971.
- Formisano, V., G. Moreno, F. Palmiotto, and P. C. Hedgecock, Solar wind interaction with the earth's magnetic field, 1, Magnetosheath, J. Geophys. Res., 78, 19, 3714, 1973.
- Freeman, J. W., The morphology of the electron distribution in the outer radiation zone and near the magnetospheric boundary as observed by Explorer 12, J. Geophys. Res., 69, 1961, 1964.
- Freeman, J. W., Jr., M. A. Fenner, H. K. Hills, R. A. Lindeman, R. Medrano, and J. Meister, Suprathermal Ions Near the Moon, Icarus, 16, 2, 328, 1972.
- Greenstadt, E. W., Binary index for assessing local bow shock obliquity, J. Geophys. Res. 77, 28, 5467, 1972.
- Greenstadt, E. W., Statistics of Bow Shock Nonuniformity, J. Geophys. Res., 78, 13, 2331, 1973.

- Howe, H. C., Jr., Explorer 33 and Explorer 35 plasma observations of the interaction region between the solar wind and the magnetic field of the earth, Ph. D. Thesis, M.I.T., 1971.
- Olbert, S., Physics of the magnetosphere (R. L. Carovillano, J. F. McClay, and H. R. Radoski, eds.), 641, D. Reidel Publishing Co., Dordrecht, Holland, 1969.
- Schatten, K. H. and J. M. Wilcox, Response of the geomagnetic activity index  $K_p$  to the interplanetary magnetic field, J. Geophys. Res., 72, 5185, 1967.
- Spreiter, J. R. and A. Y. Alksne, Plasma flow around the magnetosphere, Rev. of Geophys. 7, 11, 1969.
- Vasyliunas, V. M., Deep Space plasma measurements, Methods of Experimental Physics, IX, 1969.
- Wolfe, J. H. and D. D. McKibbin, Pioneer 6 observations of a steady state magnetosheath, Planet. Space Sci., 16, 953, 1968.

## FIGURE CAPTIONS

- Figure 1. The Suprathermal Ion Detector Experiment (SIDE) is shown as it was deployed on the moon by Apollo 14 Astronauts. The instrument stands 45 cm above the lunar surface.
- Figure 2. The look directions of the Apollo 12, 14 and 15 detectors are shown for various positions of the Moon in its orbit as it crosses the tail of the earth's magnetosphere.
- Figure 3. Distribution function spectra in velocity space are plotted as a function of time. The units are  $\text{ions/m}^3/(\text{m/sec})^3$ . The heavy reference line at the beginning of the plot represents a constant counting rate of 1 count in each energy channel. Comparing the spectra after 20 hr UT with this line indicates an absence of magnetosheath spectra after a boundary crossing.
- Figure 4. The plasma parameters -- pressure, energy density ratio, temperature, bulk flow velocity, and number density are plotted for part of a dusk magnetosheath crossing. A magnetopause crossing is seen just before 20 hr UT. For a time after this none of the parameters are calculated except the energy density ratio. The magnetosheath spectrum is absent at this time.

Figure 5. A summary of plasma parameters is given for both the dusk and dawn magnetosheath crossings during 10 lunations. Data from the three instruments are identified by an x (Apollo 14), solid dot (Apollo 15) and open dot (Apollo 12). One average value of a parameter is plotted for each sheath crossing for a single instrument. Above the parameter plots, a plot of average  $K_p$  is given. For each sheath crossing,  $K_p$  was averaged during the time the moon was in the magnetosheath (approximately two days).

Figure 6. The average energy density ratio for each of the 10 lunations plotted versus the average  $K_p$  over the entire magnetosheath crossing. A linear regression gives a straight line fit to the dusk data. The dawn data are random as seen by a correlation (r) of .05.

Figure 7. The product of  $v^3$  and the kappa = 2 distribution function  $f(v)$  is plotted for three values of bulk velocity. The energy density is represented by the area under the curve.

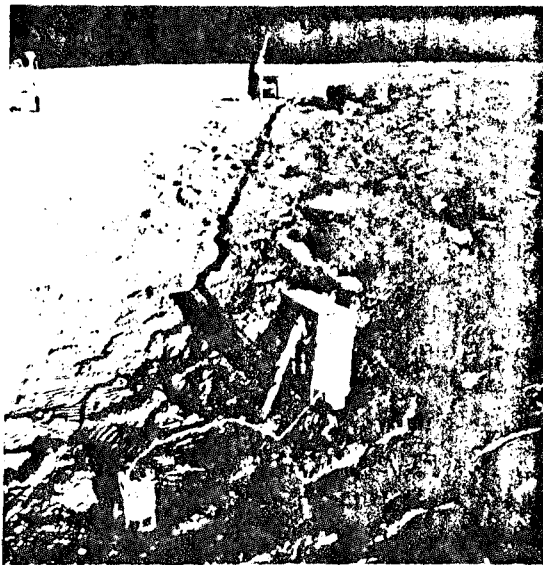
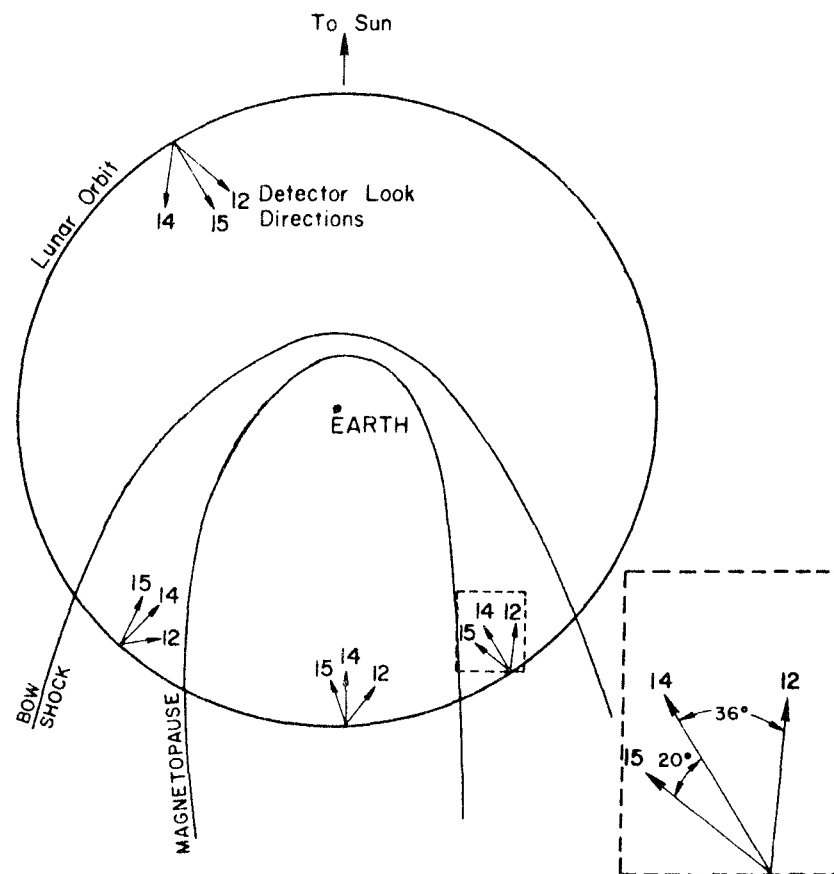
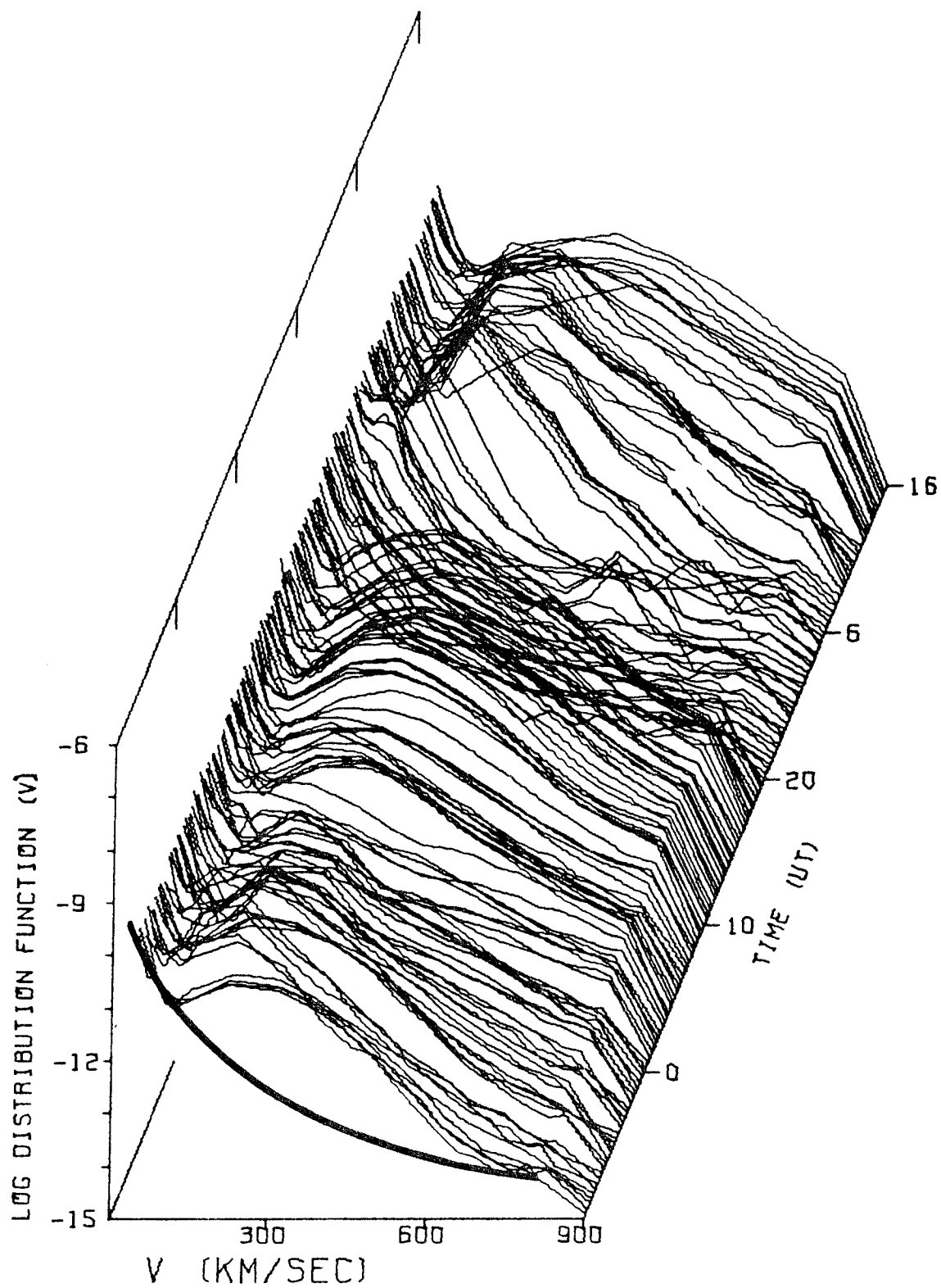


Figure 1



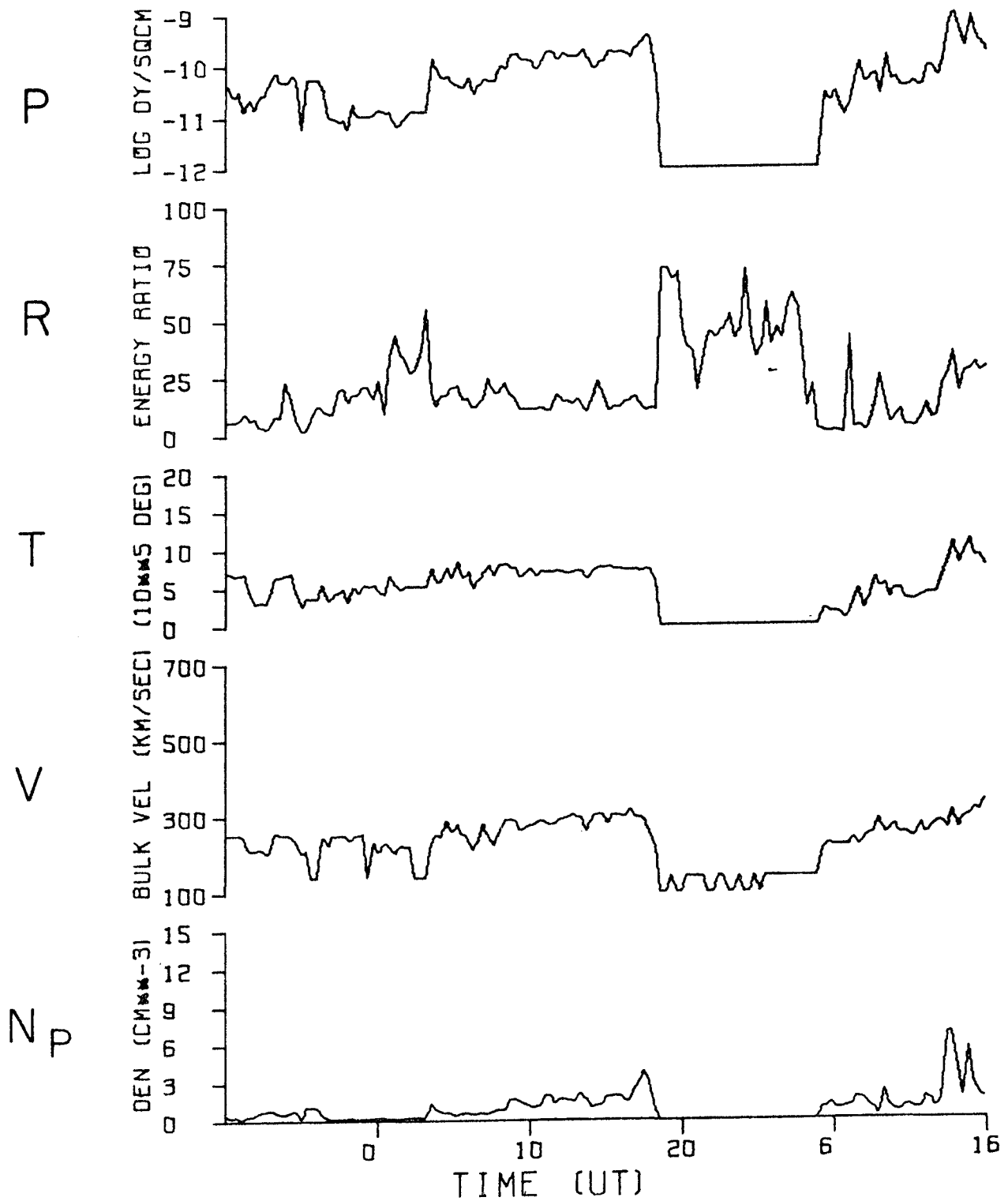
Boundaries shown are average values from Explorer data.

FIGURE 2



1972 APOLLO 14  
DAY 06 HR 14 MIN 2

FIGURE 3



1972 APOLLO 14  
DAY 06 HR 14 MIN 9

FIGURE 4



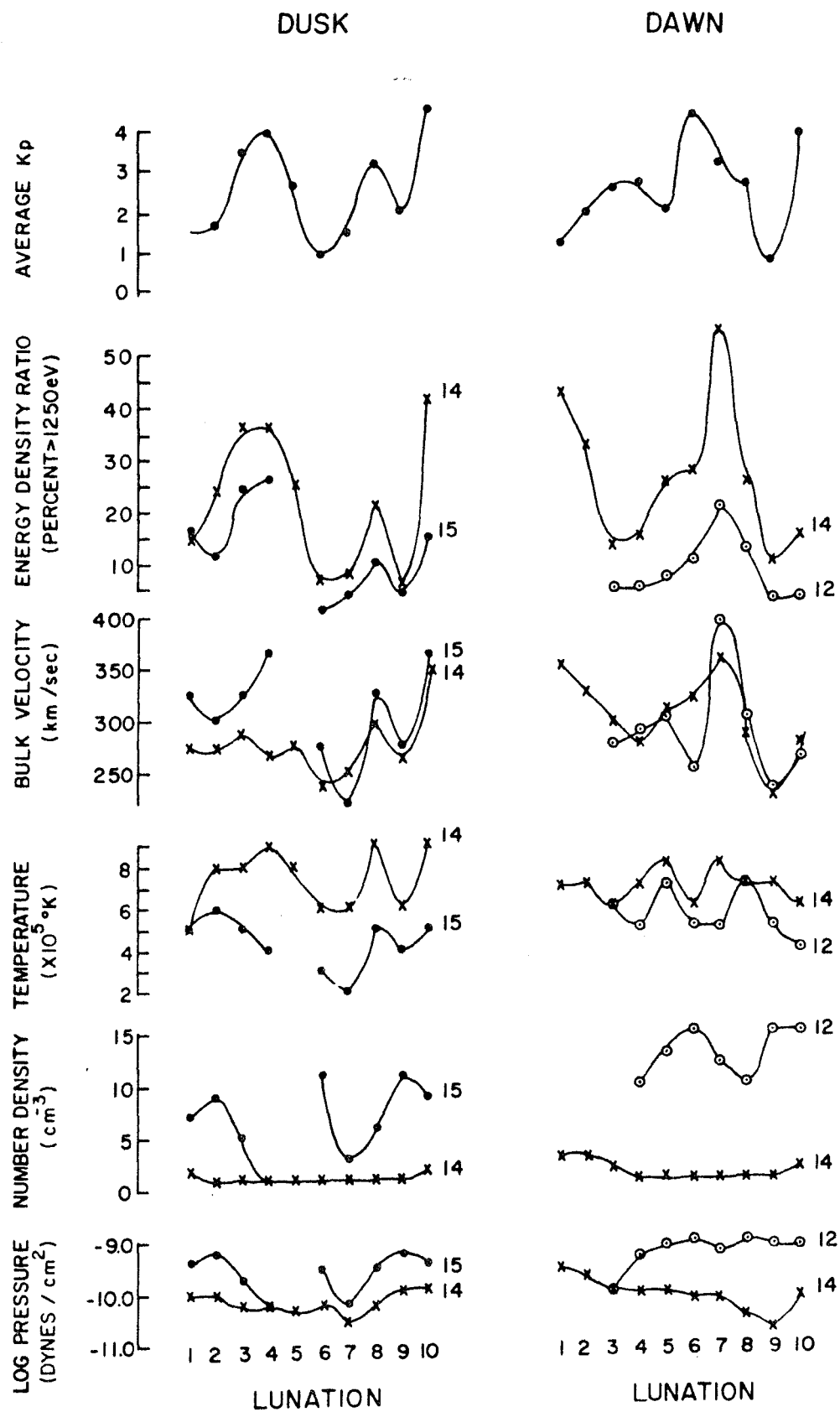


FIGURE 5

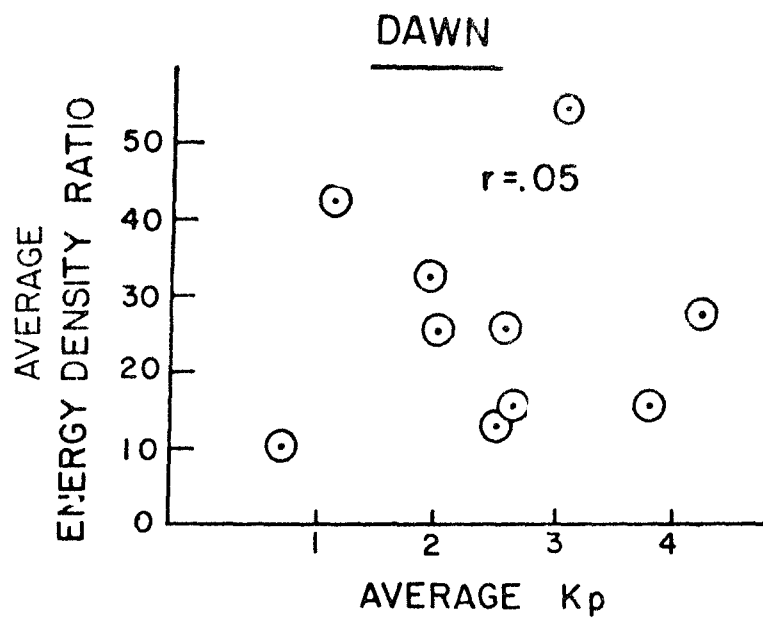
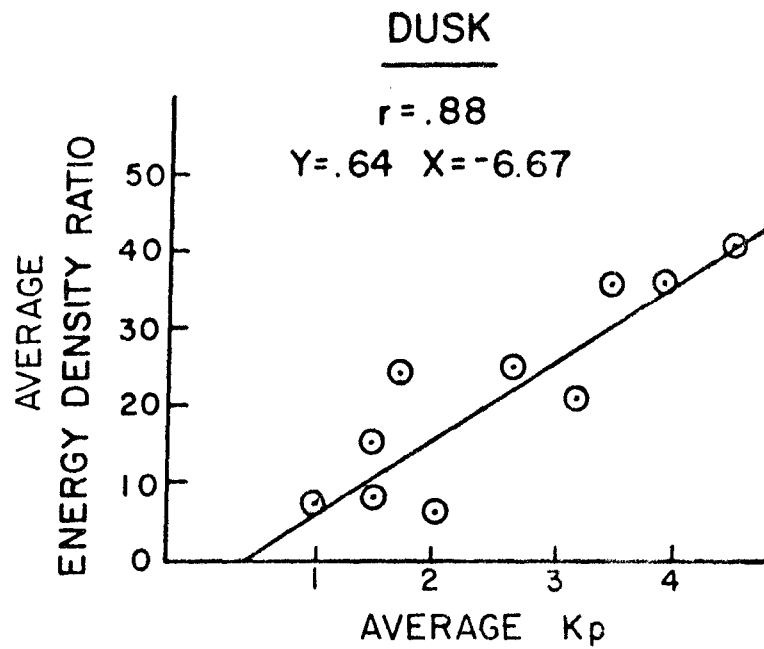


Figure 6

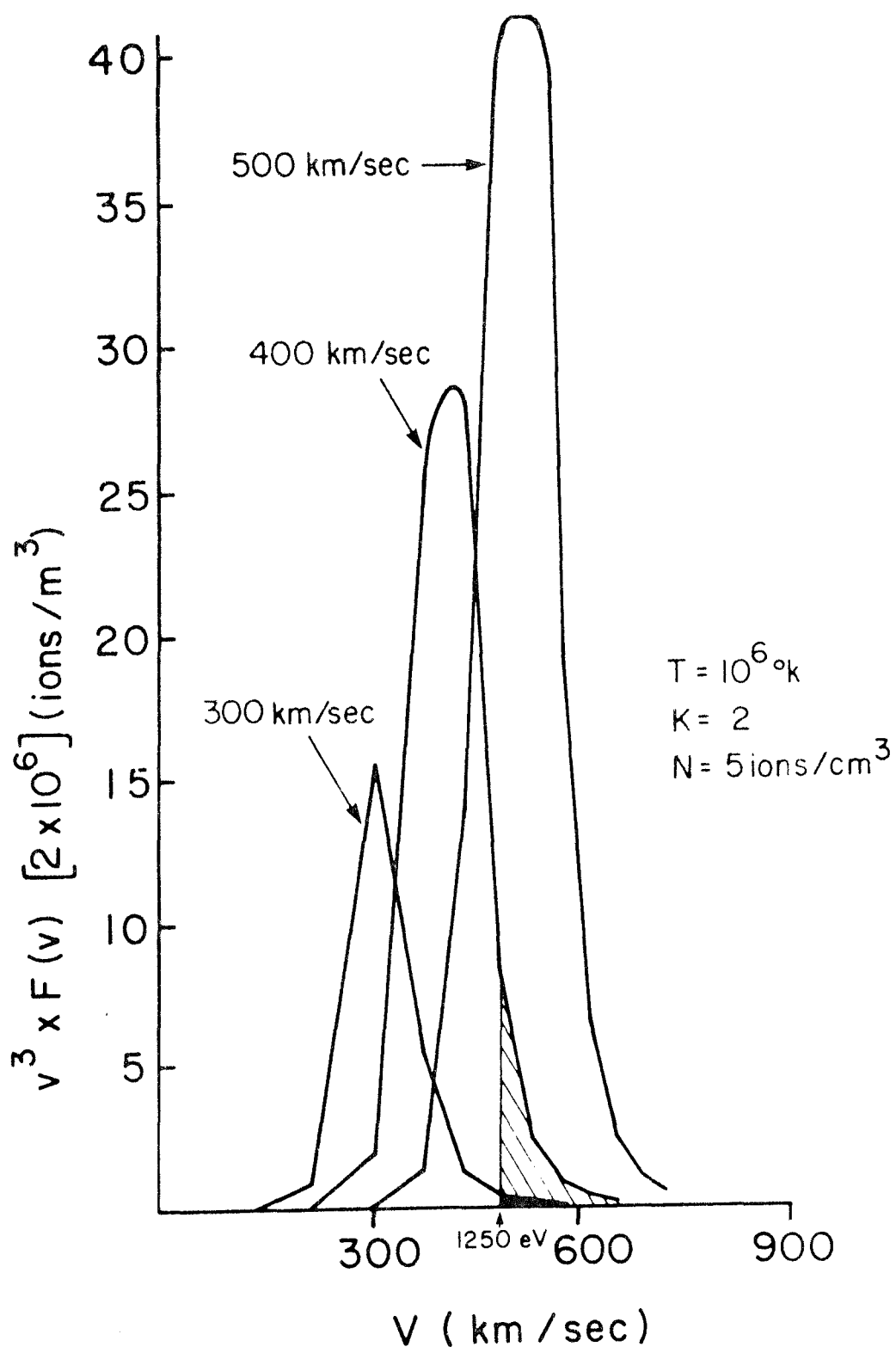


Figure 7



## A NEW PLASMA REGIME IN THE DISTANT GEOMAGNETIC TAIL

D. A. Hardy, H. K. Hills, and J. W. Freeman

Rice University  
Houston, Texas 77001

**Abstract.** The three Rice Suprathermal Ion Detector Experiments have detected an extensive region of low energy plasma flow antisunward along the ordered field lines in the lobes of the geomagnetic tail at lunar distances. This particle regime resembles the "boundary layer" and "plasma mantle" observed at smaller geocentric distances and an interior flow region parallel to the magnetopause in the dayside magnetosphere. It possesses plasma characteristics uniquely different from the plasma sheet and magnetosheath. Spatially the particle regime is found exterior to the plasma sheet across essentially the entire tail and adjacent to the magnetopause on both the dawn and dusk sides of the magnetosphere. The integral flux varies from  $10^5$  to  $10^8$  ions/cm<sup>2</sup> sec ster with the differential flux peak between 50 and 250 eV/q. Temperatures range from  $4 \times 10^4$  to  $5 \times 10^5$  °K and number densities from .1 to 5/cm<sup>3</sup>.

## Introduction

Freeman et al. [1968] reported observations of a region of plasma flow antisunward just inside the dayside magnetopause during an intense magnetic storm. This plasma resembled magnetosheath plasma but appeared connected with cold plasma flow deeper within the magnetosphere. More recently experimental evidence has accumulated as to the existence of regions of similar plasma flow in the antisunward direction along the ordered field lines of the high and low latitude lobes of the geomagnetic tail. Observations have been made in the ecliptic at  $18 R_E$  with the Vela satellite (Hones et al., 1972, Akasofu et al. 1973) and in the distant polar magnetosphere with the HEOS satellite (Rosenbauer et al., 1975). The region of plasma flow observed forms a relatively thin ( $<4 R$ ) "plasma mantle" or "boundary layer" between the tail and the magnetopause. The particles in this region exhibit fluxes and temperatures slightly less than those observed in the magnetosheath and bulk velocities in the range of 100 to 200 km/sec. There is also a general decrease in density, temperature, and bulk velocity as the distance of the spacecraft from the magnetopause increases.

This paper reports similar observations of low energy particles (LEPs) possessing many of these same characteristics, but also significant variations. These are seen in the geomagnetic tail at distances of  $60 R_E$  using the three Suprathermal Ion Detector Experiments (SIDEs) deployed on the lunar surface during the Apollo 12, 14, and 15 missions. The region of space in which these LEPs are found lies adjacent to the magnetopause but also across the tail as a border to the plasma sheet. Its extent away from the plasma sheet near the center of the tail cannot yet be determined.

Each of the SIDEs consists of two instruments; a Total Ion Detector (TID) capable of discriminating positive ions according to their energy/charge in a range from 10 eV/q to 3500 eV/q, and a Mass Analyzer (MA) capable of discriminating positive ions according to their mass/charge up to 750 amu/q and their energy/charge in a range from .2 to 48.6 eV/q. Post-analysis acceleration to 3500 eV insure efficient detection of the low energy positive ions by a funnel-channel electron multiplier. The SIDE's are deployed such that each instrument's look direction is approximately in the ecliptic plane. The look directions of the three SIDEs span a total azimuthal fan in the ecliptic of 56 degrees. (For a more detailed description see Hills and Freeman, 1971.)

## Observations

Using data principally but not exclusively from the Apollo 14 SIDE we have studied twelve passes of the moon through the tail in 1972 and the first three tail passes of 1973. These passes have yielded 265 separate encounters with the LEPs. These data comprise approximately 200 hours of observations; 16% of the time the moon was in the tail.

The LEPs form a separate regime in that their spectral characteristics are radically different from those of the magnetosheath or plasma sheet. A typical encounter with the LEP regime near the center of the tail is shown in Figure 1a where we have plotted 20 minute averages of the counting rate of the TID for a 24 hour period commencing on April 27 0000 GMT, 1972, 18 hours after the moon has passed into the tail. (The moon takes

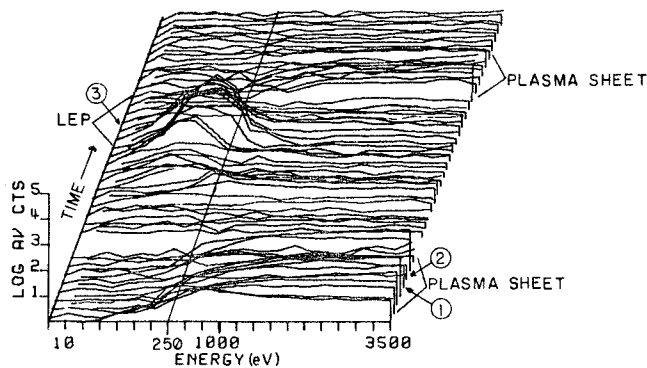


Figure 1a. Twenty minute averages of the counting rates in the 20 energy channels of the TID for the period April 27 0000 GMT to April 28 0000 GMT, 1972. The seven lowest energy channels are centered at 10, 20, 30, 50, 70, 100 and 250 eV/q respectively. The remaining channels are evenly spaced at 250 eV/q intervals up to 3500 eV/q. The numbers 1, 2, and 3 refer to the spectra in Figure 1b.

about 3 to 4 days to pass through the tail.) The times for which the plasma sheet is observed are characterized by significant counts in the energy channels from 250 eV/q to the limit of the instrument at 3500 eV/q. The low energy particles in contrast are seen only in the seven lowest energy channels covering the range from 10 to 250 eV/q. Note that the LEP and plasma sheet regions are not contiguous in this event. Differential flux spectra for the two regions are shown in figure 1b. The low energy particles (LEPs) are much colder than the plasma sheet particles ( $kT = 2-8\text{ eV}$  versus  $kT > 400\text{ eV}$ ) and also differ significantly in bulk velocity and number density. In general, the LEPs seldom exhibit temperatures above  $5 \times 10^4\text{ K}$  ( $kT \sim 40\text{ eV}$ ) or extend in energy above 500 eV. They clearly form a separate plasma regime from the plasma sheet.

From differential flux measurements we calculate a distribution function for the particles. The assumption is made that the majority of the particle energy is in the flow. This is confirmed by the lunar surface solar wind spectrometer (B. Goldstein, private communication). The bulk velocity,  $V_B$ , and temperature,  $T$ , are then calculated by taking the usual moments of the distribution function. The number density is calculated by multiplying the integral flux by the solid angle (estimated to be a cone with full angle of 50 degrees) over which the flux is considered isotropic, and dividing by the bulk velocity.

These plasma parameters and the magnetic field characteristics for part of one tail pass are illustrated in

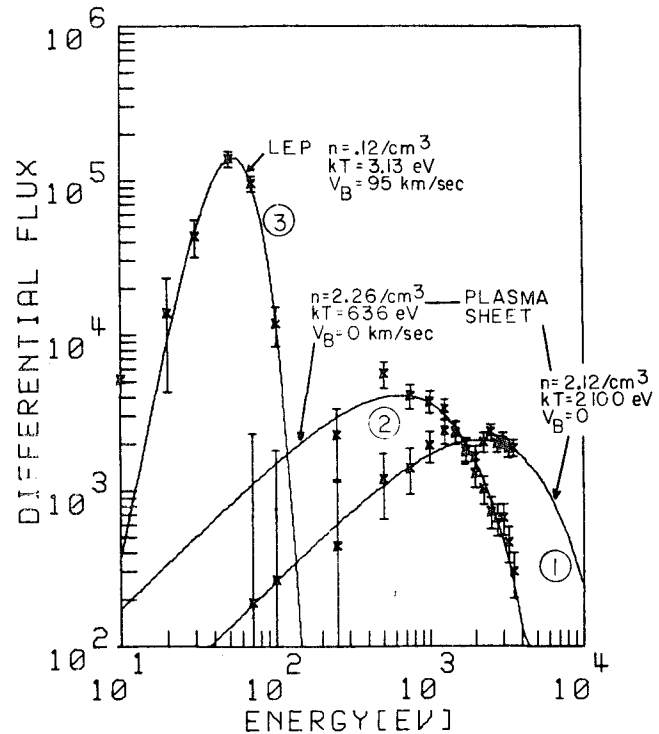


Figure 1b. Comparative differential flux spectra for the low energy particles, and plasma sheet. The differential flux is measured in ions/cm<sup>2</sup>-sec-ster-eV.

Figure 2. The figure covers a portion of the third tail pass of 1972. This pass was chosen because it provides the most hours of data for the phenomenon of the fifteen tail passes studied. Altogether 42.7 hours of observation of the low energy fluxes were recorded during this tail pass; a time equal to 60% of the total duration.

The figure shows the magnetic field and the plasma parameters for the two day period as the moon approaches the magnetosheath. Although there is variation in the plasma characteristics, the LEPs, which cover the first 32 hours, generally display an integral flux of between  $10^5$  and  $4 \times 10^7$  ions/cm<sup>2</sup> sec ster, bulk velocities of from  $\sim 90$  to 200 km/sec, temperatures in the range from  $4 \times 10^4$  to  $5 \times 10^5\text{ K}$  and number densities from 0.2 to 2/cm<sup>3</sup>. These are typical values for the LEP region. Cases have been observed where the integral flux was as high as  $10^8$  ions/cm<sup>2</sup> sec ster with corresponding number densities of  $\sim 5/\text{cm}^3$ .

The mass analyzer indicates that the ions are mainly protons but the fluxes are not sufficiently intense for us to establish the presence of alphas or other more massive ions. We may be able to report more on this after a more complete examination of the data.

The magnetic field data in Figure 2, obtained from the Ames magnetometer

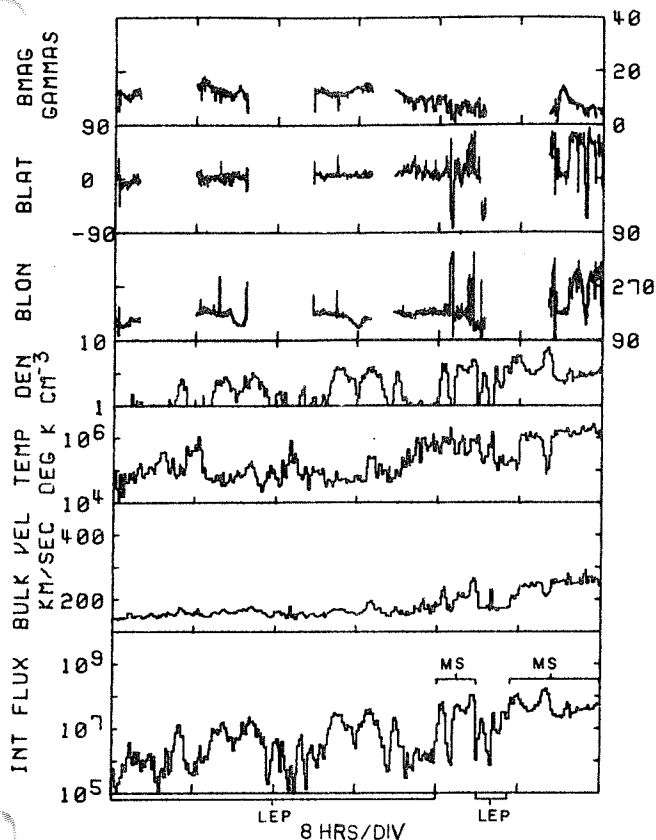


Figure 2. Magnetic field and plasma characteristics for the period March 30, 0230 GMT, to April 1, 0230 GMT, in 1972. The magnetosheath is labeled by MS and the region for the low energy particles by LEP.

aboard the Explorer 35 spacecraft orbiting the moon, display data gaps due to spacecraft circumstances. Nonetheless, the observations which are available show that the field displays lobe characteristics during the times the Moon was in the region of the LEPs. The solar equatorial latitude of the field is close to zero degrees and the solar equatorial longitude is close to 180 degrees with a field magnitude of  $\sim 14$  gammas. Furthermore, no deviations in the field are seen to correspond with variations in the intensity of the LEPs. Such behavior reflects the magnetic field character during the encounters with the region for the five tail passages for which magnetic data have been obtained.

One sees that the low energy fluxes shown in Figure 2 are observed over a time span of approximately 39 hours. During this period the Moon traveled distances of  $\sim 16 R_e$  in the solar-magnetospheric  $Y_{sm}$  coordinate direction and  $\sim 10 R_e$  in the  $Z_{sm}$  direction ( $Y_{sm} = 3R_e$  to  $Y_{sm} \sim 19 R_e$  and  $Z_{sm} \sim -7 R_e$  to  $Z_{sm} \sim -17 R_e$ ). This wide extent over which the ions are observed is seen in many of the tail passages. It indicates that the size of the region in which the LEPs are found is considerably larger

at the lunar distance than at the smaller  $X_{sm}$  distances of the Vela and HEOS satellites. In general we find that the Moon encounters the particles sporadically for a full day after it enters the tail and a full day before it exits the tail. This corresponds to a region extending a  $Y_{sm}$  distance of at least  $12 R_e$  into the tail from both the dawn and dusk sides of the magnetopause. The region, however, excludes the plasma sheet since the low energy particles are seldom observed simultaneously with the plasma sheet particles and the two regions need not be contiguous. The region of LEPs appears to extend away from the plane of the plasma sheet to the limit of observation at about  $16 R_e$ .

Figure 3 shows the portions of the lunar orbit, for the fifteen tail passages studied, over which the LEPs were encountered. It is apparent that the region must be significantly larger at  $60 R_e$  than at lesser geocentric distances.

It is impossible at present to know the exact extent of the region due to the spatial limits imposed by the orbit of the Moon. This limit arises from the fact that diurnal excursions in the  $Z_{sm}$  direction rapidly decrease for decreasing  $Y_{sm}$ . It is possible that the scarcity of events deep in the tail arises from the inability of the instrument to sample significantly the lobes exterior to the plasma sheet in this region.

Determination of the spatial extent is further complicated by the fact that the amount of time over which the particles are observed varies between tail passages from as little as 2.1 hours to as much as 42.7 hours. Such a wide variation could arise from several sources. First,

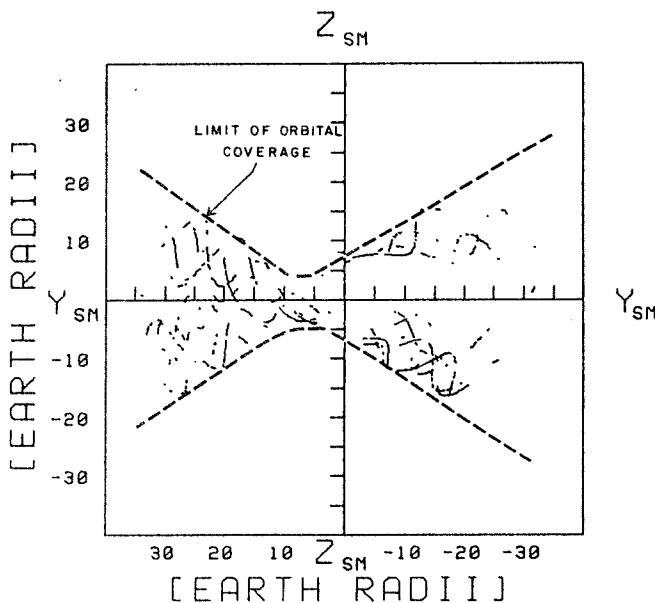


Figure 3. Sections of the lunar orbits in SM coordinates for which the low energy particles were observed.

since the events are seldom seen in the plasma sheet an increase in the thickness of the plasma sheet would tend to decrease the amount of time the moon was in regions where these low energy particles might be seen. Alternatively, such a wide variation might arise from a real change in the spatial extent of the region in which these particles are found. A third possibility is that the seasonal variation in the location of the moon's orbit relative to the plane of the plasma sheet increases or decreases the frequency of encounters with the region. Lastly, the mechanism which injects the particles onto these field lines may vary with time so that for some tail passages the conditions are not favorable for injection. Further studies are underway to determine which of these is dominant.

#### Discussion and Summary

The new plasma regime reported here, LEP, is qualitatively similar to the "boundary layer" reported by Hones et al. and Akasofu et al. and the plasma flow regime found inside the dayside magnetopause by Freeman et al. during an intense magnetic storm. It is also similar to the "plasma mantle" at high latitudes reported by Rosenbauer et al. We propose as the simplest hypothesis that all four regions are simply connected along the inner surface of the magnetopause and are in fact the same phenomenon. A consequence is that antisunward flowing plasma would generally be found everywhere inside and adjacent to the magnetopause. We believe that a consistent name should be established for this plasma, however, "boundary layer" and "plasma mantle" do not appear to be sufficiently descriptive for the region as it appears in the distant tail.

The relationship between the LEP and the plasma sheet is not clear. It has been suggested that the LEPs may be a source for the plasma sheet (R. A. Wolf, private communication).

In summary, the three Rice Suprathermal Ion Detector Experiments stationed on the lunar surface have detected a region of low energy plasma flowing along the ordered field lines of the lobes of the geomagnetic tail. This particle region exhibits the following characteristics:

1. The region of flow is encountered within the geomagnetic tail but exterior to the plasma sheet. The magnetic field characteristics in the region are indicative of the high and low latitude lobes. No consistent deviations in the field have been found to correspond with the encounters with the region.
2. The encounters with the region occur over a wide spatial extent with continual observations of the particles over distances as great as  $\sim 16 R_E$  in the  $Y_{SM}$

direction and  $10 R_E$  in the  $Z_{SM}$  direction. The majority of the encounters, however, are observed within a region extending  $12 R_E$  into the tail from the magnetopause.

3. The particles (mostly protons) display a narrow differential flux spectrum peaked normally between 50 and 250 eV. The spectrum is usually stable over the duration of the events. Some cases of spectral variation in the events are seen to occur during transitions into or out of the plasma sheet or magnetosheath. Such variations appear as a broadening of the spectrum and a shifting of the peak towards higher energy.

4. The plasma has been ascertained to have the following parameters; integral flux between  $10^5$  and  $10^8$  ions/cm<sup>2</sup> sec ster, bulk velocities between 90 and 250 km/sec, temperatures in the range from  $4 \times 10^4$  to  $5 \times 10^5$ °K, and number densities of the order .1 to 5/cm<sup>3</sup>.

5. The region appears to be the qualitatively similar to be the "boundary layer" and "plasma mantle" observed at lesser geocentric distances, and the magnetopause-adjacent flow on the dayside. The region is, however, significantly larger at lunar distances and the plasma characteristics appear to be more variable.

**Acknowledgements.** This research has been supported by NASA contract NAS9-5911 and the Atmospheric Science Section, National Science Foundation.

#### References

- Akasofu, S. -I., E. W. Hones, Jr., S. J. Bame, J. R. Asbridge and T. T. Y. Lui, Magnetotail and boundary layer plasma at a geocentric distance of approximately  $18 R_E$ ; Vela 5 and 6 observations, *J. Geophys. Res.*, **78**, 31, 7257, 1973.
- Freeman, J. W., Jr., C. S. Warren, and J. J. Maguire, Plasma flow directions at the magnetopause on January 10 and 14, 1969. *J. Geophys. Res.*, **73**, 17, 5719, 1968.
- Hills, H. K. and J. W. Freeman, Jr., Suprathermal Ion Detector Experiment (Lunar Ionosphere Detector), *Apollo 14 Preliminary Science Report*, NASA SP272, 1971.
- Hones, E. W., Jr., J. R. Asbridge, S. J. Bame, M. D. Montgomery, S. Singer, and S. I. Akasofu, Measurement of magnetotail plasma flow made with Vela 4B, *J. Geophys. Res.*, **77**, 28, 5503, 1972a.
- Rosenbauer, H., H. Grünwaldt, M. D. Montgomery, G. Paschmen, and N. Sckopke, HEOS 2 plasma observations in the distant polar magnetosphere: The Plasma Mantle, in press, *J. Geophys. Res.*, 1975.

(Received January 24, 1975;  
revised March 17, 1975;  
accepted March 27, 1975.)





# The Interaction Between an Impact-Produced Neutral Gas Cloud and the Solar Wind at the Lunar Surface

R. A. LINDEMAN,<sup>1</sup> R. R. VONDRAK, AND J. W. FREEMAN

*Space Physics and Astronomy Department, Rice University, Houston, Texas 77001*

C. W. SNYDER

*Jet Propulsion Laboratory, California Institute of Technology, Pasadena, California 91103*

On April 15, 1970, the Apollo 13 S-IVB stage impacted the nighttime lunar surface approximately 140 km west of the Apollo 12 Alsep site and 410 km west of the dawn terminator. Beginning 20 s after impact the Suprathermal Ion Detector Experiment and the Solar Wind Spectrometer observed a large flux of positive ions (maximum flux  $\sim 3 \times 10^8$  ions/cm<sup>2</sup> s sr) and electrons. Two separate streams of ions were observed: a horizontal flux that appeared to be deflected solar wind ions and a smaller vertical flux of predominantly heavy ions ( $>10$  amu), which probably were material vaporized from the S-IVB stage. An examination of the data shows that collisions between neutral molecules and hot electrons (50 eV) were probably an important ionization mechanism in the impact-produced neutral gas cloud. These electrons, which were detected by the Solar Wind Spectrometer, are thought to have been energized in a shock front or some form of intense interaction region between the cloud and the solar wind. Thus strong ionization and acceleration are seen under conditions approaching a collisionless state.

The interaction between a neutral gas and the solar wind has been the subject of much investigation in recent years. The ionization mechanisms in type I comets [Beard, 1966; Biermann *et al.*, 1967], the upper atmospheres of Venus and Mars [Cloutier *et al.*, 1969; Michel, 1971], and possibly even the formation of the solar system [Alfvén, 1954] are all dependent on this type of interaction. We present here data pertaining to the observation of such an interaction. The neutral gas cloud resulted from the impact of the spent Apollo 13 S-IVB stage rocket on the lunar surface. The data are from the nearby particle detectors on the lunar surface at the Apollo 12 landing site.

At 01h 09m 40s on April 15, 1970, the upper stage (S-IVB) of the Apollo 13 Saturn launch vehicle impacted the moon in the Ocean of Storms approximately 138 km due west and 9 km north of the Apollo 12 Lunar Surface Experiments Package (Alsep) site. The experiments observed clouds or streams of ions and electrons that we interpret as resulting from the interaction between the impact-produced neutral gas cloud and the solar wind. It appears that strong ionization and acceleration mechanisms were operating under conditions that approached a collisionless state. Beginning 20 s after impact the Suprathermal Ion Detector Experiment (SIDE) and the Solar Wind Spectrometer (SWS) observed fluxes of suprathermal ions that reached large values several times in the next 13 min. The impact site was 410 km west of the dawn terminator and 290 km west of an 'idealized' solar wind terminator (assuming a 5° aberration angle) and thus 'downwind' of Alsep. Under normal idealized conditions the solar wind would have been streaming 50 km overhead. This geometry is shown in detail in Figure 1.

The relevant impact parameters are shown in Table 1.

Both the SIDE and the SWS have been described previously [Freeman *et al.*, 1970b, 1971b; Snyder *et al.*, 1970,

1971], but a comparison of the two instruments is helpful for an understanding of the data. This is given in Table 2.

The SWS contains an array of seven Faraday cup sensors and can record charged particles arriving from all directions above the lunar surface with varying sensitivities. The cups are arranged to look radially outward, cup 7 sampling the vertical flux and the remaining cups detecting particles moving more nearly horizontally.

The SIDE contains two separate detectors, the Total Ion Detector (TID) and the Mass Analyzer (MA). Each accepts positive ions in a narrow entrance cone pointed 15° west of vertical in the plane of the ecliptic. Any ion flux observed by either the TID or the MA would enter the vertically oriented cup (cup 7) in the SWS.

The MA requires 12 s for a complete mass spectrum at each energy. Since there are six energy steps, the MA energy-mass cycle is 72 s.

The cycle times for the TID and SWS are similar, but even these detectors are unable to provide detailed time variations of transient events shorter than about half a minute.

One picoampere in a single cup of the SWS corresponds to a normal parallel beam flux of  $2.5 \times 10^6$  ions/cm<sup>2</sup> s or an isotropic flux over the field of view of the cup of  $4.1 \times 10^6$  ions/cm<sup>2</sup> s sr.

## OBSERVATIONS

Some SIDE data from this event have been reported previously [Freeman and Hills, 1970a; Freeman *et al.*, 1971a]. The SWS data have been discussed by C. Snyder, D. Clay, and M. Neugebauer (unpublished data, 1971). The results of these reports and additional analysis can be summarized as follows:

1. Large fluxes of ions were seen from both the horizontal and the vertical directions, the largest fluxes arriving from the horizontal direction (see Figure 2).
2. The fluxes arriving near the horizontal came initially from the east but moved to come from a more northerly direc-

<sup>1</sup> Now at Naval Weapons Laboratory, Dahlgren, Virginia 20240.

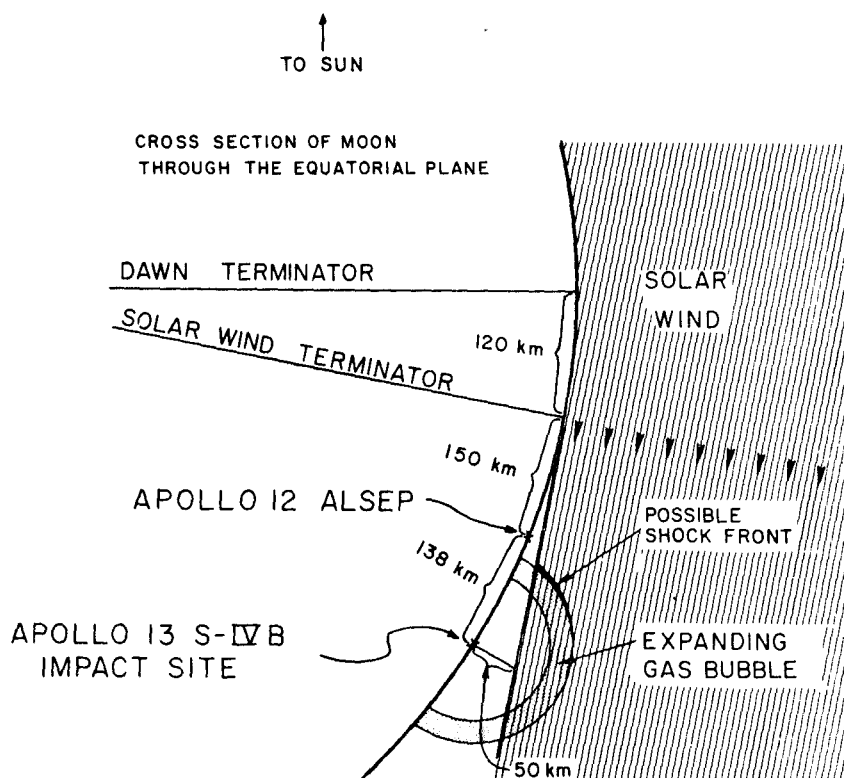


Fig. 1. An equatorial cross-sectional view of the moon (not to scale) showing the S-IVB impact point with respect to the Alsep site and the dawn and solar wind terminators (after *Freeman et al.* [1971a]). The solar wind is assumed to come from  $5^\circ$  west of the sun and to have an infinitely sharp shadow edge. We believe that the data indicate that after impact the solar wind was deviated from this configuration by interaction with the expanding gas cloud.

tion as the event proceeded. Later in the event they once again came from the east (see Figure 3).

3. The horizontal and vertical fluxes show the same onset time and a fair time correlation throughout the first  $\frac{2}{3}$  of the event, but the vertical flux disappears entirely for the final  $\frac{1}{3}$ .

4. Initially, the energy of the vertically moving positive ions was in the 35- to 55-eV/q energy range. Subsequently, it shifted to high energies. Energies characteristic of the solar wind were observed throughout the event in the horizontal fluxes (see Figure 4).

5. Massive ions were seen in the vertical flux during the onset of the event. In fact, as is shown in Figure 5, this flux is thought to have consisted to a large extent of ions of mass greater than 10 amu/q. Owing to the upward shift in particle energy the mass of the vertical ions cannot be determined later in the event. Owing to the absence of a horizontally viewing mass analyzer, no mass data are available on the horizontally moving ions.

6. The maximum vertical positive ion flux as measured by the SIDE was about  $10^8$  ions/cm<sup>2</sup> s sr. The maximum horizontal flux was a factor of 2 higher.

7. Isotropic electrons were seen throughout the event. The composite electron spectrum peaked in the channel that included energies between 20 and 50 eV (see Figure 6). The time history of the electrons generally followed that of the ions for the first  $\frac{2}{3}$  of the event. Like the vertical ions the electrons disappeared before the horizontal ions.

In the foregoing paragraphs the concepts of horizontal and vertical as they relate to the fluxes are somewhat idealized. We refer to those fluxes as horizontal that were seen by the SWS peripheral cups only. These particles had a substantial component of horizontal velocity but need not have been moving in a purely horizontal direction. Since cup 7 rarely saw any flux at 400 eV, the flow direction of the horizontal flux must have been within  $45^\circ$  of the surface.

## DISCUSSION

The differences in character between the horizontal and the vertical fluxes appear to us to be an important feature of the data.

The horizontal fluxes observed by the peripheral cups of the SWS had a peak energy similar to the solar wind energy during this event. Moreover the first direction of approach and the last direction of approach are both from the solar wind direction,  $180^\circ$  from the direction of impact. Even the peak flux in the horizontal direction (at least  $1.3 \times 10^8$  ions/cm<sup>2</sup> s) is comparable to the solar wind flux ( $10^8$  ions/cm<sup>2</sup> s) at that time (Solar Geophysical Data, 1970). From this evidence we conclude that the horizontal fluxes were solar wind ions deflected by the expanding gas cloud resulting from the S-IVB impact.

The vertical fluxes observed by the TID and cup 7 of the SWS had a low initial energy and a heavy mass component. For this reason we identify at least the early vertical fluxes as

TABLE 1. Apollo 13 S-IVB Impact Parameters

Mass*	$1.34 \times 10^4$ kg
Impact velocity	2.58 km/s
Kinetic energy	$4.46 \times 10^{17}$ ergs
Angle of impact from vertical	$13.2^\circ$
Heading angle north to west	$100.6^\circ$
S-IVB impact location	$2.75^\circ\text{S}, 27.86^\circ\text{W}$
Apollo 12 Alsep location	$3.04^\circ\text{S}, 23.42^\circ\text{W}$

Data from George C. Marshall Flight Center (unpublished report, 1970).

\* Stage dry weight: all residual propellants assumed dissipated.

TABLE 2. Comparison of SWS and SIDE

	SWS	SIDE	
	Seven Faraday Cups	TID	MA
Field of view, sr	$2\pi$	0.011	0.005
Sensitivity, particles/cm <sup>2</sup> s sr	$4.1 \times 10^6$	$1.2 \times 10^4$	$7 \times 10^4$
Detects	Positive ions and electrons	Positive ions	Positive ions
Energy range, eV			
Positive ions	5700-15	3500-10	48.6-0.2
Electrons	1376-7		
Mass range, amu	No mass analysis	No mass analysis	130-10
Cycle time, s	28	24	12/Energy step 72/Cycle

ions created in the neutral gas cloud resulting from the S-IVB impact. Whether or not all the later vertical fluxes that appear with higher energies are ionized, impact gas cannot be determined.

We now have two separate streams of ions, a horizontal flux that appears to be deflected solar wind ions and a vertical flux that is composed of massive ions (>10 amu). The horizontal flux is larger than the vertical.

There are two possible sources for the massive ions. They are either ions formed at impact or ions formed by photoionization, etc., in a neutral gas cloud released by the impact.

*Jeans and Rollins* [1970] in laboratory experiments have shown that ions can be produced in a hypervelocity impact. Although no quantitative data on the number of ions produced in such an impact are available, it seems unlikely that

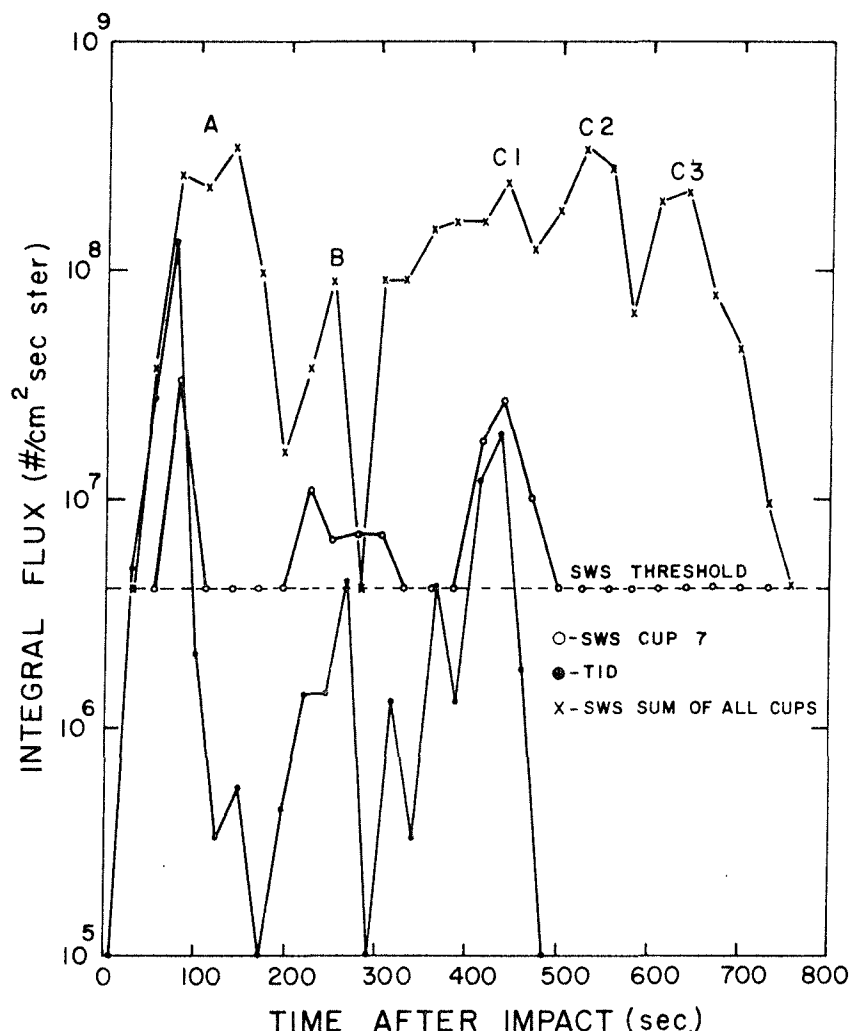


Fig. 2. Integral positive ion fluxes seen during the S-IVB impact event. The TID and cup 7 of the SWS are sensitive to ions coming from the vertical direction, whereas the sum of all cups of the SWS indicates predominantly horizontal fluxes. For purposes of comparison, the current sum of all cups has been treated as if it was coming from a single cup and due to a flux isotropic over the cup. The labeling of the peaks A, B, etc., is for illustration in Figure 3.

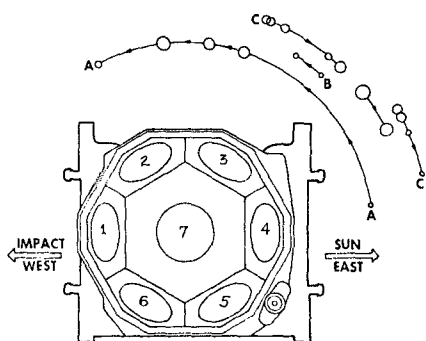


Fig. 3. Top view of the SWS showing the orientation of the Faraday cups and the azimuthal direction of arrival of the horizontal flux during various stages of the impact event (after C. Snyder, D. Clay, and M. Neugebauer, unpublished data, 1971). Each circle represents one ion measurement sequence (one point in Figure 2). The size and location of each circle suggest the amount of current observed and the direction from which the flux arrived.

enough could be formed to account for the observed fluxes. Moreover any ion formed at the impact would have to travel 140 km upstream in the solar wind. Ions of 70 eV are not energetic enough to accomplish this. Finally, the fact that the first peak occurs 75 s after impact rules out the impact as the direct source of the ions. A 70-amu ion with an energy of 70 eV has a velocity of about 14 km/s. Thus in 75 s the ion should have traveled over 1000 km.

We conclude that an expanding neutral gas cloud was partially ionized and the individual ions subsequently accelerated.

The maximum expansion velocity of this gas cloud can be estimated from the transit times required to transverse the 140 km to the Alsep site. Since the initial TID peak reached 10% of maximum 45 s after impact, the transit velocity was as high as 3 km/s. Thus at the time that the TID was measuring the peak flux the cloud front had a radius of 225 km. At the time

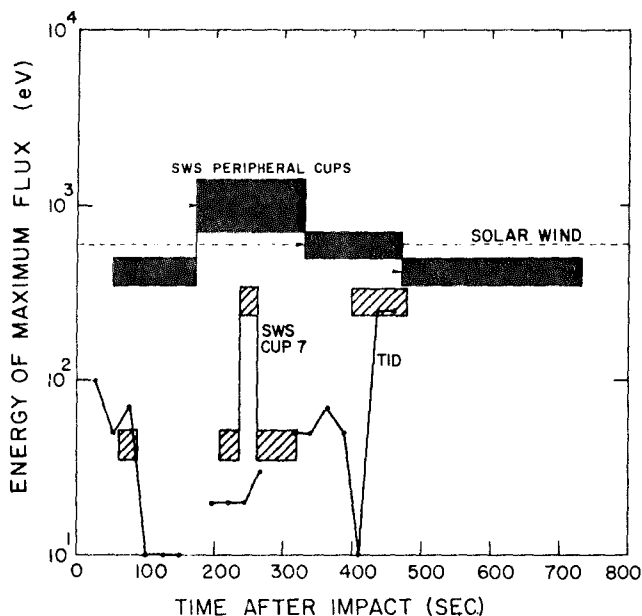


Fig. 4. Energy at which maximum ion flux was observed during the impact event. Solid bars indicate the energies of the maximum flux as observed by the horizontally viewing cups of the SWS. The TID and cup 7 of the SWS both detect ions moving in a nearly vertical direction. The solar wind energy at the time of the event was 600 eV (Solar Geophysical Data, 1970) and is given by the dotted line.

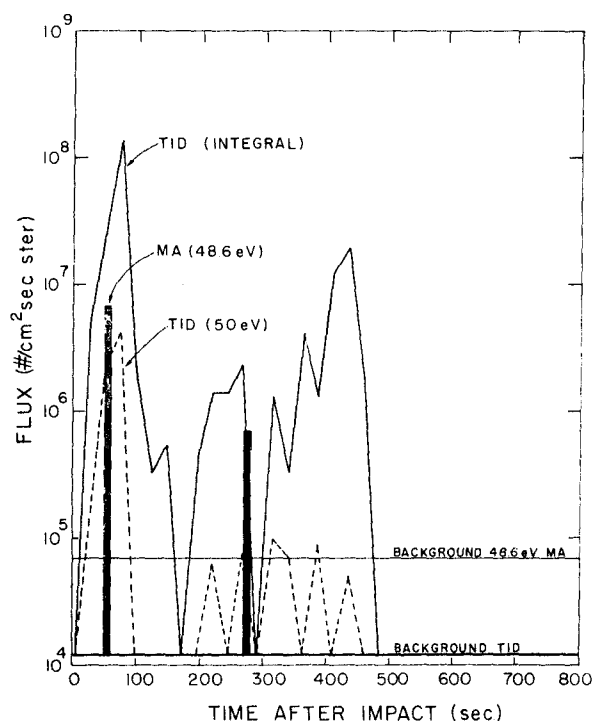


Fig. 5. Positive ion fluxes observed by the SIDE during the impact event. The solid line is the integral flux observed by the TID for energies between 10 and 3500 eV. The dashed line indicates the flux seen by the TID at 50 eV, and the solid bars show the flux seen by the MA at 48.6 eV. The TID has no mass discrimination, while the MA is sensitive only to ions with mass heavier than 10 amu.

that the SWS was measuring the maximum flux in peak A the cloud front had a radius of 420 km.

The cloud will not expand spherically owing to the flattening effect of lunar gravity. The exact shape of the pressure pulse resulting from an impulsive release of gas from the lunar surface can be calculated from kinetic theory (Appendix 1). These calculations show that the pulse duration and arrival time at any point on the surface depend upon the ratio  $\mu/T$ , where  $\mu$  is the gas molecular weight and  $T$  is the initial temperature. As is seen in Figure 7, the arrival time of the gas over the Alsep site, 75 s after impact, corresponds to a gas cloud with  $\mu/T$  of  $7 \times 10^{-3}$  amu/ $^{\circ}\text{K}$  ( $10^4$   $^{\circ}\text{K}$  for 70-amu particles). This figure plots the column density above a point 140

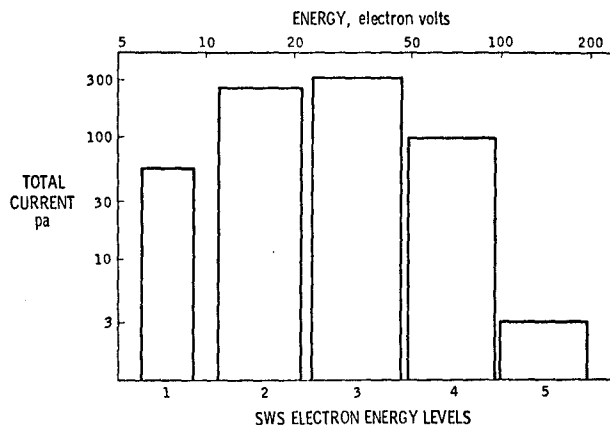


Fig. 6. Energy distribution of all electron currents in all seven cups of the SWS summed over the entire event (after C. Snyder, D. Clay, and M. Neugebauer, unpublished data, 1971).

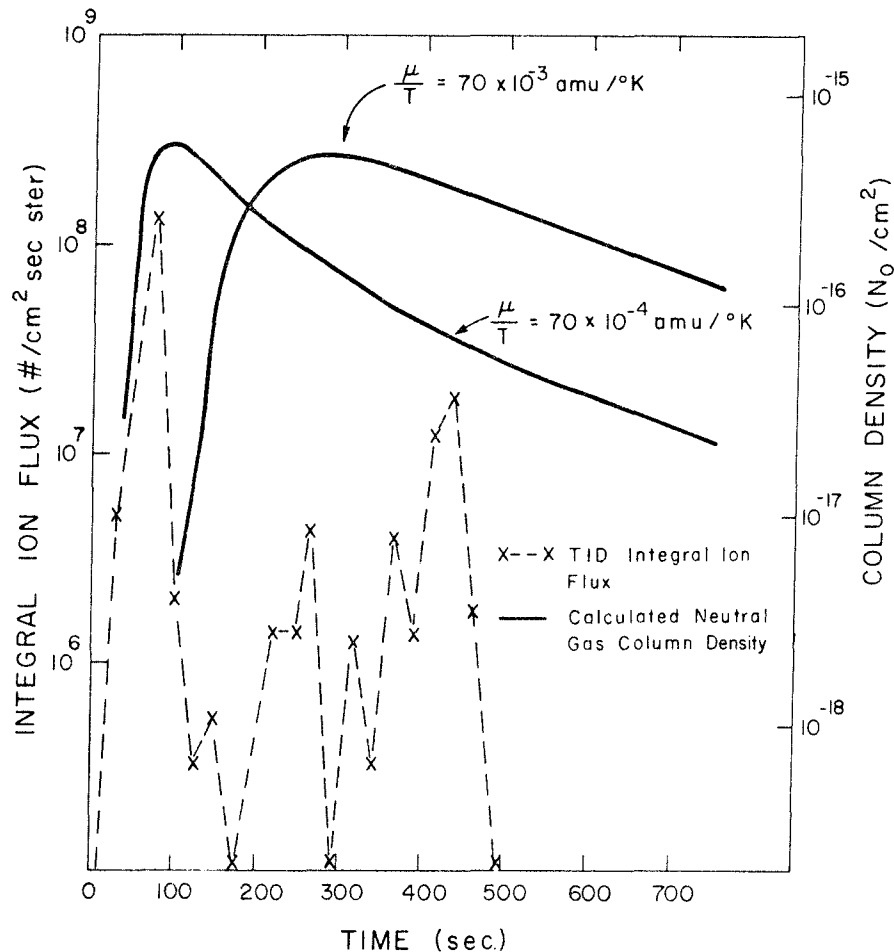


Fig. 7. Neutral gas column density at the Apollo 12 site resulting from a gas release of  $N_0$  molecules at the location and time of the S-IVB impact. The TID integral flux is also shown. The arrival time of the peak TID flux is best fit by a ratio of gas mass  $\mu$  to gas temperature  $T$  of  $70 \times 10^{-4}$  amu/°K. For comparison, the column density resulting from a gas cloud with  $\mu/T$  of  $70 \times 10^{-3}$  is also shown.

km from the source. To show the variation of column density with the parameter  $\mu/T$ , the curve for a  $\mu/T$  ratio of  $7 \times 10^{-2}$  amu/°K is also plotted.

If a steady state condition (the number of ions created in a given region per second equals the flux out of the region) is assumed, then the observed flux is proportional to the column density above the observing site:  $F = P \cdot \rho$ , where  $P$  is the total ion production rate,  $\rho$  is the column density above the observation point, and  $F$  is the observed flux.

With regard to the total vertical flux, cup 7 measured 8 pA in the 35- to 52-eV energy channel during peak A. For a normally incident parallel beam this corresponds to a flux of  $2 \times 10^7$  ions/cm² s. Just prior to this measurement the SIDE looking 15° off the vertical measured a unidirectional flux of about  $10^8$  ions/cm² sr. Assuming this flux to be uniform over 0.2 sr, including the vertical, gives a vertical flux of  $2 \times 10^7$  ions/cm² s. This is probably a lower limit since the 'vertical' flux is probably spread over a wider solid angle. Lacking further knowledge of the angular distribution, we will use a value of  $2 \times 10^7$  ions/cm² s for the vertical flux.

From Figure 7 the peak column density  $\rho$  was  $6 \times 10^{-16} N_0$ , where  $N_0$  is the total number of molecules emitted from the impact.

The ionization rates (calculated in Appendix 2) due to solar UV and charge exchange in this cloud are  $10^{-6}$  ion/s atom and  $5 \times 10^{-8}$  ion/s atom, respectively. The solar wind

parameters used in this calculation were: the proton number density equals 3/cm³, and the proton bulk velocity equals 330 km/s (Solar Geophysical Data, 1970).

A third source of ionization is the hot electrons observed by the SWS. With an assumed average thermal energy of 50 eV ( $T \sim 5 \times 10^5$  °K) this electron flux will also ionize neutrals. The peak electron current was 6 pA in each cup. This corresponds to an isotropic flux of  $2.5 \times 10^7$  el/cm² sr or  $1.6 \times 10^8$  el/cm² s for a  $2\pi$  distribution. Several electron gyroradii (<1 km) above the surface the minimum flux is  $3.2 \times 10^8$  el/cm² s. Since neither 400-eV ions nor 50-eV electrons are very efficient in producing secondary electrons from the lunar material and the electrons in the cloud are more mobile than the ions, it seems likely that the lunar surface will assume a negative potential relative to the plasma. Recent results from the SIDE indicate surface potentials as high as -100 V exist near the terminators [Lindeman et al., 1973]. The fact that the time history of the electrons followed the ion time history so closely lends support to a negative surface potential. Thus the electron flux observed at the lunar surface may have been significantly less than the actual electron flux in the cloud. With  $3.2 \times 10^8$  el/cm² s as a lower limit to the electron flux and  $2 \times 10^{-16}$  cm² as an average cross section for ionization by 50-eV electrons the production rate is  $6 \times 10^{-8}$  ion/s atom. Since the ratio between the actual and the observed flux may be as high as a factor of 10, it is possible that the electron

ionization rate may be comparable to or even greater than the photoionization rate.

We will now obtain a working lower limit for  $N_0$ . We assume first that the total production rate was dominated by photoionization. However, only part of the cloud was exposed to solar UV. The fraction of the column density over the Alsep site exposed to solar UV varies in time (Appendix 1). At the time the peak flux was observed, approximately 80% of the molecules were exposed to solar UV. Since the solar wind was presumably deviated by the interaction, the whole cloud was exposed to solar wind protons and fast electrons. Under the assumption that photoionization was active over the total volume over the Alsep site the total number of molecules released at impact can be estimated from the relation

$$N_0 = 1.6 \times 10^{15} F/P$$

$$N_0 = (1.6 \times 10^{15})(2 \times 10^7)/10^{-8}$$

$$N_0 = 3.2 \times 10^{28} \text{ molecules}$$

If solar wind charge-exchange and electron ionization are active, then at least an additional  $11 \times 10^{-8}$  ions/s atom are created, resulting in a 10% decrease in the required number of molecules emitted. Thus we conclude that if the above ionization mechanisms produced the observed ions, approximately  $3 \times 10^{28}$  molecules of neutral gas must have been released in the impact.

#### GAS CLOUD COMPOSITION

Mirtov [1969] and Johnson [1971] have proposed that meteoritic impacts may provide a significant contribution to the lunar atmosphere. McKay *et al.* [1970] have proposed a base surge origin of lunar breccias in which a hot expanding gas cloud produced by a large meteoritic impact plays an important role. Heymann and Yaniv [1971] have also proposed a similar model for one possible origin of the lunar breccias.

The S-IVB impact was not large enough to produce breccias; however, it did produce a large neutral gas cloud. Since this was an in situ measurement on the lunar surface, the mass components of the cloud are of great interest.

The MA in the operating mode then being used measured the mass per unit charge in 10 mass channels, which covered the range 10–135 amu/q. Each mass spectrum requires 12 s for completion. This spectrum is taken sequentially at six energy steps, 48.6, 16.2, 5.4, 1.8, 0.6, and 0.2 eV/q, having a narrow energy passband ( $\Delta E = 4$  eV for 48.6 eV/q step).

A large stable flux of one mass will give significant counts in two or three adjoining mass channels. By comparing the distribution data the dominant mass can be determined. This method is rather insensitive at low fluxes ( $<10^6$  ions/cm<sup>2</sup> s sr) and can prove erroneous when fluxes of two comparable

masses are observed simultaneously. The geometric factor at 48.6 eV for an element that peaks in a given mass channel varies from  $2 \times 10^{-5}$  to  $8 \times 10^{-6}$  cm<sup>2</sup> sr, depending on whether that mass is centered on the channel or near the edge of its mass window.

Only four mass spectra were obtained during this event, two at 48.6 eV/q and two at 16.2 eV/q. Owing to the rapid temporal variations as seen by the TID it is very doubtful that a constant incoming flux was maintained over 12 s, the time required for a spectrum. Recall also that the MA was not necessarily measuring the peak energy of the flux distribution. With these limitations in mind, Table 3 gives the raw data from all four mass spectra along with masses that peak in each channel.

Figure 5 shows that most of the flux at 50 eV is due to heavy masses. Table 3 shows that in the initial peak these heavy masses were predominantly between 73 and 96 amu.

The S-IVB is constructed basically of aluminum alloys (63% Al, 17% Cu, 5% Ag, 5% Fe, and 10% other). If an average molecular mass of 27 is assumed, there are  $3 \times 10^{28}$  atoms in this stage. Thus the S-IVB contains enough atoms to explain this event, but then the predominant mass peak should have been 27. The heat of vaporization for aluminum is 67.9 kcal/q atom. To vaporize the total mass of the S-IVB requires approximately  $4 \times 10^{18}$  ergs or 2 orders of magnitude more energy than that released by the impact. As a result, the metal phase of the S-IVB could only have been partially vaporized and probably contributed little to the composition of the gas cloud. This conclusion is in agreement with the work of Rehfuess [1972]. His calculations for spherical meteorites on a basalt target show that little vaporization of either the projectile or the target occurs for impact speeds of less than 12 km/s. The S-IVB impact speed was 2.58 km/s.

In addition to the metals composing the S-IVB, there were approximately 1100 kg of plastics in the form of plastic liners, tubing, etc. (T. Page, private communication, 1972). In the heat of impact these may have been vaporized. If an average mass of 80 amu is assumed for the vaporization products, it will provide  $8 \times 10^{27}$  molecules.

The remaining fuel on the S-IVB was vented before impact, so that little or no fuel remained in either the primary or the auxiliary systems.

From Rehfuess's [1972] calculations, it is not expected that the lunar regolith was vaporized. However, the regolith material contains a large quantity of trapped gaseous molecules. These molecules are either trapped in inclusions or dissolved in the solid phase within a few angstroms of the surface of the fines. The crushing and heating of the regolith material by the impact could release a large number of these molecules.

TABLE 3. Mass Analyzer Data (Counts per SIDE Frame of 1.2 s)

Time After Impact, s	Energy, eV/q	Mass Channel*									
		0, 10–14 amu	1, 15–17 amu	2, 18–22 amu	3, 23–26 amu	4, 27–31 amu	5, 32–40 amu	6, 41–55 amu	7, 56–72 amu	8, 73–96 amu	9, 97–135 amu
51	48.6	4	0	11	1	7	8	0	30	111	26
183	16.2	3	3	5	0	0	8	0	0	0	0
255	16.2	0	0	0	1	5	0	0	0	0	0
267	48.6	0	0	0	6	3	9	1	0	0	0

MA background equals 0.1 c/s.

\* Ranges of numbers denote masses peaking in each channel.

TABLE 4. Concentrations of Gases in Crater Ejecta

Molecule	Atomic Mass, amu	Concentration, cm <sup>3</sup> STP/g	Total Number of Molecules in Crater	Ionization Cross Sections by 50-eV Electrons, cm <sup>2</sup>
H	1	$7.2 \times 10^{-1}$	$8 \times 10^{28}$	$8 \times 10^{-17}$
He	4	$9.0 \times 10^{-2}$	$1 \times 10^{28}$	$2.5 \times 10^{-17}$
CH <sub>4</sub>	16	$1.0 \times 10^{-2}$	$1 \times 10^{27}$	$3.5 \times 10^{-16}$
Ne	20	$1.5 \times 10^{-3}$	$1 \times 10^{26}$	$3.5 \times 10^{-17}$
Ne	22	$1.2 \times 10^{-4}$	$1 \times 10^{25}$	$3.5 \times 10^{-17}$
N <sub>2</sub>	28	$1.0 \times 10^{-2}$	$1 \times 10^{27}$	$2.0 \times 10^{-16}$
Ar	36	$2.7 \times 10^{-4}$	$3 \times 10^{25}$	$3.0 \times 10^{-16}$
Ar	40	$1.6 \times 10^{-4}$	$2 \times 10^{25}$	$3.0 \times 10^{-16}$
Kr	84	$1.7 \times 10^{-7}$	$2 \times 10^{22}$	$4.5 \times 10^{-16}$
Xe	132	$2.2 \times 10^{-8}$	$2 \times 10^{21}$	$6.0 \times 10^{-16}$

Table 4 shows the gases and their concentrations as given by experimenters on Apollo 12 fines and breccias. The noble gas data are the averages for bulk samples as given by *Hintenberger et al.* [1971]. The H value is based on a H/He ratio of 8 [*Hintenberger et al.*, 1970, 1971; *Oró et al.*, 1971]. The values for N<sub>2</sub> and CH<sub>4</sub> are taken from *Funkhouser* [1971].

*Whitaker* [1972] has recently identified a shallow crater 40 m in diameter and approximately 5 m in depth as the Apollo 13 S-IVB impact crater. If a regolith bulk density of 2 g/cm<sup>3</sup> is assumed, approximately  $4 \times 10^9$  g of regolith material was ejected from the crater. With this value the concentrations of gaseous molecules have been converted to the total number of molecules in the material ejected from the crater (see Table 4).

It is not expected that all of these trapped gases will be released. The energy of impact was not sufficient to cause significant melting; thus the molecules dissolved in the solid phase will probably not be liberated. With the assumption of an average heat capacity of 0.1 J/g °K for the lunar material and the conversion of all of the impact energy into thermal energy of the crater regolith material, then the temperature of this material will be raised by 100°K to a final temperature of 200°K. The gas release efficiency for an impulsive heating by 100°K is not accurately known, but it should not be very large. *Heymann et al.* [1971] estimate the percentage of gas molecules trapped in inclusions as being 12–60% for noble gases. If it is assumed that all of the trapped gases except H are released, then a cloud of  $1.2 \times 10^{28}$  molecules was emitted.

There is evidence that H may be chemically bound [*Funkhouser*, 1971] and thus would be much harder to liberate. If the cloud were predominantly H, then a resonant charge exchange with 400-eV protons ( $\sigma \sim 2 \times 10^{-15}$  cm<sup>2</sup>) would dominate and the bulk of the flux observed by the TID should have been H<sup>+</sup> and not heavy ions. The results in Figure 5 show that the bulk of the ions in the vertical flux are in fact heavy ions with masses above 10 amu.

The only other possibility is for the lighter ions to be accelerated to the peak energy as is observed by the TID (70 eV) and the heavier ions to be centered at a lower energy (50 eV). For an acceleration mechanism involving either the interplanetary electric field ( $-\mathbf{V} \times \mathbf{B}$ ) or a surface electric field, this possibility is very unlikely. Thus H does not seem to be a major component of the vertical flux from the cloud.

If the plastics are included, one would expect a gas cloud containing approximately  $2 \times 10^{28}$  molecules to be emitted.

The principal elements added to the atmosphere were C, H, Cl, F, O, and N from the plastics and He, CH<sub>4</sub>, and N<sub>2</sub> from the fines. Based on the observed masses, the majority of the plastics appear to have broken down into molecules of ap-

proximately 80 amu. Some of these molecules will immediately escape from the moon, since the maximum horizontal expansion velocity of the cloud (3 km/s) exceeds the escape velocity (2.4 km/s). Those that do hit the lunar surface will probably be re-emitted at the local surface temperature. Since the dissociation time is about 10<sup>6</sup> s, the ionization time about 10<sup>8</sup> s, and the thermal escape time about 10<sup>17</sup> s, these molecules will break down into their elemental components over a period of several days. If the resultant atoms are not chemisorbed by the lunar surface within a few weeks, they will be ionized and either driven into the lunar surface or lost from the lunar environment. The reaction rates for chemisorption of these elements by the lunar surface are not known, but it seems likely that at least the very reactive elements, F and Cl, will be chemisorbed.

As a result, the contaminants released in the lunar atmosphere should have no long term effects on the lunar environment in general. However, in the immediate vicinity of impact the surface chemistry may have been drastically changed by the addition of these reactive chemicals. This change is evident from the blackened lunar surface surrounding all the impact craters formed by man-made objects on the lunar surface. [*Whitaker*, 1972; T. Page, private communication, 1972].

Since the presence of hydrocarbons and other organic molecules makes an exact mass identification impossible, the MA data were evaluated by assuming that each peak was produced by only one mass component. In this manner the two 48.6-eV spectra were analyzed by using the most probable mass for each peak as is shown in Table 5.

#### NEUTRAL GAS-SOLAR WIND INTERACTION

A model based on kinetic theory has been used to calculate the expansion of the neutral gas cloud released by the S-IVB impact. The parameters of this model have been computed so that the maximum amount of gas arrives over the A1sep site during the observation of the peak vertical flux, 75 s after im-

TABLE 5. Identification of Ions Observed by MA

Spectra	Mass	Flux, ions/cm <sup>2</sup> s sr
1 (57 s)	12	$1.8 \times 10^8$
	20	$4.9 \times 10^8$
	32	$6.1 \times 10^8$
	84	$4.9 \times 10^8$
2 (267 s)	25	$3 \times 10^8$
	35	$4 \times 10^8$



pact. The ionization rates in this expanding cloud have been calculated by using cross sections in the upper range of the measured values. Using a minimum value for the observed vertical flux and a maximum ionization rate (the photoionization rate) over the total volume of the cloud yields a value for the total number of molecules released at impact of  $3 \times 10^{28}$  molecules. This value represents a lower limit.

This value has been compared to the total number of gas molecules that were available either as plastics or as trapped gases at the impact site. An upper limit of  $2 \times 10^{28}$  molecules could be vaporized by the impact. Since  $10^{28}$  of these molecules are He and the comparison of the MA and TID data showed that the bulk of these molecules had masses greater than 10 amu, it is likely that an upper limit of  $10^{28}$  molecules can be placed on the gas cloud. Moreover the ionization rates for He are a factor of 10 larger than the rates used in this calculation. Thus the calculated lower limit should be raised by an order of magnitude if He is the major species in the cloud.

Thus the calculated lower limit for the total number of molecules released by the impact is at least 1.5 times and probably 3 times larger than the upper limit of the gas molecules that are available for vaporization by the impact. This discrepancy is within the possible errors of the experimental observations and those of the computed values of the ionization rates and gas-cloud spreading parameters. However, there would be a more comfortable agreement if the ionization rate was larger. Both an increased ionization rate and the detection of the hot (50 eV) electrons by the SWS can be consistently explained by the existence of a rapid interaction between the solar wind and the neutral gas cloud. Some insight into this process can be gained by considering the various stages of expansion of the neutral cloud.

The cloud expanded in a vacuum for the first 50 km. At this point the cloud has a volume of  $2.5 \times 10^{20}$  cm<sup>3</sup> and an average number density of  $8 \times 10^7$  molecules/cm<sup>3</sup> ( $N_0 = 2 \times 10^{28}$  molecules). The mean free path for elastic collisions between neutrals in the cloud ( $\sigma \sim 3 \times 10^{-15}$  cm<sup>2</sup>) was 35 km, and the mean free path for charge exchange with solar wind protons ( $\sigma \sim 5 \times 10^{-16}$  cm<sup>2</sup>) was 250 km. The production rate of ions was 4 ions/cm<sup>3</sup> s.

The cloud continued to expand into the solar wind until the ion production rate in a column (in units of grams per square centimeter second) along a solar wind stream line became comparable to the mass flux of the solar wind. At this point the solar wind could no longer accommodate the additional mass, and a shock wave was set up at the front of the cloud, which slowed and thermalized the solar wind. This shock wave formed when the cloud had a radius of about 70 km. (See Cloutier *et al.* [1969] for a one-dimensional analysis of this situation.) The solar wind was deflected by the shock wave and detected by the peripheral cups of the SWS.

At 90 km the cloud first emerged into the solar UV. The average number density was now  $2 \times 10^7$  molecules/cm<sup>3</sup>, and the mean free path for elastic collisions in the cloud had risen to 200 km. The ion production rate due to solar UV was 14 ions/cm<sup>3</sup> s, but this was over a very small volume of the cloud. The ion production rate due to charge exchange was 0.7 ion/cm<sup>3</sup> s. The increased ionization rate in the upper regions of the cloud may have altered the jump conditions of the shock and the postshock streamlines, but basically the situation remained unchanged.

At the time that the TID was measuring the initial ion peak the cloud had a radius of 225 km. The average number density

was  $10^6$  molecules/cm<sup>3</sup>, and the elastic mean free path and solar wind charge exchange mean free path were of the order of several thousand kilometers. The ion production rate was 1 ion/cm<sup>3</sup> s owing to solar UV and 0.05 ion/cm<sup>3</sup> s owing to charge exchange. The streaming pressure of the cloud at this point (see Appendix 3) was  $1 \times 10^{-8}$  dyn/cm<sup>2</sup> as compared with the pressure of the solar wind,  $5 \times 10^{-9}$  dyn/cm<sup>2</sup>.

The key to the explanation of this event is probably the hot electrons. By assuming that only solar wind electrons with a number density of 3 el/cm<sup>3</sup> are being energized and by giving these electrons a thermal energy of 50 eV the flux of hot electrons would be  $10^{10}$  el/cm<sup>2</sup> s or a production rate of  $2 \times 10^{-6}$  ion/s atom. This is slightly larger than the photoionization rate, and since the solar wind seems to have been deviated through the cloud, these electrons will be ionizing over a much larger volume than the solar UV. With the use of this production rate the calculated number of molecules emitted is only  $1.6 \times 10^{28}$  molecules. The addition of photoionization will make this even lower. Thus the energization of solar wind electrons may explain the observations by reducing the mass of the neutral gas cloud to a more reasonable value.

Moreover if the observed hot electrons are being energized over a thicker region than the shock layer itself, then some thermal electrons resulting from the ionization of neutrals will also be energized. In this case, an avalanche effect will occur, which is limited only by the energy flux of the solar wind. The energy lost by each solar wind proton can go into proton thermal energy, electron thermal energy, and wave energy. Thus each proton can energize at least three or four electrons. This ability would raise the ion production rate to  $8 \times 10^{-6}$  ion/s atom, the number of molecules in the cloud thus being reduced to  $4 \times 10^{27}$ .

Note that this may not be inconsistent with the observed electron fluxes. As we have already noted, Lindeman *et al.* [1973] have shown the lunar surface potential to be negative as much as 100 V on the night side of the dawn terminator. This potential will repel as many electrons as necessary to balance the sum of all the currents to the surface. As a result, the observed electron flux will be less than the actual flux in the cloud.

The avalanche effect discussed above is very similar to the critical velocity hypothesis proposed by Alfvén [1954] in his theory on the origin of the solar system. Alfvén proposed that when the relative velocity between a plasma and a neutral gas in a magnetic field reaches or exceeds a certain critical value, the gas is efficiently ionized. This critical velocity  $V_c$  can be obtained by equating the kinetic energy of neutrals relative to the plasma with the ionization energy of the neutrals ( $e\phi_n$ , where  $\phi_n$  is the neutral ionization potential)

$$\frac{1}{2}M_n V_c^2 = e\phi_n$$

The exact ionization mechanism seems to vary with the prevailing conditions [Sherman, 1970; Danielsson, 1970b]. Danielsson [1970a] has found in laboratory experiments that electrons are energized and cause efficient ionization under conditions that should have been collisionless.

Reasoner and O'Brien [1972] report the observation of a large flux of electrons in the energy range 40–95 eV, which resulted from the impact of the Apollo 14 lunar module on the lunar surface 66 km away. The authors argue by the process of elimination that these energetic electrons are the result of a neutral gas-solar wind interaction and are not produced at impact.

If energetic electrons are a common feature of the interac-

tion of a tenuous plasma and a collisionless gas, then several applications become apparent. A few that have already been mentioned are the ionospheric models for Mars and Venus, the ionization mechanism in type 1 comet tails, and possibly even the existence of our solar system.

It is unfortunate that the uncertainty in the data does not clearly indicate whether the electrons are energized only at the shock front or over a much wider region. In either case it is probable that energetic electrons play an important role in this event.

Thus the neutral gas cloud seems to have been efficiently ionized by the solar wind in this interaction. Moreover the solar wind underwent large deflections in the interaction. The exact deflection mechanism has not been specified in this model, although it was probably accomplished by the shock front rather than the local lunar magnetic fields.

By means of an expansion velocity of 3 km/s the cloud had expanded over 380 km beyond the Alsep site during the observation of the maximum horizontal fluxes by the SWS. At this time the flow was from the north. It requires an 8- $\gamma$  magnetic field directed into the lunar surface to deflect a 400-eV proton by 90° in 380 km. The average local surface field at the Alsep 12 site is 36  $\gamma$  and directed into the lunar surface with a dip of 32°. The magnetic pressure exerted by a 36- $\gamma$  field is  $5 \times 10^{-9}$  dyn/cm<sup>2</sup> (Appendix 3). The pressure exerted by the solar wind after being deflected by 90° ( $K = 1$  in Appendix 3) is  $5 \times 10^{-9}$  dyn/cm<sup>2</sup>. When the local field attempts to deflect the solar wind by more than 90°, the solar wind pressure exceeds the field pressure and the local fields are then deformed by the solar wind. This qualitative discussion shows that the assumption that the horizontal fluxes are deflected solar wind ions is perhaps consistent with the available data. However, the solar wind is not deviated in this manner on other lunar mornings, so the complex time history of the horizontal fluxes may be due to the deformation of the local fields, as well as deviation of the solar wind flow by the shock front.

#### SUMMARY AND CONCLUSIONS

The impact of the S-IVB on the lunar surface vaporized the 1100 kg of plastics on the rocket and released some of the trapped gases in the lunar soil. A maximum of  $2 \times 10^{28}$  molecules were released in the resultant gas cloud, the plastics having been apparently broken down into 80-amu molecules. This cloud expanded at a mean horizontal velocity of 2 km/s over the 140 km to the Alsep site. As the cloud expanded, it came into contact with the solar wind and ionization started. When the column ion production rate exceeded the solar wind mass flux, a shock wave was set up at the front of the cloud. As a result of either this shock wave or an anomalous neutral gas-solar wind interaction, electrons were energized to 50 eV. These hot electrons then dominated the ionization rates of the neutral cloud.

The thickness of the shock wave or interaction layer can be estimated by assuming that it coincides with the initial peak as observed by the TID. From the average transit velocity and the temporal duration of the peak (full width at 10% maximum) this layer is 17 km thick. If the shock wave is at an angle with respect to the lunar surface, this value would be an upper limit.

The collisionless interaction suggested by these results has application to a wide variety of problems in space research. If the existence of energetic electrons proves to be a common feature in neutral gas-plasma interactions, the implications may be far-reaching.

#### APPENDIX 1

The distribution of gases resulting from gas sources on the lunar surface has been calculated previously by *Yeh and Chang* [1971, 1972] *Hodges et al.* [1972], and *Hall* [1973].

If  $N_0$  particles are released isotropically with a Maxwellian distribution from a point on the lunar surface ( $X_0, Y_0, Z_0$ ) at a time  $t = 0$ , then the particle distribution at the source is given by

$$f_0 = N_0 \delta(X_0) \delta(Y_0) \delta(Z_0) \left( \frac{m}{2\pi kT} \right)^{3/2} \exp \left( -\frac{m\mathbf{v}_0^2}{2kT} \right)$$

where  $m$  is the molecular mass of the emitted gas,  $T$  is the temperature at which the gas is released,  $k$  is the Boltzmann constant, and  $\mathbf{v}_0$  is the molecular velocity.

With the assumption of no collisions the distribution function will be constant along a particle trajectory in phase space. The density of a particle at a particular location at time  $t$  is obtained by integration of the distribution function with respect to the velocities. By assuming a flat lunar surface this integral is given by

$$n(R, Z, t) = \left( \frac{1}{2\pi gH} \right)^{3/2} \frac{N_0}{t^3} \cdot \exp \left[ -\frac{1}{2gH} \frac{R^2}{t^2} - \frac{gt^2}{8H} \right] \cdot \exp \left[ -\frac{Z^2}{2gHt^2} - \frac{Z}{2H} \right]$$

where  $g$  is the acceleration due to lunar gravity,  $H = kT/mg$ , and  $R^2 = X^2 + Y^2$ . This result has been obtained previously by *Hodges et al.* [1972].

The total column density  $\rho$  at a distance  $R$  is obtained by integrating over  $Z$  from 0 to infinity, the following result being given:

$$\rho(R, t) = \frac{N_0}{2\pi gHt^2} \exp(-R^2/2gHt^2) \cdot \{1 - \operatorname{erf}[t(g/8H)^{1/2}]\}$$

where

$$\operatorname{erf}(x) = [2/(\pi)^{1/2}] \int_0^x e^{-y^2} dy$$

The column density above an altitude  $y$  is given by

$$\rho_s(R, t) = \frac{N_0}{2\pi gHt^2} \exp \left( \frac{-R^2}{2gHt^2} \right) \cdot \{1 - \operatorname{erf}[t(g/8H)^{1/2}] + Z(2/gHt^2)^{1/2}\}$$

#### APPENDIX 2

The production rate is given by

$$P = \sigma FN$$

where  $\sigma$  is the ionization cross section,  $F$  is the ionization flux (particles or radiation), and  $N$  is the neutral number density.

A normalized production rate is given by

$$P/N = \sigma F$$

and is given in units of ions/s atom.

**Solar UV.** Assume an average ionization potential of 11 eV and a photoionization cross section of  $10^{-17}$  cm<sup>2</sup> for heavy atoms and simple molecules [*Hudson*, 1971]. The flux of photons with energy greater than 11 eV is about  $10^{11}$  photons/cm<sup>2</sup> s [*Hinteregger*, 1965]

$$P/N \sim 10^{-6} \text{ ion/s atom}$$

**Charge exchange.** Assume an average cross section for asymmetric charge exchange of a 600-eV proton with the neutrals composing the cloud of  $5 \times 10^{-16}$  cm<sup>2</sup> [Bernstein et al., 1963]. The solar wind flux at the time of this event was  $10^8$  protons/cm<sup>2</sup> s.

$$P/N \sim 5 \times 10^{-8} \text{ ion/s atom}$$

**Electrons.** Assume an average cross section for ionization by 50-eV electrons of  $2 \times 10^{-16}$  cm<sup>2</sup> [Kieffer, 1965]. The exact flux of electrons is not known, but a lower limit is  $3.2 \times 10^8$  el/cm<sup>2</sup> s.

$$P/N \sim 7 \times 10^{-8} \text{ ion/s atom}$$

### APPENDIX 3

The pressure required to contain the expanding cloud is given by the streaming pressure

$$p = K\rho v^2$$

where  $K$  is a constant approximately equal to 1,  $\rho$  is the mass density, and  $v$  is the expansion velocity.

If an average particle mass of 80 amu, an expansion velocity of 3 km/s, and an average density of  $10^6$  molecules/cm<sup>3</sup> are assumed, the pressure is

$$p \approx 10^{-5} \text{ dyn/cm}^2$$

The streaming pressure of the solar wind at the time of this event was ( $n \approx 3$  protons/cm<sup>3</sup>;  $v \approx 330$  km/s)

$$p \approx 5 \times 10^{-9} \text{ dyn/cm}^2$$

The pressure of the average magnetic field at the Apollo 12 Alsep site is given by

$$p \approx B^2/8\pi$$

Since the average magnetic field is 36  $\gamma$ , the magnetic pressure is

$$p \approx 5 \times 10^{-9} \text{ dyn/cm}^2$$

**Acknowledgments.** We are grateful for many useful discussions with H. K. Hills and other members of the Rice University Department of Space Physics and Astronomy and with C. G. Fälthammer of the Royal Institute of Technology, Stockholm, Sweden. This research was supported by NASA contract NAS 9-5911 and the Royal Institute of Technology, Stockholm, Sweden. The work at the Jet Propulsion Laboratory, California Institute of Technology, was sponsored by NASA contract NAS 7-100.

\* \* \*

The Editor thanks S. J. Bame and T. T. J. Yeh for their assistance in evaluating this paper.

### REFERENCES

- Alfvén, H., *On the Origin of the Solar System*, chap. 2, Oxford at the Clarendon Press, London, 1954.
- Beard, D. B., The theory of type I comet tails, *Planet. Space Sci.*, **14**, 303, 1966.
- Bernstein, W., R. Fredricks, J. Vogl, and W. Fowler, The lunar atmosphere and the solar wind, *Icarus*, **2**, 233, 1963.
- Biermann, L., B. Brosowski, and H. Schmidt, The interaction of the solar wind with a comet, *Solar Phys.*, **1**, 254, 1967.
- Cloutier, P. A., M. B. McElroy, and F. C. Michel, Modification of the Martian ionosphere by the solar wind, *J. Geophys. Res.*, **74**, 6215, 1969.
- Danielsson, L., Experiment on the interaction between a plasma and a neutral gas, *Phys. Fluids*, **13**, 2288, 1970a.
- Danielsson, L., Review of the critical velocity, 2, Experimental observations, *Rep. 70-05*, Roy. Inst. of Technol., Div. of Plasma Phys., Stockholm, 1970b.
- Freeman, J. W., Jr., and H. K. Hills, Positive ions at the Apollo 12 Alsep site resulting from the Apollo 13 S-IVB lunar impact (abstract), *Eos Trans. AGU*, **51**, 821, 1970a.
- Freeman, J. W., Jr., H. Balsiger, and H. K. Hills, Suprathermal ion detector experiment, Apollo 12 Preliminary Science Report, *NASA Spec. Publ. 235*, pp. 83-92, 1970b.
- Freeman, J. W., Jr., H. K. Hills, and M. A. Fenner, Some results from the Apollo 12 suprathermal ion detector, *Geochim. Cosmochim. Acta*, **35**, Suppl. 2, 2093, 1971a.
- Freeman, J. W., Jr., M. A. Fenner, H. K. Hills, R. A. Lindeman, R. Medrano, and J. Meister, Suprathermal ions near the moon, *Icarus*, **16**, 328, 1971b.
- Funkhouser, J., E. Jessberger, O. Muller, and J. Zahringer, Active and inert gases in Apollo 12 and Apollo 11 samples released by crushing at room temperature and by heating at low temperature, *Geochim. Cosmochim. Acta*, **35**, Suppl. 2, 1381, 1971.
- Hall, F. G., Role of pressure transients in the detection and identification of lunar surface gas sources, *J. Geophys. Res.*, **78**, 2111, 1973.
- Heymann, D., and A. Yaniv, Breccia 10065: Release of inert gases by vacuum crushing at room temperature, *Geochim. Cosmochim. Acta*, **35**, Suppl. 2, 1681, 1971.
- Hintenberger, H., H. Weber, H. Voshage, H. Wänke, F. Begemann, and F. Wlotzka, Concentrations and isotopic abundances of the rare gases, hydrogen, and nitrogen in Apollo 11 lunar matter, *Geochim. Cosmochim. Acta*, **34**, Suppl. 1, 1269, 1970.
- Hintenberger, H., H. Weber, and N. Takaoka, Concentrations and isotopic abundances of the rare gases in lunar matter, *Geochim. Cosmochim. Acta*, **35**, Suppl. 2, 1607, 1971.
- Hinteregger, A. E., Absolute intensity measurements in the extreme ultraviolet spectrum of solar radiation, *Space Sci. Rev.*, **4**, 461, 1965.
- Hodges, R. R., Jr., J. H. Hoffman, T. T. J. Yeh, and G. K. Chang, Orbital search for lunar volcanism, *J. Geophys. Res.*, **77**, 4079, 1972.
- Hudson, R. D., Critical review of ultraviolet photoabsorption cross sections for molecules of astrophysical and aeronomic interest, *Rev. Geophys. Space Phys.*, **9**, 305, 1971.
- Jeans, B., and T. Rollins, Radiation for hypervelocity impact generated plasma, *AIAA J.*, **8**, 1742, 1970.
- Johnson, F. S., Lunar atmosphere, *Rev. Geophys. Space Phys.*, **9**, 813, 1971.
- Kieffer, L. J., Electron ionization cross sections, *At. Data*, **1**, 22, 1965.
- Lindeman, R., J. W. Freeman, Jr., and R. Vondrak, Ions from the lunar atmosphere, *Geochim. Cosmochim. Acta*, **37**, Suppl. 4, 2889, 1973.
- McKay, D., W. Greenwood, and D. Morrison, Origin of small particles and breccia from the Apollo 11 site, *Geochim. Cosmochim. Acta*, **34**, Suppl. 1, 673, 1970.
- Michel, F. C., Solar wind induced mass loss from magnetic field-free planets, *Planet. Space Sci.*, **19**, 1580, 1971.
- Mirtov, B., Matter from the lunar surface in the lunar atmosphere, *Geomagn. Aeron.*, **9**, 112, 1969.
- Oró, J., D. Flory, J. Gilbert, J. McReynolds, H. Lichtenskin, and S. Wikstrom, Abundances and distribution of organogenic elements and compounds in Apollo 12 lunar samples, *Geochim. Cosmochim. Acta*, **35**, Suppl. 2, 1913, 1971.
- Reasoner, D. R., and B. J. O'Brien, Measurements on the lunar surface of impact produced plasma clouds, *J. Geophys. Res.*, **77**, 1292, 1972.
- Rehfuss, D., Lunar winds, *J. Geophys. Res.*, **77**, 6303, 1972.
- Sherman, J., Review of Alfvén's critical velocity hypothesis, 3, Theory, *Rep. 70-30*, Roy. Inst. of Technol., Div. of Plasma Phys., Stockholm, 1970.
- Snyder, C. W., D. R. Clay, and M. Neugebauer, The solar-wind spectrometer experiment, Apollo 12 Preliminary Science Report, *NASA Spec. Publ. 235*, 75-83, 1970.
- Whitaker, E., Artificial lunar impact craters: Four new identifications, Apollo 16 Preliminary Science Report, *NASA Spec. Publ. 315*, 29-39, 1972.
- Yeh, T., and G. Chang, Density and flux distributions in the lunar atmosphere due to point and line sources, *Rep. TM-71-2015-7*, Bellcomm, Inc., Wash., D. C., 1971.
- Yeh, T., and G. Chang, Density and flux distributions of neutral gases in the lunar atmosphere, *J. Geophys. Res.*, **77**, 1720, 1972.

(Received November 20, 1973;  
accepted February 27, 1974.)



# Suprathermal Ions Near the Moon

J. W. FREEMAN, JR., M. A. FENNER, H. K. HILLS, R. A. LINDEMAN,  
R. MEDRANO, AND J. MEISTER

*Department of Space Science, Rice University, Houston, Texas*

Reprinted from ICARUS, Vol. 16, No. 2, April, 1972  
All Rights Reserved by Academic Press, New York and London  
*Printed in England*

## Suprathermal Ions Near the Moon<sup>1</sup>

J. W. FREEMAN, JR.,<sup>2</sup> M. A. FENNER, H. K. HILLS,  
R. A. LINDEMAN, R. MEDRANO, AND J. MEISTER

*Department of Space Science, Rice University, Houston, Texas*

Received November 29, 1971

This paper reports some preliminary results from the Suprathermal Ion Detectors deployed on the lunar surface by the Apollo 12 and 14 astronauts. Salient features of these results include: the possible observation of sporadic venting of gas from the lunar surface; evidence for a prompt ionization and acceleration mechanism operating in the lunar exosphere; and a preliminary measurement yielding approximately 1 month for the *e*-folding decay time for the heavier components of the exhaust gases from the Apollo lunar landing systems. Prominent phenomena from which these results have been derived are: (1) ion bursts of low to moderate energy seen in conjunction with lunar sunrise and sunset; (2) solar wind energy ions detected on the night side of the Moon; (3) ions of several keV energy seen during the lunar sunset to midnight quadrant of the Moon's orbit; (4) magnetosheath ion flux enhancements; (5) ion bursts generated by the lunar impact of the Apollo 13 Saturn upper stage and other man-made objects; and (6) geomagnetic storm associated ion flux variations in the Earth's magnetotail.

### I. INTRODUCTION

The objectives of the Apollo Lunar Surface Experiment Package (ALSEP) Suprathermal Ion Detector Experiment (SIDE) are to provide an exploratory search for possible lunar exospheric phenomena and to study the interaction between these phenomena and the Solar Wind. To this end the instrument (shown in Fig. 1) is equipped with a crude positive ion mass/unit charge spectrometer and a positive ion energy/unit charge spectrometer. The first SIDE was deployed by the Apollo 12 astronauts in the Ocean of Storms (23.4°W, 3.04°S) and the second in the Fra Mauro Highlands (17.48°W, 3.65°S). A third such instrument was deployed on July 31, 1971, by the Apollo 15 astronauts in the Hadley-Apennine area. All these instruments are presently functioning. However, since the

Apollo 12 SIDE has been in operation the longest results reported herein are based principally on data from that instrument.

The purpose of this report is to provide only a brief summary of a few of the principal findings. More detailed papers addressing themselves to individual features of the data are in preparation or have been presented by Freeman *et al.* (1970), Freeman and Hills (1970), Fenner *et al.* (1971), Freeman (1972), Freeman *et al.* (1971), Garrett *et al.* (1971), Hills and Freeman (1971), and Lindeman *et al.* (1971).

### II. THE SIDE EXPERIMENT

Figure 2 shows the operating principles of the instrument. The ion mass/*q* spectrometer consists of a crossed electric and magnetic field (Wien) velocity filter followed by an electrostatic curved-plate energy/*q* filter. The sensor is a channel-electron-multiplier with its input biased at -3.5 kV so that only positive ions can be detected. The device is sequenced through the six energies, 0.2, 0.6, 1.8, 5.4, 16.2, and 48.6 eV. While at each energy, twenty

<sup>1</sup> Presented at the XVth General Assembly of the International Union of Geophysics and Geodesy, Moscow, August, 1971.

<sup>2</sup> Present address: Department of Plasma Physics, Royal Institute of Technology, S-100 44 Stockholm 70, Sweden.

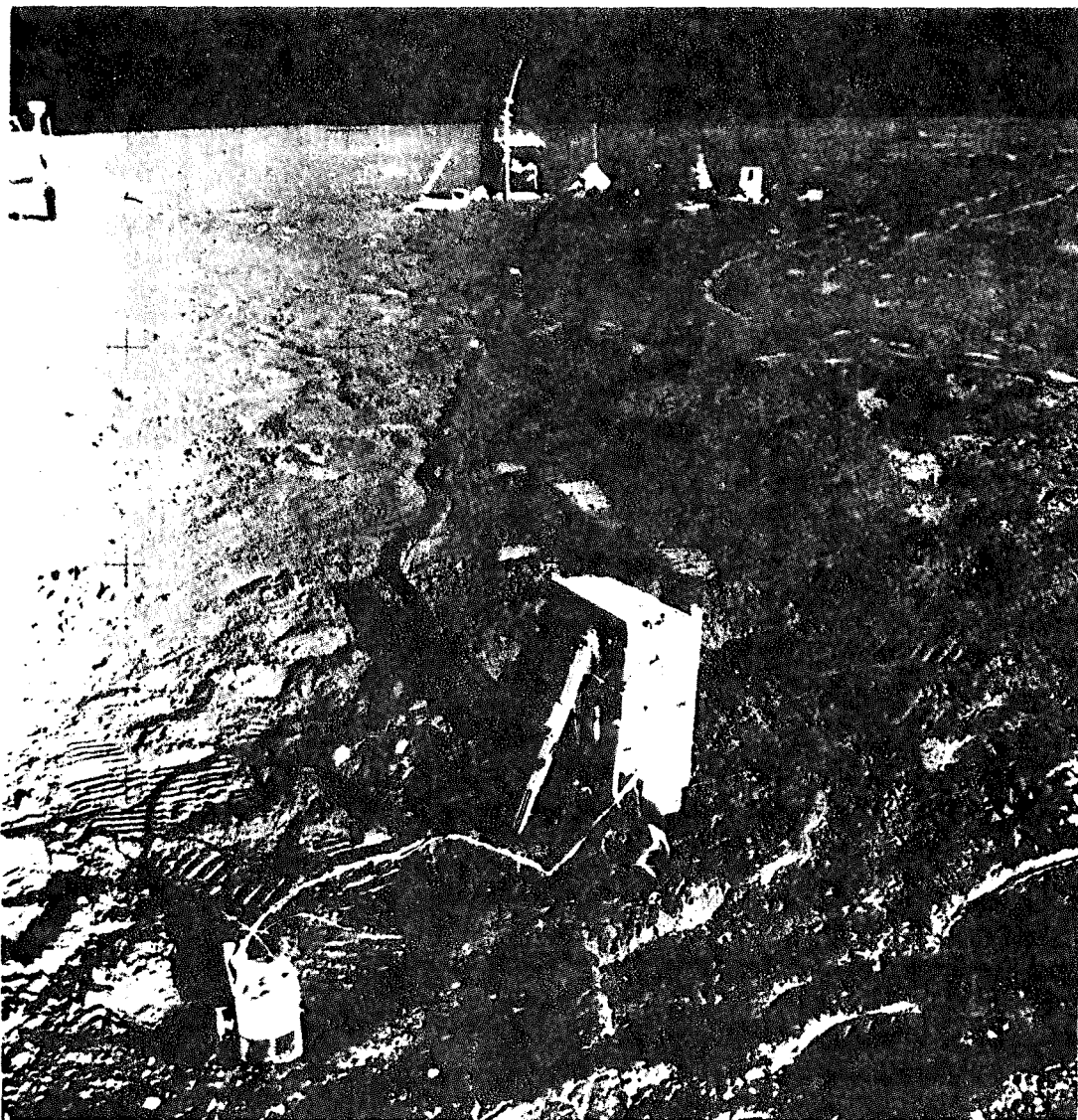


FIG. 1. The Apollo 14 SIDE deployed on the lunar surface. The ALSEP central station, radio-isotope thermal generator, and additional experiments can be seen in the background. The cold cathode ionization gage is in the lower left foreground (Johnson *et al.*, 1971). The entrance apertures for the MA and TID are on the SIDE top horizontal surface. At the time of this photograph they are protected by a dust cover subsequently removed by radio command. The SIDE top horizontal surface is about 20 in above the lunar surface. A bubble level is used by the astronaut to level the instrument within 5°.

velocity steps (corresponding to 20 mass/ $q$  ranges) are sampled by stepping the voltage on the electric field plate in the Wien filter. Thus the mass/ $q$  range from approximately 10 to 1500 amu/ $q$  (for the Apollo 12 SIDE) is sampled in 20 steps at six energies up to

48.6 eV. This detector is called the Mass Analyzer or MA. A complete energy-mass scan is accomplished in 2.58 min.

The second detector called the Total Ion Detector or TID is identical to the MA but possesses no velocity filter. It is also tuned

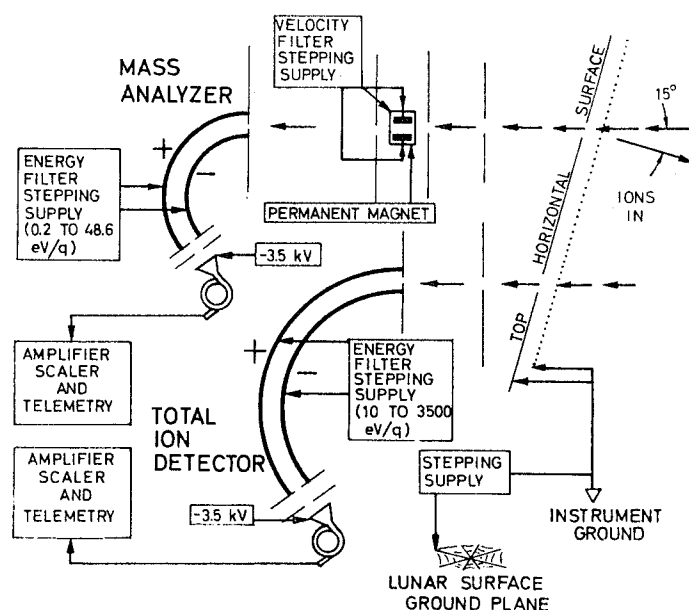


FIG. 2. SIDE principal elements. The lunar surface ground plane and its stepping supply periodically alter the electric potential between the instrument ground (also a wire mesh screen on the top surface) and the lunar surface. The potential range is from  $+27.6$  to  $-27.6$  V in 23 steps including 0. See the text for a description of the other elements of the experiment.

to include higher energies. It covers the energy range from  $10\text{ eV}$  to  $3500\text{ eV}$  in 20 differential steps. Results of the TID can be compared with those of the MA to determine the flux of positive ions in the mass/ $q$  range not covered by the MA.

The geometric factors for the Apollo 12 detectors are  $10^{-4}\text{ cm}^2\text{-sr}$  and  $0.5 \times 10^{-4}\text{ cm}^2\text{-sr}$  for the TID and MA respectively. Both fields of view are approximately square and  $6^\circ$  on a side and the look-axes are  $15^\circ$  west and east of local vertical for Apollo 12 and 14 respectively. They lie approximately in the ecliptic plane. Additional details of the experiment can be found in Freeman *et al.* (1970) and Hills and Freeman (1971).

### III. SUMMARY OF THE DATA

Phenomena reported by the SIDE can be broadly divided into two categories: diurnal, that is, recurring on successive lunar orbits; and sporadic or singular events whose occurrence may be independent of lunar phase.

Figure 3 shows the lunar orbit location of various diurnal phenomena that have been observed with the Apollo 12 instrument. Also shown are the look directions for the field of view of the two detectors. The look-axes lie approximately in the ecliptic plane.

Note first the indicated presence of intermediate and low energy ion bursts (IBs) usually seen within a few days either side of the ALSEP passage by the sunrise and sunset terminators (Lindeman *et al.*, 1971). Here intermediate and low energy refers to ions in the 10 to approximately  $1250\text{ eV}/q$  range. The brief and sporadic appearance of IBs contrasts to the more steady and sustained count-rate enhancement produced, for example, by the magnetosheath or solar wind plasma flow.

Note also the appearance of higher energy (up to  $3500\text{ eV}/q$ ) ions in the pre-midnight quadrant. These are thought to be high energy protons that have escaped upstream from the Earth's bow shock to impinge on the night side of the Moon. Such protons have been reported pre-



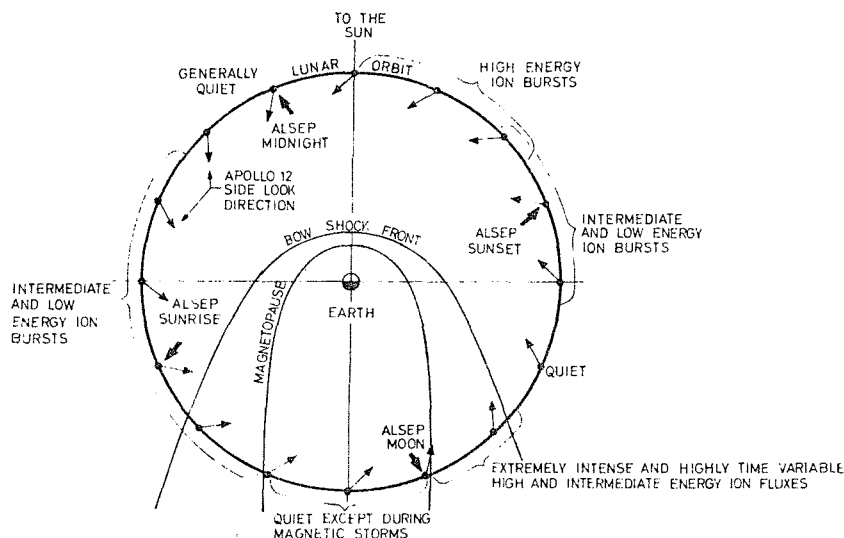


FIG. 3. Capsule summary of the location of diurnal phenomena along the lunar orbit.

viously (Asbridge *et al.*, 1968) but were not known to extend as far as the Moon.

Extensive data are also available from both the Apollo 12 and 14 instrument on the characteristics of the magnetosheath ion flow since during passage through the magnetosheath these detectors look directly upstream (Fenner *et al.*, 1971). These data deal less directly with the Moon and hence will not be the main subject of this paper.

Garrett *et al.* (1971) have reported enhancements of plasma-sheet ions seen with the SIDE in the magnetotail during a geomagnetic storm. At times other than this the plasma flux in the tail has remained at or below the TID high lunar day background level.

#### IV. ION BURSTS

We return now to the subject of the IBs seen near sunrise and sunset. Using data from the Apollo 12 TID, Lindeman *et al.* (1971) have performed a preliminary statistical study of the spectral types and their location in lunar orbit. The results of this study are shown in Fig. 4. Here it is seen that at least five spectral types have been tentatively identified. Whether or not these are all independent phenomena still remains to be seen.

The top spectrum in Fig. 4 (type I) with its lunar orbit distribution weighted to the post-sunset region, is probably the bow-shock protons already mentioned.

The type III spectrum, with its distributions weighted slightly toward the pre-sunrise region, appears to resemble solar wind that has been deflected onto the night side of the Moon. One dramatic example that appeared 4.7 days before the sunrise terminator has been reported by Freeman (1972).

A feature of particular interest is the occasional appearance of a low energy peak, often around 50 eV, that may be found superimposed on any of these spectral types or standing alone. This is illustrated by the dotted peak in type III. It is in this type of spectrum that higher mass/ $q$  ions are sometimes found. When the MA indicates the presence of higher mass/ $q$  ions the event is referred to as a HIB for heavy ion burst.

One of the most interesting examples of a HIB event occurred on March 7 and was observed by the Apollo 14 SIDE. The mass/ $q$  spectrum typical of this event is shown in Fig. 5. Here we see the raw data from a single spectrum taken at 48.6 eV/ $q$ . The mass/ $q$  of the ions producing the strong peak in mass channel 5 was between 18 and 23 amu/ $q$ . This spectrum is one of 5 similar

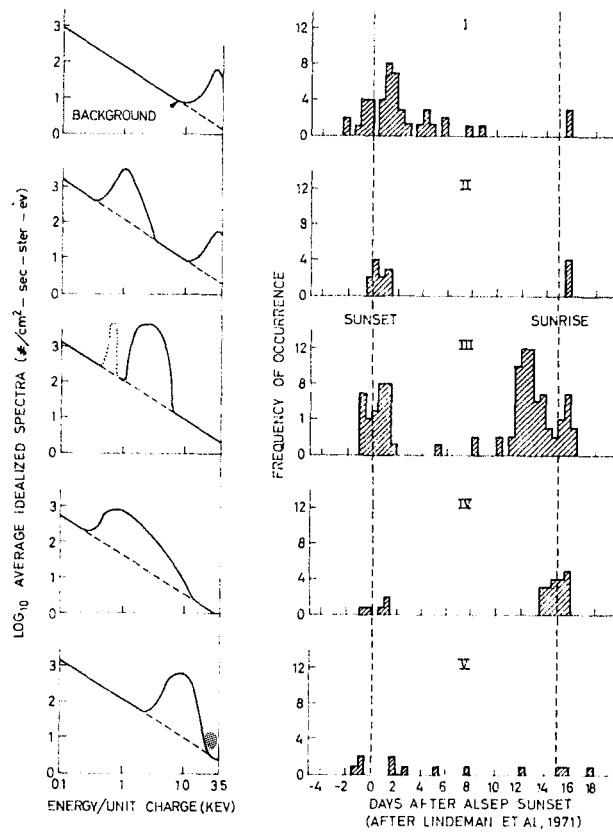


FIG. 4. Spectral types and lunar orbit frequency distribution of TID ion bursts, November 19, 1969 May 16, 1970. The spectral types are labeled I through V. The lower energy dotted peak shown superimposed on the type III spectrum is not always present and may be found occasionally in other spectral types as well.

spectra that occurred within a 50 min period late in the event. The entire event consisted of intermittent bursts of heavier ions lasting nearly 14 hr. During that time the highest flux recorded by the MA was  $10^7$  ions/cm<sup>2</sup>-sec-sr and was in mass channel 5. At the same time the adjacent mass channel, channel 4, indicated statistically significant counts. This suggests that the ions producing the beam were toward the lower end of the channel 5 passband, probably water vapor. During laboratory calibrations water vapor showed up predominantly in channel 5.

At the time of the mass/ $q$  spectrum illustrated in Fig. 5 the TID indicated an energy spectrum as shown in Fig. 6, an intense monochromatic peak near 50 or

70 eV/ $q$  superimposed on a broader spectrum peaking at around 250 eV/ $q$ . A similar pattern of a peak at or below 100 eV/ $q$  is common whenever mass spectra are discernible with the MA. For the event illustrated here the low energy peak was exceptionally intense, monochromatic, and highly variable in amplitude: varying as much as two orders of magnitude within 25 sec.

The foregoing HIB occurred 29 days after the Apollo 14 landing. Its peak intensity exceeded any other HIB observed to date by over one order of magnitude, and all other such events have been clearly identifiable by their close time proximity to lunar surface operations or man-made events. Further, this event appears different

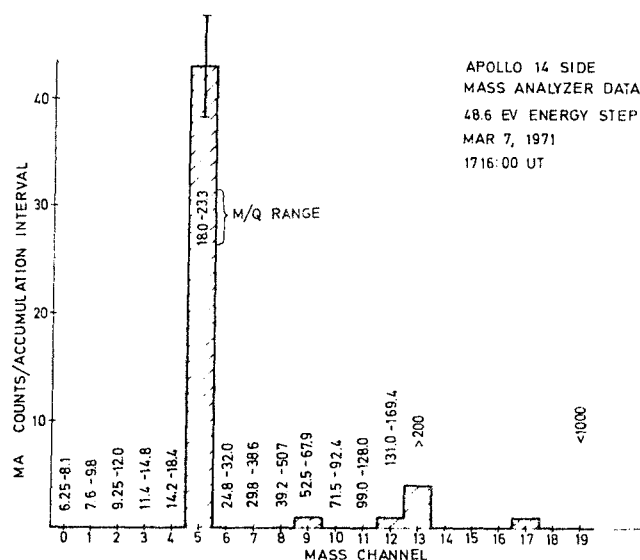


FIG. 5. Mass/ $q$  spectrum typical of the March 7, 1971 event. The mass/ $q$  ranges shown for each channel (in amu/unit charge) represents worst-case limits obtained by plotting the results of a series of laboratory calibration runs with known gases and taking the two straight line envelopes that included all points to define the range of each mass channel. These ranges therefore indicate approximately the mass/ $q$  range included in each channel. More detailed knowledge of the actual ions present is generally possible by computer solution of 20 simultaneous equations involving the laboratory obtained response functions. This detailed work is in progress.

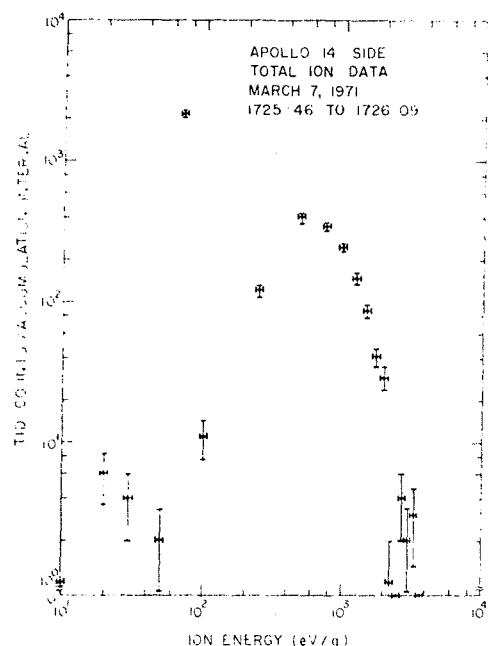


FIG. 6. TID energy spectrum at the time of the March 7, 1971 HIB event. The vertical error bars represent the  $1\sigma$  limits based on the count statistics and the horizontal bars, the detector energy passband widths.

in character (e.g. event duration and energy) from several other IBs recorded by more than one SIDE (and the ALSEP Passive Seismic Experiment) at energies too high to allow a mass/ $q$  determination but believed to be due to meteoroid impacts (Hills and Freeman, 1971). For these reasons, together with the narrow mass/ $q$  spectrum, we suspect that the March 7 event may represent a natural spontaneous emission of gas from the lunar surface.

An example of a HIB identified with lunar surface activities is shown in Fig. 7. This spectrum occurred during the Apollo 14 2nd EVA and shortly after the LM cabin depressurization for that activity. This spectrum, with its strong peak in mass channel 6, is thought to have arisen from the molecular oxygen released by the cabin depressurization process. (During laboratory calibrations  $O_2$  showed up predominantly in channel 6.) This flux lasted only a minute or so.

Not all the mass/ $q$  spectra have been as narrow as these two. Figure 8 illustrates a composite spectrum from an HIB of extended duration seen approximately 2

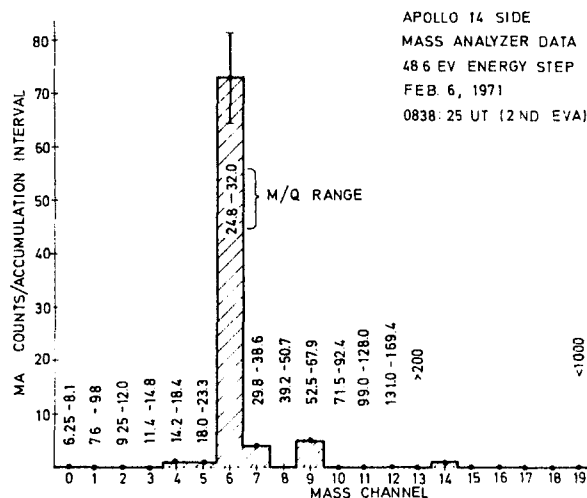
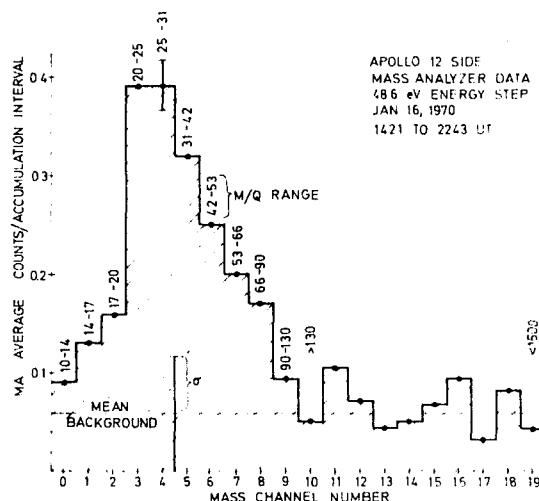


FIG. 7. Same as Fig. 5 for February 6, 1971.

months after the Apollo 12 landing. The broad mass/ $q$  spectrum seen here is very similar to that shown in Fig. 9 taken 14 hr after the Apollo 12 lunar landing. By comparison with predicted spectra (Simoneit *et al.*, 1969) we believe these spectra to result from residual or exhaust gases from the LM ascent and descent engines.

According to diffusion calculations by Chang (1969) the descent stage exhaust gases should reach a uniform distribution

over a hemisphere about 20 hr after landing. If we assume satisfactory uniformity by the time of the spectrum shown in Fig. 9 (i.e. local gas inhomogeneities have died away), similar ion accelerating conditions for the occasions of the two spectra, and an exponential decay curve, we can calculate the  $e$ -folding time for dissipation of the exhaust gases from the lunar surface. The result is approximately 30 days. In obtaining this number we have corrected for the subsequent additional input of gas from

FIG. 8. Composite mass/ $q$  spectrum for the specified interval on January 16, 1970. The same comments regarding mass/ $q$  ranges apply as stated for Fig. 5.

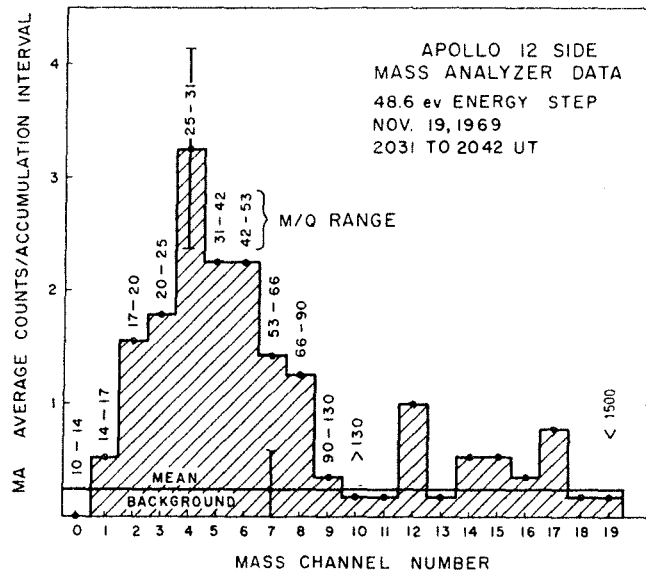


FIG. 9. Composite mass/ $q$  spectrum for the specified interval on November 19, 1969. The same comments regarding mass/ $q$  ranges apply as stated for Fig. 5.

the LM ascent stage by assuming these gases to be captured by the Moon in an identical proportion as those for the descent stage.

This preliminary figure of 1 month for the mean lifetime of rocket exhaust gases is somewhat shorter than the approximately 100 day lifetime that might be expected from pure ionization escape of these heavier gases (Johnson *et al.*, 1971); on the other hand it is longer than the several days predicted by Chang (1969). A more complete examination of the SIDE data and the ALSEP cold-cathode-gage experiment data is bound to yield a more refined figure.

#### V. S-IV B IMPACT

The foregoing discussion is taken as evidence for the prompt ionization and acceleration of gas from local natural or man-made sources. Further support for such an ionization and acceleration mechanism (or mechanisms) is provided by data from the lunar impacts of portions of the Apollo system (Freeman *et al.*, 1971; Freeman and Hills, 1970). The Apollo 13 S-IV B impact was some 140 km west of the Apollo 12 ALSEP. About 20 sec

following the impact an intense flux of ions was detected at the ALSEP site. Figure 10 illustrates the mass/ $q$  spectrum obtained by the MA at 48.6 eV/ $q$  during the early part of this burst of ions. The strong peak near heavy masses is thought to represent vaporized and ionized lunar surface material. This was the first occurrence of a mass spectrum showing such heavy ions thus verifying that the ions were from the impact.

The kinetic energy of the impact was approximately  $5 \times 10^{10}$  J. Figure 11 illustrates the time history of the ion flux and energy for the event as reported by the TID. Note that an initial burst of ions was seen 21 sec following the impact. At this time the ion energies were between 50 and 100 eV/ $q$ . After this the energies fell to low values and then rose again to as high as 500 eV/ $q$  as the flux increased some 4 min later. Ions of similar energies but with lower intensities were also observed immediately following the Apollo 12 LM ascent stage impact and the Apollo 14 and 15 S-IV B impacts (Hills and Freeman, 1971; O'Brien and Reasoner, 1971; Freeman *et al.*, 1971).

For the Apollo 13 S-IV B impact the maximum integrated flux seen from the

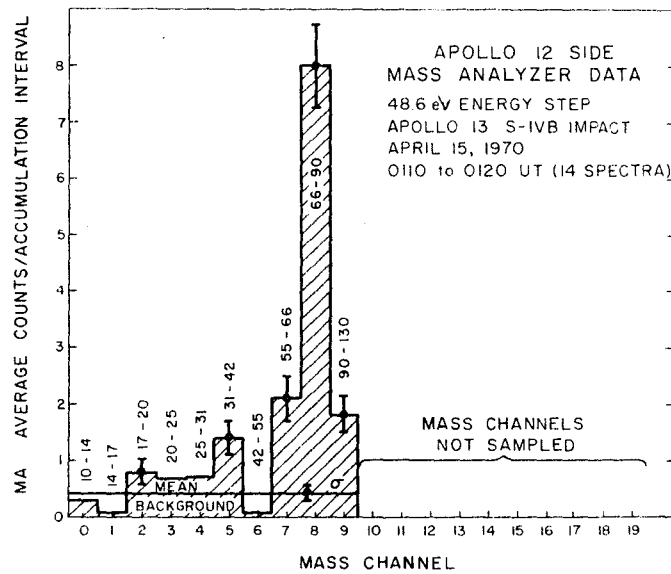


FIG. 10. Composite mass/ $q$  spectrum for the Apollo 13 S-IVB impact event. The same comments regarding mass/ $q$  ranges apply as stated for Fig. 5. At the time these data were taken the SIDE had been commanded into an operating mode where the sampling of channels 10 through 19 was eliminated.

near vertical direction by the SIDE was  $3 \times 10^7$  ions/cm<sup>2</sup>-sec-sr. The Solar Wind Spectrometer (another ALSEP experiment) saw much higher fluxes arriving simultaneously from more nearly horizontal directions (C. Snyder, private communication). If one assumes the entire

mass of the Apollo 13 S-IV B stage,  $1.34 \times 10^4$  kg (Marshall Space Flight Center Report, 1970), to represent the mass of the vaporized material a conservative upper limit estimate can be obtained for the expected ion flux due to classical photoionization and charge-exchange reactions.

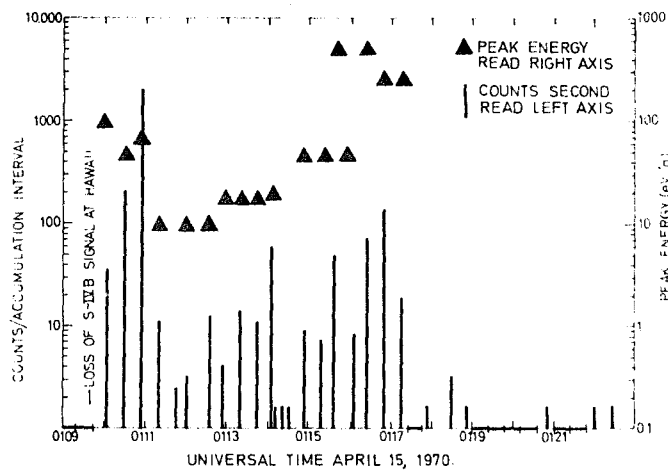


FIG. 11. Time history of the TID response following the Apollo 13 S-IVB lunar impact. The vertical bars are the peak counting rate in a given energy/ $q$  spectrum and the triangles indicate the energy at which the peak count occurred.

Assuming a spherical gas cloud whose radius is the distance from ALSEP to the impact point this estimate is  $10^6$  ions/cm<sup>2</sup>-sec-sr; at least one order of magnitude below the observed flux. This discrepancy suggests the need for an anomalous interaction mechanism between the neutral gas cloud and the solar wind. Such a mechanism has been proposed by Alfvén (1954) whereby when the relative velocity between a plasma (in this case the solar wind) and a neutral gas in a magnetic field exceeds a critical value highly efficient ionization of the gas takes place. This phenomenon is being investigated by the Stockholm group (Danielsson, 1970; Fahleson, 1961). Manka and Michel (1970) have discussed the acceleration fate of lunar exospheric ions as a result of the interplanetary electric field however in the present case the rapid ionization must also be explained.

## VI. SUMMARY

Several examples now exist of energized ions of mass/ $q$  greater than singly ionized hydrogen or multiply ionized heavier elements close to the lunar surface. While most of these can be identified with man's activities pertaining to the Moon at least one event may have had a natural origin and is suggestive of a transient lunar surface gas emission.

A most important universal feature of these events is that the ions appear promptly and are found in a substantially accelerated state. This indicates the activity of one or more important ionization and acceleration mechanisms such as acceleration by the interplanetary electric field or an anomalous interaction with the solar wind. Such mechanisms must be taken into account in calculations of planetary atmospheric losses and the gas content of lunar rocks.

For the case of the Apollo rocket exhaust gases preliminary data indicate a mean lifetime for the heavier gas components of about one month.

Finally we again wish to emphasize the preliminary nature of these interpretations of a large body of data of which only a small fraction has been examined to date.

## ACKNOWLEDGMENT

The authors would like to acknowledge the help of Dr. H. Balsiger in the calibration and interpretation of the SIDE data.

This research was supported by NASA Contract NAS 9-5911, Rice University, Houston, Texas, and the Royal Institute of Technology, Stockholm, Sweden.

(Authors' note: Since the preparation of this paper additional data have been obtained supporting the conclusion regarding transient lunar surface gas emission [New York Times, 1971]. Rather than update the present manuscript, for historical reasons, the authors prefer to submit the paper in its present form.)

## REFERENCES

- ALFVÉN, H. (1954). "On the Origin of the Solar System." Oxford University Press.
- ASBRIDGE, J. R., BAME, S. J., AND STRONG, J. B. (1968). Outward flow of protons from the Earth's bow shock, *J. Geophys. Res.* **73**, 5777.
- CHANG, G. K. (1969). Lunar Atmosphere Contamination Due to an Apollo Landing. Belconm Rept. TM-69-2015-5.
- DANIELSSON, L. (1970). Experiment on the interaction between a plasma and a neutral gas. *Phys. Fluids* **13**, 2288.
- FAHLESON, U. V. (1961). Experiments with plasma moving through neutral gas. *Phys. Fluids* **4**, 123.
- FENNER, MARTHA A., FREEMAN, J. W., JR., HILLS, H. K., MEDRANO, R. A., AND LINDEMAN, R. A. (1971). Magnetosheath plasma observations at the Moon's surface. *EOS* **52**, 326.
- FREEMAN, J. W., JR., BALSIGER, H., AND HILLS, H. K. (1970). Suprathermal Ion Detector Experiment Apollo 12 Preliminary Science Report, NASA SP 235, Section 6.
- FREEMAN, J. W., JR., AND HILLS, H. K. (1970). Positive Ions at the Apollo 12 ALSEP site resulting from the Apollo 13 S-IV B Impact. *EOS* **51**, 821.
- FREEMAN, J. W., JR., HILLS, H. K., AND FENNER, M. A. (1972). Same results from the Apollo 12 suprathermal ion detector. *Proc. Apollo 12 Lunar Sci. Conf. Houston, January 1971*. The MIT Press.
- FREEMAN, J. W., JR. (1972). Energetic ion bursts on the night side of the Moon. *J. Geophys. Res.*, **77**, 1.
- GARRETT, H. B., HILL, T. W., AND FENNER, M. A. (1971). Plasma-sheet ions at lunar

- distance preceding substorm onset. *Planet. Space Sci.* **19**, 1413.
- HILLS, H. K., AND FREEMAN, J. W., JR. (1971). Suprathermal Ion Detector Experiment. Apollo 14 Preliminary Science Report, NASA SP-272, Section 8.
- JOHNSON, F. S., EVANS, D. E., AND CARROLL, J. M. (1971). Cold-Cathode-Gage Experiment, Apollo 14 Preliminary Science Report, NASA, SP-272, Section 9.
- LINDEMAN, R. A., FREEMAN, J. W., JR., AND HILLS, H. K. (1971). Recurring ion clouds at the lunar surface. *EOS* **52**, 340.
- MANKA, R. H., AND MICHEL, F. C. (1970). Lunar atmosphere as a source of argon-40 and other lunar surface elements. *Science* **169**, 278-280.
- Marshall Space Flight Center Report MPR-SAT-Fe 70-2, 1970.
- New York Times* (1971). Water vapor found on the Moon, 16 October, p. 1.
- O'BRIEN, BRIAN J., AND REASONER, DAVID L. (1971). Charged-Particle Lunar Environment Experiment, Apollo 14 Preliminary Science Report, NASA SP-272, Section 10.
- SIMONEIT, B. R., BURLINGAME, A. L., FLORY, D. A., AND SMITH, I. D. (1969). Apollo lunar module engine exhaust products. *Science* **166**, 733-738.





# OBSERVATIONS OF WATER VAPOR IONS AT THE LUNAR SURFACE\*

J. W. FREEMAN, JR., H. K. HILLS, R. A. LINDEMAN, and  
R. R. VONDRAK

*Dept. of Space Science, Rice University, Houston, Tex., U.S.A.*

(Received 7 December, 1972)

**Abstract.** The Apollo 14 Suprathermal Ion Detector Experiment observed a series of bursts of 48.6 eV water vapor ions at the lunar surface during a 14-h period on March 7, 1971. The maximum flux observed was  $10^8$  ions  $\text{cm}^{-2} \text{s}^{-1} \text{sr}^{-1}$ . These ions were also observed at Apollo 12, 183 km to the west. Evaluation of specific artificial sources including the Apollo missions and the Russian Lunokhod leads to the conclusion that the water vapor did not come from a man-made source. Natural sources exogenous to the Moon such as comets and the solar wind are also found to be inadequate to explain the observed fluxes. Consequently, these water vapor ions appear to be of lunar origin.

## 1. Introduction

The existence of water at or beneath the lunar surface is a question of great importance in theories of formation of lunar surface features and of the Moon itself (cf. Urey, 1969 for a review). If the Moon were devoid of water now or in the past it would be unique among the terrestrial (i.e. high density) planets about which detailed information is now available. At the Third Lunar Science Conference we presented preliminary observational evidence for the occurrence of endogenous water vapor at the lunar surface (Freeman *et al.*, 1972b). In this paper we review this evidence, present a more detailed description of the event, and discuss more completely arguments pertaining to the identification of the source.

The Apollo 14 Suprathermal Ion Detector Experiment (SIDE), part of the Apollo Lunar Surface Experiments Package (ALSEP), observed ions of mass 18 amu/q during an event of approximately 14 hours duration on March 7, 1971. Because of their mass per unit charge, these ions are believed to be constituents of the water vapor group. Several gas sources associated with the Apollo 14 mission one month earlier have been suggested as possible sources of this water vapor. However, all of these appear to us to be inadequate to explain the observed phenomena.

The SIDE consists of two positive-ion detectors: the mass analyzer (MA) and the total ion detector (TID). The location of the Apollo 12 and 14 SIDEs and the concept of acceleration of ions into the instruments are illustrated in Figure 1. The MA consists of a velocity filter and an energy per unit charge (energy/q) filter followed by an ion detection system. The velocity filter and energy/q filter are sequenced through a series of steps to provide coverage of twenty mass/q ranges at each of six energy/q steps: 0.2, 0.6, 1.8, 5.4, 16.2 and 48.6 eV/q. The TID is an ion energy/q spectrometer that records ions without mass discrimination in 20 differential energy channels from

\* Paper dedicated to Prof. Harold C. Urey on the occasion of his 80th birthday on 29 April 1973.

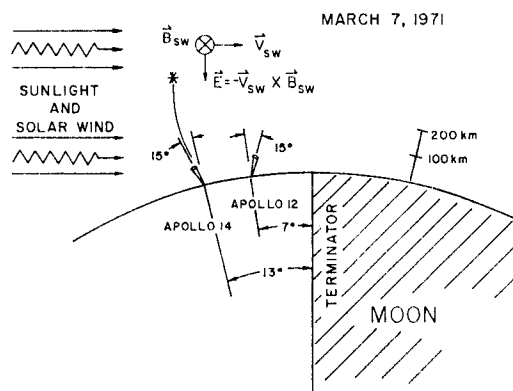


Fig. 1. Conceptual operation of the SIDE as a mass spectrometer, showing geometry of the March 7 event. Photo-ionization by solar UV and charge exchange processes with the solar wind ionize the lunar exosphere. These ions are then accelerated by the interplanetary electric field associated with the motion of the solar wind (Manka and Michel, 1970; Manka, 1972), as illustrated, or some other acceleration mechanism operating in the lunar environment. Full details of the operation of the SIDE can be found in Freeman *et al.* (1970), and Hills and Freeman (1971).

3500 eV/q down to 10 eV/q. The lowest energy channels can be used as a check on the MA data. Each SIDE has a field of view  $6^\circ$  square centered on a direction  $15^\circ$  from the local vertical. The Apollo 12 SIDE look direction is toward the west and the Apollo 14 SIDE views toward the east.

The efficacy of the SIDE system has been demonstrated by numerous observations of mass spectra associated with the LM rocket exhaust gases (Freeman *et al.*, 1972a), LM cabin venting (Hills and Freeman, 1971), and gas emission from the S-IVB and LM lunar impact events (Freeman *et al.*, 1971). The exhaust gas spectrum obtained 14 hours after the Apollo 12 LM landing exhibited a broad range of masses (Freeman *et al.*, 1972b), in good agreement with the laboratory measurements of Simoneit *et al.* (1969). As shown in Figure 2, two months later the exhaust gas ion intensities had decreased generally by an order of magnitude, but the spectrum was still very broad and readily identifiable as due to exhaust gases. There were several changes in the spectrum due to the operation of ionization, loss, dissociation, and recombination processes over the two months. Most striking was the disappearance of mass 18 ions and the appearance of a significant quantity of mass 16 ions. These mass 16 ions presumably came from the dissociation of the more massive molecules in the original spectrum; principally water vapor. For comparison, the maximum water vapor ion intensity observed by the Apollo 14 SIDE during the March 7 event is indicated in Figure 2 (see next page). It is more than *three orders of magnitude greater* than the intensity observed by the Apollo 12 SIDE 14 h after lunar landing.

## 2. Water Vapor Observations, March 7, 1971

The Apollo 14 MA data from the March 7 event are shown in Figure 3. The time

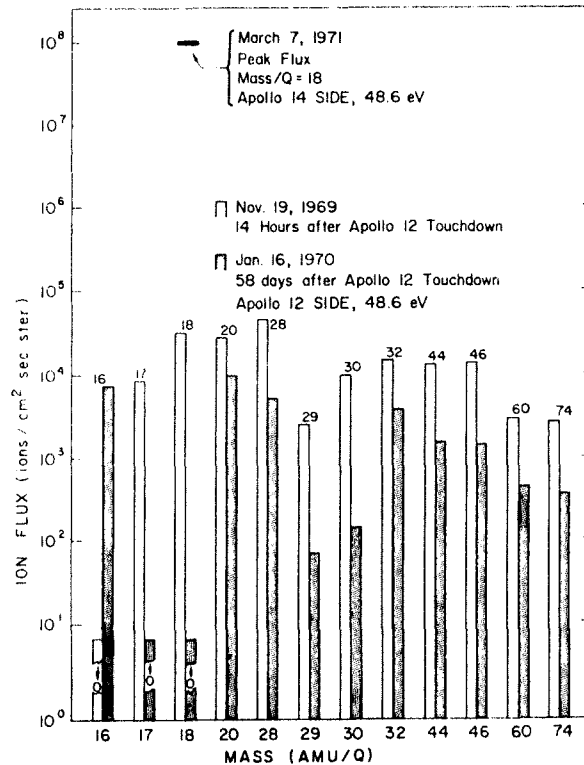


Fig. 2. Observed decrease in exhaust gas fluxes over a 58 day period. For comparison, the peak flux seen in the March 7 water vapor event is shown.

history of the events leads to a separation of the data into three parts. The mass spectra accumulated in each part are shown in the upper portion of the figure, together with the best fit to the observations, based on laboratory calibration data. In Part I, the accumulated spectrum can be fitted by a mixture of 85% mass 18 amu/q and 15% mass 16 amu/q while in Parts II and III the data is fitted well with 100% mass 18 amu/q. For Part I a fit including a percentage of mass 17 amu/q is also possible but presses the resolution of the experiment. This apparent change in the mass spectrum during the event is suggestive of the injection of fresh gas and thereby a dynamic rather than a static event.

The Apollo 14 TID recorded data consistent with that of the MA, showing sporadic bursts of low energy ions throughout the event. Figure 4 shows two successive energy spectra obtained with the TID. The broad high energy spectrum at 250–1000 eV is due to ions in the Earth's magnetosheath, and is not of interest in this event. The important feature is the high mono-energetic flux of low-energy ions (70 eV in this spectrum). The narrow low-energy portion of the spectrum occurred at various energies, but usually was observed in only one channel at a time (at 30, 50, or 70

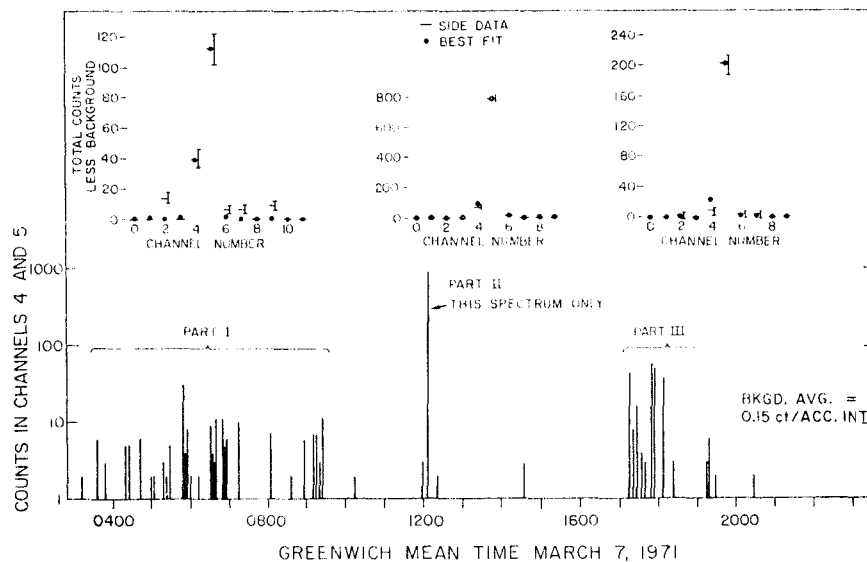


Fig. 3. Time history of the Apollo 14 Mass Analyzer data for the March 7 water vapor event. Laboratory calibrations indicate that water vapor ions are recorded primarily in channel 5 of this instrument with channel 4 recording approximately 12% as many counts. Consequently, to show the principal features of the March 7 event, the total counts in adjacent channels 4 and 5 at 48.6 eV are displayed in the lower portion of the figure. Ions were observed during the March 7 event only at the highest energy level, 48.6 eV, and not at the next lower level, 16.2 eV. Twenty-channel mass spectra at 48.6 eV were obtained in 24 s every 2.58 min. Insets display the observed mass spectra summed over each part of the event as well as a fit to the observations. One count in channel 5 corresponds to a flux of  $\text{H}_2\text{O}^+$  of  $1.2 \times 10^5 \text{ ions cm}^{-2} \text{ s}^{-1} \text{ sr}^{-1}$ .

eV/q). The two illustrated spectra indicate the sporadic nature of this flux.

The SIDE MA at the Apollo 12 site 183 km to the west (see Figure 1) was quite noisy at the time, so no usable mass spectra were obtained. There was, however, good correlation between the TID responses of the two instruments during the event. Both instruments detected significant fluxes starting at 0300-0400 UT on March 7. The Apollo 14 SIDE was turned off at 2100 UT on March 7, according to its scheduled cycle for thermal control. The Apollo 12 SIDE continued to detect ions until the end of the event at ~0400 UT on March 8. The time history of the TID data is indicated in Figure 5. The ion energies observed at the Apollo 12 site during Part I of the event were higher than those at Apollo 14, being generally in the 100 eV/q and 250 eV/q channels, whereas the energies at Apollo 14 were in the range 50 eV/q to 100 eV/q. During Part II of the event the energies observed by the Apollo 12 TID decreased to a level matching those observed at the Apollo 14 site. Again we see the suggestion of a dynamic rather than a static event. Fluxes observed by the Apollo 12 TID were typically  $1\text{--}5 \times 10^5 \text{ ions cm}^{-2} \text{ s}^{-1} \text{ sr}^{-1}$ , while the Apollo 14 TID detected typical fluxes of  $4\text{--}10 \times 10^5 \text{ ions cm}^{-2} \text{ s}^{-1} \text{ sr}^{-1}$ . Peak fluxes for each instrument were generally about 5 times greater than these typical fluxes.

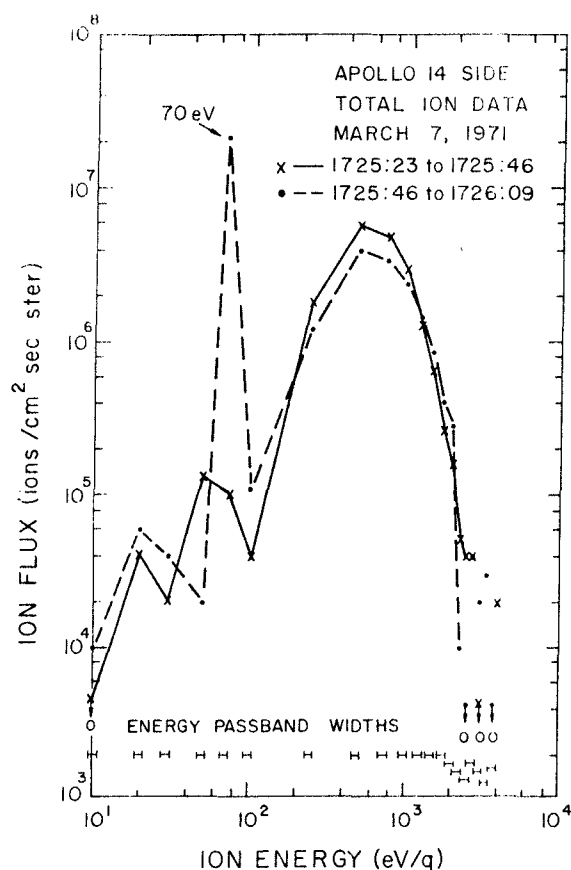


Fig. 4. Total Ion Detector data from the Apollo 14 SIDE for two successive spectra during the March 7 event. The width of an energy channel is approximately 10% FWHM. The peak at 70 eV corresponds to the water vapor ions seen in the mass analyzer. The broad spectrum peaking near 500 eV is that of magnetosheath ions and occurs independently of the water vapor ions.

Simultaneous with the SIDE observations, ions were also detected by the Charged Particle Lunar Environment Experiment (CPLEE). The CPLEE has two charged particle analyzers, one of which looks in a vertical direction and the other 60° west of vertical. The low energy (60–300 eV/q) detectors of both analyzers recorded an apparently isotropic flux of ions between ~0400 UT, March 7 and ~0900 UT, March 8 with maximum fluxes between 1200 UT and 1600 UT on March 7 (F. Rich and D. Reasoner, private communication). Fluxes of such low energy ions are not normally detected by CPLEE in this portion of the lunar orbit due to the high threshold of the low energy ion channels and large angle between the magnetosheath flow direction and instrument look direction. A complete analysis of the CPLEE data and calculations of the total flux have not yet been made.

### 3. Comparison with Electric Field Data

In an attempt to determine whether the sporadic nature of the March 7 event was due to either an intermittent source or simply a variability in observing conditions, the ion data have been compared with simultaneous data concerning the interplanetary electric field. The interplanetary electric field  $\mathbf{E}$  is related to the solar wind velocity  $\mathbf{V}$  and magnetic field  $\mathbf{B}$  by the expression  $\mathbf{E} = -\mathbf{V} \times \mathbf{B}$ . It has been shown (Manka *et al.*, 1972; Manka, 1972) that this electric field can be an important acceleration mechanism for ions produced in the lunar exosphere. The interplanetary electric field undergoes rapid temporal fluctuations in both magnitude and direction. Consequently, temporal variations in the ion observations could be a result of changes in the solar wind parameters rather than changes in the source of the ions.

The solar wind data, the MA data, and the TID data are shown in Figure 5. The solar wind magnetic field data was measured by Explorer 35 in lunar orbit and was generously supplied by Dr David Colburn. The solar wind velocity as recorded by the Apollo 14 Solar Wind Spectrometer varied between 275 and 340 km s<sup>-1</sup> during the March 7 event (Conway Snyder, private communication). Since only the magni-

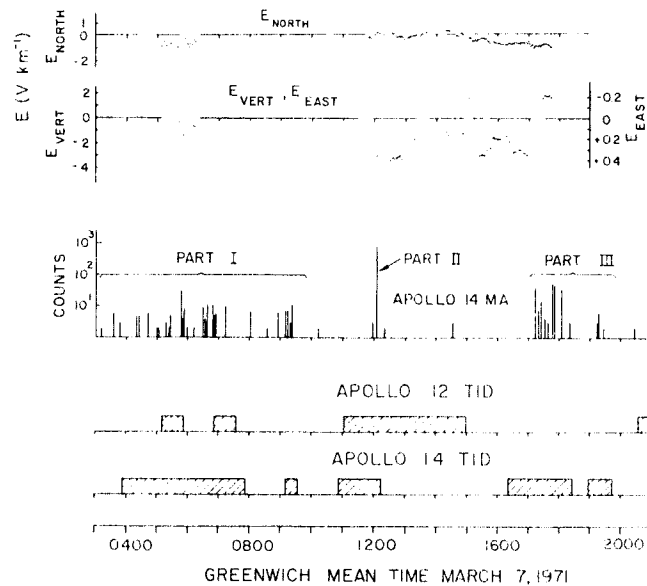


Fig. 5. Comparison of SIDE data and the interplanetary electric field on March 7, 1971. The electric field is derived from 1 min 22 s averages of the magnetic field measured by Explorer 35 in lunar orbit. The time delay between field fluctuations measured in lunar orbit and at the lunar surface is estimated to be less than one minute. Gaps in the electric field data result from unavailability of magnetometer data during these times. The three components of the electric field are given in the local coordinate system at the Apollo 14 site. A negative vertical electric field would accelerate positive ions towards the lunar surface. The MA data is the same as that shown in Figure 3. Periods when significant low-energy ion fluxes were observed in the Apollo 12 and 14 SIDEs are indicated.

tude of the electric field and not its direction is related to the solar wind speed, a uniform speed of  $300 \text{ km s}^{-1}$  has been assumed in computing the electric field components.

In the simplest model of ion acceleration by the interplanetary electric field, the field orientation most favorable for ion detection would be one in which the field is pointed directly into the instrument look angle. This requires a negative vertical component and a zero (or small) northward component.

From the data comparison we see that there is some positive correlation between the ion data and the interplanetary electric field vector. In particular, the large vertical field near 1200 UT corresponds very well with the large ion flux (Part II) observed at that time. Also, some of the sporadic ion activity in Part I correlates with times of favorable electric field orientation. However, there are periods from 1200 to 1600 UT when the field was favorable for acceleration of ions into the detectors, but no ions were detected. Also, ions were observed in the Apollo 12 instruments during the period following 1700 UT when the electric field was oriented so as to accelerate ions away from the lunar surface. This is true for all of Part III of the event for which data is available. A lack of simple correlation with the interplanetary electric field is further indicated by the fact that the observed ions were nearly monoenergetic, while acceleration of ions in an exponential atmosphere by a uniform electric field would result in a broader energy distribution (Manka, 1972). Thus, the features of the ion observations for this event are not completely determined by the interplanetary electric field vector. Numerous other examples exist in the SIDE data where the surface gas pressure is enhanced and massive ions are seen regardless of a favorable or unfavorable interplanetary electric field (Freeman *et al.*, 1972a). Until the acceleration mechanism operating in the lunar environment at that time is well understood, we will be unable to determine whether the sporadic nature of the March 7 event is due to the source or the acceleration mechanism.

Mass separation of ions may occur in the local surface magnetic fields, resulting in the apparent mass purity of an event, while in fact a mixture of ions is present. However, a preliminary estimate of such effects indicates that it would be difficult to produce a significant mass separation. Moreover, in light of the large fluctuations in the interplanetary electric field, it would be extremely difficult to maintain any mass separation for the duration of the March 7 event.

#### 4. Quantity of Water

It is of course desirable to have some estimate of the total quantity of water represented in this event. The SIDE is an *ion* detector and determination of the quantity of *neutral* gas present requires certain assumptions. A lack of knowledge of the location and extent of the source and the details of the ionization and acceleration mechanisms precludes a precise quantitative determination. However, we have looked for a similar event where the quantity of gas released is known in order to 'calibrate' the water vapor event. In general, Apollo mission activities have resulted in counting



rates far lower than those seen on March 7. For example, the Apollo 12 LM exhaust introduced approximately 2000 kg of water into the lunar environment, yet when observed 14 h after landing resulted in an ion flux that was less than one thousandth the peak flux seen on March 7.

The only event that yielded MA counting rates as high as those during the March 7 event was the detection of the Apollo 14 LM ascent engine exhaust gases by the Apollo 12 SIDE (Hills and Freeman, 1971). The Apollo 14 SIDE was not operating at that time. The maximum counting rates for this event in both the TID and MA were within a factor of 2 of those for the March 7 event and the ion energies were comparable. However, the ion flux duration was only 2 min compared to some 14 h (intermittent) for the March 7 event. Ions were recorded starting 1 minute after the LM had passed by the minimum slant range of 27 km at an altitude of approximately 15 km. The total gas released by the LM was approximately 2200 kg (of which  $\sim 500$  kg was water) at a constant emission rate of  $5.2 \text{ kg s}^{-1}$  ( $1.1 \text{ kg s}^{-1}$  of  $\text{H}_2\text{O}$ ). Therefore, if we assume equivalent ion accelerating conditions for the two events and if the water vapor source was no closer than 27 km we conclude that *at least* 500 kg of water was involved in the March 7 event. Alternatively, if an emission rate of  $1 \text{ kg s}^{-1}$  of  $\text{H}_2\text{O}$  was maintained on March 7 for a period of 14 h, a total water emission of the order of  $10^4$  kg is implied. The source characteristics and accelerating conditions (including ion trajectories) may be greatly different in the two events. Consequently, this estimate of the source strength may be in error. However, given a non-local source, as discussed below, these quantities serve as reasonable preliminary estimates.

### 5. The Apollo Lunar Module as a Possible Source

The mass spectra of LM exhaust shown in Figure 2 indicate that the exhaust spectrum is readily identifiable by its broad mass range, and does not resemble the spectrum obtained in the March 7 event. This fact, together with the unprecedented intensity of the latter event, indicates that the March 7 event was not due to LM exhaust gases. Separation of the  $\text{H}_2\text{O}$  in the LM exhaust from the other exhaust components could conceivably result from selective adsorption of the water onto the lunar surface followed by selective emission. However, such a mechanism, which could explain the purity of the event, fails to account for the more than three orders of magnitude increase between the  $\text{H}_2\text{O}$  fluxes measured 14 h after the LM exhaust release and those seen on March 7, one month after the Apollo 14 mission.

The maximum flux of water vapor ions observed at the Apollo 14 SIDE during this event was approximately  $10^8 \text{ ions cm}^{-2} \text{ s}^{-1} \text{ sr}^{-1}$ . For comparison, when the LM cabin was vented during the Apollo 14 mission prior to the 2nd EVA, the SIDE observed a short-lived (approximately one minute) flux of  $4 \times 10^5 \text{ ions cm}^{-2} \text{ s}^{-1} \text{ sr}^{-1}$  at 50 eV. At the same time the ALSEP Cold Cathode Gauge Experiment (CCGE) measured a high neutral gas pressure (Johnson *et al.*, 1971). This is important, for it establishes that the CCGE would have seen a large neutral gas pressure rise if enough gas were liberated *locally* to cause the high counting rate seen by the SIDE on March

7. There was no such increase (Johnson *et al.*, 1972) therefore the source must have been further away than the LM or the other debris left on the surface nearby. A gas source at a great distance could lead to the production of ions which subsequently reach the SIDE, while the neutral gas density at the instrument might never be high enough to be observed by the CCGE. The simultaneous observation of the event by the Apollo 12 SIDE further implies a distant or wide-spread source.

### 6. The Apollo CSM as a Possible Source

The 43 kg of waste water, mostly excess  $\text{H}_2\text{O}$  from the fuel cells, (C. Staresinich, private communication) dumped from the Apollo 14 Command/Service Module (CSM) in lunar orbit one month earlier has been suggested as a possible source (F. El-Baz, private communication; Page, 1972). An attractive feature of such a source is the presumed narrow altitude distribution of gas, resulting in a narrow energy spectrum after acceleration through an electric field. However, we note that a narrow altitude distribution is not a prerequisite for the narrow energy spectrum observed, since a narrow energy spectrum seems to be a general feature of heavy mass ion events *regardless of the source*. For example, narrow energy spectra of approximately 50 eV energy have been observed during the Apollo 14 cabin vent (Hills and Freeman, 1971), in association with Apollo 12 LM exhaust (Freeman *et al.*, 1970), and also at times when the source is less obvious (Freeman *et al.*, 1972b). Furthermore, as shown in Figure 5, the interplanetary electric field strength was  $\sim 3\text{V km}^{-1}$  at 1200 GMT on March 7. Thus, if the observed 50–70 eV water vapor ions seen at that time resulted from simple vertical acceleration, they were produced at an altitude of 15–25 km. This is much lower than the 100 km orbit of the CSM.

Most of the water dumped from the CSM will freeze promptly and then rapidly vaporize by sublimation. Sharma and Buffalano (1971) estimate the *e*-folding lifetime of the ice crystals to be less than 30 h. Exposure of this water vapor to the solar ultraviolet and the solar wind particles results in the production of  $\text{H}_2\text{O}^+$  ions as well as the dissociation of  $\text{H}_2\text{O}$  into H and OH. Later the production of  $\text{OH}^+$ , and finally that of  $\text{O}^+$ , will dominate as further dissociation and ionization takes place and as the quantity of  $\text{H}_2\text{O}$  becomes depleted. Figure 6 shows the calculated rates of production for these ions as a function of ultraviolet exposure time. If the event of March 7 were due to water ejected from the Apollo 14 CSM a month earlier, then ions of masses 16 and 17 would be more abundantly produced than ions of mass 18, contrary to observation. In fact, in Part I of the event there is an indication of mass 16 and possibly mass 17 ions, but only a small amount. The later parts of the event showed only mass 18 ions. As was noted earlier, this change of spectrum is suggestive of a possible injection of fresh gas during the event.

The ion flux expected at the SIDE due to the CSM water dump can be estimated as simply the total number of 50 eV ions formed in one second in the  $\text{cm}^2$  column over the detector. If all of the ice had become vapor within a few days, dissociation and ionization by solar UV at a rate of  $10^{-5}\text{ s}^{-1}$  (Werner *et al.*, 1964) would reduce the

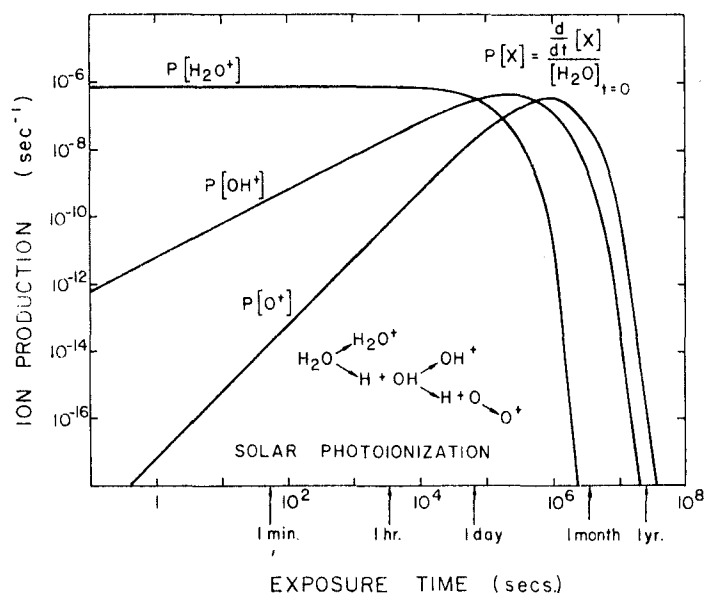


Fig. 6. Production rates of ions resulting from exposure of water to solar ultraviolet at the Moon. These curves are obtained from solution of the differential equations describing the depicted reaction chain. Production rates are normalized to the initial number of  $\text{H}_2\text{O}$  molecules; the change in production rate is due to the change in composition. The appropriate reaction rates were obtained from Hinteregger (1960), Werner *et al.* (1967), and Mukherjee and Siscoe (1973).

initial 43 kg of water to about  $4 \times 10^{15}$  molecules of  $\text{H}_2\text{O}$ . Also, since the counting rates in Part I of the ion event were present for longer than the 2-h orbital period of the CSM, then if the source gas was in orbit it must have been dispersed relatively uniformly throughout the orbital path. (After one month the gas cloud would be expected to be widely dispersed since the molecular sublimation velocity is about  $\frac{1}{3}$  of the initial orbital velocity.) In this case the average volume rate of  $\text{H}_2\text{O}^+$  production is simply the number of neutral molecules times the ion production rate (Mukherjee and Siscoe, 1973) divided by the volume over which the original gas has become dispersed. A conservative estimate of this volume is  $4 \times 10^8 \text{ km}^3$ , obtained by assuming dispersal over 100 km in altitude along the initial orbit and  $10^\circ$  in latitude transverse to the orbit. Finally, integration over the narrow altitude range ( $\sim 1 \text{ km}$ ) in which the observed ions originate results in an upper limit on the flux measured by the SIDE of  $4 \times 10^{-8} \text{ ions cm}^{-2} \text{ s}^{-1} \text{ sr}^{-1}$ , much less than the observed peak flux of  $10^8 \text{ cm}^{-2} \text{ s}^{-1} \text{ sr}^{-1}$ .

F. El-Baz (private communication; Page, 1972) has suggested that the ice cloud remained intact for one month and then impacted the Moon due to orbital decay. We know of no way to inhibit sublimation for one month. However, even if we assume the worst case where dissociation and ionization do not begin until just at the time of observation (implying  $\sim 10^{27}$   $\text{H}_2\text{O}$  mole present), we obtain a flux of only  $2 \times 10^4 \text{ ions cm}^{-2} \text{ s}^{-1} \text{ sr}^{-1}$ . This is also an upper limit to the  $\text{OH}^+$  or  $\text{O}^+$  flux at any time.

Orbital decay is an additional mechanism for  $\text{H}_2\text{O}$  loss and would reduce the estimated ion fluxes, diminishing even further the possibility of the CSM being the source of the observations. Water molecules that impact the surface are equivalent to a surface source and can be ruled out as a possible source due to the small quantities involved.

We conclude that the CSM waste water dump is unlikely to be the source because it has been shown to lead to a counting rate much smaller than observed, and because consideration of the observation of the Apollo 14 LM ascent indicates a much greater quantity of water as the source. Also the appeal of the CSM as a source is diminished when it is recognized that a narrow altitude distribution for the gas is not required. Furthermore, the time history of the event suggests an impulsive injection of fresh gas during the event, long after the CSM has left the Moon.

### 7. The Lunokhod as a Possible Source

It has been brought to our attention (K. P. Florensky, private communication) that the Russian Lunokhod research vehicle (located approximately 1400 km from Apollo 14) occasionally vents 'a few liters' of water from its cooling system.

After a quantity of water vapor  $N_0$  is released from the Lunokhod it will diffuse outward from the landing site. The water molecules move along ballistic trajectories in the lunar exosphere, traveling a distance  $L$  of  $\sim 300$  km in a time  $\tau$  of  $\sim 600$  s. between contact with the surface. This diffusing cloud of water vapor will expand to a radius  $R$  of 1400 km in a time equal to  $R^2\tau/L^2 \approx 4$  h (cf. Hall, 1973). An upper limit to the height-integrated density (mole  $\text{cm}^{-2}$ ) at a distance  $R$  of 1400 km is given by  $N_0/\pi R^2 = 1.6 \times 10^{-7} N_0$ . This value is an upper limit since in such a diffusion process, the columnar density is always greater the nearer to the source point (Hall, 1973). This upper limit equals  $5 \times 10^8$  mole  $\text{H}_2\text{O cm}^{-2}$  for each liter of  $\text{H}_2\text{O}$  released and is a factor  $10^3$  smaller than the columnar density of the ambient lunar exosphere (Johnson, 1971). It would result in a count rate for the SIDE MA of  $\sim 0.02$  counts  $\text{s}^{-1}$ . Thus, the Lunokhod ventings are not sufficiently large enough to account for the March 7 event.

### 8. Comets and the Solar Wind as Possible Sources

Having considered all artificial sources we will now evaluate two natural sources which are exogenous to the Moon: comets and the solar wind.

An impact of a comet or cometary debris could be a source of water vapor in localized areas of the Moon. The impact of a solid comet of a mass of a thousand kilograms (the approximate mass of water inferred for this event) on March 7, can be firmly ruled out by the lack of any seismic activity characteristic of such an impact. Furthermore, March 7 is neither a date of known meteor showers nor a date when the Earth-Moon system is near known old comet orbits (Thornton Page, private communication). Also, comets and comet remnants contain significant quantities of other materials, such as  $\text{CO}_2$ , which were not detected during the March 7 event. Conse-

quently, it appears unlikely that a comet or cometary remnant could be the source of the observed water.

Interactions between the solar wind and the lunar material as a source of water at the lunar surface was suggested by Michel (1964). The details of such a production mechanism have been evaluated by Mukherjee and Siscoe (1973) who concluded that the maximum density of the solar wind-produced  $\text{H}_2\text{O}$  near the lunar surface would be about  $6 \times 10^{-3} \text{ cm}^{-3}$ , a factor of  $10^7$  smaller than the ambient lunar exospheric density (Johnson, 1971). Thus, the solar wind is an insufficient source for the March 7 observations.

### 9. The Moon as a Possible Source

Examination of the lunar samples has indicated them to be remarkably devoid of water (Lunar Sample Preliminary Examination Team, 1969, 1970). However, at least one hydrated mineral has been found in the Apollo 14 surface samples (Agrell *et al.*, 1972). Further, preliminary analysis of the Apollo 16 soil samples from the Descartes region indicates large amounts of hydrated minerals (Gregory, 1972). It has been suggested that a comet impact may have been responsible for the Apollo 16 results. However, Williams and Gibson (1972) have raised some questions regarding the chemical feasibility of such a process.

The high orders of hydrogen and oxygen in the cosmic and solar abundances of the elements lead to the expectation of water as a common constituent of the planets. Possible exceptions would occur if extremely efficient defluidization or loss processes have been operable (see Green, 1964 for a review of defluidization processes on the Moon) or if the Moon accreted inhomogeneously as an original satellite of the Earth (Anders, 1970).

There have been numerous suggestions of subsurface water on the Moon, trapped below an ice layer beneath the lunar surface (Gold, 1960; Green, 1964; Schubert *et al.*, 1970) and liberated occasionally by the flexing or fracture of the lunar crust. The so-called Lunar Transient Phenomena have been shown (Moore, 1971) to occur with a preference for times near lunar perigee passage and at likely positions for crustal stress. There were seismic signals ('swarms', not due to impact events) observed by the Passive Seismic Experiment during this event (G. Latham, private communication), although such seismic signals have been observed many times without simultaneous observations of high ion intensities. Thus there may be no meaningful relation between the seismic signals and the water vapor event. However, there is a possibility that such seismic signals are linked to a release of gas, but that the probability for the gas to be eventually detected as ions by the SIDE is quite low. If the acceleration of the ions occurs as illustrated in Figure 1 and discussed by Manka and Michel (1970), then the SIDE can detect the ions only when the interplanetary electric field points approximately antiparallel to the local vertical. This can occur only within a few days of sunrise and sunset and when the interplanetary magnetic field points nearly normal to the ecliptic plane. The magnetic field can be expected to have the correct direction less than 2% of the time (Burlaga and Ness, 1968). In addition, the

gas source must be large enough and near enough to produce observable fluxes of ions. Thus the probability that a random venting of gas will result in ions observed by the SIDE is quite low if the solar wind electric field is the only acceleration mechanism.

We emphasize that the March 7 event was an intense event of extended duration and we have not yet seen another event like it. The question of lunar venting vs. artificial sources would be more unambiguously resolved if another event similar to that of March 7 were found displaced further in time from an Apollo mission. Although there exist a few other events which may be attributable to transients in the lunar atmosphere, none of these has yet been found to include water vapor as a constituent. Since water vapor is the subject of this paper, these will be discussed in a future report.

### 10. Conclusions

None of the suggested artificial sources for the observed water ions appears to us to be capable of producing the observed ion fluxes. Table I lists the prominent source candidates and the objections to each. Therefore, we conclude that the only possible source is a natural source endogenous to the Moon.

TABLE I

Source	Difficulties
LM	1. event duration and intensity 2. simultaneous observation at 2 sites 3. not observed by CCGE
Residual exhaust gases	1. event intensity 2. exhaust spectrum maintains identity for at least 58 days, with H <sub>2</sub> O dissociation 3. time history suggests impulsive injection of fresh gas during event
CSM waste water	1. event intensity and duration 2. interplanetary electric field strength implies source altitude lower than CSM orbit 3. narrow altitude distribution not required in order to explain observed narrow energy spectrum 4. time history suggests injection of fresh gas during event
Lunokhod	1. event intensity
Comets	1. no known cometary impact or cometary remnant 2. event purity
Solar wind	1. event intensity
Moon	???

### Acknowledgements

We are grateful to Drs D. Colburn, C. Snyder, and D. Reasoner for allowing us access to their data. F. Rich provided much useful information concerning interpretation of the CPLEE data and magnetometer data. Discussion with members of the Rice University Space Science Department and the staff of the Royal Institute of Technol-

ogy in Stockholm were also useful in the interpretation of the data. Dr Hans Balsiger was helpful in various portions of the data analysis. One of us (JWF) was a Visiting Scientist at the Lunar Science Institute in Houston during the preparation of this paper. This work was supported by NASA contract NAS9-5911.

### References

- Agrell, S., Scoon, J., Long, J., and Coles, J.: 1972, in C. Watkins (ed.), *Lunar Science III*, p. 7, Lunar Sci. Inst. Contrib. No. 88.
- Burlaga, L. and Ness, N.: 1968, *Can. J. Phys.* **46**, 5962.
- Freeman, J. W., Jr., Balsiger, H., and Hills, H. K.: 1970, 'Suprathermal Ion Detector Experiment', in *Apollo 12 Preliminary Science Report*, NASA SP-235, 83.
- Freeman, J. W., Jr., Hills, H. K., and Fenner, M. A.: 1971, *Proc. 2nd Lunar Sci. Conf., Geochim. Cosmochim. Acta, Suppl.* **2**, 3, 2093.
- Freeman, J. W., Jr., Fenner, M. A., Hills, H. K., Lindeman, R. A., Medrano, R., and Meister, J.: 1972a, *Icarus* **16**, 328.
- Freeman, J. W., Jr., Hills, H. K., and Vondrak, R. R.: 1972b, *Proc. 3rd Lunar Sci. Conf., Geochim. Cosmochim. Acta, Suppl.* **3**, 3, 2217.
- Gold, T.: 1960, in Z. Kopal and Z. K. Mikhailov (eds.), 'The Moon', *IAU Symp.* **14**.
- Green, J.: 1964, 'Lunar Defluidization and Volcanism', North American Aviation Report SID 64-1340.
- Gregory, W.: 1972, *Av. Wk. Space Tech.* **97**, 15, 18.
- Hall, F. G.: 1973, *J. Geophys. Res.*, in press.
- Hills, H. K. and Freeman, J. W., Jr.: 1971, 'Suprathermal Ion Detector Experiment', in *Apollo 14 Preliminary Science Report*, NASA SP-272, 175.
- Hinteregger, H.: 1960, *Astrophys. J.* **132**, 801.
- Johnson, F. S.: 1971, *Rev. Geophys. Space Phys.* **9**, 813.
- Johnson, F. S., Evans, D. E., and Carroll, J. M.: 1971, 'Cold-Cathode-Gage Experiment', in *Apollo 14 Preliminary Science Report*, NASA SP-272, 185.
- Johnson, F. S., Evans, D. E., and Carroll, J. M.: 1972, *Proc. 3rd Lunar Sci. Conf., Geochim. Cosmochim. Acta, Suppl.* **3**, 3, 2231.
- Lunar Surface Preliminary Examination Team: 1969, *Science* **165**, 1211.
- Lunar Surface Preliminary Examination Team: 1970, *Science* **167**, 1325.
- Manka, R. H. and Michel, F. C.: 1970, *Science* **169**, 278.
- Manka, R. H., Michel, F. C., Freeman, J. W., Jr., Dyal, P., Parkin, C. W., Colburn, D. S., and Sonett, C. P.: 1972, in C. Watkins (ed.), *Lunar Science III*, p. 283, Lunar Sci. Inst. Contrib. No. 88.
- Manka, R. H.: 1972, 'Lunar Atmosphere and Ionosphere', Ph.D. Thesis, Rice University, Houston, Texas.
- Michel, F. C.: 1964, *Planetary Space Sci.* **12**, 1075.
- Moore, P.: 1971, 'Transient Phenomena on the Moon', *XVth General Assembly IUGG* (Moscow, 1971).
- Mukherjee, N. R. and Siscoe, G. L.: 1973, *J. Geophys. Res.*, in press.
- Page, T.: 1972, *Sky Telesc.* **43**, 145.
- Schubert, G., Lingenfelter, R., and Peale, S.: 1970, *Rev. Geophys. Space Sci.* **8**, 199.
- Sharma, R. D. and Buffalano, C.: 1971, *J. Geophys. Res.* **76**, 232.
- Simoneit, B. R., Burlingame, A. L., Flory, D. A., and Smith, I. D.: 1969, *Science* **166**, 733.
- Urey, H. C.: 1969, *Bull. Atom Sci.* **25**, 9, 46.





# Solar Cosmic Ray 'Square Wave' of August 1972

R. A. MEDRANO,<sup>1</sup> C. J. BLAND,<sup>2</sup> J. W. FREEMAN, H. K. HILLS, AND R. R. VONDRAK<sup>3</sup>

*Department of Space Physics and Astronomy, Rice University, Houston, Texas 77001*

Three Rice University suprathermal ion detector experiments (Sides) were deployed on the lunar surface during the Apollo 12, 14, and 15 missions. During the exceptional period of solar activity in August 1972, penetrating particles were observed by all Side detectors on the night side of the moon. The penetrating particles are tentatively identified as solar protons with energies ( $\sim 25$  MeV or greater) that were able to penetrate the shielding of all detectors. Of particular interest is the occurrence on August 5 of a 'square wave' flux enhancement of 2-hour duration. Data from a variety of ground-based and space experiments are examined in relation to the square wave. Based on the results of this investigation a model relating the square wave to the flare plasma propagation is proposed. This model hypothesizes transport of energetic particles along a 'corridor' formed by the tangential discontinuity produced by the driver gas of a flare-induced shock wave. This model could explain other frequently observed delayed particle events.

## INTRODUCTION

Early in August 1972 there occurred a series of impressive solar flares. The flares observed during this time were associated with some of the largest emissions of energetic particles ever recorded [McKinnon, 1972; *World Data Center A*, 1973]. Photospheric magnetograms indicated strong field activity during this period [Livingston, 1972]. Interplanetary space was disturbed with drastic changes in the solar wind [Wolfe *et al.*, 1972; Armstrong *et al.*, 1972; Rosenbauer *et al.*, 1972; Medrano *et al.*, 1973a] and in the interplanetary magnetic field [Colburn *et al.*, 1972; Smith *et al.*, 1972].

In this paper we present the analysis and results of the data taken by the Rice University suprathermal ion detector experiments (Sides) pertaining to one particular penetrating particle feature of the August event. The Sides were deployed on the lunar surface by the astronauts of Apollo 12, 14, and 15 and continuously transmit data to earth on the plasma environment of the moon. Since the Sides were not intended as solar cosmic ray detectors, the information provided by the instruments in this event is necessarily crude; however, the significance of the results to be discussed is not diminished.

## COSMIC RAY RESPONSE OF THE SIDES

Each Side instrument consists of two detectors, a mass analyzer (MA) and a total ion detector (TID). Together these measure the differential fluxes of positive ions in the energy range 0.2–3500 eV per unit charge. The sensors for these detectors are funnel-type channel electron multipliers manufactured by the Bendix Corporation. The channel electron multipliers have their entrance apertures biased at  $-3500$  V and hence can collect, accelerate, and count low-energy ions generated in or near the input funnel by penetrating radiation traversing the instrument side walls. The detectors thus become crude cosmic ray monitors. Further details of the Side design are given by Freeman *et al.* [1972] or Hills and Freeman [1971]. The Sides deployed at the three Apollo sites (12, 14, and 15) are essentially identical.

The shielding in the detector side walls is a complicated function of direction, since the absorbing material consists of electronic components, encapsulation material, thermal paint, etc. Accordingly, we have calculated the minimum energy that protons must have to penetrate to the sensor. We find that approximately 25-MeV protons are able to penetrate to the MA and 50-MeV protons to the TID. The equivalent numbers for electrons are 1.4 and 4.7 MeV, respectively.

To check these calculations, we placed a spare Side instrument in a cyclotron proton beam of 50-MeV maximum energy. The results indicated these to be good working numbers to within 50%. The cyclotron beam could not be used for absolute efficiency calibrations because of the short duration of the cyclotron beam pulse.

As a further independent check on the energy thresholds of the MA and TID detectors we have compared data on solar particle decay times with results from the proton detector aboard the Imp 5 and Imp 6 spacecraft [Kohl *et al.*, 1973]. These results indicate thresholds of  $32 \pm 7$  MeV and  $73.5 \pm 17$  MeV for the MA and TID, respectively.

The area of the channel electron multiplier funnel is approximately  $0.5 \text{ cm}^2$ . At 100% efficiency this yields an omnidirectional geometric factor  $G_0$  of  $0.5 \text{ cm}^2$ . The quiet nighttime background count rate of four of the six sensors is usually about 0.5 c/s or less. This is consistent with the calculated  $G_0$  and with most of the background being due to galactic cosmic rays.

During a separate solar cosmic ray event we compared the background count rate registered by the Side detectors with the omnidirectional solar proton flux measured by the ATS 1 spacecraft. In this case we found  $G_0 = 1.2 \pm 0.8 \text{ cm}^2$ . There are two reasons to suspect that this  $G_0$  is too high. First, the ATS 1 detector provided no information on protons above 70 MeV, and second, the investigators have reported the possibility of sensor degradation in the ATS 1 detectors [World Data Center A, 1972].

A more careful analysis of the galactic cosmic ray flux using the differential energy spectra of several investigators [Comstock *et al.*, 1972] compared with the long time average of the Side detector backgrounds taken on the night side of the moon gives the result  $G_0 = 0.3 \text{ cm}^2$ . We favor this result and believe it to be applicable to the August 1972 event to within a few factors of 2.

Figure 1 shows the location of the moon at the time of local

<sup>1</sup> Now at Instituto de Pesquisas Espaciais, 12200 São José dos Campos, São Paulo, Brasil.

<sup>2</sup> Permanent address: Physics Department, University of Calgary, Alberta, Canada.

<sup>3</sup> Now at Radio Physics Laboratory, Stanford Research Institute, Menlo Park, California 94025.

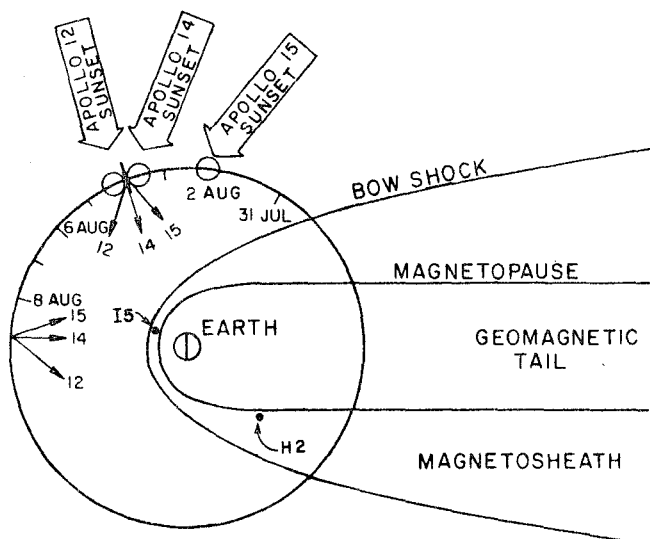


Fig. 1. Lunar orbit and the positions of the moon at the local sunsets of Apollo 12, 14, and 15. The data reported in this paper were obtained between the two positions where the detector look directions are indicated. The geomagnetic cavity is shown for reference, and the positions of the Imp 5 and Heos 2 spacecraft on August 5 are indicated by I5 and H2, respectively.

sunset at the Apollo 12, 14, and 15 sites early in August 1972. Table 1 gives the times of local sunset and the angular distances past the sunset terminator for each of the sites. It is seen that all three sites are well onto the night side of the moon by 0400 UT on August 5. The Apollo 12 and 14 sites are 138 km apart and in global terms can be considered to be at the same location. Apollo 15 is 1100 km away.

#### SIDE OBSERVATIONS

The complete results of the Side experiments during the August 1972 solar events have been reported by Medrano *et al.* [1973a, 1973b]. For review, we will here summarize the penetrating particle results shown in Figures 2 and 3.

Starting at 0730 UT on August 4, 1972, the background count rates of each detector in all three Sides increased abruptly. The count rates remained elevated for approximately 3 days and passed through a maximum some 6–14 hours after the onset. The maximum counting rate exceeded by three orders of magnitude the background associated with galactic cosmic rays. This burst of solar cosmic rays is attributed to the class 3B flare which began at 0520 UT on August 4 [World Data Center A, 1972]. The transit time for the initial flare particles is then 2 hours and 10 min.

A second similar abrupt increase was seen on August 7 at 1547 UT. This enhancement was 2 orders of magnitude less intense and lasted only 2 days. The flare associated with this burst was the 3B flare that began at 1445 UT, indicating a transit time of 1 hour and 2 min.

The purpose of this paper is not to discuss these general enhancements but rather a most interesting feature of these penetrating particle events, a 'square wave' flux enhancement that started at 0310 UT and ended at 0459 UT on August 5. This feature is shown in detail in Figure 4. The rise and fall times for this square wave were both about 8.5 min. It was preceded by a precursor spike at 0259 lasting only 7 min. There is no flare feature reported that can be directly associated with this interesting event. The flux enhancement indicated is about one order of magnitude above the decreasing penetrating particle flux from the first 3B flare.

#### RELATED SQUARE WAVE OBSERVATIONS

The square wave under discussion was seen by experiments aboard several spacecraft near the earth: the Imp 5 and Imp 6 [Kohl and Bostrom, 1972; Bostrom, 1973; Lanzerotti and MacLennan, 1973] and the ATS spacecraft [Paulikas *et al.*, 1972]. Another particle experiment on the lunar surface also recorded the square wave [Moore *et al.*, 1973]. Pioneer 9 and 10 did not see it; however, they were located at 46°E from the earth-sun line at 0.8 and 2.2 AU, respectively [Lezniak and Webber, 1972; Webber *et al.*, 1972].

Among the experiments that saw the square wave there was generally good time correlation when transit and diffusion times are taken into consideration. A puzzling exception is the slightly early end to the square wave at the moon compared with Imp 5 data (C. Bostrom, private communication 1973).

Interplanetary magnetic field data from Heos 2 (P. Hedgecock, private communication) and Explorer 41 [Venkatesan *et al.*, 1975] indicate a significant change in the field vector during the passage of the square wave. The field was roughly radially outward both before and after but changed polarity to radially inward during passage. Also there existed a strong component north of the ecliptic before and after. This disappeared during passage [Bostrom, 1973].

During the first days of August 1972, ground-based neutron monitors recorded large variations in the cosmic ray intensity. Figure 5 illustrates hourly data from several stations. During the early morning of August 5 the neutron monitors observed a transient feature similar in appearance to the square wave recorded by lower-energy detectors in space. Figure 6 illustrates the detailed features of this transient increase as recorded by the Sulphur Mountain neutron monitor. This enhancement was due to relativistic particles of solar origin or galactic origin or particles accelerated in the interplanetary medium. A galactic origin is indicated by the following evidence:

1. The ratios of the amplitudes of this transient feature from pairs of nearly adjacent neutron monitors at differing altitudes (e.g., Sulphur Mountain and Calgary, McMurdo, and South Pole) are close to those recorded during short-term modulations of the galactic intensity rather than during solar particle events.
2. Equatorial stations responded to this transient, whereas solar particle events are generally apparent only at polar stations (e.g., the solar particle event on the preceding day).
3. The spectrum of the transient increase derived from data from underground detectors is estimated to vary as about  $E^{-1.5}$  [Sekido *et al.*, 1973] and was seen underground at 20 m water equivalent (i.e.,  $\bar{E} = 70\text{--}100$  GeV) [Filippov *et al.*, 1973].

TABLE 1. Deployment Characteristics of Alsep-Sides on Apollo 12, 14, and 15 and Angular Distances From the Terminator at the Time of the Solar Cosmic Ray Square Wave

	Apollo 12	Apollo 14	Apollo 15
Time of local sunset			
Hour	0348 UT	1706 UT	2338 UT
Date	Aug. 4	Aug. 3	Aug. 1
Alsep selenographic coordinates			
Latitude	3.2°S	3.7°S	26.01°W
Longitude	23.4°W	17.5°W	3.6°E
Angular distance past the sunset terminator at 0400 UT Aug. 5	11.9°	17.6°	36.0°

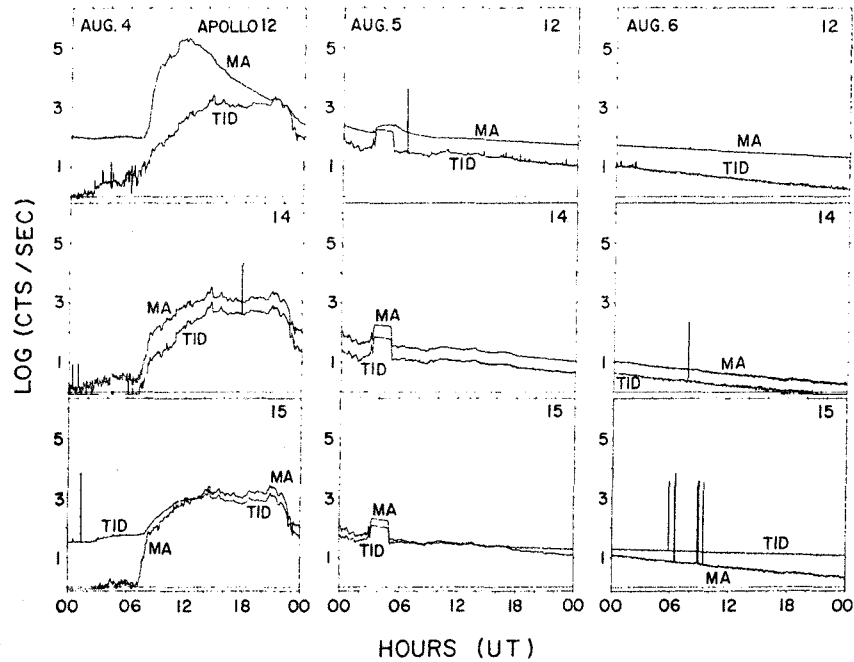


Fig. 2. Time history of the penetrating particle event. Every row of blocks displays 3 days of data from each Apollo experiment. The counts per second, plotted on a logarithmic scale, very nearly represent also the omnidirectional flux in particles  $\text{cm}^{-2} \text{s}^{-1}$ . MA and TID represent protons with energies of  $\geq 25$  MeV and  $\geq 50$  MeV, respectively.

In contrast, the preceding solar particle event on August 4 had a spectrum with an exponent between  $-5$  and  $-6$  [Pomerantz and Duggal, 1973].

The transient increase in the neutron monitor variations therefore appears to manifest features which are typical of a short-term modulation of the galactic intensity. A solar origin for this enhancement at the energies responsible for neutron monitor variations has been rejected by other workers [e.g., Pomerantz and Duggal, 1974; Agrawal et al., 1974].

#### DISCUSSION OF THE RESULTS

The solar activity of the first half of August 1972 consisted of at least four major solar flares as observed in the  $\text{Ly } \alpha$  line. All four flares were produced by the same region of activity (McMath plage region 11976). The first flare (of importance 1B) started at 0316 UT on August 2, and it took place at  $13^\circ\text{N}$  and  $35^\circ\text{E}$  on the sun. It generated a shock wave which was probably registered by Pioneer 9 between 1100 and 1500 UT

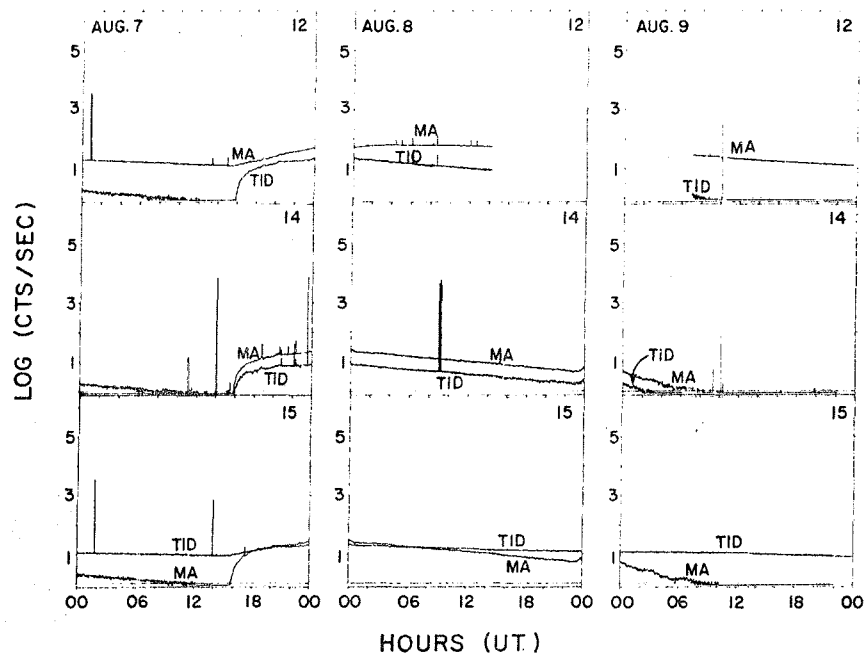


Fig. 3. Time history of the penetrating particle event. See Figure 2 legend for details.

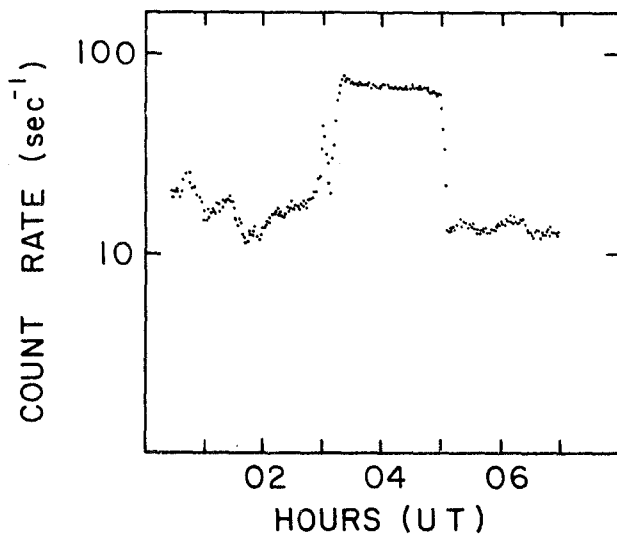


Fig. 4. Square wave enhancement as seen by the TID of the Apollo 14 Side on August 5, 1972. A nearly identical square wave structure was seen by the other Side detectors. The counting rate very nearly represents the omnidirectional flux in particles  $\text{cm}^{-2} \text{s}^{-1}$  of protons of  $\geq 50$  MeV.

on August 3 and produced an sc on earth at 0119 UT on August 4 (see Figure 7). Pioneer 9, which was at  $46^\circ\text{E}$  and at 0.8 AU, observed a significant enhancement in the proton fluxes between 0730 and 1200 UT on August 2. Detectors on board Imp 5 and Imp 6 noticed a gradual increase in their lowest energy ( $>10$  MeV) threshold detector at 0945 UT [Kohl *et al.*, 1973].

A second flare (of importance 2B) produced another shock wave which probably was overtaking the previous shock when it passed the earth. The mean speed of the shock at 0.8 AU derived directly from the transit time is 1740 km/s. The bulk speeds measured by Pioneer 9 at 1100 and 1500 UT were 350 and 585 km/s, respectively. If these values were representative of the preshock and postshock conditions and if we assume a jump in the number density by a factor of 10 (a reasonable assumption for strong shocks), we can make an estimate of the possible shock speed. In the stationary reference frame of the propagating shock, mass conservation requires

$$n_1(V_1 - U) = n_2(V_2 - U)$$

where  $n_1$ ,  $V_1$  and  $n_2$ ,  $V_2$  are the number density and speed of the solar wind on both sides of the shock front and  $U$  is the shock speed for a radial propagation. Under the assumptions mentioned above we estimate  $U \approx 610$  km/s, which is lower than that derived from the mean transit time. Using adjacent extreme values ( $V_2 = 730$  km/s,  $V_1 = 290$  km/s), we find an upper limit  $U \approx 780$  km/s. This implies a shock deceleration by the ambient plasma, as is currently accepted [Gosling *et al.*, 1968]. If the shock deceleration from 0.8 to 1 AU were not important (the energy density of the solar wind decreases as  $1/r^2$  as one goes out from the sun), the shock would propagate to the earth's orbit in approximately 10 hours. However, the time between the first measured jump in the wind speed by Pioneer 9 and the sc on earth was more than 12 hours. This simple calculation gives us an idea of the nonspherical propagation of this shock.

Solar proton events apparently were not exceptionally important during these first two flares, at least not at the earth's position.

The flare of August 4 at 0530 UT produced one of the

strongest plasma and solar cosmic ray events ever recorded. The flare was located at  $14^\circ\text{N}$  and  $09^\circ\text{E}$  on the sun. The observed onset of the solar protons corresponding to this flare was between 0400 and 0800 UT in Pioneer 9 and at around 0730 UT in the Alsep-Sides, Alsep-CPLEE, and the Imp 5 and Imp 6 experiments. Since the location of the flare was slightly to the east of the sun's central meridian, these protons might have reached the detectors by diffusion processes. The shock wave originated by this flare was presumably observed by Pioneer 9 between 2000 and 2400 UT on the same day of the flare. The Heos 2 magnetometer and ground-based magnetometers recorded a jump in the interplanetary magnetic field vector at about 2100 UT. The transit time of this shock implies a very high mean speed of propagation (2410 km/s) which is not commonly observed [Hundhausen, 1970]. About 6 hours later (at 0230 UT on August 5) Heos 2 measured a significant change in the magnetic field magnitude and direction. After a short delay the solar proton fluxes at the moon increased sharply and stayed almost constant for about 2 hours and then decreased suddenly down to the level of the normal decay (see Figures 2 and 3). The time interval between the observations of the magnetic field discontinuity by Heos 2 and the onset of solar proton fluxes detected by the Side instruments was 30 min. This is only a short time (less than 3 min) longer than the time a corotating region in space would take to reach the moon's position starting at the Heos 2 satellite's relative position. (The moon's instantaneous position can be visualized in Figure 1, and the Heos 2 was at  $138.96^\circ$  and  $32.66^\circ$  geocentric solar ecliptic longitude and latitude, respectively, and at  $33 R_E$  from the earth.) The Side instruments were past their local sunsets during this time; therefore the moon shielded them from particles flowing directly from the sun. However, the interplanetary magnetic field lines are bent and piled up at the magnetosphere on the day side [Spreiter *et al.*, 1966], forming a tangential discontinuity that is commonly known as the magnetopause. Solar protons following interplanetary field lines as guiding centers could mirror at the magnetopause depending on their pitch angle and head back upstream toward the sun. This may be the method by which the square wave protons reached the dark side of the moon.

The observed interplanetary magnetic field discontinuity can be identified with the surface that separates the ambient (disturbed) plasma and the plasma released by the flare from the chromosphere. The driver gas normally appears to follow the shock wave by 5–12 hours [Hirshberg *et al.*, 1970]. Theoretical considerations [Hundhausen, 1972] indicate that the surface that separates the ambient plasma (i.e., the transition region) and the plasma released by the flare is a tangential discontinuity. A detailed analysis of one of these driver gas tangential discontinuities has been made by Medrano [1973]. It seems reasonable to assume that the magnetic discontinuity observed by Heos 2 at 0230 UT on August 5 was the signal of the driver gas arrival. The field lines of the discontinuity on the side of the driver gas connect directly to the center of activity of the flare. These interplanetary field lines have small-scale irregularities convected from the chromosphere which are the major cause for the cosmic ray perpendicular diffusion. If there exist mechanisms that smooth these irregularities, then the perpendicular diffusion of the energetic particles would be reduced. (Possible smoothing mechanisms will be mentioned later.) Under these circumstances the tangential discontinuity is transformed into a 'free corridor' for the propagation of energetic charged particles. Therefore if the flare site is still actively injecting energetic particles [Roelof and Krimigis, 1973],

these will follow the tangential discontinuity field lines. When this corridor sweeps past the earth, it would cause a square wave like enhancement in the proton fluxes measured by a spacecraft.

The rise and fall times of the square wave, as measured by the Side instruments, correspond to a thickness of about  $7 \times 10^6$  km, whereas the gyroradius of a 50-MeV proton in a 30- $\gamma$

field (measured by Heos 2) is  $3 \times 10^4$  km. Assuming that the magnetic corridor was free of inhomogeneities, the rise time of the square wave would be expected to be related to a few gyroradii of the solar protons. Since the actual thickness is only slightly larger (by about a factor of 20) than the gyroradius, little diffusion through the sides during transit from the sun is indicated.

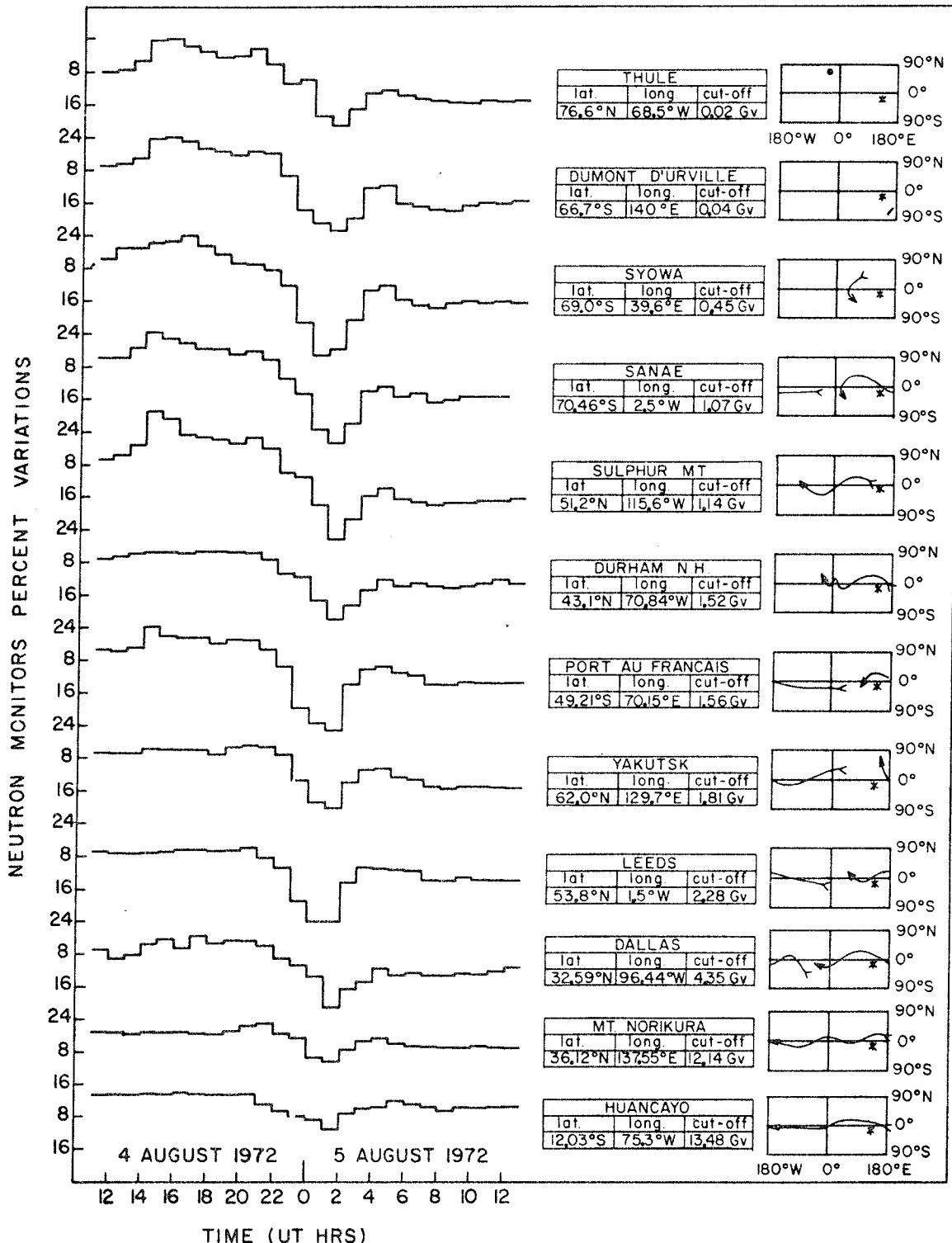


Fig. 5. Percentage variations of the galactic cosmic radiation as recorded by a selection of ground level neutron monitors. Variations are plotted with the same vertical scale as a function of time in UT. For each station the geographic coordinates and vertical cutoff magnetic rigidity are given. In the rightmost column we illustrate the asymptotic viewing directions (in geographic coordinates) of higher magnetic rigidities.

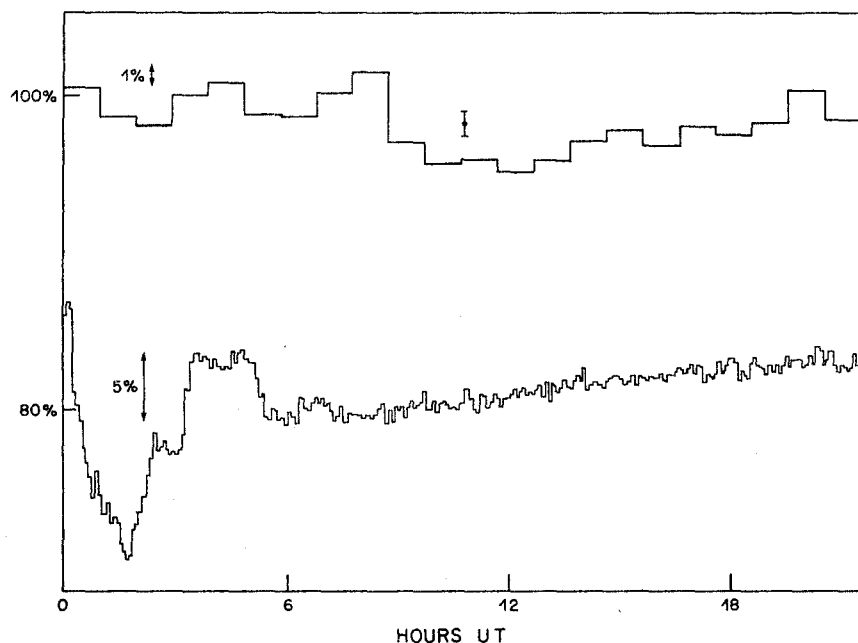


Fig. 6. Illustration of the different time variations recorded during the morning of August 5, 1972, by detectors responding to cosmic rays of different mean primary energy for (top) Yakutsk mesons at 60 m water equivalent and (bottom) Sulphur Mountain neutrons. Five-minute data from the Sulphur Mountain neutron monitor reveal a short-lived recovery peak at primary energies of a few GeV; in the hundreds of GeV primary energy range ( $\bar{E} = 200\text{--}280$  GeV), the underground meson monitor at Yakutsk registers a decrease late in the morning. Data from Sulphur Mountain are reproduced by courtesy of T. Mathews; Yakutsk data are reproduced from *Filippov et al.* [1973].

The relativistic particles observed by the ground-based neutron monitors can be related to the magnetic discontinuity and corridor in one of two ways. The first possibility is that these relativistic particles are of solar origin and are simply a high-energy extension of the spectrum of solar particles in the square wave recorded by the detectors in space. This interpretation, however, implies continuous injection of relativistic (GeV) particles at the flare site even hours after the original burst. Since this does not appear to be experimentally confirmed, we are unable to state any definite conclusion regarding this possibility.

A second possible interpretation is that the square wave enhancement recorded by the neutron monitors results from a short-term modulation of the galactic cosmic ray intensity. Let us assume that the transient increase is the result of the superposition of two sequential Forbush decreases. Around 2200 UT on August 4 a very large Forbush decrease occurred. The existence of a second Forbush decrease mechanism operative at high primary energies is indicated by the Yakutsk underground data presented in Figure 6. It will be noted that this detector hardly responded at all to the huge Forbush decrease late on August 4 but recorded a second Forbush decrease in the late morning of August 5. In the light of the observations therefore we are led to postulate that the first Forbush decrease was caused by the passage of the earth through a shock front, the transient increase by the passage through a region being replenished with galactic cosmic rays by means of parallel diffusion along the tangential discontinuity, and that the increase was terminated by the entry into a closed loop structure capable of excluding cosmic rays up to very high energies. Recently *Barnden* [1973] has independently arrived at similar conclusions in his analysis of the September 1966 and December 1971 events. Such an interplanetary magnetic configuration is consistent with and substantiated by the evidence that the relativistic particle square wave results from modula-

tion of galactic cosmic rays. The lower-energy square wave seen by detectors in space is certainly of solar origin.

#### MODEL OF PROPAGATION

At this point we present a model representing the dynamics of the particles and fields in the interplanetary space corresponding to the solar proton square wave of August 5, 1972.

The model is based on the current and generally accepted picture of a shock and blast wave propagation following a solar flare [*Hundhausen*, 1972]. Fresh plasma supersonically ejected during a flare propagates through the ambient plasma. Due to the highly conductive nature of both plasmas, interpenetration is forbidden, so the ambient plasma and field lines accumulate in front of the fresh plasma. Consequently, a shock wave is built up ahead of the driver gas. Between the shock and the driver gas there exists a transition region where both the ambient plasma and fields are highly disturbed. Between the transition region and the fresh plasma a tangential discontinuity exists. The field lines on the side of the driver gas at the tangential discontinuity connect directly to the center of activity of the flare. If this center of activity continues to inject energetic protons, these protons will propagate with their guiding centers following the field lines of the discontinuity. Furthermore, if the field lines are free of inhomogeneities (an idealized case), the discontinuity will provide a type of free corridor for the propagation of energetic solar protons. Figure 7 is an artistic representation of the shock wave propagation several hours after the flare. The tongue-shaped flare plasma ejected follows the description made by *Hundhausen* [1972] and is based upon the observations. The solar proton corridor follows the tangential discontinuity. The spreading of the particles on the sides of the corridor is due to the diffusion across field lines. Figure 8 is intended to illustrate the geometry of the event some days later. An observer at the point A will traverse the corridor noticing a

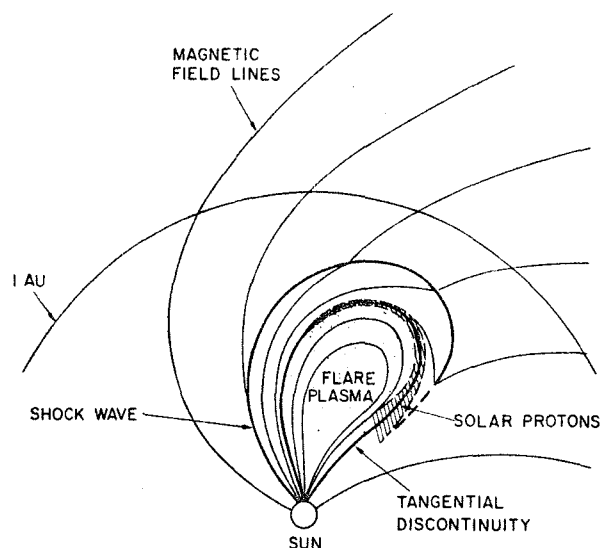


Fig. 7. Sketch of the propagation of a flare-induced shock wave several hours after the flare time [after *Hundhausen*, 1972]. Energetic solar protons (solar cosmic rays) propagate along the tangential discontinuity formed by the fresh plasma. Gradual diffusion perpendicular to the field lines makes the population of the solar protons extend over the shaded area (observed to be  $7 \times 10^6$  km at 1 AU).

square wave like enhancement in the cosmic ray fluxes. Another observer at the point B will notice a solar proton flux enhancement that is less intense than A but occurs over a longer period of time.

According to this model, after a major solar proton flare an enhancement in the solar cosmic ray fluxes should be expected before (observer B) or with (observer A) the arrival of the tangential discontinuity. The time and the shape of this enhancement will depend not only on the heliographic coordinates of the flare but also on the diffusion processes across field lines. If the perpendicular diffusion of charged particles were mostly due to the uneven configuration of the field lines along the general pattern, then this type of diffusion could be expected to be inversely proportional to the solar wind speed. The smoothing of the interplanetary field lines by the solar wind can be analogized by a rubber band fixed at both extremes across a river. The speed of the fluid controls the smoothness and distention of the rubber band. This type of smoothing can be carried out by MHD waves (primarily Alfvén waves) propagating from the sun along the tangential discontinuity. The wave activity is likely to be enhanced at the surface of the discontinuity by the speed of the driver gas. Another smoothing mechanism can be provided by the pressure exerted on the field lines by the energetic particles injected at the flare site. Both of these mechanisms are currently under investigation.

The square wave particle enhancement on August 5 must have had little diffusion across field lines, since its rise and decay times are small (only about 20 times the equivalent Larmor radius). This unusually small perpendicular diffusion is probably due to the remarkably high speed of the wind and unprecedented emission of solar cosmic rays.

The width of the square wave (2 hours and 8 min) corresponds to 0.07 AU. This shell is within the range of the estimated thickness of a helium-enriched region in front of the driver gas [*Hundhausen*, 1972]. Because of the lack of solar wind data we cannot confirm this suggestion.

Enhancements in the solar proton fluxes in association with

the sudden storm commencements and Forbush decreases have been reported in the literature [*Bryant et al.*, 1962; *Axford and Reid*, 1962; *Lockwood and Razdan*, 1963; *Haurwitz et al.*, 1965; *Ahluwalia*, 1966; *Kahler*, 1969; *Engelmann et al.*, 1969; *Ogilvie and Arens*, 1971; *Balogh et al.*, 1971; *Datlowe*, 1972]. Several interpretations including trapped solar protons behind the shock front [*Bryant et al.*, 1962; *Haurwitz et al.*, 1965], acceleration in the transition region [*Axford and Reid*, 1962; *Datlowe*, 1972], temporary leakage of galactic cosmic rays through the plasma cloud under 'certain instabilities' [*Lockwood and Razdan*, 1963], etc., have been made. However, these models bear some inconsistencies with the observations [*Datlowe*, 1972].

A difficulty in the present model is that it assumes continuous injection of energetic particles. Long-lived solar proton streams of MeV energies for as much as a complete solar rotation have been reported by *Bryant et al.* [1963]. Recently *Roelof and Krimigis* [1973] have lent new support to the idea of time-extended injection. It seems to us that continuous injection of energetic protons at the flare's center of activity is the most favorable explanation at this time.

#### SUMMARY AND CONCLUSIONS

Data analysis of the Alsep-Side experiments of Apollo 12, 14, and 15 has been made in relation to the solar activity of early August 1972. Observations of solar wind ions during this active period are reported in other works [*Medrano et al.*, 1973a, b; *Medrano*, 1973]. While the solar wind activity was still in progress, solar cosmic ray protons with fluxes never before seen by Side arrived on the night side of the moon. The estimated minimum energies for these protons to penetrate the shielding of the MA and TID detectors are 25 MeV and 50 MeV, respectively. The observations of the solar proton event can be summarized as follows:

1. Two major enhancements in the solar proton fluxes are directly related to two solar flares: 3B on August 4 at 0525 UT and another 3B flare on August 7 at 1445 UT. During this time the Side experiments were in the lunar night and could not observe directly protons coming from the sun. It is suggested

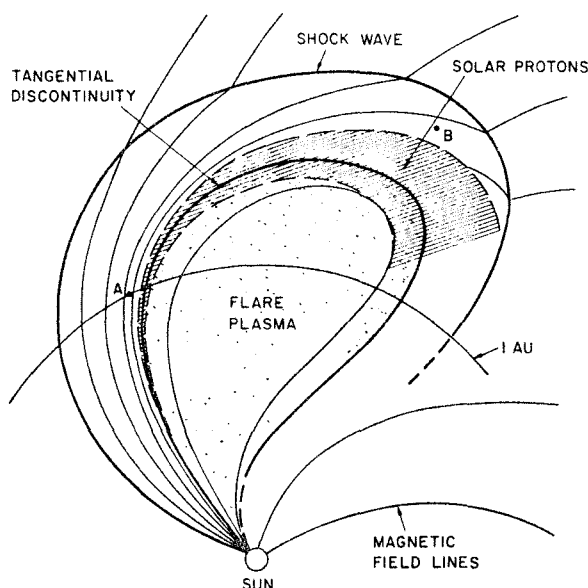


Fig. 8. Sketch of the propagation of a flare-induced shock wave several days after the flare time. The diffusion of the solar protons on the sides of the tangential discontinuity makes their confinement wider than that in Figure 7.

that these protons following the field lines mirrored on the nose of the magnetopause and then headed back toward the sun.

2. A third solar proton enhancement cannot be directly related to any solar flare. It took place at 0310 UT on August 5 during the decay time of the proton event of August 4. The peculiar characteristic of this event is the square wave shape of the enhancement with rise and fall times of 8 min and a duration of approximately 2 hours.

In connection with this last-mentioned singular event, data from a variety of ground-based and space experiments have been examined. The result of this analysis appears to show that the onset of the square wave corresponds to the tangential discontinuity that signals the arrival of the driver gas ejected by the flare of August 4.

A model to explain the square wave particle propagation has been elaborated. The model hypothesizes continuous injection of energetic solar protons into interplanetary space by the active center of the flare site for hours after the flare time. The tangential discontinuity serves as a magnetic corridor for the propagation of the energetic protons and as a mechanism for subsequent modulation of galactic cosmic rays. The width of this corridor at 1 AU, as derived from the duration of the square wave, is 0.07 AU. The rise and fall time of the square waves is approximately 20 times larger than the Larmor radius of a 50-MeV proton. This is interpreted as an indication of only slight diffusion across field lines. At larger distances from the sun this diffusion process should be expected to intensify the cosmic ray fluxes in the transition region behind the shock front.

It is suggested that the frequently observed energetic solar protons in association with ssc and Forbush decreases (delayed solar particle events) can be explained by this model.

**Acknowledgments.** We wish to acknowledge enlightening discussions with R. A. Wolf and other members of the Rice University Department of Space Physics and Astronomy. Unpublished data from Heos 2 and 1971-39A satellite were made available, thanks to the kindness of P. C. Hedgecock and G. A. Paulikas. We made use of neutron monitor data kindly supplied to the University of Calgary by various investigators. One of us (C. J. Bland) wishes to acknowledge the hospitality received while a guest of Rice University. We gratefully acknowledge the facilities made available at Texas A&M University for the calibration of the Side in a cyclotron beam. This research has been partially supported by NASA under contract NAS 9-5911. The paper is based in part on a Ph.D. thesis submitted by R. A. Medrano to the Department of Space Physics and Astronomy of Rice University.

The Editor thanks G. A. Paulikas for his assistance in evaluating this paper.

## REFERENCES

- Agrawal, S., A. Ananth, M. Bemalkhedkar, L. Kargathra, U. Rao, and H. Razdan, High-energy cosmic ray intensity increase of non-solar origin and the unusual Forbush decrease of August 1972, *J. Geophys. Res.*, **79**, 2269, 1974.
- Ahluwalia, H. S., A case of transient anisotropy during the recovery phase of a Forbush decrease, *Planet. Space Sci.*, **14**, 791, 1966.
- Armstrong, J. W., W. A. Coles, J. K. Harmon, S. Maagoe, B. J. Rickett, and D. G. Sime, The solar wind velocity during August 1-15, 1972 (abstract), *Eos Trans. AGU*, **53**, 1057, 1972.
- Axford, W. I., and G. C. Reid, Polar-cap absorption and the magnetic storm of February 11, 1958, *J. Geophys. Res.*, **67**, 1692-1697, 1962.
- Balogh, A., P. C. Hedgecock, R. J. Hynds, and J. Sears, Propagation of low energy protons associated with the 24 January 1969 solar flare, *Solar Phys.*, **20**, 150, 1971.
- Barnden, L. R., The large-scale magnetic field configuration associated with Forbush decreases, *Proc. Int. Conf. Cosmic Rays 13th*, **2**, 1277, 1973.
- Bostrom, C. O., Convection of energetic solar particles and entry into the magnetotail during the August 4, 1972 event, paper presented at the 2nd General Assembly, International Association of Geomagnetism and Aeronomy, Kyoto, Japan, Sept. 9-21, 1973.
- Bryant, D. A., T. L. Cline, V. D. Desai, and F. B. McDonald, Explorer 12 observations of solar cosmic rays and energetic storm particles after the solar flare of September 28, 1961, *J. Geophys. Res.*, **67**, 4983, 1962.
- Bryant, D. A., T. L. Cline, V. D. Desai, and F. B. McDonald, New evidence for long-lived solar streams in interplanetary space, *Phys. Rev. Lett.*, **11**, 144, 1963.
- Colburn, D. S., B. F. Smith, and C. P. Sonett, Pioneer 9 magnetic field observations during the solar storm of early August, 1972 (abstract), *Eos Trans. AGU*, **53**, 1058, 1972.
- Comstock, G. M., K. C. Hsieh, and J. A. Simpson, Cosmic ray source and local interstellar spectra deduced from the isotopes of hydrogen and helium, *Astrophys. J.*, **173**, 691, 1972.
- Datlowe, D., Association between interplanetary shock waves and delayed solar particle events, *J. Geophys. Res.*, **77**, 5374, 1972.
- Engelmann, J., A. Hautdidier, and L. Koch, Energy spectra and time profile of protons emitted during the solar flare of June 9, 1968, paper presented at the 11th Conference on Cosmic Rays, International Union of Pure and Applied Physics, Budapest, Aug. 25-Sept. 4, 1969.
- Filippov, V. A., A. I. Kuzmin, A. N. Prikhodko, I. S. Samsonov, G. V. Skripin, G. V. Shafer, and A. A. Upolmikov, Data of the events of August 1972 from the cosmic ray installation complex in Yakutsk, Collected Data Reports on August 1972 Solar-Terrestrial Events, edited by H. E. Coffey, *Rep. UAG-28*, p. 469, World Data Center A, Boulder, Colo., 1973.
- Freeman, J. W., Jr., M. A. Fenner, H. K. Hills, R. A. Lindeman, R. Medrano, and J. Meister, Suprathermal ions near the moon, *Icarus*, **16**, 328-338, 1972.
- Gosling, J. T., J. R. Asbridge, S. J. Bame, A. J. Hundhausen, and I. B. Strong, Satellite observations of interplanetary shock waves, *J. Geophys. Res.*, **73**, 43, 1968.
- Haurwitz, M. W., S. Yoshida, and S. I. Akasofu, Interplanetary magnetic field asymmetries and their effects on polar cap absorption events and Forbush decreases, *J. Geophys. Res.*, **70**, 2977, 1965.
- Hills, H. K., and J. W. Freeman, Jr., Suprathermal ion detector experiment (lunar ionosphere detector), Apollo 14 Preliminary Science Report, *NASA Spec. Publ.* 272, 175, 1971.
- Hirshberg, J., A. Alksne, D. S. Colburn, S. J. Bame, and A. J. Hundhausen, Observation of a solar flare induced interplanetary shock and helium-enriched driver gas, *J. Geophys. Res.*, **75**, 1, 1970.
- Hundhausen, A. J., Composition and dynamics of the solar wind plasma, *Rev. Geophys. Space Phys.*, **8**, 729, 1970.
- Hundhausen, A. J., *Coronal Expansion and Solar Wind*, Springer, New York, 1972.
- Kahler, S. W., A comparison of energetic storm protons to halo protons, *Solar Phys.*, **8**, 166, 1969.
- Kohl, J. W., and C. O. Bostrom, Observations of the August '72 solar events by the solar proton monitor on Explorer 41 (abstract), *Eos Trans. AGU*, **53**, 1055, 1972.
- Kohl, J. W., C. O. Bostrom, and D. J. Williams, Particle observations of the August 1972 solar events by Explorers 41 and 43, Collected Data Reports on August 1972 Solar-Terrestrial Events, edited by H. E. Coffey, *Rep. UAG-28*, p. 330, World Data Center A, Boulder, Colo., 1973.
- Lanzerotti, L. J., and C. G. MacLennan, Low energy interplanetary particles during the August 1972 events, Collected Data Reports on August 1972 Solar-Terrestrial Events, edited by H. E. Coffey, *Rep. UAG-28*, p. 338, World Data Center A, Boulder, Colo., 1973.
- Lezniak, J. A., and W. R. Webber, Pioneer 9 cosmic ray observations during August 1972 (abstract), *Eos Trans. AGU*, **53**, 1054, 1972.
- Livingston, W. C., Solar magnetic fields of McMath 11976 (abstract), *Eos Trans. AGU*, **53**, 1052, 1972.
- Lockwood, J. A., and H. Razdan, Asymmetries in the Forbush decreases of the cosmic radiation, 2. Superimposed intensity variations during a Forbush decrease, *J. Geophys. Res.*, **68**, 1593, 1963.
- McKinnon, J. A., August 1972 solar activity and related geophysical effects, *NOAA Tech. Mem. ERL SEL-22*, Dec. 1972.
- Medrano, R. A., Unusual solar wind and solar proton events observed on the lunar surface, Ph.D. thesis, Rice University, Houston, Tex., 1973.
- Medrano, R. A., J. W. Freeman, Jr., H. K. Hills, and R. R. Vondrak, Penetrating solar flare particles and solar wind observations in the lunar night, August 1972, Collected Data Reports on August 1972



- Solar-Terrestrial Events, edited by H. E. Coffey, *Rep. UAG-28*, p. 361, World Data Center A, Boulder, Colo., 1973a.
- Medrano, R. A., C. J. Bland, and J. W. Freeman, The solar energetic particle "square-wave" during the August 1972 solar storm (abstract), *IAGA Bull.* 34, 196, 1973b.
- Moore, P. R., D. L. Reasoner, W. J. Burke, and F. J. Rich, Lunar surface observations of the August 1972 solar flare activity, Collected Data Reports on August 1972 Solar-Terrestrial Events, edited by H. E. Coffey, *Rep. UAG-28*, p. 356, World Data Center A, Boulder, Colo., 1973.
- Ogilvie, K. W., and J. F. Arens, Acceleration of protons by interplanetary shocks, *J. Geophys. Res.*, 76, 13, 1971.
- Paulikas, G. A., J. B. Blake, and E. F. Martine, Energetic solar proton observations 3-10 August 1972 (abstract), *Eos Trans. AGU*, 53, 1055, 1972.
- Pomerantz, M. A., and S. P. Duggal, Remarkable cosmic-ray storm and associated relativistic solar particle events of August 1972, Collected Data Reports on August 1972 Solar-Terrestrial Events, edited by H. E. Coffey, *Rep. UAG-28*, World Data Center A, Boulder, Colo., 1973.
- Pomerantz, M., and S. Duggal, Interplanetary acceleration of solar cosmic rays to relativistic energy, *J. Geophys. Res.*, 79, 913, 1974.
- Roelof, E. C., and S. M. Krimigis, Analysis and synthesis of coronal and interplanetary energetic particle, plasma, and magnetic field observations over three solar rotations, *J. Geophys. Res.*, 78, 5375, 1973.
- Rosenbauer, H., H. Gruenwaldt, and M. D. Montgomery, Extreme solar wind conditions observed after the activity related to McMath region 11976 (abstract), *Eos Trans. AGU*, 53, 1058, 1972.
- Sekido, Y., K. Nagashima, I. Kondo, H. Ueno, K. Fujimoto, and Z. Fujii, Multi-directional meson intensities at Mt. Norikura and Nagoya, August 1972, Collected Data Reports on August 1972 Solar-Terrestrial Events, edited by H. E. Coffey, *Rep. UAG-28*, p. 479, World Data Center A, Boulder, Colo., 1973.
- Smith, E. J., D. E. Jones, L. Davis, Jr., P. J. Coleman, Jr., C. P. Sonett, P. Dyal, and D. S. Colburn, Response of the distant interplanetary magnetic field: Pioneer 10 (abstract), *Eos Trans. AGU*, 53, 1058, 1972.
- Spreiter, J. R., A. L. Summers, and A. Y. Alksne, Hydromagnetic flow around the magnetosphere, *Planet. Space Sci.* 14, 223, 1966.
- Venkatesan, D., T. Mathews, L. Lanzerotti, D. Fairfield, and C. Bostrom, Cosmic ray intensity variations during 0200-0700 UT, August 5, 1972, *J. Geophys. Res.*, 80, in press, 1975.
- Webber, W. R., E. C. Roelof, F. B. McDonald, B. J. Teegarden, and J. H. Trainor, Pioneer 10 cosmic ray observations during August 1972 (abstract), *Eos Trans. AGU*, 53, 1054, 1972.
- Wolfe, J., H. Collard, D. McKibbin, and J. Mihalov, Preliminary interplanetary solar wind profile for the August 2-7, 1972, solar events (abstract), *Eos Trans. AGU*, 53, 1057, 1972.
- World Data Center A for Solar-Terrestrial Physics, Preliminary compilation of data for retrospective world interval July 26-August 14, 1972, compiled by J. V. Lincoln and H. I. Leighton, *Rep. UAG-21*, Boulder, Colo., Nov. 1972.
- World Data Center A for Solar-Terrestrial Physics, Collected Data Reports on August 1972 Solar-Terrestrial Events, edited by H. E. Coffey, *Rep. UAG-28*, Boulder, Colo., 1973.

(Received May 9, 1974;  
accepted December 19, 1974.)

